EVALUATION OF CONCRETE MIXES FOR SLAB REPLACEMENT USING THE MATURITY METHOD AND ACCELERATED PAVEMENT TESTING

By

KITTI MANOKHOON

A DISSERTATION PRESENTED TO THE GRADUATE SCHOOL
OF THE UNIVERSITY OF FLORIDA IN PARTIAL FULFILLMENT
OF THE REQUIREMENTS FOR THE DEGREE OF
DOCTOR OF PHILOSOPHY

UNIVERSITY OF FLORIDA

2007

© 2007 Kitti Manokhoon

To my grand father
To my father and mother

ACKNOWLEDGMENTS

I would like to express my heartfelt appreciation and deep gratitude to my supervisory committee chair, Prof. Mang Tia, for continuously helping, guiding and supporting me at the University of Florida (UF). Appreciation is also extended to supervisory committee co-chair, Prof. Fazil T. Najafi, as well as committee members, Dr. Scott Washburn, Dr. Bouzid Choubane and Dr. Malisa Sarntinoranont, whose opinions and guidance have been invaluable in the completion of this study.

Special gratitude is expressed to the Royal Thai Government and the Thai people for financially supporting my studies at the University of Florida.

I wish to express my sincere thanks to the Florida Department of Transportation (FDOT) for sponsoring the research that made this dissertation possible. I also give thanks to FDOT Materials Office personnel, particularly Dr. Bouzid Choubane, Michael Bergin, Tom Byron, Steve Ross, Charles Ishee, Richard DeLorenzo, and others. Gratitude is also conveyed to the staff of the Department of Civil and Coastal Engineering, especially Nancy Been, Carol Hipsley, Doretha Ray, Ketty Fizer, Anthony Murphy, and others. Sincere appreciation also goes to Irene Scarso for her expert editing of this dissertation.

I would like to also express my appreciation to my friends and colleagues at UF who have helped with this research, as well as my friends in the Thai Student Association at UF for their kind support.

Finally, the deepest appreciation goes to my parents, to my family members, especially to my sister (Nonglak Manokhoon) and my brother (Sukho Manokhoon), and last but not least Kanthida Deopanich, for their patience, understanding, support and love throughout my time in the US.

TABLE OF CONTENTS

page

LIST OF TABLES

LIST OF FIGURES

Abstract of Dissertation Presented to the Graduate School
of the University of Florida in Partial Fulfillment of the
Requirements for the Degree of Doctor of Philosophy

EVALUATION OF CONCRETE MIXES FOR SLAB REPLACEMENT USING THE MATURITY METHOD AND ACCELERATED PAVEMENT TESTING

By

Kitti Manokhoon

December 2007

Chair: Mang Tia
Major: Civil Engineering

Five instrumented full-size concrete slabs were constructed and tested under accelerated pavement testing by means of a Heavy Vehicle Simulator (HVS) to study the behavior of concrete replacement slabs at early age and the effects of concrete properties on the performance of the replacement slabs. The maximum stresses in the concrete slabs were calculated using the FEACONS (Finite Element Analysis of CONcrete Slabs) program, which considers the effects of the applied load, temperature differential in the slab, elastic modulus and coefficient of thermal expansion of concrete, slab thickness, joint characteristics and effective subgrade stiffness. The model used was calibrated by comparing the computed strains with the measured strains from embedded strain gauges in the test slabs which were loaded by the HVS.

The use of maturity method to determine the flexural strength of the in-place concrete at early age was evaluated in this study. It was found that the maturity method was convenient to use and produced reliable determination of the flexural strength of the in-place concrete.

Investigation was also made to evaluate the use of the maximum stress to flexural strength ratio of the concrete at the early age as an indicator of potential performance of a concrete replacement slab. This was done by comparing the stress strength ratio with the observed

performance of test slabs in this study. This method was found to be effective in predicting the potential performance of the replacement slabs. A systematic method for evaluation of concrete mixes for potential performance in replacement slab was recommended as the result of this study.

CHAPTER 1
INTRODUCTION

1.1 Background

In Florida, full slab replacement is a typical method to repair existing badly deteriorated concrete pavement slabs. This type of repair work is generally performed at night, and the repaired slabs are opened to traffic by the next morning. It is essential that this repair work be finished in a minimal amount of time. High early strength concrete is normally used in this application in order to have sufficient strength within a few hours after placement.

The Florida Department of Transportation (FDOT) currently specifies that slab-replacement concrete must have a minimum 6-hour compressive strength of 2,200 psi and a minimum 24 hour compressive strength of 3,000 psi [FDOT standard for slab replacement section 353, 2007]. The California Department of Transportation (Caltrans) has developed a guideline for concrete slab replacement that requires a minimum flexural strength at opening to traffic of 400 psi [Caltrans, Slab replacement guideline, 2004].

A research study entitled "Evaluation of Early Strength Requirement of Concrete for Slab Replacement Using APT" has just recently been completed. In this study, five 9-inch thick concrete replacement slabs were constructed and tested at the accelerated pavement testing facility at the FDOT Materials Research Park in Gainesville, Florida. The results of this experiment showed that two slabs performed well, while the other three slabs cracked prematurely under 12-kip wheel loads [Tia, M. and Kumara, W., 2005].

The performance of the test slabs was found to be independent of the cement content of the concrete used as two concrete slabs with the same concrete mix design were found to have drastically different performance. The performance of a concrete replacement slab depends on whether or not the concrete has sufficient flexural strength to resist the anticipated temperature-

load induced tensile stresses in the concrete slab. The strength development of concrete depends not only on the mix design but also the condition under which the concrete is cured. The temperature-load induced stresses are a function of the slab thickness, effective modulus of subgrade reaction, modulus of the concrete, coefficient of thermal expansion of the concrete, loads and temperature differentials in the concrete slab. The flexural strength of the concrete must be greater than the tensile stress in the slab at all times to ensure good performance. In addition, in order to minimize the chance for shrinkage cracking, the cement content of the concrete mix must be kept to a minimum [Tia, M. and Kumara, W., 2005].

Due to the limited amount of testing performed in this previous study, no recommendation for changes in the FDOT specifications for concrete replacement slabs was made. There was a need to perform further testing and research to substantiate these findings, [Tia, M. and Kumara, W., 2005].

This current research is aimed to better understand the behavior of concrete replacement slabs at early age, so that a concrete mix can be effectively designed, evaluated and controlled to ensure good performance in concrete replacement slabs.

1.2 Hypothesis of Research

The following hypotheses were tested in this research study:

- The maximum stresses in the concrete slab can be calculated from an appropriate finite element model which considers the effects of the applied load, temperature differential in the slab, elastic modulus and coefficient of thermal expansion of concrete, slab thickness, joint characteristics and effective subgrade stiffness. The model used can be calibrated by comparing the computed strains with the measured strains from embedded strain gages in test slabs loaded by a heavy vehicle simulator (HVS).
- The flexural strength of the in-place concrete at the early age can be determined accurately and conveniently by the maturity method.
- The maximum stress to flexural strength ratio of the concrete at the early age can be used as an indicator of potential performance of a concrete replacement

slab. This hypothesis was tested by comparing the stress strength ratio with the observed performance of test slabs in this study.

1.3 Research Objectives

The main objectives of this research were as follows:

- To verify analytical models for calculating the load and temperature induced stresses in a concrete replacement slab after it is open to traffic under typical Florida conditions. The applicability of the model will be validated by comparing the predicted results to the experimental results in this study.
- To develop a systematic method for evaluation of concrete mixes to ensure satisfactory performance in replacement slabs.
- To evaluate the current FDOT specification for slab replacement for its adequacy and effectiveness and to make recommendations for changes if needed.

1.4 Approach and Scope of Research

The envisioned approach was to develop a rational method where (1) the maximum anticipated tensile stresses in the concrete slab can be accurately determined, (2) the flexural strength of the in-place concrete can be reliably determined, and (3) the ratio of the maximum tensile stress to the flexural strength of the concrete can be used as an indicator of performance. The stress ratio must be less than 1 at all times to avoid cracking in the concrete.

The scope for this study consists of the following:

- To design an experiment to evaluate the performance of different concrete mixes in replacement slabs using accelerated pavement testing by means of a Heavy Vehicle Simulator (HVS).
- To develop an instrumentation plan for the experiment for an effective collection of temperature, strain and deflection data based on the results of stress analyses.
- To perform maturity calibration of concrete mixtures to be used in the HVS experiments.

- To select an appropriate model and calibrate the model parameters for analysis of concrete replacement slabs under typical Florida conditions, and to perform stress analysis for the conditions of the test sections under HVS loading.
- To verify the analytical models by comparing the computed strains to the measured strains from the embedded strain gages in the test section, and to make necessary adjustments to the analytical model.
- To evaluate the drying shrinkage properties and coefficient of thermal expansion of the concrete used in the test slabs.
- To determine the relationships among the material and pavement parameters and the performance of the test slabs.
- To identify possible improvements to the current FDOT specification for slab replacement.

1.5 Significance of the Research

In the past, there have been a lot of analytical models developed for analysis of concrete pavements [Westergaard, 1926, 1933, 1947, Tabatabaie and Barenberg, 1978, Tayabji and Colley, 1981, Tia et al, 1989, Huang 1993]. There have also been some experimental studies done to evaluate the performance of concrete pavements in the past [Melhem et al, 2003, Turan et al, 2005, Suh, 2005]. However, there has been very little research done where the experimental results were compared successfully to the analytical results. For example, in experiments by Melhem et al, [2003] all gauges used in the experiment were positioned to measure longitudinal strains at the bottom of the PCC overlays. While some tensile and compressive strains measured were reported, the remaining gauges did not give any useful strain readings. These researchers were not able to relate measured strains to observed performance.

One of the objectives of this research was to develop a reliable model for analysis of concrete pavements which is verified by experimental results. The development of such an analytical model which is validated by experimental results represents a significant contribution in this field.

Past specification for this type of application usually required a compressive strength or a flexural strength at a certain age [FDOT standard for slab replacement section 353, 2007, Caltrans, slab replacement guideline, 2004]. However, little work has been done in verifying that this type of specification is sufficient to ensure satisfactory performance. In its slab replacement guideline, Caltrans recommends test procedures to help ensure the proper curing of the beams for flexural testing such that the strength of the beams can match the strength of the concrete in the pavement. These flexural strength test results are not used as the criteria for opening to traffic. The Caltrans field laboratory flexural strength test results are used to determine pay factors for the contractor, as the contractor may choose to open the lanes to traffic at less than specified strength to avoid penalties associated with delays.

This research investigated the adequacy of this type of specification, and whether additional criteria, based on factors such as anticipated temperature distribution in the slab and coefficient of thermal expansion of the concrete, need to be added to the specification to ensure satisfactory performance. Little work has been done in this area, and the useful results from this work represent a significant contribution in this area.

In recent years, the maturity method has been used in many states in the U.S. as a convenient tool to evaluate the strength of in-place concrete [Tikalsky et al, 2001, Luke et al, 2002, Rasmussen, 2003, Mancio et al, 2004, Zhang et al, 2004, Trost et al, 2006]. However, it is a fairly new practice, and further research and experience with this method is needed to refine it and to make it an effective tool. Most of the practice of the maturity method uses compressive strength as the predicted result and relates the predicted compressive strength to the predicted flexural strength [Zhang et al, 2004].

In this research, the flexural strength was used as the primary predicted property, while the relationship between compressive strength and flexural strength of in-place concrete was evaluated. Little work has been done in this area. Zhang also stated that the strength-maturity correlation has been generally developed for concrete cylinders tested under uniaxial compressive strength, because this is usually the most important strength index for conventional structures [Zhang et al, 2004]. This research work represents the first effort in using the flexural strength directly in evaluation of replacement slabs for Florida conditions.

CHAPTER 2
LITERATURE REVIEW

2.1 General Review on Slab Replacement

The Florida Department of Transportation is often restricted to very short construction time windows for pavement rehabilitation, due to high traffic demand for most of Florida's urban freeways. Often the available time for lane closure may be as short as 6 hours and nighttime construction may be required, depending on the direction of peak traffic and the day of the work.

Many concrete pavements are restored to an acceptable performance level using slab and base repairs. The effectiveness of this repair strategy depends on proper evaluation of the extent and severity of the slab distresses, as well as the condition of the underlying pavement layers.

NCHRP report 540 states that, because of its unique requirements, early-opening-to-traffic (EOT) concrete is more susceptible to durability-related distress than conventional concrete. For example, the use of high cement contents and multiple admixtures can lead to increased shrinkage, altered microstructure, and unexpected interactions. Further, the ability of standard testing to detect durability-related problems is limited, and thus deficiencies may go undetected through the mixture design and construction process [NCHRP report 540, 2005].

This NCHRP study was conducted to evaluate the durability characteristics of EOT concrete for materials, mixtures, and construction techniques that enhance long-term durability of EOT concrete for pavement rehabilitation. The research dealt with concrete mixtures that are suited for opening to traffic within (a) 6 to 8 hour and (b) 20 to 24 hours after placement and was limited to full-depth rehabilitation, such as a full-depth repair and slab replacement. In the experiment, the EOT concrete mixtures obtained from four states (Ohio, Georgia, Texas and New York) were evaluated to determine their mixture properties and performance characteristics [NCHRP report 540, 2005].

The California Department of Transportation (Caltrans) has developed guidelines for concrete slab replacement. These guidelines include several key factors that help reduce the time necessary to accomplish slab replacement and improve the quality of repaired concrete pavement, including the proper selection of the slab removal boundaries and concrete material. Also included are the recommended procedures for saw cutting, slab removal, subgrade and base preparation, concrete placing and curing, sampling and testing procedures, grinding and joint sealing, and opening to traffic criteria. A practical checklist that provides a quick summary of the entire process is also provided [Caltrans, Slab replacement guideline, 2004].

In Florida, many forms of functional or structural distresses have been reported from the newly replaced concrete slabs within a short time after construction. A survey on I-10 in Florida of 100 replacement slabs ranging in age between 1 to 3 years showed that 35% of the slabs had developed cracks. In these slabs, fatigue damage was clearly ruled out as a cause of early cracking. Investigators of this study hypothesized that the micro cracks were developed in the slabs as a result of shortcoming in pavement design, concrete mix or construction [Kumara, Tia, Wu, and Choubane, 2002].

High early strength concrete has been used for slab replacement concrete to allow earlier use of the paved sections for moving construction equipment and speeding up construction. High early strength concrete often uses high quantities of cement content. Increasing the cement content in concrete mixture tends to increase the heat development in the mixture. For the investigation of effects of cement type, curing method, and joint type on the performance of high early strength concrete in slab replacement, forty two test sections were constructed on the outside lane of I-10. Fourteen different combinations of the above factors were included in the design of test sections with 3 slabs for each design. Frequent condition surveys of 42 sections on

I-10 showed that mid slab cracking occurred in 39 of the 42 slabs. The cracks developed at different times ranging from 24 hours to one year [Kumara, Tia, Wu, and Choubane, 2002].

Doweled joints are expected to perform better than undoweled joints. A reduction of 20% in deflection and lower stresses are expected in doweled joints [Armaghani, 1993]. An extensive crack survey on Florida's I-10 showed that dowelled pavement sections had 30% less faulting and fewer corner cracks as compared with undoweled sections [Kumara, Tia, Wu, and Choubane, 2002].

2.2 Analytical Models for Concrete Pavement

2.2.1 Foundation Models for Concrete Pavement

In many engineering applications, the response of the supporting soil medium under the pavement is an important consideration. To accurately evaluate this response, we must know the complete stress-strain characteristics of the foundation. Accurately describing the stress-strain characteristics of any given foundation medium is usually hindered by the complex soil conditions, which are markedly nonlinear, irreversible, and time-dependent. Furthermore, these soils are generally anisotropic and inhomogeneous. Certain assumptions about the soil medium were used for these idealizations. The assumptions are necessary for reducing the analytical rigor of such a complex boundary value problem. Two of the most frequently applied assumptions are linear elasticity and homogeneity.

Winkler foundation model

The Winkler foundation model or dense-liquid foundation model is the foundation that is considered as a bed of evenly spaced, independent, linear springs. The model assumes that each spring deforms in response to the vertical stress applied directly to the spring, and does not transmit any shear stress to the adjacent springs. The stiffness of the springs is represented by the k value as the modulus of subgrade reaction.

No transmission of shear forces means that there are no deflections beyond the edges of the plate or slab. The liquid idealization of this foundation type was derived for its behavioral similarity to a medium using Archimedes' Buoyancy principle. It was applied to analyze pavement support systems in studies [Westergaard, 1926, 1933, 1947].

In the field, the *k*-value for use in analysis can be determined by back calculation from measured deflections of the slab surface obtained from nondestructive tests, using devices such as falling weight deflectometers (FWD).

Boussinesq foundation

The Boussinesq foundation or the elastic-solid foundation model treats the soil as a linearly elastic, isotropic, homogenous material that extends semi-infinitely. It is considered a more realistic model of subgrade behavior than the dense-liquid model, because it takes into account the effect of shear transmission of stresses to adjacent support elements. Consequently, the distribution of displacements is continuous; that is, deflection of a point in the subgrade is due to stress acting at that particular point, and also is also influenced to a lesser extent by stresses at points farther away.

The elastic solid foundation model considers the shear force interaction between different elements in the foundation. Although it presents an improvement over Winkler foundation model by considering the shear forces in the foundation, field tests showed that the solutions were not exact for many foundation materials. It was reported that the surface displacements of foundation soil outside the loaded region decreased faster than the prediction by this model [Foppl and Teubner, 1909].

Modification of Winkler Foundation

The dense liquid and elastic solid foundation models may be considered as two extreme idealizations of actual soil behavior. The dense liquid model assumes complete discontinuity in the subgrade and is better suited for soils with relatively low shear strengths (e.g. natural soils). In contrast, the elastic solid model simulates a perfectly continuous medium and is better suited for soils with high shear strengths (e.g., treated bases). The elastic response of a real soil subgrade lies somewhere between these two extreme foundation models. In real soils, the displacement distribution is not continuous, and neither is it fully discontinuous. The deflection under a load can occur beyond the edge of the slab and it goes to zero at some finite distance. In an attempt to bridge the gap between the dense liquid and elastic solid foundation models, researchers have developed some improved foundation models. Improved foundation models have been developed in either of the following two ways: (a) starting with the Winkler foundation and, in order to bring it closer to reality, some kind of interaction between spring elements may be assumed, or (b) starting with the elastic solid foundation, simplifying assumptions with respect to expected displacements or stresses may be introduced.
A major problem in applying these models, however, has been the lack of guidance in selecting the governing parameters which have limited or no physical meaning.

2.2.2 Finite Element Method for Concrete Pavement

Finite element (FE) techniques have been used to successfully simulate different pavement problems that could not be modeled using the simpler multi-layer elastic theory. Further, it provides a modeling alternative that is well suited for applications involving systems with irregular geometry, unusual boundary conditions or non-homogenous composition. Three different approaches have been used for FE modeling of pavement system: plane-strain (2D), axisymmetric, and three-dimensional (3D) formulation. In the FE method, the level of accuracy

obtained depends upon different factors, including the degree of refinement of the mesh (element dimensions), the order and type of element and location of evaluation.

Various finite element models have been developed for analyzing the behavior of concrete pavement systems. Most of the finite element models use an assemblage of two-dimensional plate bending elements to model behavior of a concrete slab. A plate with medium thickness is thick enough to carry the load by bending action but is thin enough such that the transverse shear deformation can be considered negligible. The subgrade is usually assumed to behave like either a Winkler (dense liquid) or an elastic solid foundation. The Winkler foundation can be modeled by a series of vertical springs at the nodes, which means that the deflection at any point of the foundation surface depends only on the forces at that point and does not depend on the forces or deflections at any other points. The stiffness of the foundation is represented by a spring constant. The use of an elastic solid foundation assumes a homogeneous, elastic and isotropic foundation with a semi-infinite depth. The deflection at any point depends not only on the forces at that point but also on the forces or deflections at other points. The following section briefly describes the basics and applications of a few finite element computer programs.

The FEACONS (Finite Element Analysis of CONcrete Slabs) program was developed by the University of Florida for the analysis of concrete pavement behavior for the Florida department of Transportation. FEACONS program was modified several times to upgrade its capabilities. The latest version, FEACONS IV program can be used for analysis of plain jointed concrete pavements subjected to load and temperature differential effects. In the FEACONS program, a concrete slab is modeled as an assemblage of rectangular plate bending elements with three degrees of freedom at each node. The three independent displacements at each node are (1) lateral deflection, w, (2) rotation about the x-axis, θ_x, and (3) rotation about the y-axis, θ_y. The

corresponding forces at each node are (1) the downward force, f_w , (2) the moment in the x direction, $f_{\theta x}$, and (3) the moment in the y direction, $f_{\theta y}$. The FEACONS IV program has the option of modeling a composite slab made up of a concrete layer bonded to another layer of a different material. The subgrade is modeled as a liquid or Winkler foundation which is modeled by a series of vertical springs at the nodes. A spring stiffness of zero is used when a gap exists between the slab and the springs due to subgrade voids. Either a linear or nonlinear load-deformation relationship for the springs can be specified [Tia et al, 1989].

Load transfers across the joints between two adjoining slabs are modeled by shear (or linear) and torsional springs connecting the slabs at the nodes of the elements along the joint. Looseness of the dowel bars is modeled by a specified slip distance, such that shear and moment stiffnesses become fully effective only when the slip distance is overcome. Frictional effects at the edges are modeled by shear springs at the nodes along the edges [Tia et al, 1989].

The JSLAB program [Tayabji and Colley, 1981]: The pavement slab, the base or subbase layer and the overlay are modeled as rectangular plate bending elements based on the classical theory of thin plates with small deflections. These layers can be bonded or unbonded. The subgrade is modeled as a Winkler foundation represented by vertical springs. The effect of temperature gradient in the concrete slab is incorporated. The temperature is assumed to vary linearly along the slab depth. The subgrade stiffness is set to be zero at the locations where loss of support occurs.

Dowel bar at the joints are modeled as bar elements with the ability to transfer both moment and shear forces across the joints. The effects of looseness of dowel bars can also be considered. Aggregate interlock and keyway are modeled by spring elements transferring shear forces only.

In the WESLIQUID and WESLAYER programs, the modeling of a slab is also based on the classical theory of a thin plate with small deflections. The slab is modeled as an assemblage of rectangular plate bending elements with three degrees of freedom at each node in both programs. The difference between these two models is that the WESLIQUID model considers the sublayers as a Winkler foundation, while the WESLAYER model uses an elastic layered foundation. The Winkler foundation is modeled by a series of vertical springs. For the elastic foundation, the Boussinesq's solution is used to compute the deflections at subgrade surface for the case of a homogeneous elastic foundation and the Burmister's equations are used to compute those for the case of a layered elastic foundation.

The two programs are able to take into account the effects of loss of support from the sublayer to the pavement slab. The loss of support can be due to linear temperature gradient in the slab or due to voids in the sublayer.

Load is transferred across a joint by both shear forces and moment transfer. Shear forces are transferred either by dowel bars, key joint or aggregate interlock. The two models have three options for specifying shear transfer and one for moment transfer. The three methods of determining shear transfer are (1) efficiency of shear transfer, (2) spring constant and (3) diameter and spacing of dowels. Moment transfer across joints or cracks is specified by the efficiency of moment transfer which is defined as a fraction of the full moment.

In *KENSLAB* [Huang, 1993], the slab treated in this model is composed of two bonded or unbonded layers with uniform thickness. The two layers can be either a high modulus asphalt layer on top of a concrete slab, or a cement-treated base. Rectangular thin-plate elements with three degrees of freedom per node (a vertical deflection and two rotations) are used to represent the slab. Load transfer through doweled joint or aggregate interlock can be considered in this

model. Three types of foundation are included in this model, namely the Winkler foundation, the semi-infinite elastic solid foundation and layered elastic solid foundation. Three contact conditions between slab and foundation can be considered: full contact, partial contact without initial gaps, and partial contact with initial gaps. Load transfer effects can be considered in analyzing the pavement slab system.

ILLI SLAB program [Tabatabaie and Barenberg, 1978] can be used to analyze a jointed or continuously-reinforced concrete pavement with a base or subbase, and with or without an overlay, which can be either fully bonded or un-bonded to the concrete slab. A concrete slab is modeled as an assemblage of rectangular plate bending elements with three degree of freedom at each node. When a base or subbase layer and/or an overlay are used, they are also modeled as assemblages of plate bending elements. If there is no bond between the layers, the overall stiffness matrix for the multiple layers is obtained by simply adding up the stiffness matrices of the concrete slab, the base or subbase and the overlay. For the case of perfect bond between layers, full strain compatibility at the interface is assumed. Thus, an equivalent layer can be obtained based on a transformed-section concept.

Load transfer across the joints is modeled in various ways depending on the transfer devices used. Dowel bars are modeled as bar elements with two degrees of freedom at each node. The two displacement components are a vertical displacement and a rotation about a horizontal transverse axis. The bar element is capable of transferring both a vertical shear force and a moment. If the loads are transferred across a joint only by means of aggregate interlock or keyway, they are modeled by vertical spring elements with one degree of freedom at each node. Only vertical forces are transferred across the joint by the spring element. The moment transfer can be neglected for such a joint.

2.3 Maturity Method in Concrete Pavement

The concept of concrete maturity was first introduced by Saul in 1951. He defined "maturity of concrete" as "its age multiplied by the average temperature above freezing that it has maintained." Based on this definition, he further developed the law for relationship between concrete strength and maturity: "Concrete of the same mixture at the same maturity (measured as temperature-time) has approximately the same strength whatever combination of temperature and time goes to make up that maturity." Since then, many studies on maturity have been done by other researchers and Saul's law for maturity has been confirmed and proven to be a useful tool to predict concrete strength. The Maturity method has been standardized by ASTM as Standard Practice C1074.

Strength Measurements Using Maturity for Portland Cement Concrete Pavement Construction at Airfields [Rasmussen, 2003]: The objective of this project was to demonstrate a non-complex solution for monitoring concrete strengths in real time using concrete maturity technology. The project team evaluated a number of commercially available maturity measurement devices coupled with an innovative strength assessment and prediction system, termed Total Environmental Management for Paving (TEMP).

This project included a field evaluation of a concrete pavement placement at Des Moines International Airport (DSM). The research team evaluated the following maturity measuring devices: 1) T-Type Thermocouple, 2) Dallas Semiconductor Thermocron iButton®, 3) Nomadics Construction Labs intelliRock™ Maturity, Temperature, and prototype Strength Loggers, and 4) Identec Solutions i-Q Tags. As a result of this field evaluation, it has been concluded that current maturity technology can be used successfully to assess the strength of a concrete airfield pavement in real-time. Furthermore, it is believed that the adoption of maturity-based

technologies can result in expedited airfield repair and construction, and an improved knowledge of the behavior of concrete pavements at early age.

Using Maturity Testing for Airfield Concrete Pavement Construction and Repair [Trost et al, 2006]: The primary benefits include: better decision-making, reduced runway and taxiway closure times, faster construction, fewer beam specimens, and improved concrete quality control. Concrete maturity enables better decision-making with respect to open-to-traffic decisions. This occurs because concrete maturity enables real-time, in-place flexural strength measurements that are more accurate and more cost-effective than field-cast beam specimens. The improved open-to-traffic decision-making applies not only to aircraft traffic but also to construction-vehicle traffic.

Concrete maturity results in shorter runway and taxiway closures as a direct result of the improved open-to-traffic decision-making. Rather than having to wait for field-cast beam specimens to reach the required strength (and the guesswork associated with when to break them), the pavement can be opened to traffic at the earliest possible moment because the in-place flexural strength can be obtained instantaneously.

Faster construction also directly results from the improved open-to-traffic decision making. This is due to the benefits of allowing staged open-to-traffic criteria rather than the standard "14-day or 550-psi" requirements. With staged open-to-traffic, the pavement can be monitored in real-time until the required flexural-strength threshold is reached for each major type of construction equipment. As such, lighter vehicles can be allowed on the pavement soon after placement, with heavier equipment being allowed somewhat later, but typically much sooner than the wait period based on conventional methods.

Concrete maturity testing can result in fewer beam specimens required on a project, particularly the number of field-cast beams. This is because a single maturity sensor can provide an infinite number of in-place flexural strength measurements at a given location.

As such, multiple sets of beams to support open-to-traffic decisions are no longer required. In addition, alternative methods of field verification, such as splitting tensile, direct tension, or compressive strength testing can be used to further reduce the need for field-cast beams.

With respect to quality, the concrete maturity method, when used as a mix-verification tool, provides the framework for an extremely effective and robust concrete quality control plan that can result in improved concrete quality control. This benefit is the direct result of the mix-specific nature of the method. The strength-maturity relationship for a given concrete mix is unique to that mix design. As such, the maturity method is extremely sensitive to any changes that affect the rate of strength gain or the ultimate strength of the concrete mix, such as the quality or proportioning of the raw materials. This sensitivity enables a maturity-based quality control plan to catch mix-related or batching-related errors in a matter of days or even hours rather than weeks.

To summarize the benefits, concrete maturity empowers the field engineer and the contractor to make critical decisions based on the actual in-place strength of the pavement using real-time measurements that take into account the physical properties, dimensions, and curing conditions of the pavement structure.

Implementation of Concrete Maturity Meters [Luke et al, 2002]: The major intent of this study was to explain how the maturity method can be used to estimate the strength of in-place concrete for highway construction. NJIT started studying the maturity method for NJDOT in 1995 to verify the strength of very early strength concrete patches. Since then, several other

studies on the maturity method have been conducted for NJDOT. Collectively, these studies presented a convincing case for utilizing the maturity method to predict the strength of early age concrete in highway structures. The purpose of this project was to move the method from an experimental to a practical setting.

Manual for the Maturity Method," describes the instrumentation and methods for making temperature measurements, performing maturity computations and predicting concrete strength. The procedures manual is based on ASTM C 1074 "Standard Practice for Estimating Concrete Strength by the Maturity Method." Nine important modifications of ASTM C 1074 were made in order to practically implement the maturity method on NJDOT projects.

Three innovations were presented among these modifications. The first is the requirement that the strength-maturity relationship be verified. For strength critical applications, companion cylinders are cast and match cured along with the structure. When the strength-maturity relationship was able to reasonably predict the strength of those cylinders at three different early ages, the relationship is considered validated and can be applied to the structure. The second innovation is that the results of verification testing should be added to the data set from which the predictions are made and then the predictive equation is recomputed. By this procedure, confidence in the prediction grows as more test results become available. The third innovation is a method for starting a quality assurance program with no prior laboratory testing. An assumed prediction is checked and refined through the verification process.

The field trials also revealed that elevated curing temperatures, approaching that of mass concrete, frequently occur in highway structures. The reason is thought to be the increased use of more active cements at higher cement factors and lower water-cement ratios. Such behavior can occur where it is least expected, like on bridge decks, which have large surface to volume ratios

that should readily dissipate heat. Temperature monitoring is useful for identifying these situations and avoiding the detrimental effects of high temperatures on concrete durability.

During the course of this study, field trials using the maturity method were held in all three NJDOT regions. These trials revealed two significant findings. First, it was found that current winter concreting procedures may overheat concrete pours, creating high temperature conditions that exceed even the worst of summer concreting operations. The second finding has to do with the effects of a typical chloride inhibitor on the temperature behavior of concrete. It was found that calcium nitrite modified the rapid temperature rise normally associated with the early strength gain of concrete. Chloride inhibited mixes followed ambient temperature changes quite closely, with positive effects on the rate of strength gain and the ultimate strength.

Current Field Application

Because of its simplicity and low cost, the application of the maturity concept has received wide attention as a prospective in-situ testing method for concrete pavements. For example, in a survey reported by Tikalsky et al., 32 states reported conducting research on the use of the maturity method. However, at that time, 29 states did not have any protocol, and only four states reported the use of maturity to determine pavement opening times. Although this scenario was rapidly evolving at the time of the survey, it clearly shows that the application of maturity for concrete pavements is indeed very new and a topic of great interest across the country. The application to flexural strength was not identified in the survey, and California may be the first state to consider this extension of the maturity concept [Tikalsky et al, 2001].

For the past decade, the Federal Highway Administration has been encouraging state DOTs to evaluate the maturity method and to refine procedures for its application. Among the advantages of the maturity method over the traditional concrete strength tests that justify the

growing interest in the method, one could cite 1) the maturity method allows contractors to determine the precise times at which a specified strength is achieved, and 2) the maturity method provides results that could represent the in-situ strength [Mancio et al, 2004].

Indeed, maturity is a very well established and standardized method, being described by both ASTM 1074-98 (Standard Practice for Estimating Concrete Strength by the Maturity Method) and AASHTO TP 52-95 (Estimating the Strength of Concrete in Transportation Construction by Maturity Tests) standards. However, as discussed previously, the maturity concept was developed based on the determination of compressive strength of conventional concretes made with Type I/II cements with no chemical or mineral admixtures. Recent advances in concrete technology make the material today different from that of fifty years ago [Mancio et al, 2004].

The strength-maturity correlation has been generally developed for concrete cylinders tested under uniaxial compressive strength, because this is usually the most important strength index for conventional structures. In pavements, where concrete is submitted to bending stresses, flexural strength is the preferred measure for quality control. The indirect correlation between the concrete maturity and flexural strength has been seen practiced in the field. In some cases, the laboratory established compressive strength versus maturity curve has been used to predict the compressive strength, from which the flexural strength in the field is derived by correlating the compressive (F'_c) and flexural (MR) strength in the lab. However, this relation (F'_c *to* MR) may have large variability, and changes significantly depending on the mix, age, and other variables [Zhang et al, 2004].

2.4 Verification of Analytical Results with Measured Results

The following section presents some current research in concrete pavement focusing on instrumentation and strain measurement and verification of analytical results with measured results.

Accelerated Testing for Studying Pavement Design and Performance [Melhem et al, 2003]: This study presented an instrumentation plan on placing soil pressure cells below the aggregate base, which were used to determine the vertical pressure in the subgrade, and to monitor its variation due to the deterioration of the overlay or the rubblized base. Thermocouples were placed below, in, and on top of the overlay slabs to monitor the slab temperature and see if there is a correlation between overlay slab temperature and stress/curling of the slabs. Strain gauges were installed in the overlay to monitor the deterioration of the overlay slab and to determine a correlation between the slab movement due to loading and temperature. Linear Variable Displacement Transformers (LVDT's) were used to measure horizontal joint movements. The report also showed that stress and strain measurements were taken at the start of the test and at 20,000 repetition intervals until the end of the test. The vertical stress data were compared with the number of ATL passes.

All gauges used in this experiment were positioned to measure longitudinal strains at the bottom of the PCC overlays. Some tensile and compressive strains (in microstrain) measured were reported, while the remaining gauges did not give any useful strain readings. Similar to the trend observed for vertical compressive stresses in the subgrade, the measured strains at the bottom of the overlay did not show a continuous increase; the general trend is that the strains increase with the number of applied ATL passes. Therefore, from the strain data alone, it was difficult to determine which overlay gave the best performance.

Early-Age Behavior of Jointed Plain Concrete Pavement Systems [Turan et al, 2005]: This paper mainly focuses on the early-age behavior of concrete pavement systems under varying temperature and moisture gradients upon construction. In an effort to better understand the early-age behavior of the jointed plain concrete pavements under varying environmental conditions, a field study was conducted on instrumented portland cement concrete slabs in Platteville, Wisconsin. The study involved on-site measurements, extensive laboratory testing, and analyses of the concrete pavement systems under temperature and moisture profiles using finite element methodology-based analytical tools. The aim of the study was to summarize the laboratory test results for concrete samples and the analysis of the early-age slab deflection data captured with linear variable displacement transducers (LVDTs). In the analytical modeling of the slabs, the ISLAB2000 finite element model was used. Based on the large number of comprehensive finite element analyses, a good match has been observed with the analytical solutions and field measurements, thus capturing the early-age behavior of concrete pavement systems under temperature and moisture profiles. Comparison between the predicted FEM results and the measured results showed that the FEM estimated the shape of the curves reasonably well.

The Effect of Early Opening to Traffic on Fatigue Life of Concrete Pavement [Suh, 2005]: Concrete pavements are subjected to many traffic-load repetitions prior to achievement of their full design strength. The effect of early opening to traffic on the life of Portland cement concrete pavement systems was evaluated using experiments and mathematical model. To quantify the loss of life due to early opening of a rigid pavement system, an appropriate fatigue equation is required. A series of laboratory fatigue tests were performed on simply supported beams to develop appropriate fatigue relationships for typical, normal strength Texas paving

concrete mixture designs. After completion of the laboratory testing, accelerated fatigue tests on full-scale concrete slabs were performed under constant cyclic loading. Six full-scale rigid pavement slabs were constructed and tested under constant cyclic loading for fatigue. During fatigue loading, cracks began at the loading points and propagated along the bottom of the slab centerline, which was the maximum stress path. Vertical crack propagation at the edge and stress redistribution occurred as part of the slab's fatigue life. The concept of equivalent fatigue life was applied to correct the effect of the different stress ratio between the field and the laboratory testing. The laboratory beams and full-scale field slabs showed an almost identical *S*-*N* relationship after the correction for the variance of stress ratio.

CHAPTER 3
MATERIALS AND TEST METHODS

3.1 Introduction

Three laboratory-prepared mixes and five concrete mixes from test slabs were tested and evaluated in this research. This chapter describes the mix proportions and ingredients of the concrete mixes, fabrication and curing condition of concrete specimens, tests on fresh and hardened concretes as well as a procedure to calibrate maturity curves of concrete used in this study.

3.2 Concrete Mixes Evaluated

3.2.1 Mix Proportion of Concrete

The first target concrete mix in this study was a typical mix design used for slab replacement in Florida and has a cement content of 850 lb per yd^3. This concrete mix was used as a target mix to evaluate performance of the first two test slabs.

Another target concrete mix had a cement content of 725 lb per yd^3, while keeping the same water cement ratio and other mix ingredients. The second target concrete mix was used to evaluate performance of the last three test slabs.

The concrete used in each test slab was obtained and tested for its properties. The same concrete mixes were also prepared in the laboratory and used in the calibration of the concrete maturity before placement of the test slabs.

Table 3-1 shows the mix design details for the actual concrete mixes used in Test Slabs 1 and 2. Table 3-2 shows the mix design details for Test Slabs 3, 4 and 5.

Table 3-1. Mix design of the concrete mix used in Slabs 1 and 2.

Material	Target (/yd^3)	Actual Slab 1 (/yd^3)	Actual Slab 2 (/yd^3)
Cement	850 lb	842 lb	822 lb
Stone # 08-012	1650 lb	1670 lb	1722 lb
DOT Sand # 76-349	991 lb	1040 lb	1069 lb
Coarse aggregate moisture	-	28.4 lb	22.4 lb
Fine aggregate moisture	-	46.8 lb	42.8 lb
Air-entraining admixture (Darex)	1 oz (0.065 lb)	0.0625 lb	0.0625 lb
Superplasticizer (Adva-540)	50 oz (3.26 lb)	2.125 lb	4.017 lb
Accelerator (Daraccel)	384 oz (25 lb)	25.04 lb	25.04 lb
Water	283 lb	185 lb	195 lb
W/C	0.364	0.341	0.351
Theoretical unit weight	140 pcf (2% Air)	139 pcf (3% Air)	142.1 pcf (2% Air)

Table 3-2. Mix design of the concrete mix used in Slabs 3, 4 and 5.

Material	Target (/yd^3)	Actual Slab 3 (/yd^3)	Actual Slab 4 (/yd^3)	Actual Slab 5 (/yd^3)
Cement	725 lb	729.4 lb	705.0 lb	715.8 lb
Stone # 08-012	1650 lb	1675.6 lb	1676.6 lb	1681.8 lb
DOT Sand # 76-349	1215 lb	1268.8 lb	1187.1 lb	1190.5 lb
Coarse aggregate moisture	-	25.1 lb	30.7 lb	36.1 lb
Fine aggregate moisture	-	53.3 lb	45.5 lb	52.1 lb
Air-entraining admixture (Darex)	1 oz (0.065 lb)	0.0652 lb	0.0719 lb	0.0723 lb
Superplasticizer (Adva-540)	50 oz (3.26 lb)	3.26 lb	3.60 lb	3.22 lb
Accelerator (Daraccel)	384 oz (25 lb)	25.03 lb	24.55 lb	24.69 lb
Water	236 lb	153.33 lb	150.40 lb	148.89 lb
W/C	0.365	0.357	0.362	0.370
Theoretical unit weight	143.1 pcf (2% air)	142.9 pcf (2.25% air)	139.0 pcf (3.0% air)	139.5 pcf (2.0% air)

3.2.2 Mix Ingredients

The mix ingredients used in producing the concrete mixture both in the laboratory and from concrete plant are the same and described as follows:

Water

Potable water from the local city water supply system was used as mixing water for production of the concrete mixtures. The water temperature was around 64^{o}F

Cement

Type-I/II Portland cement from Florida Rock Industry was used. The physical and chemical properties of the cement analyzed by Florida State Materials Office are shown in Tables 3-3 and 3-4

Table 3-3. Physical properties of the Type I/II cement.

Tests	Specification	Cement	Specification Limits
Loss on Ignition	ASTM C114	0.30%	<= 3.0
Autoclave Expansion	ASTM C151	0.04%	<= 0.80
Time of Setting (Initial)	ASTM C266	190 min.	>= 60
Time of Setting (Final)	ASTM C266	290 min.	<= 600
3-Day Compressive Strength	ASTM C109	2,723 psi	>=1,450
7-Day Compressive Strength	ASTM C109	4,770 psi	>= 2,470

Table 3-4. Chemical properties of the Type I/II cement.

Constituents	Percent
Silicon Dioxide	20.50%
Aluminum Oxide	5.20%
Ferric Oxide	3.80%
Magnesium Oxide	0.60%
Sulfur Trioxide	2.80%
Tricalcium Aluminate	7%
Tricalcium Silicate	54%
Total Alkali as Na_2O	0.25%

Fine Aggregate

Fine aggregate used was silica sand from Goldhead of Florida, mine# 76-349. The physical properties of the fine aggregate analyzed by Florida State Materials Office are shown in Table 3-5. The gradation of the fine aggregate is shown in Figure 3-1. The fine aggregate was oven-dried before it was mixed with the other mix ingredients in the production of the concrete mixtures.

Table 3-5. Physical properties of the fine aggregate.

Fineness Modulus	2.2
SSD Specific Gravity	2.640
Apparent Specific Gravity	2.651
Bulk Specific Gravity	2.634
Absorption	0.20%

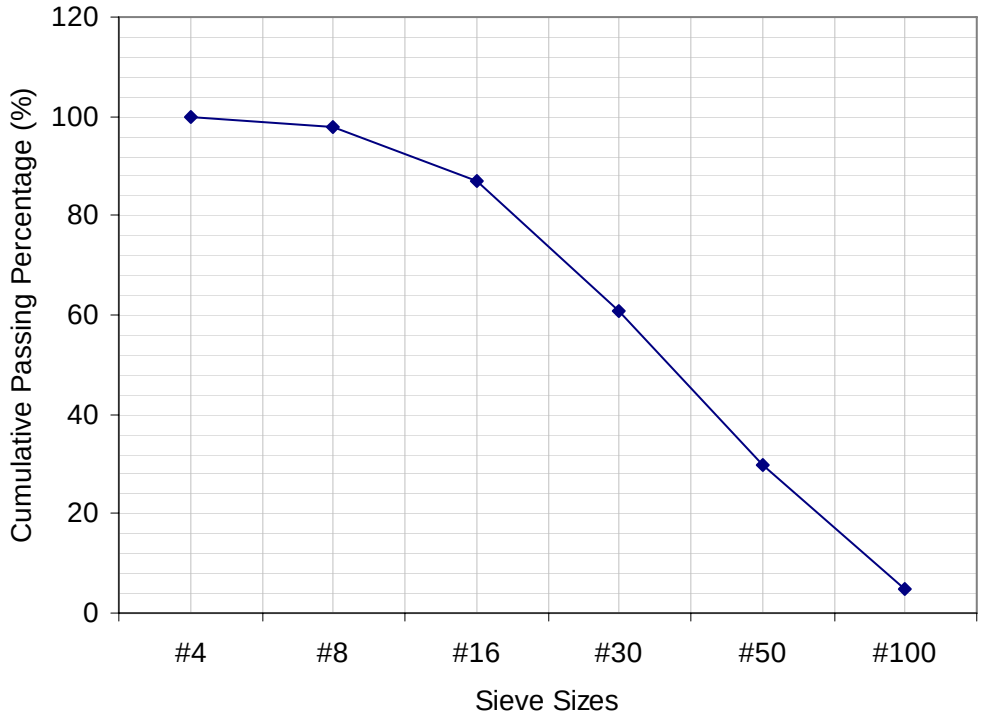

Figure 3-1. Gradation of fine aggregate (Goldhead silica sand#76349).

Coarse aggregate

The coarse aggregate used was a #57 limestone obtained from mine# 08-012. The physical properties of the fine aggregate analyzed by Florida State Materials Office are shown in Table 3-6. The gradation of the fine aggregate is shown in Figure 3-2. In order to have the coarse aggregate moisture content in well-controlled, saturated-surface-dry coarse aggregate was used to produce concrete. So, the coarse aggregates were soaked in water for at least 48 hours and then drained off the free water on the surface of aggregate before they were mixed with the other mix ingredients in the production of the concrete mixtures.

Table 3-6. Physical properties of the fine aggregate.

SSD Specific Gravity	2.384
Apparent Specific Gravity	2.546
Bulk Specific Gravity	2.280
Absorption	5.47%

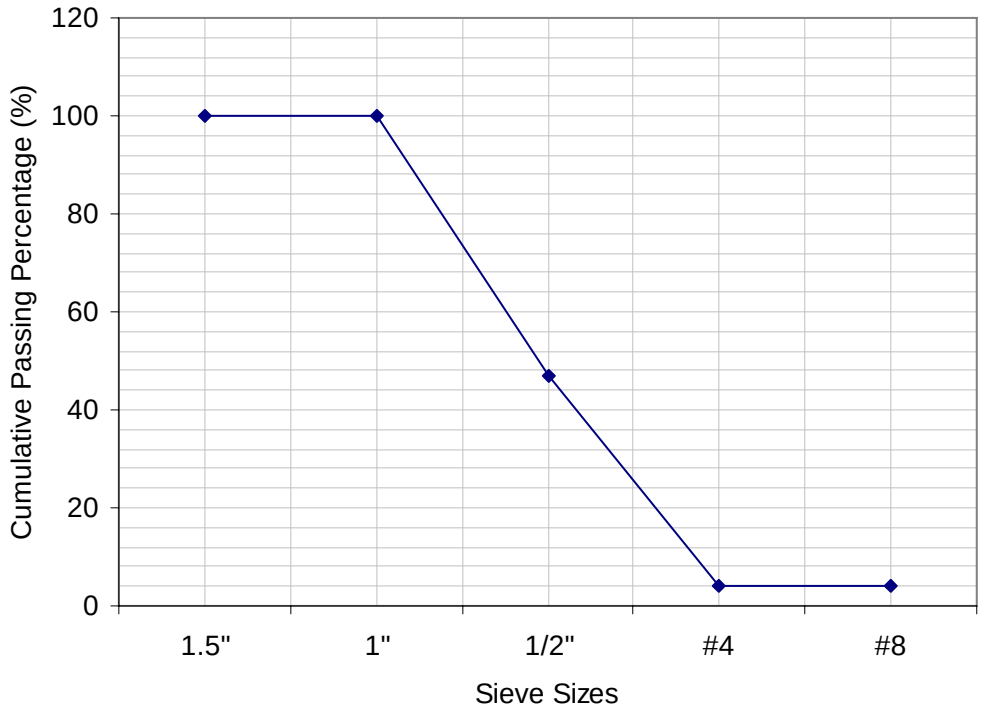

Figure 3-2. Gradation of the coarse aggregate (Limestone #08012).

Air-Entraining Admixture

The air-entraining admixture used was a liquid admixture Darex AEA from W.R. Grace & Co. It also contains a catalyst for more rapid and complete hydration of Portland cement. In this study, Darex AEA was mixed with the water used in the production of the concrete mixtures before adding the water to other ingredients.

Superplasticizer

The superplasticizer used in this study is ADVA Cast 540 from W.R. Grace & Co. ADVA Cast 540 is high efficiency polycarboxylate based superplasticizer. It has been formulated to impart extreme workability without segregation to concrete, and to achieve high early compressive strength as required by the precast industry. The ADVA is optimized for the production of Self Consolidating Concrete (SCC) in precast applications. It was recommended that dosage rate can normally range from 325 to 1300 mL/100 kg (5 to 20 fl oz/100 lbs) of cementitious material.

Accelerating Admixture

The accelerator used is Daracel from W.R. Grace & Co. Daraccel® is a liquid admixture formulated to provide faster set acceleration and increased early strength development of concrete. It contains calcium chloride as well as other chemicals to enhance the effect of the calcium chloride. Daraccel is specifically designed for use in cold weather concreting or whenever accelerated properties of concrete are desired. Daraccel is a water-reducing accelerator formulated to comply with the requirements of ASTM C 494 as a Type E admixture with a Type I or Type II cement. The resulting reduction in water requirement, shorter setting time, and higher early strengths permit earlier finishing and earlier form removal with significant job economies. Daraccel is used at an addition rate of 520 to 2600 mL/100 kg (8 to 40 fl oz/100 lb)

of cement. The amount used will depend upon the setting time of the non-admixtured concrete and the temperature at placement.

3.3 Fabrication and Curing Condition of Concrete Specimen

Two conditions of producing concrete mixes in this study are 1) laboratory-prepared mixes and 2) plant-prepared mixes used in test slabs.

The laboratory-prepared concrete mixtures were produced in the laboratory using compulsive pan mixer with capacity of 17 cubic feet, as shown in Figure 3-3. Concrete used to construct each test slab was also obtained from the truck to fabricate concrete specimens, as also shown in Figure 3-3. For each concrete mix, about nine cubic feet of fresh concrete was produced or obtained to fabricate forty four cylinders (4" x 8"), eleven beams (6" x 6" x 20") and three square prism specimens (3" x 3" x 11.25"). Table 3-7 shows a list of concrete samples obtained to perform tests for each mix in this research.

Table 3-7. Concrete samples obtained to perform tests.

Test	Specimen Size	#	Testing Times
Compressive/ Elastic Modulus	4"x8" cylinder	21	At 4 hr, 6 hr, 8hr, 1, 7 and 28 days, and start of HVS loading
Temperature	4"x8" cylinder	2	Every 30 minutes for 48 hour, then every hour
Splitting Tensile	4"x8" cylinder	12	At 6 hr, 1, 7 and 28 days
Coefficient of Thermal Expansion	4"x8" cylinder	9	At 1, 7 and 28 days
Flexural + Temperature	6"x6"x20" beam	10+1	At 4, 6 hours, 1 and 28 days, and start if HVS loading
ASTM C157	3"x3"x 11.25" square prism	3	At 6, 8 hours, 1, 7 and 28 days

A


B

Figure 3-3. Mixer used for this study. A) Concrete mixer used in the laboratory. B) Concrete truck.

3.3.1 Laboratory-Prepared Mixes

The procedures to fabricate the specimens in the laboratory were presented as follows:

- Based on mix proportion design, measure out the coarse aggregate, fine aggregate, cement, admixtures, water, air-entraining agent, superplasticizer and accelerating admixture.
- Place coarse aggregate and fine aggregate into the pan mixer to mix about 30 seconds.
- Place two thirds of the water together with the air-entraining admixture into the mixer and mix for 1 minute.
- Place cement and mix for 3 minutes, followed by a 2-minute rest, then followed by 3-minute mixing.
- Add the superplasticizer and mix for 3 minutes, followed by a 2-minute rest.
- Perform a slump test (ASTM C143) and other fresh concrete properties which will be presented in Section 3.4.
- Add the accelerating admixture and mix for 2 minutes.

- Measure fresh concrete properties again, while at the same time, start filling each mold.
- For cylinder and square prism molds, after filling each mold to half of it height, place the mold on the vibrating table for 45 seconds. Then fill the mold and vibrate again for 45 seconds. Finish the surface of the samples.
- For beam molds, after filling each beam mold to half of it height, place the vibrating stick to the concrete for 45 seconds. Then fill the mold and vibrate again for 45 seconds. Finish the surface of the samples.
- For maturity calibration, put the thermocouples into two cylinders and one beam to monitor the hydration temperature, and start obtaining the temperature and time every 30 minutes for 48 hours, then every 1 hour after that.
- For the early strength concrete used in the study, allow the concrete to be cured in the cylinder molds for about 3 to 4 hours before demolding to perform the first test.
- For cylinder and beam specimens, set the demolded concrete specimens in the standard moist curing room for the specified curing time before testing.

3.3.2 Plant-Prepared Concrete Mixes Used in Test Slabs

The procedures to fabricate the specimens of concrete used in each slab obtained from the truck were presented as follows:

- Based on the target mix design, the contractor mixes the concrete with all the concrete ingredients except adding accelerating admixture.
- When truck arrives at the test section, perform a slump test (ASTM C143) and other fresh concrete tests which will be presented in Section 3.4.
- Add the accelerating admixture and mix for 2 minutes.
- Perform fresh concrete tests again, while at the same time start filling each mold.
- For cylinder and square prism molds, after filling each cylinder mold to half of it height, place the mold on the vibrating table for 45 seconds. Then fill the mold and vibrate again for 45 seconds. Finish the surface of the samples.
- For beam molds, after filling each beam mold to half of it height, place the vibrating stick to the concrete for 45 seconds. Then fill the mold and vibrate again for 45 seconds. Finish the surface of the samples.

- For maturity calibration, put the thermocouple into two cylinder molds and one beam to monitor the hydration temperature, and start obtaining the temperature and time, every 30 minutes for 48 hours, then every 1 hour after that.

- For the early strength concrete used in the study, allow the concrete to be cured in the cylinder molds for about 3 to 4 hours before demolding to perform the first test.

- For cylinder and beam specimens, set the demolded concrete specimens in the standard moist curing room for the specified curing time before testing.

- Two beam and three cylinder molds are placed aside to the test slab to cure under the same condition with the test slab. This set of samples are to be tested at the starting time of HVS loading.

Figure 3-4 shows some photos of the concrete specimens fabricated and cured in this study.


A

B

C

D

E

F

Figure 3-4. Concrete specimens fabricated and cured. A) Molds for concrete specimens. B) Using vibrating table to consolidate cylinder samples. C) Using internal vibrators to consolidate beam samples. D) and E) Samples allowed to be cured in the molds for about 3 to 4 hours before demolding to perform the first test. F) Demolded samples in the standard moist room.

3.4 Tests on Fresh Concrete

ASTM standard tests as listed in Table 3-8 were performed on the fresh concrete used in this study to determine and control the quality of each concrete mix before and after adding the accelerating admixture. The properties of the fresh concrete for each of the five concrete mixes obtained from the test slabs are presented in Tables 3-9 and 3-10.

Slump Test

Slump test was run in accordance with ASTM C143. It was used to measure the consistency of concrete. A high slump value is indicative of a wet or fluidic concrete. The test should be started within 5 minutes after the sample has been obtained and the test should be completed within 2 and half minutes, as concrete loses slump with time.

Air Content Test

Air Content test was run in accordance with ASTM C173. It was used to measure the air content of freshly mixed concrete. The test should also be started within 5 minutes after the sample has been obtained.

Temperature Test

Temperature test was run in accordance with ASTM C1064. It was used to measure the temperature of fleshly mixed concrete. The result of the test was used to check whether it was within the normal range. The test should be finished within 5 minutes after obtaining the sample. The result should be reported to the nearest 1 ˚F or 0.5 ˚C.

Unit Weight

The procedures of ASTM C138 standard was followed in running the unit weight test. This test was carried out to verify the density of concrete mixtures for quality control.

Table 3-8. Testing program on fresh concretes.

Test	Test Standard
Slump	ASTM C143
Air Content	ASTM C173
Temperature	ASTM C1064
Unit Weight	ASTM C138

Table 3-9. Properties of fresh concrete used in Slabs 1 and 2.

Fresh concrete properties	Slab 1		Slab 2	
Adding the accelerating admixture	Before	After	Before	After
Slump	2.75"	3.00"	3.75"	4.25"
Temperature	92 °F	95 °F	95 °F	98 °F
Air Entrainment	1.75%	3.00%	1.75%	2.00%
Unit Weight (pcf)	142	142	-	141
Theoretical Unit Weight (pcf)	-	139	-	142

Table 3-10. Properties of fresh concrete used in Slabs 3, 4 and 5.

Fresh concrete properties	Slab 3		Slab 4		Slab 5	
Adding the accelerating admixture	Before	After	Before	After	Before	After
Slump	6.25"	8.00"	9.50"	8.50"	8.00"	4.25"
Temperature	83 °F	84 °F	98 °F	98 °F	100 °F	100 °F
Air Entrainment	2.00%	2.25%	3.00%	3.00%	2.00%	2.00%
Unit Weight (pcf)	141.6	139.8	144	143	142	140
Theoretical Unit Weight (pcf)	144.4	143.1	139	139	139.6	139.5

3.5 Tests on Hardened Concrete

ASTM and AASHTO standard tests on the hardened concrete specimens are given in Table 3-11. The detailed description of these tests is presented as follows:

Table 3-11. Testing program on hardened concrete.

Test	Test Standard
Compressive Strength	ASTM C39
Flexural Strength	ASTM C78
Splitting Tensile Strength	ASTM C496
Elastic Modulus	ASTM C469
Dry Shrinkage	ASTM C157
Co-efficient Of Thermal Expansion	AASHTO TP60-00

3.5.1 Compressive Strength Test

Compressive strength tests were performed on all concrete mixes investigated in this study. Compressive strength is presently used for quality control of concrete mix in FDOT standard for slab replacement. The tests were performed at 4 hours, 6 hours, 8 hours, 1 day, 7

days and 28 days in accordance with ASTM C39. The tests were performed on three 4"x 8" cylindrical specimens at each age, and the average strength for each curing condition was computed. If a low test result is due to an obviously defective specimen, the low test result would be discarded. Before testing, the two end surfaces of each cylinder were ground evenly by using a grinding stone so that the cylinder would support the applied load uniformly.

The compressive strength of the specimens was calculated using the following equation:

$$f_c = P/A \tag{3-1}$$

Where

f_c -- Compressive strength in pound force per square inch (psi);
P -- Ultimate load attained during the test in pound (lb); and
A -- Loading area in square inch (in^2)

3.5.2 Flexural Strength Test

The flexural strength tests were run at ages of 6 h, 1 day, 7 days and 28 days in accordance with ASTM C78. Two 6" x 6"x 20" beam specimens were tested at each age and the average strength was computed for each curing condition. Before testing, the two loading surfaces of each beam were ground evenly by using a grinding stone to support the applied load uniformly.

The flexural strength was calculated according to the type of fracture in the beam as follows:

1. If the fracture initiates in the tension surface within the middle third of the span length, calculate the modulus of rupture as follows:

$$R = PL/bd^2 \tag{3-2}$$

Where:

R -- Modulus of rupture, psi,
P -- Maximum applied load indicated by the testing machine, lbf,
L -- Span length, in.,
b -- Average depth of specimen, in., at the fracture, and
d -- Average depth of specimen, in., at the fracture.

2. If the fracture occurs in the tension surface outside of the middle third of the span length by not more than 5% of the span length, calculate the modulus of rupture as follows:

$$R=3Pa/bd^2 \quad (3\text{-}3)$$

Where:

a -- Average distance between line of fracture and the nearest support measured on the tension surface of the beam, in.

3. If the fracture occurs in the tension surface outside of the middle third of span length by more than 5% of the span length, discard the results of the test.

3.5.3 Splitting Tensile Strength Test

Splitting tensile strength test is simple to perform. The strength determined from splitting tensile test is believed to be close to the direct tensile strength of concrete.

In this study, the testing procedure of ASTM C496 standard was followed in performing the splitting tensile strength test. A 4" x 8" cylindrical specimen, which is identical to that used for compressive strength test, is placed on its side in a steel frame, which is designed to keep the cylinder in place between the platens of the testing machine. Load is applied to the specimen through two thin strips of ply wood placed on the top and bottom sides of the specimen. The load is increased until failure by indirect tension in the form of splitting along vertical diameter.

The splitting tensile strength of a cylinder specimen can be calculated by the following equation:

$$T_i = \frac{2p_i}{\pi \cdot l \cdot D} \quad (3\text{-}4)$$

Where:

T_i -- Splitting tensile strength of cylinder in psi;
P_i -- Maximum applied load to break cylinder in psi;
l -- Length of cylinder in inch;
D – Diameter of cylinder in inch.

Three replicate specimens were tested at each of the curing times, which were 6 hours, 1 day, 7 days and 28 days. A total of 12 specimens per concrete mixture were tested for splitting tensile strength.

Figure 3-5 shows sample photos of strength tests and typical fracture of specimens in this research.

A

B


C

D

E


F

Figure 3-5. Strength tests and typical fracture of specimens. A) and B) Compressive strength test. C) and D) Flexural strength test. E) and F) Splitting tensile strength test.

3.5.4 Elastic Modulus Test

Modulus of elasticity tests were performed at various curing times in accordance with ASTM C469 standard. In this method, the modulus of elasticity of concrete is determined when a compressive load is applied on a concrete cylinder in the longitudinal direction. Similar to the compressive strength test, the modulus of elasticity test was performed at curing time of 4 hours, 6 hours, 8 hours, 1 day, 7 days and 28 days. Figure 3-6 show the test set-up, which consisted of a compression testing machine, a digital key panel (for controlling the testing machine and retrieving the data from the test). The output from the load cell (in the testing machine) and the output from the LVDT (Linear Variable Differential Transformer) were connected to the testing machine.

Before the elastic modulus test, one of the three 4”x 8” concrete cylinders was broken first to determine the compressive strength of concrete at each curing time in accordance with ASTM C39 standard. Then, 40 % of the ultimate compressive strength of concrete specimen was applied on the other two cylinders to perform the elastic modulus test. The data for the modulus of elasticity test were loaded and unloaded three times. Then, the first load cycle data were discarded. The average value from the last two times was recorded as the elastic modulus of the specimen.

Figure 3-6. Performing a modulus of elasticity test.

3.5.5 Drying Shrinkage Test

Shrinkage testing according to the ASTM C157 standard was performed on square prism specimens with dimensions of 3" x 3" x 11.25". Figure 3-7 shows the specimens and length comparator used in this study.

In order to obtain drying shrinkage at the early age of the concrete specimen in this study, the specimens were removed from the molds at an age of 5 ± ½ h (after the addition of water to cement and accelerator admixture during the mixing operation) and then placed in lime-saturated water, which was maintained at 73.4 ± 1 ºF (23.0 ± 0.5ºC) for a minimum of 30 min. Initial length measurement was made at an age of 6 ± ½ h. The specimens were removed from water storage, and wiped with a damp cloth. An initial reading was immediately taken with a length comparator. The specimens were then allowed to dry at ambient condition in the laboratory. Length measurement on the specimens was taken on hour 8, days 1, 7, and 28.

The length change of a specimen at any age after the initial comparator reading was calculated as follows:

$$\Delta L_x = \frac{Initial\,CRD - FinalCRD}{G} \quad (3\text{-}4)$$

Where:

ΔL_x -- Length change of specimen at any age,

CRD -- Difference between the comparator reading of the specimen and the reference bar,

G -- Gauge length.

A 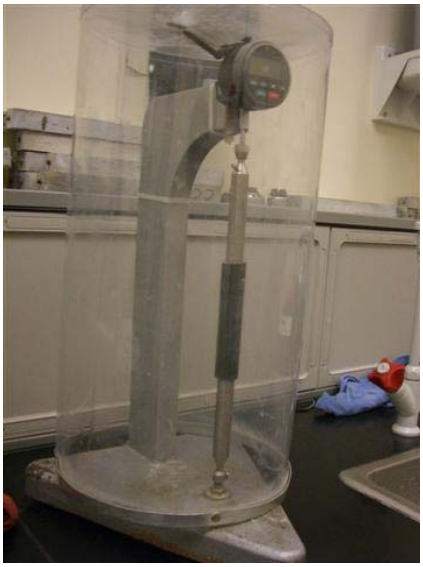 B

Figure 3-7. Drying shrinkage test. A) Square prism specimens for drying shrinkage test. B) Length comparator used in this study.

3.5.6 Coefficient of Thermal Expansion

Coefficient of thermal expansion tests (CTE) were performed in accordance with the AASHTO TP 60-00 Standard. This test method determines the CTE of a cylindrical concrete specimen, maintained in a saturated condition, by measuring the length change of the specimen due to a specified temperature change. The measured length change is corrected for any change in length of the measuring apparatus, and the CTE is then calculated by dividing the corrected

length change by the temperature change and then the specimen length. The CTE of one expansion or contraction test segment of a concrete specimen is calculated as follows:

$$CTE = (\Delta L_a / L_0) / \Delta T \quad (3\text{-}5)$$

Where:

CTE – Coefficient of Thermal Expansion,
ΔL_a -- Actual length change of specimen during temperature change, mm or in.;
L_0 -- Measured length of specimen at room temperature, mm or in.; and
ΔT -- Measured temperature change (average of the four sensors), ºC.

$$\Delta La = \Delta Lm + \Delta Lf \quad (3\text{-}6)$$

Where:

ΔL_a – Measured length change of specimen during temperature change, mm. or in.;
ΔL_m – Length change of the measuring apparatus during temperature change, mm. or in.;

$$\Delta L_f = C_f \, x \, L_o \, x \, \Delta T \quad (3\text{-}7)$$

Where:

C_f – Correction factor accounting for the change in length of the measurement apparatus with temperature, $in.^{-6}/in./^{o}C$.

The test result is the average of the two CTE values obtained from the expansion test segment and contraction test segment, and is calculated as follows:

$$CTE = (CTE_{expan.} + CTE_{cont.}) / 2 \quad (3\text{-}8)$$

In this study, three of 4" x 8" concrete cylinders were evaluated in the CTE test at various curing times such as 1 day, 7 days and 28 days for each concrete mix. The cylinders at each set were sawed to the length of 7.0 ± 0.1 in. and submersed in saturated limewater at 23 ± 2 ^{o}C before testing.

The saturated specimens were removed from the tank and measured of their lengths at room temperature to the nearest 0.004 in. After measuring the length, place the specimens in the measuring apparatus located in the controlled temperature bath. The lower end of the specimen is firmly seated against the support buttons, and the LVDT tip is seated against the upper end of the specimen.

The water in the bath was initially set to 10 ± 1 ^{o}C. When the bath reaches this temperature, allow the bath to remain at this temperature until thermal equilibrium of the specimens has been reached, as indicated by consistent readings of the LVDT to the nearest 0.00001 in. taken every 10 minutes over a one-half hour time period. Then the water temperature was set to 50 ± 1 ^{o}C to get the second value of the LVDT reading. Then, set the water temperature again to 10 ± 1 ^{o}C to get the final reading.

An average of CTE values from three specimens was represented the CTE measurement in each curing time of concrete mix.

Figure 3-8 shows the test set-up for Coefficient of Thermal Expansion measurement

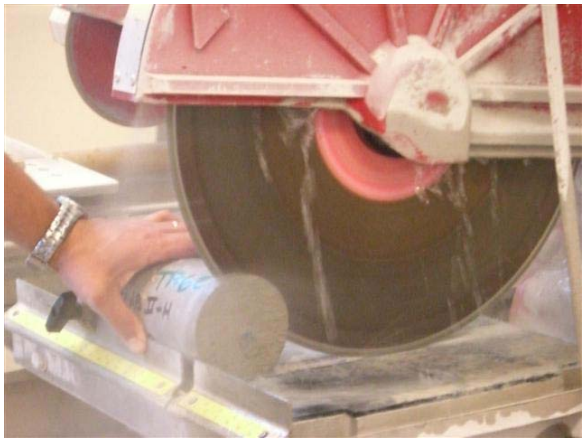
A


B

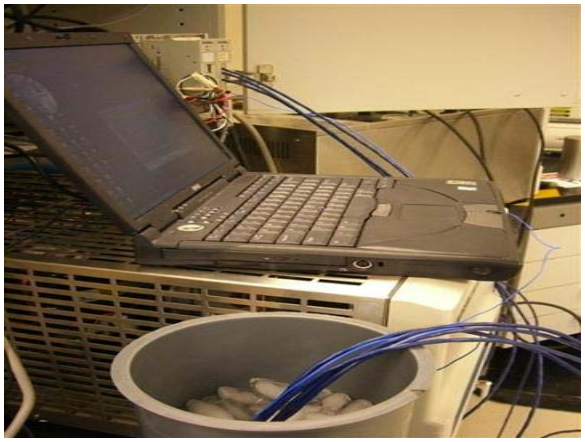
C


D

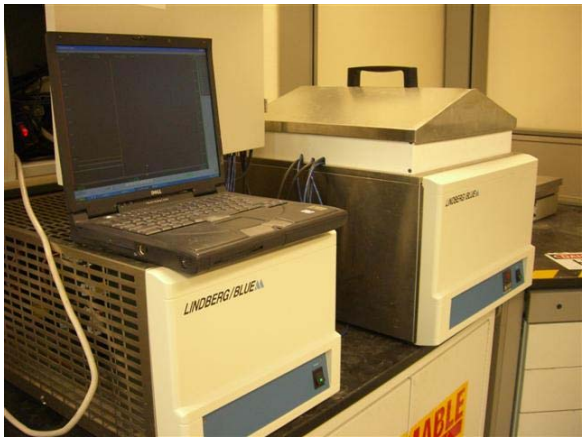

E

F

Figure 3-8. Test set-up for Coefficient of Thermal Expansion measurement. A) Cylindrical specimen length of 7.0 ± 0.1 in. B) Frame calibration. C) Thermocouples calibration. D) LVDT, frame and temperature bath. E) Length change measured at 10 & 50 ^{o}C. F) LVDT and Temperature recording.

3.6 Concrete Maturity Characteristics

3.6.1 Introduction of Maturity Concept

The concept of concrete maturity was first introduced by Saul in 1951. He defined "maturity of concrete" as "its age multiplied by the average temperature above freezing that it has maintained." Based on this definition, he further developed the law for relationship between concrete strength and maturity: "Concrete of the same mixture at the same maturity (measured as temperature-time) has approximately the same strength whatever combination of temperature and time goes to make up that maturity." Since then, many studies on maturity have been done by other researchers and Saul's law for maturity has been confirmed and proven to be a useful tool to predict concrete strength. The Maturity method has been standardized by ASTM as Standard Practice C1074.

3.6.2 Maturity Functions

According to ASTM C1074, there are two alternative functions for computing the maturity index. The first is the Nurse Saul equation that is used to calculate the temperature-time factor (TTF) as follows:

$$M(t) = \sum (T_a - T_0)\Delta t \tag{3-9}$$

where:

$M(t)$ -- Temperature-time factor at age t, degree-days or degree-hours,
Δt -- Time interval, days or hours,
T_a -- Average concrete temperature during time interval, Δt, ºC, and
T_0 -- Datum temperature, ºC.

The Arrthenius equation is another maturity function, which is used to compute equivalent age (AGE) as follows:

Error! Objects cannot be created from editing field codes.
(3-10)

Where:

t_e -- Equivalent age at a specified temperature T_s, days or h,

Q -- Activation energy divided by the gas constant, K,
T_a -- Average concrete temperature during time interval, Δt, K,
T_s -- Specified temperature, K, and
Δt -- Time interval, days or hours.

Though both functions can predict the strength of in-place concrete equally well, the Nurse Saul equation was preferred in this project for its simplicity.

3.6.3 Maturity Test Apparatus

In order to determine the concrete maturity, a temperature-time recording device is required. Acceptable devices include thermocouples or thermistors connected to strip-chart recorders or digital data-loggers. Figure 3-9 shows one of the popular maturity meters, which is also used in this project. This device is a multi-channel maturity meter, giving digital maturity number calculation, instant readout, and temperature history. All four channels can be used simultaneously. All data are on menu-driven alphanumeric displays. Communication port allows data transfer from meter to meter, printer, or computer. The main specifications for this maturity meter are given in Table 3-12.

Figure 3-9. Model H-2680 system 4101 concrete maturity meter.

Table 3-12. Specifications for models H-2680 system 4101 concrete maturity meter.

Temperature Measurement			Data Record	
Sensor measurement	Accuracy	Thermocouple Wire	Data Capacity	Recording Interval
-10ºC to 90 ºC	+/-1 ºC	Type "T"	10 months x 4 channels	Every ½ hour up to 48 hrs, then every hour
Mechanical		Maturity Value Calculations		
Dimensions	Weight	Datum Temperature	Equivalent Age Temperature	Activation Energy Constant
7.8" x 4.7"x 2.9"	1.75lbs	-20 ºC to 40 ºC	0 ºC to -40ºC	0ºK to 20,000 º K

3.6.4 Procedure for Maturity Test

The maturity test is a two-step process (Figure 3-10). Step 1: develop a relationship between the maturity values and the concrete strength from beams or cylinders. This step includes four processes: 1) determine datum temperature (T_0) via mortar testing; 2) measure temperature history of concrete, which is used to calculate maturity index: temperature-time factor (*TTF*); 3) run strength test on beams or cylinders; 4) establish relationship between strength values and *TTF*. Step 2: predict strength of in-place concrete. This step includes two processes: 1) measure maturity of in-place concrete; 2) determine strength from maturity-strength curve developed in step 1.

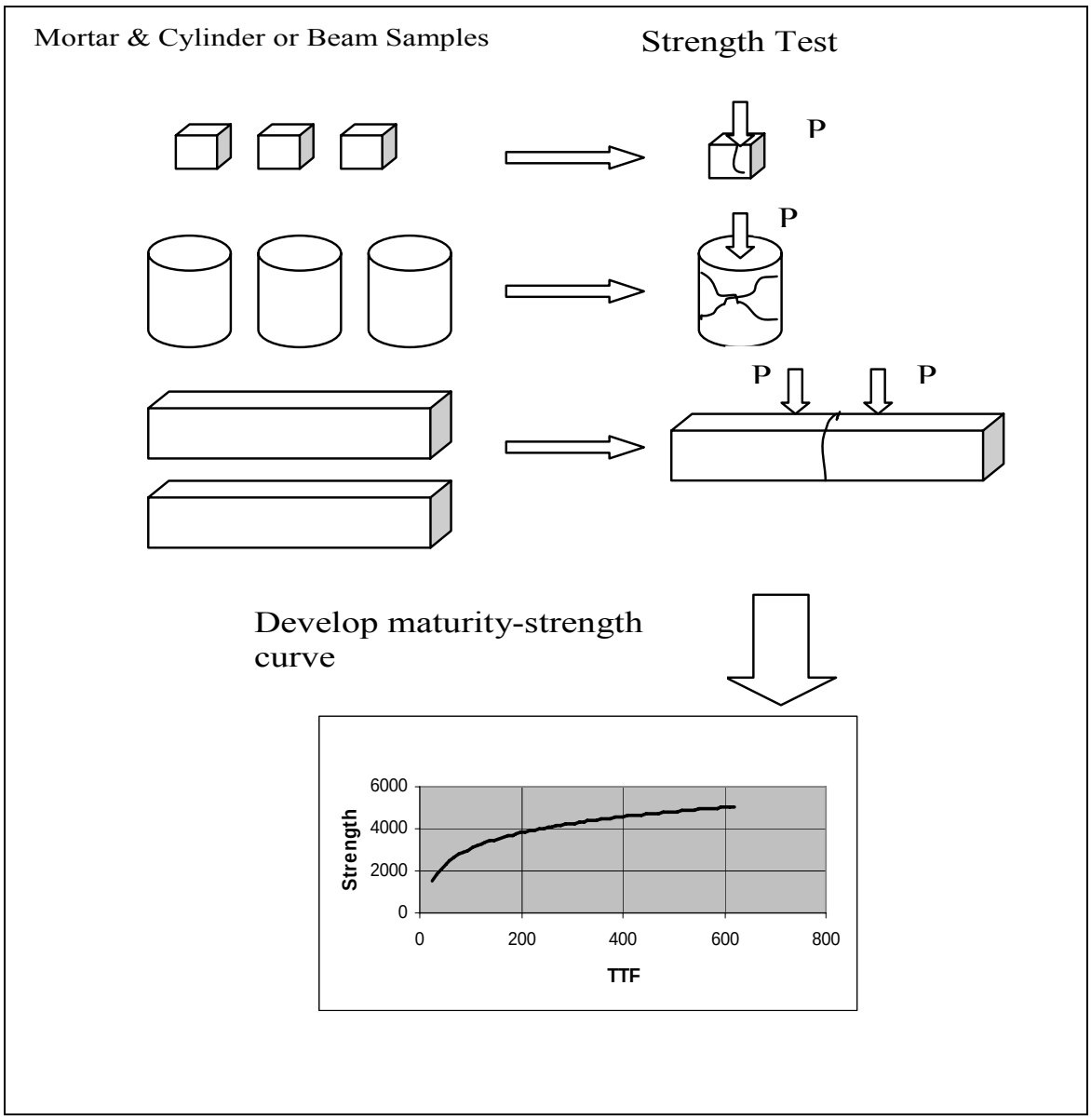

A

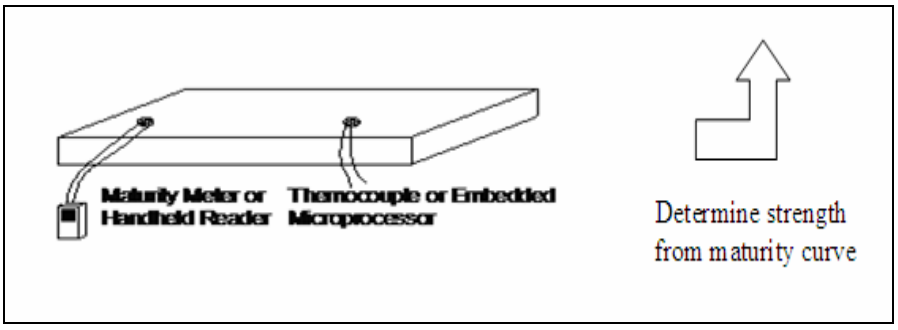

B

Figure 3-10. Procedure for maturity testing. A) Step 1: Develop maturity – strength curve. B) Step 2: Predict strength of in-place concrete.

3.6.5 Establishment of Maturity Strength Relationship

It is to be noted that the concrete must be made of the same material and same proportions as in-place when developing the maturity-strength relationship. The detailed procedures for establishing the maturity-strength relationship are shown in this section as follows.

Determine Datum Temperature (T_0)

Procedure for determining datum temperature (T_0) is given as follows:

1. Prepare a mortar

   The mixture proportions of the mortar used are given in Table 3-13. The Fine Aggregate/Cement ratio of the mortar was the same as the Coarse Aggregate/Cement ratio of the concrete to be evaluated. The same proportions of admixtures used in the concrete were also used in the mortar.

Table 3-13. Mix proportions of the mortar.

Cement (lbs/yd^3)	FA (lbs/yd^3)	Water (lbs/yd^3)	Admixtures (oz)			W/C
			AE(darex)	ADVA	Daraccel	
850	1650	283	1	34	384	0.365

2. Prepare three temperature baths

   The three temperatures used were:
   1) 5ºC = the minimum temperature expected for the in-place concrete
   2) 40ºC = the maximum temperature expected for the in-place concrete
   3) 23ºC = the midway temperature between the extremes expected for the in-place concrete

3. Prepare 50-mm mortar cubes

   Three sets of mortar cubes were prepared, one set for each bath temperature. For each set, 6 testing times were used, and 3 replicates were used per test condition. For each set, 3 additional cubes were also used to estimate the time when the mortar reached a compressive strength of 4 MPa. Thus a total of 21 mortar cubes were made for each set.

4. Run compressive strength test

   For each set of mortar cubes, compressive strength test was first run on 3 cubes at an early age to estimate the time when the mortar would reach a compressive strength of 4 MPa. Compressive strength test was then run on 3 mortar cubes at the time when the

compressive strength was around 4 MPa. Subsequent compressive strength tests were performed on 3 cubes at ages that were approximately twice the age of the previous tests.

5. Determine K-values

   Steps in determining the K-values are as follows:
   1) Using the strength-age data for the last four test ages, plot the reciprocal of strength (y-axis) versus the reciprocal of age (x-axis). Determine the y-axis intercept. The inverse of the intercept is the limiting strength, S_u .
   2) Calculate A = $S/(S-S_u)$, where S = strength at age t, from the first 4 tests.
   3) Plot A versus age for the first 4 tests at each curing condition.
   4) Determine K = slope of the best-fit straight lines for each curing temperature.

6. Determine the datum temperature (T_0)

   The datum temperature is determined as follows:
   1) Plot K-values versus temperature
   2) T_0 = intercept of x-axis

7. Determine Q (activation energy/gas constant)

   The Q value is determined as follows:

   1) Plot Ln (K) versus 1/temperature (in °K).
   2) Determine the best-fitting straight line through the points. The negative of the slope of the line is Q.

Figures 3-11 shows datum temperature determination process and equipment.

A


B
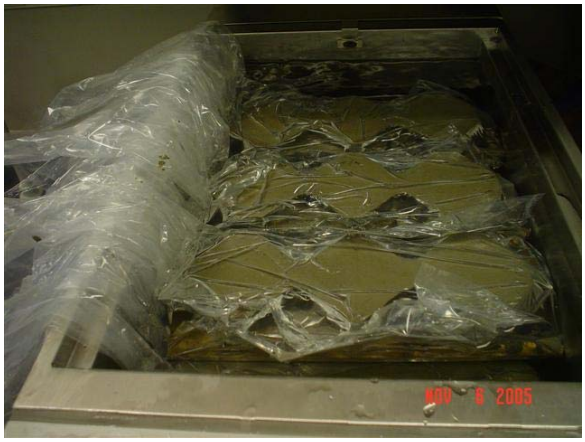

C


D


E

F

Figure 3-11. Datum temperature determination process and equipment. A) 50-mm cube mold. B) Mixing the mortar mixtures. C) Curing mortars in the bath at 5 oC. D) Curing mortars in the room temperature of 23 oC. E) Curing mortars in the oven at 40 oC. F) Running compressive test of the cube specimen.

The plots for determination of the datum temperature and Q value are shown in Figure 3-12 and 3-13 respectively. The measured datum temperature was determined to be -10.1 ˚C, and the Q value was determined to be 3,568 K. These values were used to calculate the time-temperature factor (TTF) and equivalent age (t_e) to develop the strength maturity relationships for the concrete.

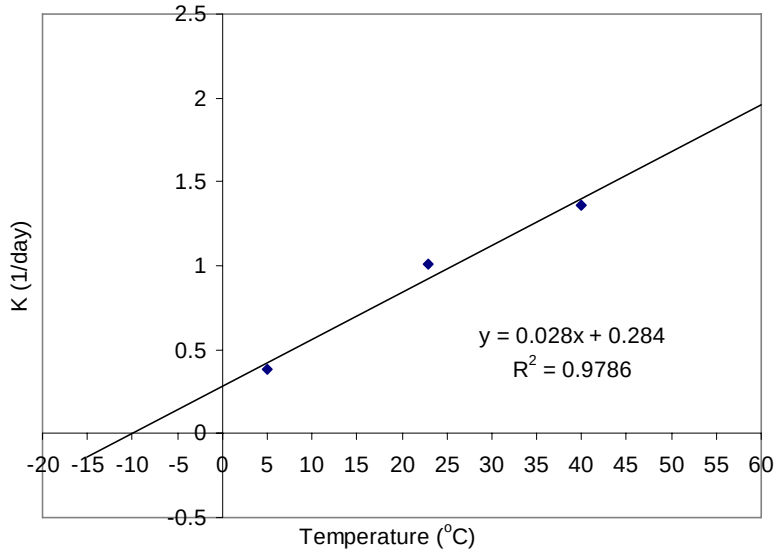

Figure 3-12. Plot for determination of datum temperature, T_o.

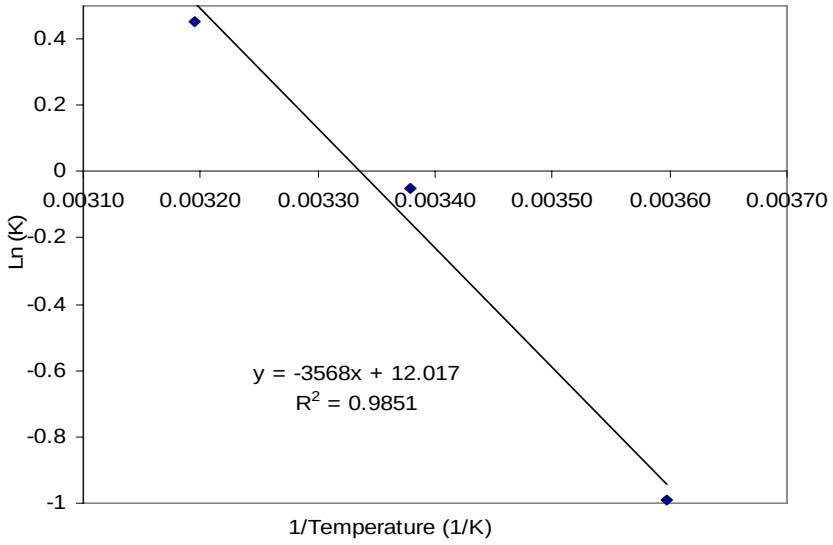

Figure 3-13. Plot of determination of Q-value.

Concrete Specimens Preparation and Measuring Temperature of Concrete Specimens

The concrete specimens for maturity calibration were prepared as described in Section 3.3, 3.4 and 3.5 of this Chapter. Strengths obtained from this study are used to develop strength-maturity relationship. The strength-maturity relationships were used to estimate in-place strength of concrete test slabs.

The maturity meter, as described in Section 3.6.3, was used to record the temperature history of concrete specimens. The procedure to measure the temperatures of the concrete specimens is as follows:

1) Embed thermocouple wires into approximately mid-depth of two cylinders and one beam (see Figure 3-14). Secure any wires to prevent them from being inadvertently pulled out of the specimens.
2) Connect thermocouple wires to maturity meter and turn on the meter to start recording temperature at once. Make sure that thermocouple wires are working normally.
3) Place the other cylinder and beam specimens together for curing.
4) Download temperature data from the maturity meter to a computer when finished.

The typical temperature history of the specimens in this research is shown in Figure 3-14. Both the cylinders and beams were kept in a moist curing room at a constant temperature of 23 ºC after 28 hours.

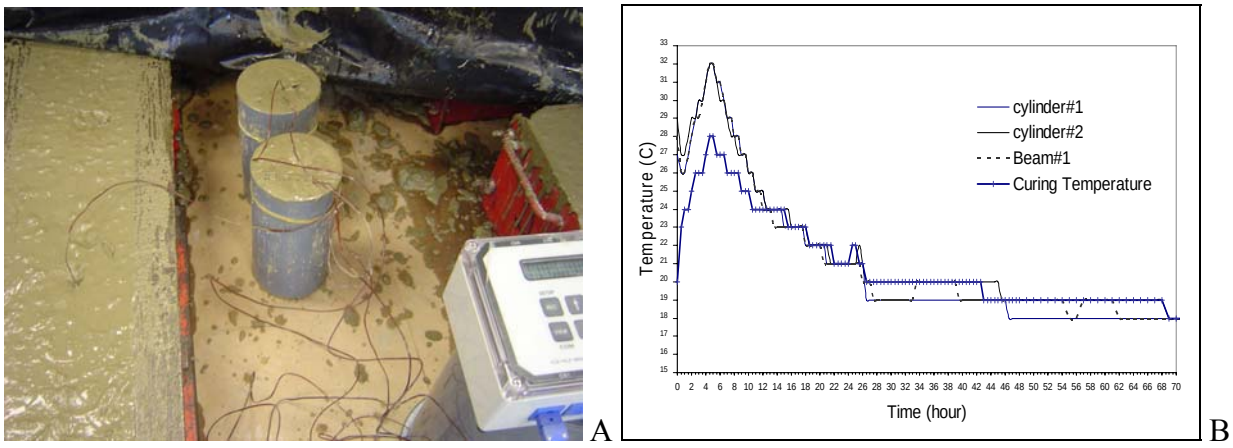

Figure 3-14. Measuring temperature of concrete specimens. A) Measuring concrete temperature using a maturity meter. B) Typical temperature history of the specimens.

Develop Maturity-Strength Relationship Curve

Figures 3-15 shows the typical plots of compressive strength and flexural strength versus TTF. Maturity calibration was also performed on the concrete sampled from all the test slabs in this research, which is presented in Chapter 5.

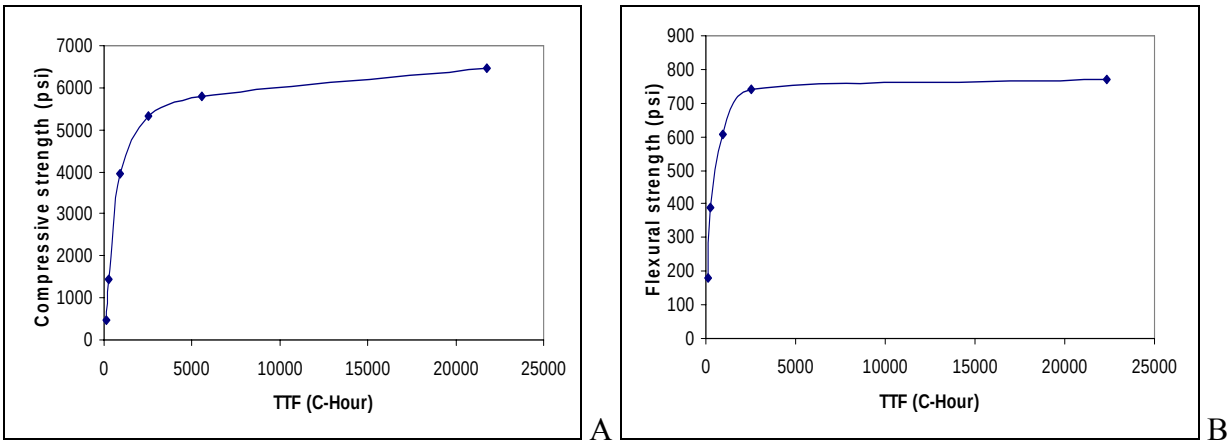

Figure 3-15. Typical plots of compressive strength and flexural strength versus TTF. A) Compressive strength vs. TTF. B) Flexural strength vs. TTF.

CHAPTER 4
INSTRUMENTATION AND CONSTRUCTION OF THE TEST SLABS

4.1 Description of Experiment

The research was planned to test the performance of concrete slabs made with different concrete mixtures using the Accelerated Paving Testing (APT) by means of a Heavy Vehicle Simulator (HVS). The concrete test track to be used for this study was constructed at the APT facility at the Florida Department of Transportation (FDOT) State Materials Research Park on September 25, 2002. This concrete test track consists of two 12-foot wide lanes. Each test lane consists of three 12 ft. x 16 ft. test slabs, placed between confinement slabs. The thickness of the concrete slabs is 9 inches.

To construct a test slab, a 12 ft. x 16 ft. slab was first removed from the concrete test track, and a replacement slab was constructed in its place. The instrumentation and construction of the test slab was done with the HVS parked over the test slab area. The HVS was used to apply repetitive moving loads along the edge of the test slab, which is the most critical wheel loading position on the concrete slab.

Analysis of the potential stress distributions within the concrete test slabs when subjected to the HVS loads was performed using FEACONS IV, a finite element program described in the following section of this dissertation. Based on the results of the analysis, optimum locations of the strain gauges to be placed on the test slabs were determined.

Maturity calibration was performed and used to predict strength of the concrete in each test slab. HVS testing was to start when the predicted strength reached a certain value by using the maturity method.

The HVS testing was continued until visible cracks developed. Dynamic strains at gauge locations were recorded every 30 minutes. The temperatures were recorded in 5 minutes intervals

during the testing period at the corners and center of the slab using the thermocouples placed in the concrete slab in 2 inch intervals from the surface of the concrete slab. The temperature in base layer was also recorded in the same time intervals.

The concrete used in each test slab was also obtained to fabricate concrete specimens to evaluate their properties. Measurement of surface profiles, joint movement and Falling Weight Deflectometer (FWD) deflection of test slabs were performed to characterize the test slabs. The material and slab characterization are presented in Chapter 6.

Parameters used in the FEACONS model were calibrated by deflection and strain data, and the calibrated model was then used to calculate potential temperature-load induced stresses. This portion of the work is presented in Chapter 7.

The evaluation of the performance of concrete test slabs is presented in Chapter 8**.**

4.2 Stress Analysis for Instrumentation Plan

The FEACONS IV (Finite Element Analysis of CONcrete Slabs version IV) program was used to analyze the anticipated stresses on the test slabs when loaded by the HVS. The FEACONS program was developed by the University of Florida for the FDOT for analysis of concrete pavements subjected to load and temperature effects.

Since the most critical loading condition is when the wheel load is applied along the edge of the concrete slab, this loading condition is used in the HVS loading of the test slabs in this study. The FEACONS program was used to analyze the stresses in the test slab when a 12-kip single wheel load with a tire pressure of 120 psi is applied along the edge of the concrete slab. Analysis was done for two critical load positions for this edge loading condition, namely (1) load at the corner of the slab, and (2) load at the middle of the edge, as shown in Figure 4-1.

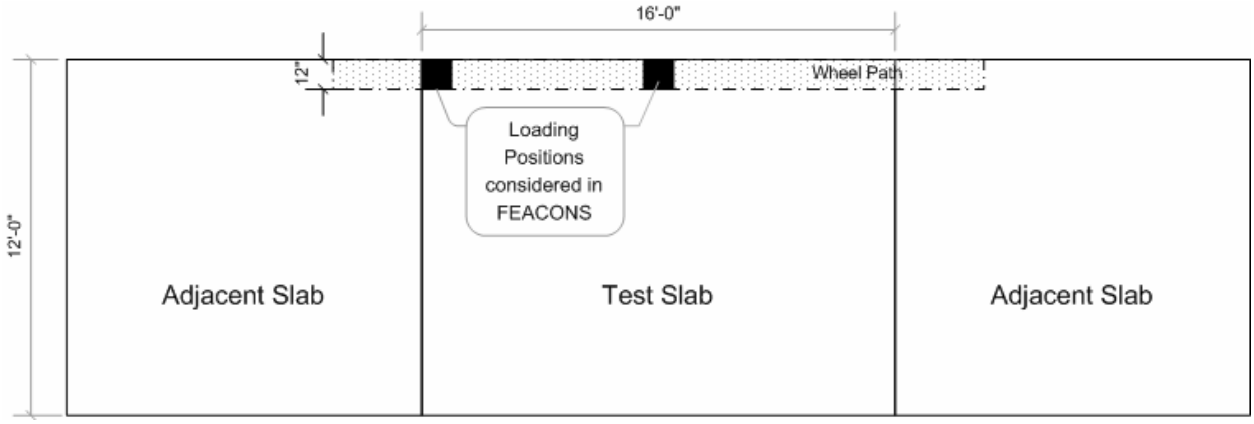

Figure 4-1. Loading positions used in the stress analysis.

In the FEACONS analysis, an elastic modulus of 3,800 ksi (as measured from the concrete sampled from Test Slab 1 and at a curing time of 28 days) was used for the concrete. The thickness of the concrete slabs was 9 inches. Other pavement parameter inputs needed for the analysis are the joint shear stiffness (which models the shear load transfer across the joint), the joint torsional stiffness (which models the moment transfer across the joint) and the edge stiffness (which models the load transfer across the edge joint). The values for these parameters are usually determined by back-calculation from the deflection basins from NDT loads (such as FWD) applied at the joints and edges. In this analysis, the values for these parameters determined previously in Phase I of this study were used. The modulus of subgrade reaction was determined to be 1.1 kci. A joint shear stiffness of 200 ksi, a joint torsional stiffness of 600 k-in/in, and an edge stiffness of 10 ksi were used. A temperature differential of zero was assumed in this analysis.

Figures 4-2 and 4-3 show the 3D plots of the distribution of the maximum computed stresses in the x (longitudinal) direction at the top of the slab caused by a 12-kip wheel load at the slab corner and slab mid-edge, respectively. Figures 4-4 and 4-5 show the contour plots of maximum stresses in the x direction caused by a 12-kip wheel load at the slab corner and slab

mid-edge, respectively. Figures 4-6 and 4-7 show the contour plots of maximum stresses in the y direction caused by a 12-kip wheel load at the slab corner and slab mid-edge, respectively.

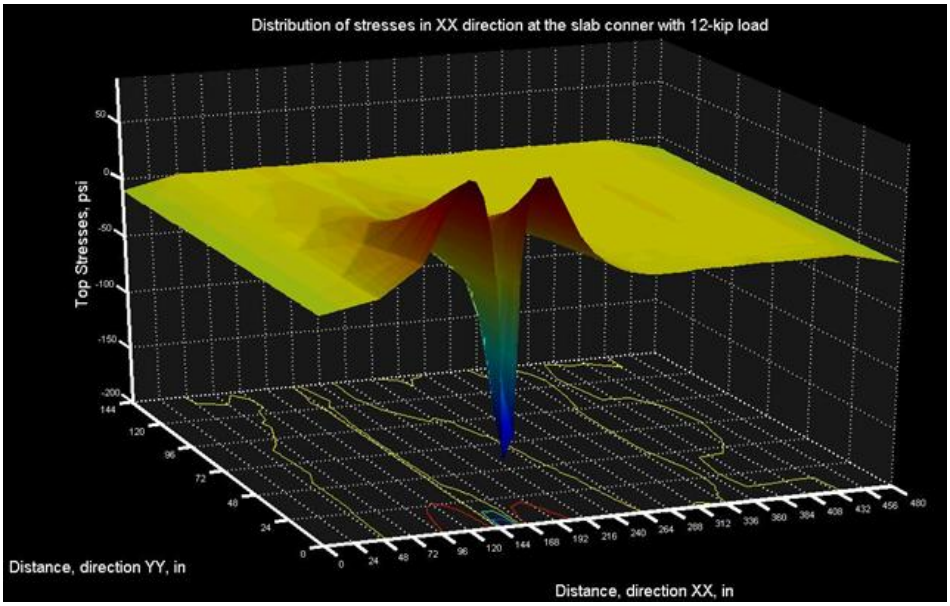

Figure 4-2. Distribution of the maximum stresses in the x (longitudinal) direction caused by a 12-kip wheel load at the slab corner.

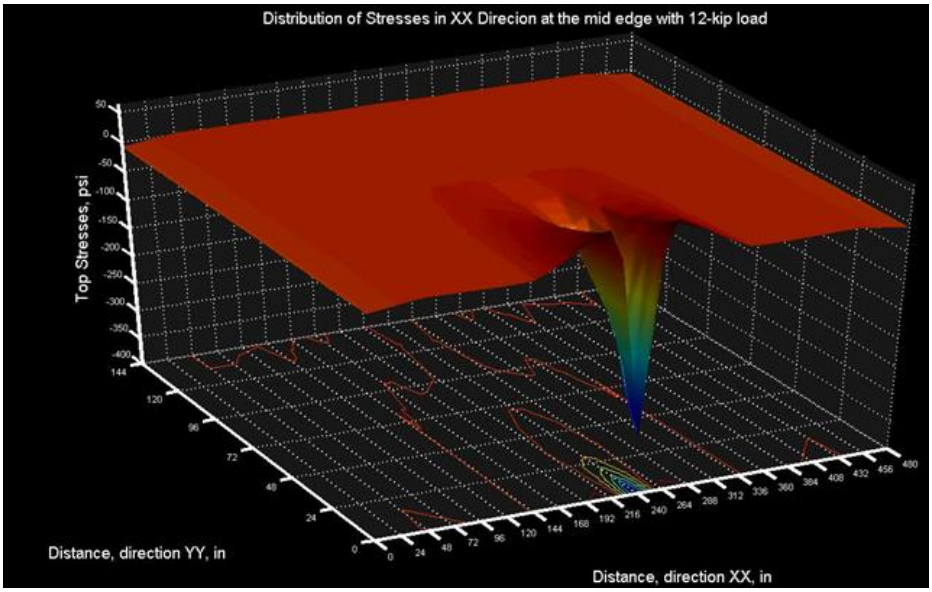

Figure 4-3. Distribution of the maximum stresses in the x (longitudinal) direction caused by a 12-kip wheel load at the slab mid-edge.

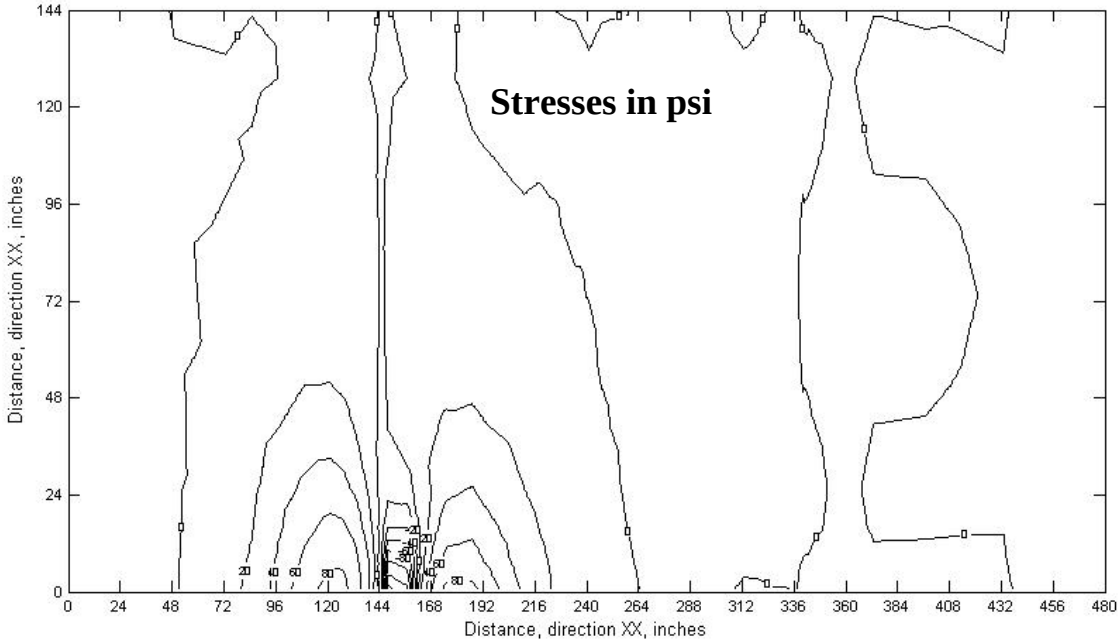

Figure 4-4. Contour plots of maximum stresses in the x direction caused by a 12-kip wheel load at the slab corner.

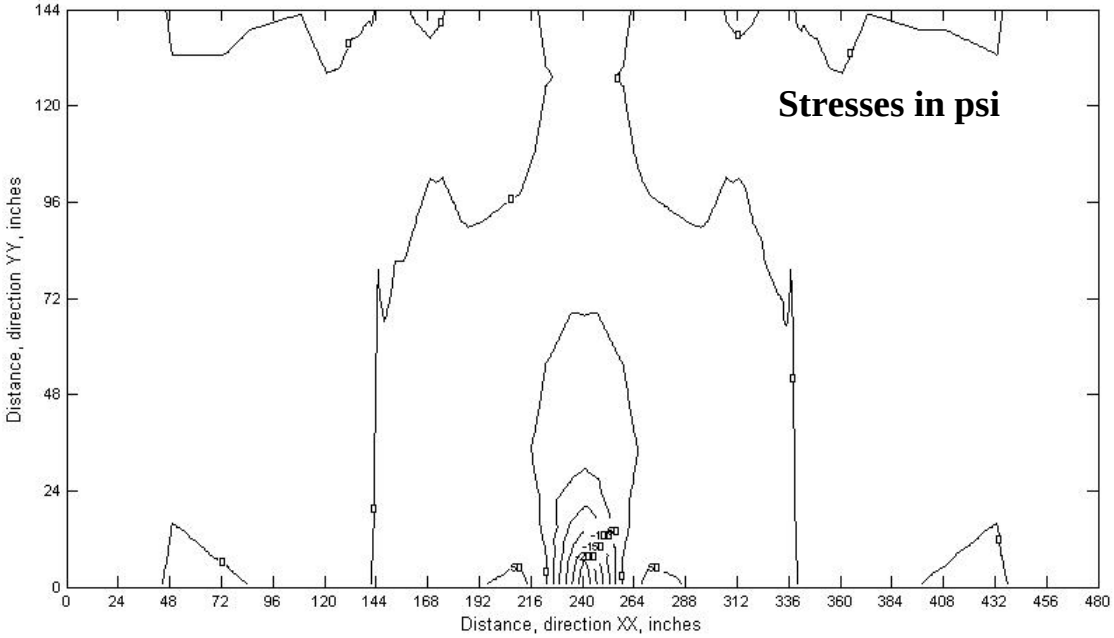

Figure 4-5. Contour plots of maximum stresses in the x direction caused by a 12-kip wheel load at the slab mid-edge.

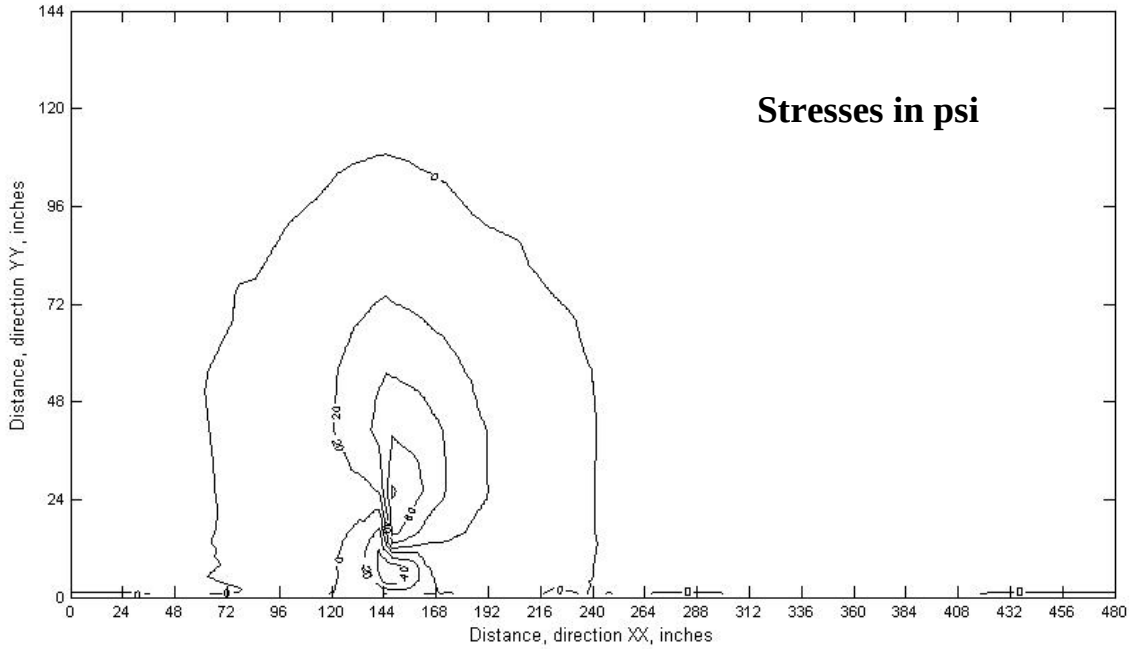

Figure 4-6. Contour plots of maximum stresses in the y direction caused by a 12-kip wheel load at the slab corner.

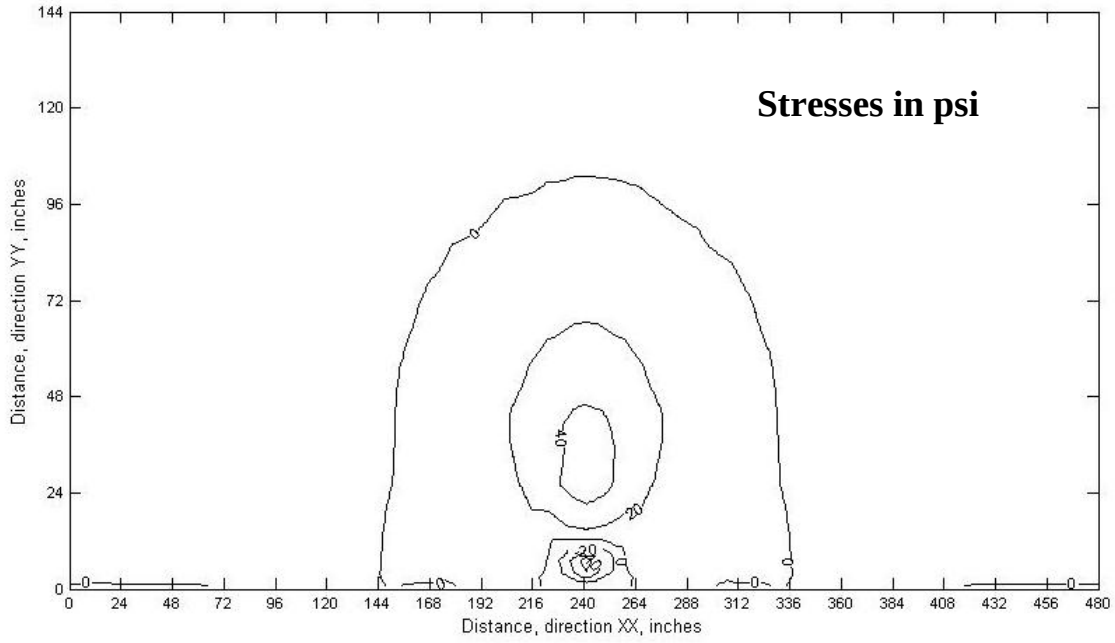

Figure 4-7. Contour plots of maximum stresses in the y direction caused by a 12-kip wheel load at the slab mid-edge.

The instrumentation plan was designed so that strain gauges would be placed at the location of maximum anticipated stresses during the HVS loading. Thermocouples were also to be placed in the concrete slab to monitor the temperature distribution in the slabs. Figure 4-8 shows layout of the instrumentation for Test Slabs 1, 2 and 3, showing the location of the strain gauges, and thermocouples. Figure 4-9 is for Test Slabs 4 and 5.

Two strain gauges are to be placed at each of the seven strain gauge locations. At each strain gauge location, one strain gauge is to be embedded in the concrete at a depth of 1 inch from the surface and another one at 1 inch above the asphalt layer. Three strain gauge positions are on the wheel path in the longitudinal (x) direction - two are at 30 inches from each joint, and the other one is at mid edge of the slab. Four additional strain gauges positions are outside the wheel path.

Thermocouples are to be placed in three locations, namely (1) the slab corner on the side of the slab not loaded by the HVS wheel, (2) the slab corner on the wheel path, and (3) the slab center. At each location, six thermocouples will be placed at 0.5, 2.5, 4.5, 6.5, 8.5 inches from the concrete surface and at 1 inch below the surface of the asphalt base.

Figure 4-10 shows also the vertical position of thermocouples and strain gauges.

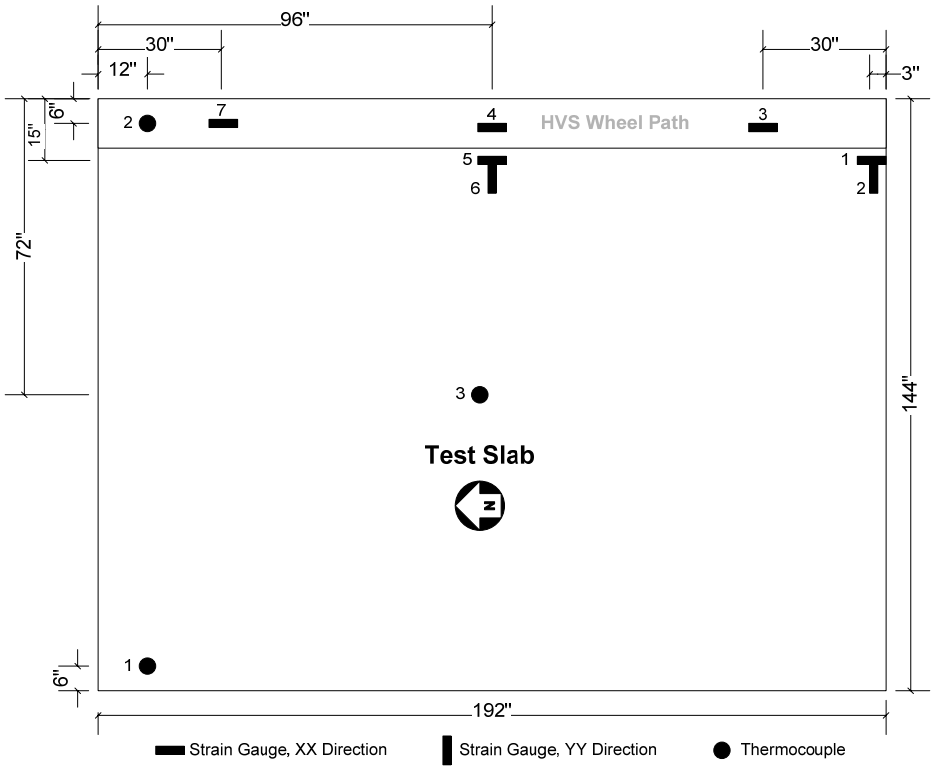

Figure 4-8. Instrumentation layout plan A for Test Slabs 1, 2 and 3.

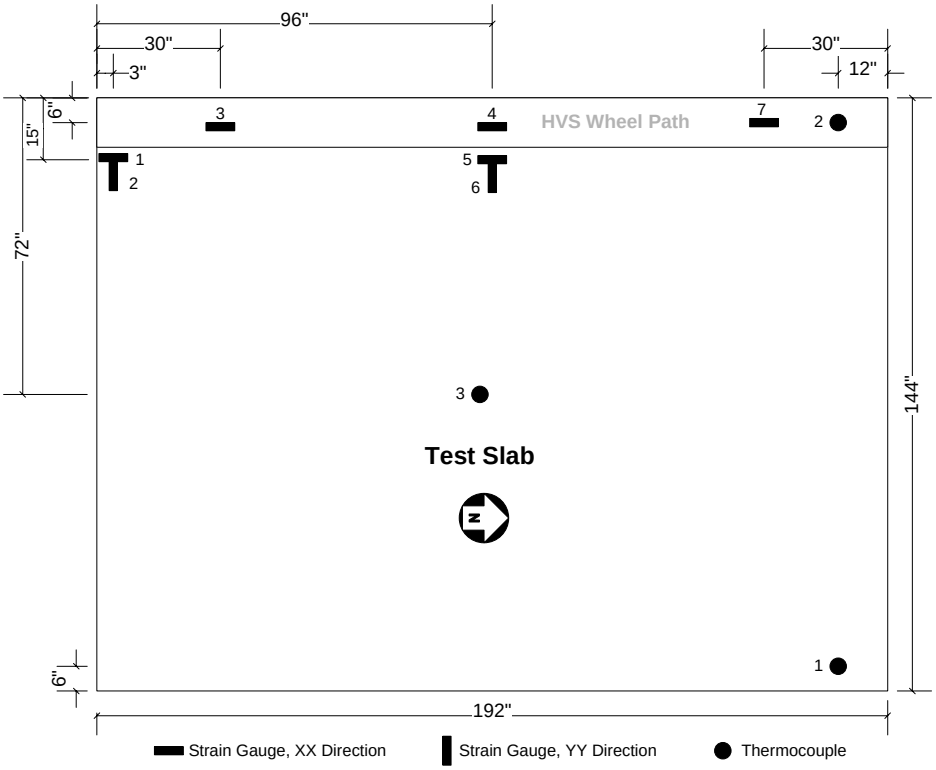

Figure 4-9. Instrumentation layout plan A for Test Slabs 4 and 5.

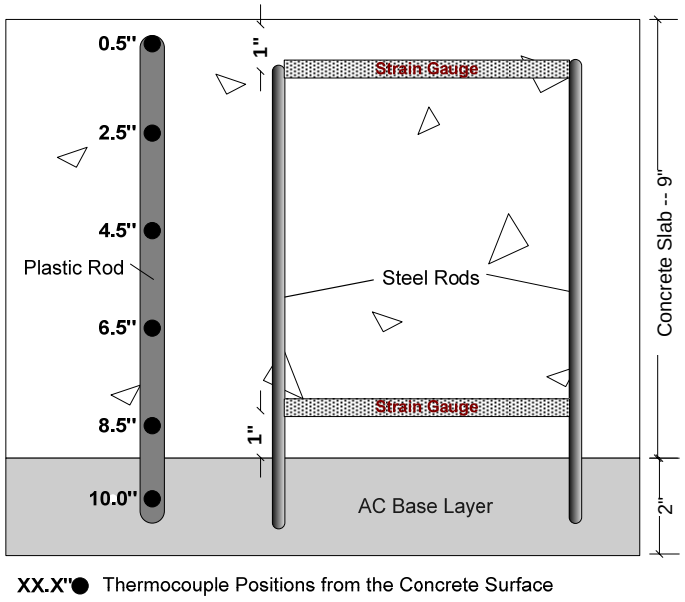

Figure 4-10. Vertical Positions of Thermocouples and Strain Gauges.

4.3 Construction of the Test Slabs

Five instrumented full-size concrete test slabs, namely Slab 1 to Slab 5, were placed on the concrete test track at the APT facility at the FDOT State Materials Research Park on March 21, 2006, June 1, 2006, April 5, 2007, July 21, 2007 and August 20, 2007, respectively by a concrete contractor under the supervision of FDOT personnel. Slabs 1 and 2 used the same target concrete mix design with a cement content of 850 lbs per cubic yard. Another concrete mix design with a cement content of 725 lbs per cubic yard was used as the target concrete mix design for Slabs 3, 4 and 5.

4.3.1 Concrete Test Track

The concrete test track for this study was constructed during Phase I of this study. It is located at the Accelerated Pavement Testing (APT) test area at the FDOT State Materials Research Park. This concrete test track consists of six 12 ft. x 16 ft., 9-inch thick concrete slabs, placed between confinement slabs.

The concrete slabs were placed over an existing two-inch thick asphalt surface. The asphalt surface was placed over a 10.5-inch limerock base that was placed over a 12-inch stabilized subgrade. This asphalt layer acts as a leveling course and provides the concrete slab with a firm and consistent foundation that is not affected by moisture changes throughout the experiment. Figure 4-11 shows a picture of the test track and a cross section of the test track and layers underneath.

A

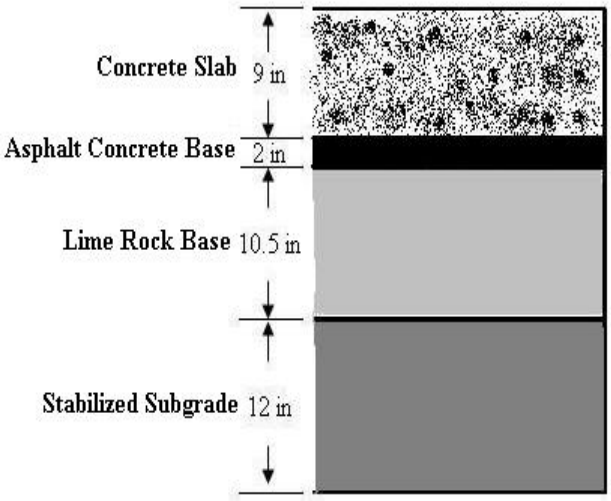

B

Figure 4-11. Concrete test track. A) Picture of the test track. B) Typical cross section of the concrete slab and layers underneath.

4.3.2 Removal of Concrete Slabs

In the preparation for the placement of a replacement test slab, an existing concrete slab on the test track was first removed. Full-depth saw cuts were made around the entire perimeter of the marked area that was to be removed. The saw cuts separated the concrete slab into small pieces (approximately 3 ft. x 4 ft.). Then the pieces were removed by using a lifter. Damaged areas on the asphalt base after the removal of the concrete slab were patched with a cold asphalt mix. Figure 4-12 shows the removal of an existing slab and patching of the damaged areas.

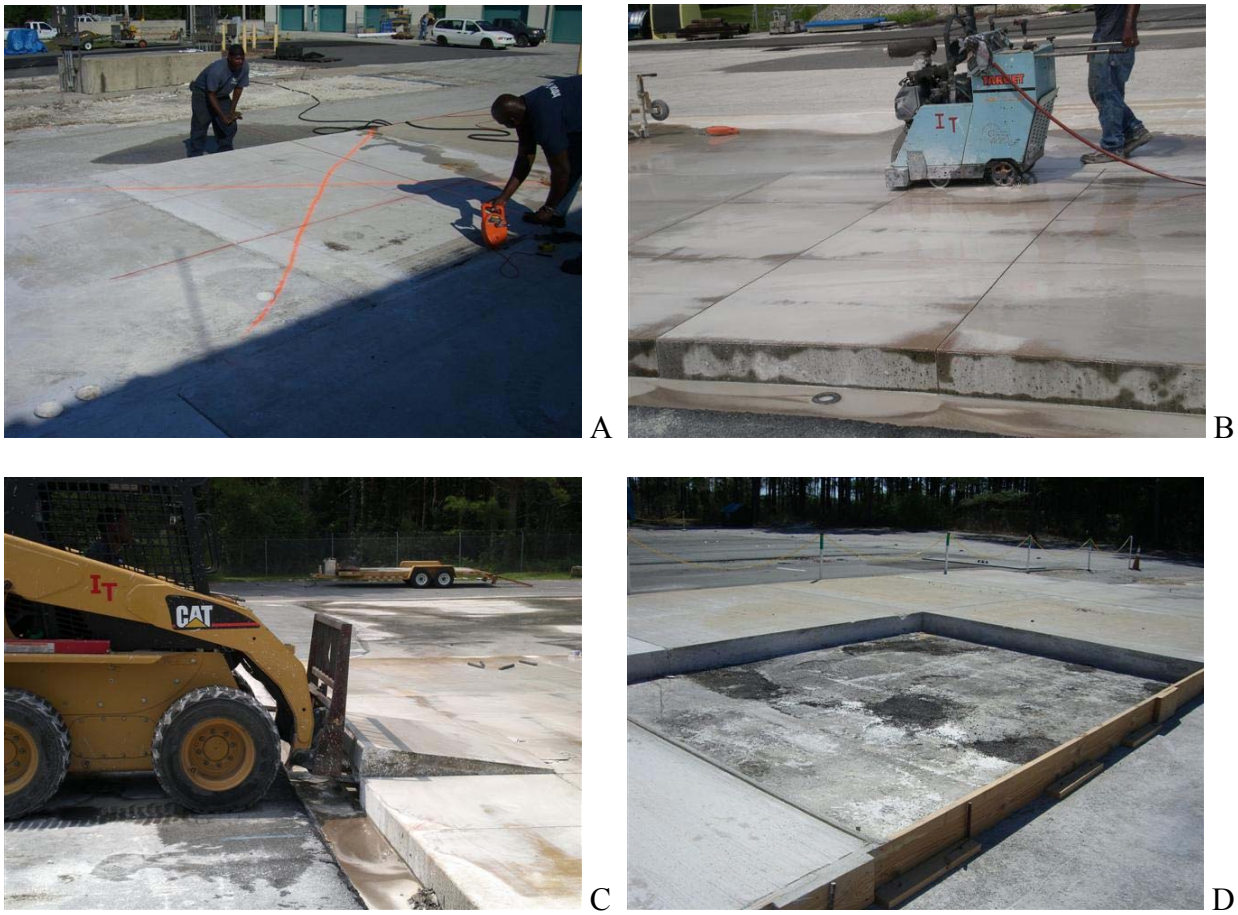

Figure 4-12. Removal of Test Slab. A) Marking a location for test slab. B) Separation of concrete slab (12 ft. x 16 ft.) into small pieces (3 ft by 4 ft). C) Removal of separated pieces using the lifter. D) After removal of separated pieces and patching of damaged base.

4.3.3 Installation of Dowel Bars and Fiber Sheets

To simulate typical replacement slabs in Florida, dowel bars were installed at the joints of the test slabs. Dowel bars were placed at one-foot intervals starting at six inch from the edge. Holes for dowel bars were drilled to a 9-inch depth to the adjacent slabs. After drilling, the drilled holes were cleaned out by inserting an air nozzle into the hole to force out all dust and debris. An epoxy was used to bond the dowels to the adjacent slab, and a lubricant was applied at the other end to allow movement in the longitudinal direction (Figure 4-13).

Figure 4-13. Placement of dowel bars. A) Drilling holes for dowel bars to the adjacent slabs. B) Clean the drilled holes with air pressure. C) Dowel bar with epoxy. D) 9-inch dowel bars to test slab with lubricant.

All the test slabs to be replaced were confined with three adjacent slabs and had one free edge. A fiber sheet was placed along the longitudinal edge of the adjacent slab to prevent the test slab from adhering to the adjacent slab, so that the edge of the test slab would behave as free longitudinal slab edge (Figures 4-14).


A


B

Figure 4-14. Placement of fiber sheet. A) Attaching fiber sheets to side of adjacent slab. B) Fiber sheet attached.

4.3.4 Placement of Strain Gauges and Thermocouples

Fourteen strain gauges and three sets of six thermocouples were placed in each test slab according to the instrumentation plan as described in Section 4.2. Before placement of concrete, the strain gauges to be embedded in the concrete were fixed in position by two steel rods, which were fixed to the asphalt base in a vertical direction. Similarly, each set of six thermocouples were fixed on a plastic rod, which was fixed to the asphalt base. Figure 4-15 show the placement of strain gauges and thermocouples.

Figure 4-15. Installing of instrumentation. A) Strain gauges held in position by steel rods. B) Thermocouples held in position by a plastic rod. C) Strain gauges and thermocouples protected by PVC pipes before placement of concrete. D) Strain gauge cables and thermocouple wires hooked up to the data acquisition box.

4.3.5 Data Acquisition

Strain data were record at every ½ hour interval, for 30 seconds each time, at a rate of 100 values per second. Temperature data were retrieved at five minute intervals from placement of concrete throughout the HVS testing period.

Wheatstone quarter-bridge circuits were used to measure strains in concrete from the strain gauges in this study. Figure 4-16 shows the quarter-bridge circuit along with the circuit for calibration and amplification of the output signal. The following symbols apply to the circuit diagram:

- R_1 and R_2 are half-bridge completion resistors.
- R_3 is the quarter-bridge completion resisters.
- R_4 is the active element measuring tensile strain ($+\varepsilon$)
- V_{EX} is the excitation voltage.
- R_L is the lead resistance.
- V_{CH} is the measured voltage.

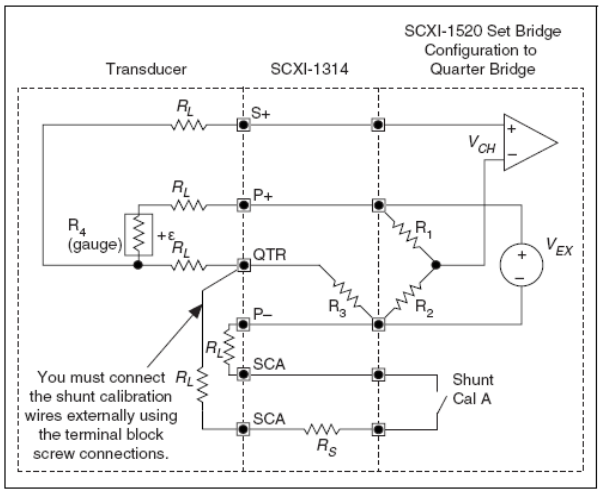

Figure 4-16. Wheatstone Quarter-bridge circuit diagram for measuring strain.

The data acquisition used is a National Instrument Model SCXI-1000. It consists of a 12-slot chassis which holds various data acquisition modules and one digitizer/communications module. Two strain/bridge modules and one thermocouple module were plugged into the chassis. Each strain/bridge module provides for 8 strain gauge inputs, and each thermocouple module provides for 32 thermocouple inputs. The digital/communications module provides a USB output to the control computer. The data acquisition system is controlled by the computer through the software LabVIEW.

The data acquisition system and control computer were placed in a temperature control chamber (Figure 4-17A), which was placed next to the test slab during the experiment (Figure 4-17B), so that the strain gauge and thermocouple wires could be conveniently connected to the data acquisition system without having to run long wires between the test slabs and the

instrumentation room. The control computer was networked with another computer through wireless networking so that the control computer can be accessed conveniently from the instrumentation room.

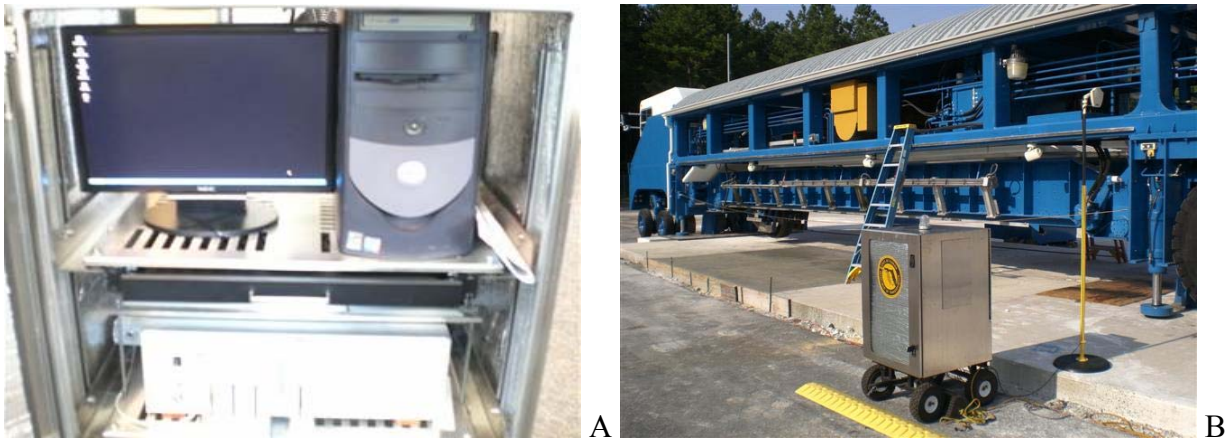

A B

Figure 4-17. Data acquisition box. A) Inside the data acquisition box. B) Set up of the data acquisition box and antenna near the test slab.

4.3.6 Placement and Finishing of Concrete Test Slabs

Two different target mixes were used for the test slabs as described in Chapter 3 of this dissertation. Before placement of concrete on test track, samples of concrete were collected from the truck to determine the plastic properties of the concrete for quality assurance and evaluation of the mixes. First, samples of concrete were taken before the accelerating admixture was added for conductance of the slump, unit weight, air content and temperature tests. Samples of concrete were again taken after adding accelerating admixture for the plastic property tests and for fabrication of test specimens for compressive strength, flexural strength, splitting tensile strength, elastic modulus, drying shrinkage and coefficient of thermal expansion. Concrete mix properties and characteristics will be presented in Chapter 6 of this dissertation.

PVC pipes were placed around the strain gauges and the thermocouples to protect them from concrete handling instruments during the placement of concrete. The concrete was placed

manually around the strain gauges and the thermocouples inside the PVC pipes. After the concrete was placed to the same thickness on both the inside and outside of the PVC pipe, the PVC pipe was then pulled out manually.

After concrete was placed into the formwork for the test slab, vibrators were used to consolidate the fresh concrete. A vibrating leveling bar was also used to level off the concrete. The concrete surface was finished manually. After placement and finishing of the concrete, 3" deep cuts were made to form the joints for the slabs. Curing compound was sprayed to the surface to cure the concrete slab. The finished test slab was protected until the start of the HVS loading. Figure 4-18 shows placement and finishing of test slab.

Figure 4-18. Placement and finishing of test slab. A) Fresh concrete properties obtained before and after adding accelerating admixture for quality assurance and evaluation of the mixes. B) Adding the accelerating admixture. C) Strain gauges and thermocouple trees protected with the PVC pipes. D) Vibrating leveling bar used to level off the concrete. E) Curing compound sprayed. F) Finished test slab with data acquisition box and a set of samples tested at the start of HVS loading.

CHAPTER 5
HVS TESTING AND OBSERVATION OF PERFORMANCE OF TEST SLABS

5.1 Introduction

This chapter presents the HVS testing and observed performance of the test slabs.

The testing plan was to start the HVS loading when the concrete reached a certain strength. The strength to signal the start point of the HVS testing at each test slab was predicted from maturity calibration for the concrete used.

Two beam and three cylindrical specimens made with an actual concrete mix used in each test slab were placed next to the slab in order to have the same curing condition as the test slab. These specimens were tested for their flexural and compressive strengths to obtain average actual strengths of the test slab at the time of start of loading.

HVS loading at 12 kips was to be applied to each test slab for 7 days, then at 15 kips for 3 days, and then at 18 kips for 3 more days before stopping the HVS.

The HVS loading were applied using a super single tire with a contact pressure of 120 psi, traveling at about 6 mph in a uni-directional mode with no wander along the longitudinal edge of the test slab. Loading along the edge was chosen because it represents the most critical loading condition for a concrete slab.

Strain data were recorded at every ½ hour interval, for 30 seconds each time, at a rate of 100 values per second. Temperature data were retrieved at five minute intervals from the time of placement of concrete and throughout the HVS testing period.

Condition surveys were made and crack maps drawn when cracks were observed during the HVS testing. Figure 5-1 shows HVS loading on a test slab.

Figure 5-1. HVS loading on a test slab.

5.2 Slab 1

5.2.1 Start of HVS Loading on Slab 1

The concrete mix used in Slab 1 had a cement content of 850 lb per cubic yard of concrete. The current FDOT concrete specification for replacement slab requires a minimum compressive strength of 2,200 psi at 6 hours. This strength requirement was used as a criterion for the start of HVS loading on Slab 1. HVS loading of Slab 1 was to start when the in-place concrete attained an estimated compressive strength of 2,200 psi.

The compressive strength of the in-place concrete was determined using the maturity method. Temperature readings from thermocouples embedded in the test slab were used to compute the Time Temperature Factor (TTF) of the in-place concrete, which was used to determine the compressive strength using the maturity calibration of the same concrete. The maturity calibration of a laboratory-prepared concrete of the same mix design was used in this case.

Figure 5-2 shows the relationship between the compressive strength and the TTF of the laboratory-prepared mix. To attain a compressive strength of 2,200 psi, the TTF has to be equal to or greater than 400 C-hr. Figure 5-3 shows the plot of TTF versus time for the in-place concrete in Slab 1. It can be seen that TTF was equal to 400 C-hr. at approximately 7 hours. Thus, HVS loading of Slab 1 was started at 7 hours after concrete placement.

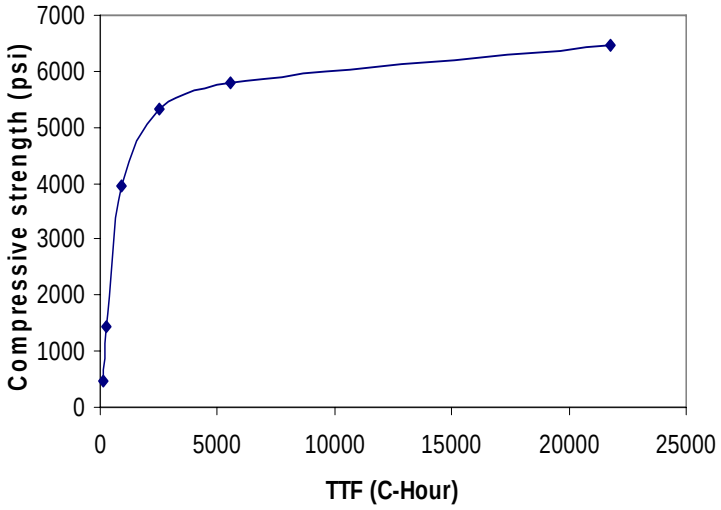

Figure 5-2. Compressive strength vs. TTF for laboratory-prepared mix.

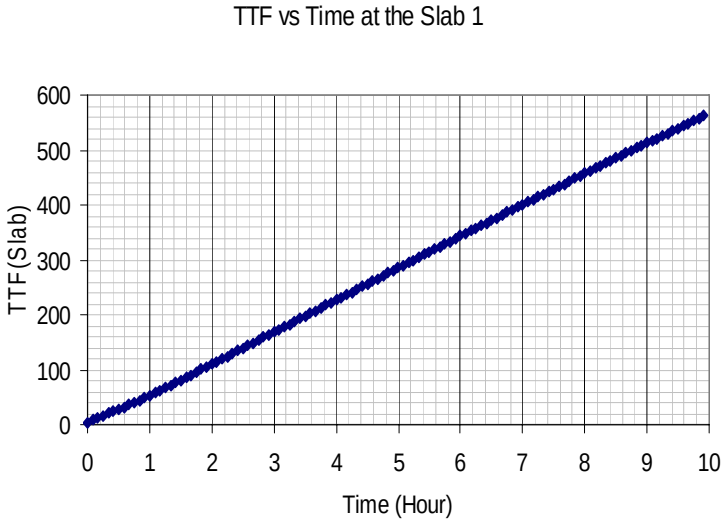

Figure 5-3. TTF vs. time for in-place concrete in Slab 1.

5.2.2 Strength Determination using Maturity Calibration of Concrete Mix from Slab 1

Samples of the concrete mix used in Slab 1 were taken and used to perform the maturity calibration. The maturity calibration of the actual concrete used in Slab 1 was used to determine the strength of the in-place concrete at different times. Table 5-1 shows the compressive strength, flexural strength and TTF of the laboratory cured samples of the concrete from Slab 1, which were used to determine maturity calibration of this mix. Table 5-1 also shows the computed compressive strength and flexural strength of the in-place concrete in Slab 1 by using this maturity calibration.

Three cylindrical specimens made with the concrete mix from Slab 1 were placed next to the slab in order to have the same curing condition as the slab. These specimens were tested for their compressive strength at the time of start of loading (7 hours). An average compressive strength of 1,760 psi was obtained. This value was slightly less than the value of 2,200 psi as predicted by the maturity calibration of the laboratory-prepared specimen. However, this value matched well with the predicted strength values from the maturity calibration of the actual concrete from Slab 1.

Table 5-1. Strength analysis for concrete in Slab 1 using maturity method.

Time	TTF (Lab)	TTF (Slab)	R (Lab)	R (Slab)	f_c (Lab)	f_c (Slab)
Start	0	0	0	0	0	0
5-hour	-	280.4	-	320	737.4	1,400
6-hour	250.1	338.5	291.8	360	1,222.8	1,600
7-hour	-	396.0	-	400 **(397*)**	-	1,850 **(1760*)**
9-hour	-	507.8	-	480	1,851.5	2,100
24-hour	846.4	1,195.9	592.2	620	3,630.9	3,900
168-hour	5,079.3	5,697.5	762.1	780	5,633.6	5,700
672-hour	21,252.2	-	800.9	-	6,428.8	-

Note: * -Actual strength of samples placed by the test slab
TTF = time-temperature factor, hr-°C
R = Flexural strengths, psi
f_c = Compressive strengths, psi

5.2.3 Observed Performance of Slab 1

HVS loading using a12-kip super single wheel with a tire contact pressure of 120 psi was applied to Slab 1 along its free edge for 7 days with a total load repetitions of 85,254 passes. The wheel load was increased to 15 kips, and the slab was loaded for 3 days with an additional 37,880 passes of the 15-kip wheel load. The load was then increased to 18 kips, and the slab was loaded for 3 days with an additional 35,676 passes of the 18-kip load. A corner crack was observed on the north end of the slab at that time and the slab was loaded with an additional of the 18-kip load for 20,506 passes before the HVS testing was stopped.

Figure 5-4 shows a picture of the corner crack and the transverse cracks at the mid-edge of the slab. The corner crack had the shape of a quarter-circle with a radius of about 3 feet. In addition to the corner crack, a few transverse cracks had also occurred at the mid-edge of the slab. Crack pattern and locations of the cracks after testing with 18-kip loads are shown in Figure 5-5.

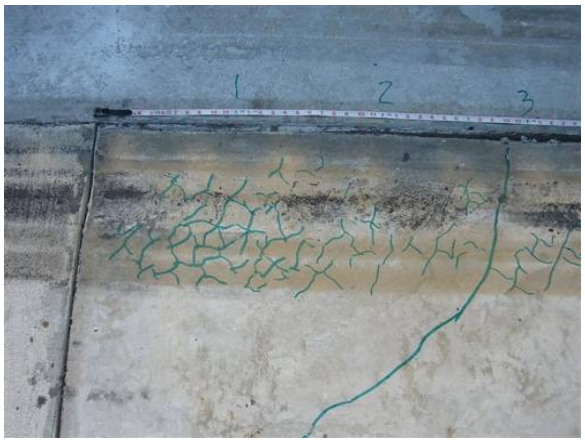

A  B

Figure 5-4. Cracks after HVS loading with 18-kip load. A) Corner crack at the north end of Slab 1. B) Transverse cracks at mid edge of Slab 1.

A

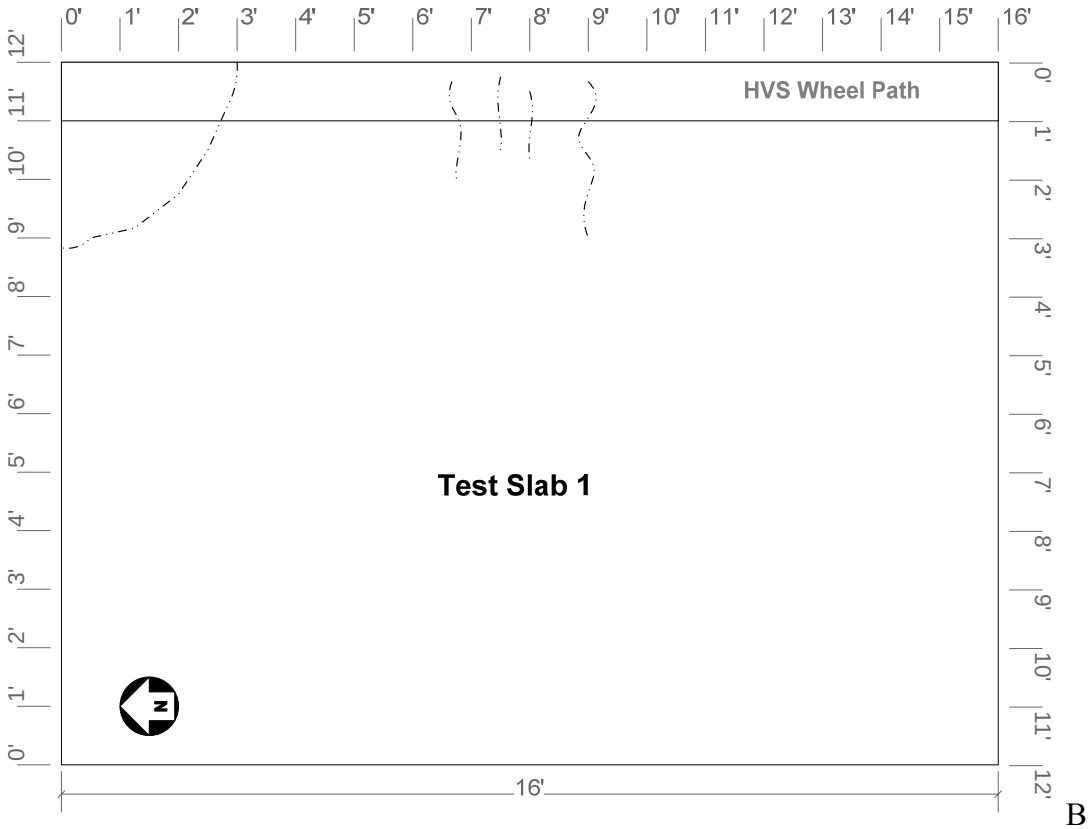

B

Figure 5-5. Observed cracks on Test Slab 1. A) Crack Pattern (corner crack and transverse Cracks after Testing with 18-kip Loads, at locations of computed maximum stresses). B) Locations of Corner Crack and Transverse Cracks after Testing with 18-kip Load.

5.3 Slab 2

5.3.1 Start of HVS Loading on Slab 2

The concrete mix used in Slab 2 had the same mix design as that used in Slab 1, which had a cement content of 850 lb per cubic yard of concrete. HVS loading of Slab 2 was to start when the in-place concrete attained an estimated flexural strength of 300 psi.

The TTF of the in-place concrete was used to predict the flexural strength of the concrete using the maturity calibration of the concrete from Slab 1. This was a reasonable thing to do since Slab 2 used the same concrete mix as Slab 1. Figure 5-6 shows the relationship between the flexural strength and the TTF of the concrete used in Slab 1. To attain a flexural strength of 300 psi, the TTF has to be equal to or greater than 300 C-hr. Figure 5-7 shows the plot of TTF versus time for the in-place concrete in Slab 2. It can be seen that TTF was equal to 300 C-hr. at approximately 5 hours. Thus, HVS loading of Slab 2 was started at 5 hours after concrete placement.

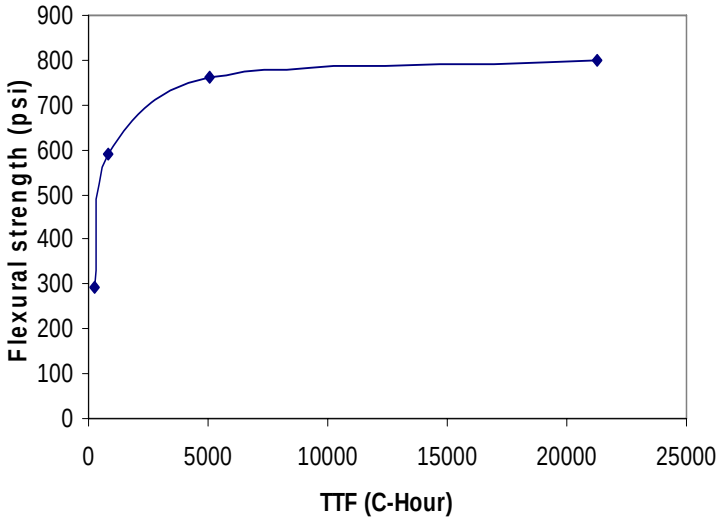

Figure 5-6. Flexural strength vs. TTF for concrete mix from Slab 1.

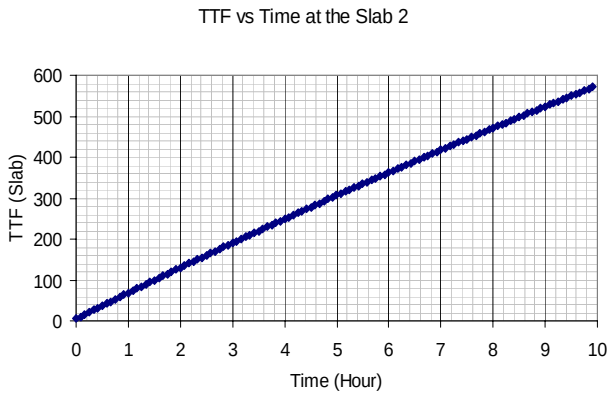

Figure 5-7. TTF vs. time for in-place concrete in Slab 2.

5.3.2 Strength Determination using Maturity Calibration of Concrete Mix from Slab 2

Samples of the concrete mix used in Slab 2 were taken and used to perform the maturity calibration. The maturity calibration of the actual concrete used in Slab 2 was then used to determine the flexural and compressive strengths of the in-place concrete at different times. Table 5-2 shows the compressive strength, flexural strength and TTF of the laboratory cured samples of the concrete from Slab 2, which were used to determine the maturity calibration of this mix. Table 5-2 also presents the computed compressive strength and flexural strength of the in-place concrete in Slab 2 by using this maturity calibration.

Two beam specimens made with the actual concrete mix used in Slab 2 were placed next to the slab in order to have the same curing condition as this test slab. These specimens were tested for their flexural strength at the time of start of loading (5 hours). An average flexural strength of 402 psi was obtained from these samples at 5 hours. This value was substantially higher than the value of 300 psi as predicted by the maturity calibration of concrete mix sampled from Slab 1. However, this measured flexural strength of 402 psi at 5 hours matched well with the other predicted strength values from the maturity calibration of the actual concrete from Slab 2.

Table 5-2. Strength analysis for concrete in Slab 2 using maturity method.

Time	TTF (Beam)	TTF (Cylinder)	TTF (Slab)	R (Lab)	R (Slab)	f_c (Lab)	f_c (Slab)
Start	0	0	0	0	0	0	0
4-hour	-	171.2	244.2	-	360.0	890.5	1,000.0
5-hour	-	-	301.7	-	390.0 **(401.5*)**	-	1,350.0 **(1,433.3*)**
8-hour	261.1	250.1	358.0	389.5	450.0	1,094.5	1,850.0
24-hour	-	324.3	466.8	-	500.0	1,560.0	2,600.0
168-hour	890.6	846.4	1,237.7	575.7	590.0	3,225.0	3,650.0
672-hour	5,145.3	5,079.3	5,794.2	723.7	730.0	5,951.1	6,150.0

Note: * -Actual strength of samples placed by the test slab
TTF = time-temperature factor, hr-°C
R = Flexural strengths, psi
f_c = Compressive strengths, psi

5.3.3 Observed Performance of Slab 2

Similar HVS loading as used on Slab 1 was used on Slab 2. Slab 2 was loaded for 7 days with a total of 87,785 passes of a 12-kip super single wheel load. The wheel load was increased to 15 kips, and the slab was loaded for an additional 42,239 passes of the 15-kip wheel load. The load was then increased to 18 kips, and the slab was loaded for an additional 37,617 passes of the 18-kip load. Some transverse cracks across the wheel path were observed at this point. Figure 5-8 shows pictures of these transverse cracks on the wheel path. Crack pattern and locations of the cracks after testing with 18-kip load are shown in Figure 5-9.

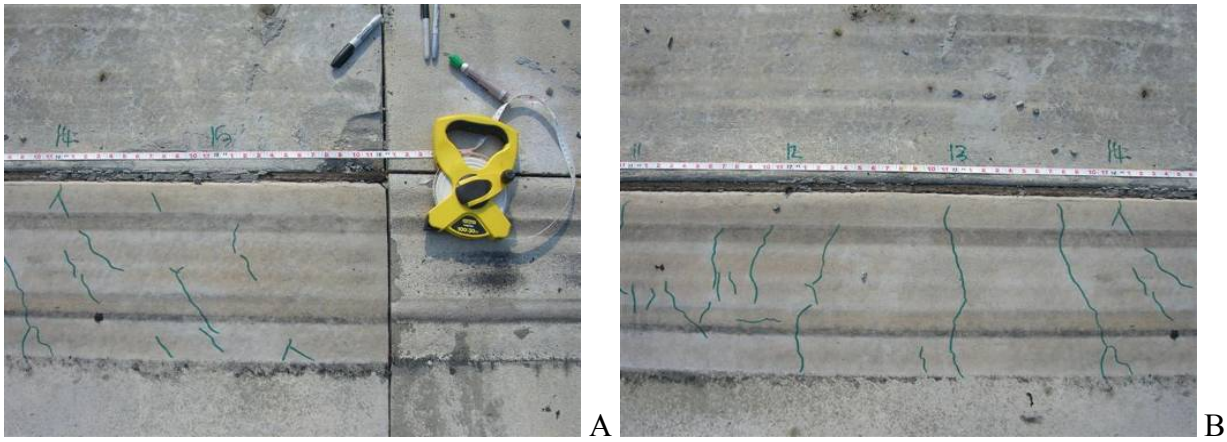

A B

Figure 5-8. Transverse cracks on Test Slab 2. A) Cracks at the south end. (b) Cracks at mid edge.

A

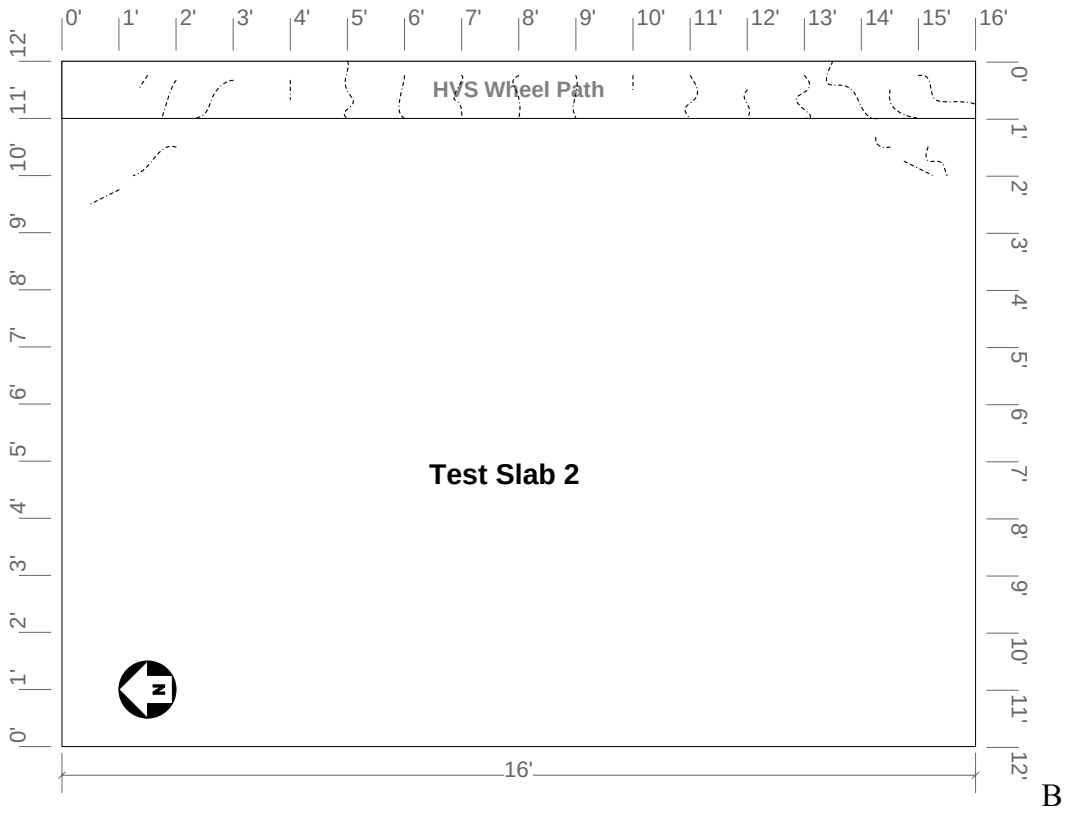

B

Figure 5-9. Cracks on Test Slab 2. A) Crack pattern (Cracks after Testing with 18-kip Loads). B) Locations of Cracks on Test Slab 2 after Testing with 18-kip Loads.

5.4 Slab 3

5.4.1 Start of HVS Loading on Slab 3

The concrete mix for Slab 3 had a cement content of 725 lb per cubic yard of concrete. HVS loading of Slab 3 was to start when the in-place concrete attained an estimated flexural strength of 300 psi. The TTF of the in-place concrete was used to predict the flexural strength of the concrete using the maturity calibration of the laboratory-prepared Mix 2. Figure 5-10 shows the relationship between the flexural strength and the TTF of the concrete according to the maturity calibration of the laboratory-prepared mix. To attain a flexural strength of 300 psi, the TTF had to be equal or greater than 160 C-hr. Figure 5-11 shows the plot of TTF versus time for the in-place concrete in Slab 3. It can be seen that TTF was equal to 190 C-hour at approximately 4 hours. Thus, HVS loading of Slab 3 was started at 4 hours after concrete placement.

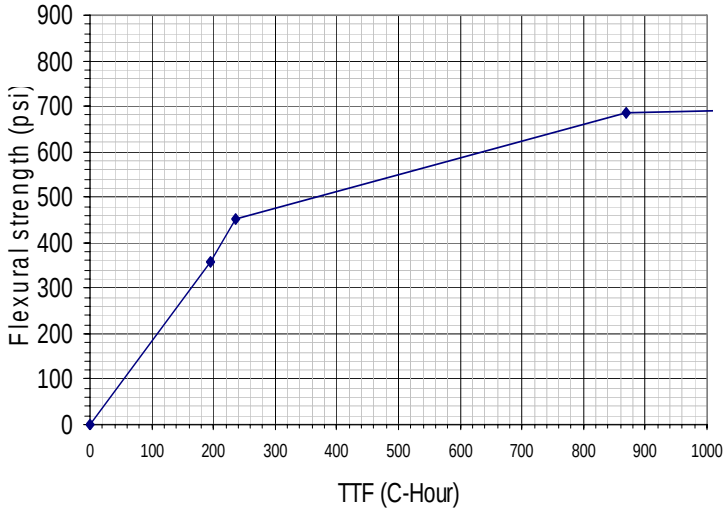

Figure 5-10. Flexural Strength vs. TTF for Laboratory-Prepared Mix 2.

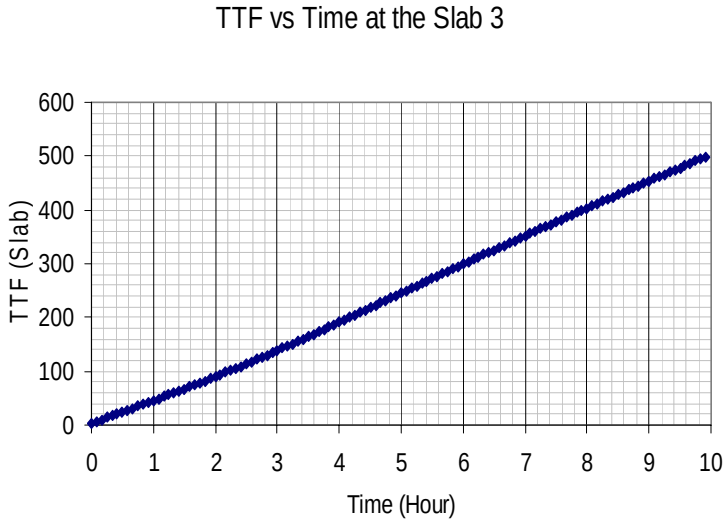

Figure 5-11. TTF vs. Time for In-Place Concrete in Slab 3.

5.4.2 Strength Determination using Maturity Calibration of Concrete Mix from Slab 3

Samples of the concrete mix used in Slab 3 were taken and used to perform the maturity calibration. The maturity calibration of the actual concrete used in Slab 3 was used to determine the strength of the in-place concrete at different times. Figures 5-12 show the plots of compressive strength and flexural strength versus TTF, respectively, for the concrete mix used in Slab 3.

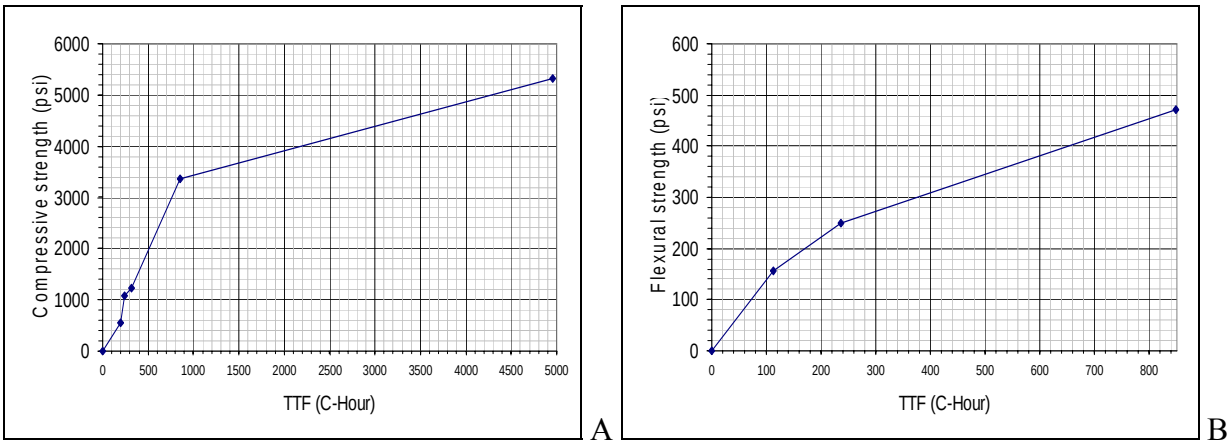

Figure 5-12. Strengths vs. TTF for the concrete from Slab 3. A) Compressive Strength vs. TTF. B) Flexural Strength vs. TTF.

Table 5-3 shows the compressive strength, flexural strength and TTF of the laboratory cured samples of the concrete from Slab 3, which were used to determine maturity calibration of this mix. Figure 5-13 shows the temperature history of these specimens. Table 3.1 also shows the computed compressive strength and flexural strength of the in-place concrete in Slab 3 by using this maturity calibration.

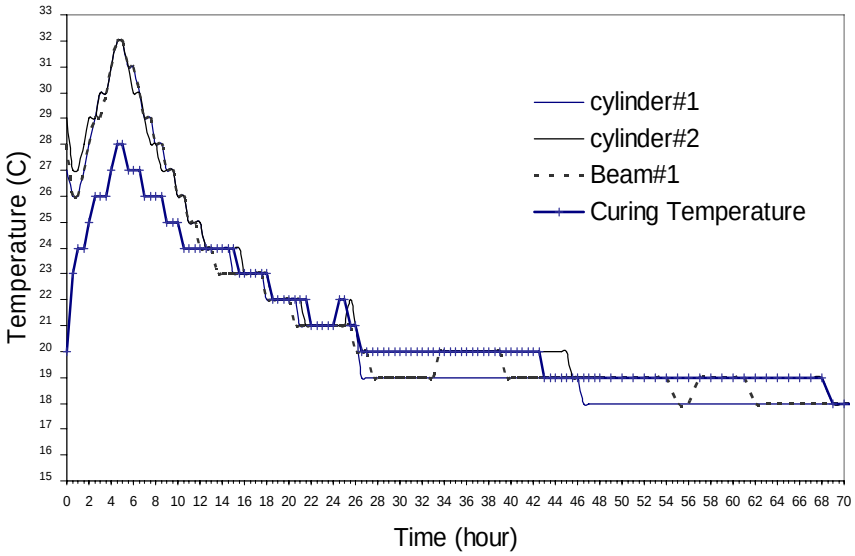

Figure 5-13. Temperature history of the specimens from Slab 3.

Table 5-3. Strength analysis for the concrete in Slab 3 using maturity method.

Time	TTF (Beam)	TTF (Cylinder)	TTF (Slab)	R (Lab)	R (Slab)	f_c (Lab)	f_c (Slab)
3-hour	112.6	-	134.2	156	170	-	450
4-hour	-	-	186.7	-	215 (**184*)**	-	550 (**485*)**
5-hour	-	194.8	240.8	-	235	563	1,150
6-hour	235.9	236.1	294.6	250	255	1,076	1,200
8-hour	-	315.1	398.9	-	285	1,2340	1,550
24-hour	848.6	851.4	1,086.9	472	475	3,370	3,500
168-hour	4,999.6	4,961.1	5,702.1	-	560	5,324	5,700
672-hour	19713.5	19650.5	-	805	-	6,810	-

Note: * -Actual strength of samples placed by the test slab
TTF = time-temperature factor, hr-°C
R = Flexural strengths, psi
f_c = Compressive strengths, psi

Two beam specimens made with the actual concrete mix used in Slab 3 were placed next to the slab in order to have the same curing condition as the test slab. These specimens were tested for their flexural strength at the time of start of loading (4 hours). An average flexural strength of 184 psi was obtained from these samples at 4 hours. This measured flexural strength was very close to the predicted flexural strength value (215 psi) from the maturity calibration of the actual concrete from Slab 3. However, this value was substantially lower than the value of 300 psi as predicted by the maturity calibration of laboratory-prepared Mix 2, which was done in October 2006. Using the relationship between flexural strength and TTF (as presented in Figure 5-10) had resulted in over-predicting the strength of the in-place concrete.

5.4.3 Observed Performance of Slab 3

HVS loading of Test Slab 3 was started 4 hours after concrete placement. A 12-kip super single wheel with a tire contact pressure of 120 psi was applied repetitively along the free edge of the slab.

On the second day, a 12-inch transverse crack was observed at the mid-edge of the slab, as shown in Figure 5-14-A. After 47,170 passes of the 12-kip load, a few small transverse cracks had also occurred at the mid-edge of the slab as shown in Figure 5-14-B. The slab was continuously loaded with the 12-kip load for 7 days with a total load repetition of 95,042 passes. The wheel load was then increased to 15 kips, and the slab was loaded for an additional 3 days with an additional 35,915 passes of the 15-kip wheel load when a corner crack of about 3 feet radius was observed at the north end, as shown in Figure 5-14-C. The load was then increased to 18 kips, and the slab was loaded for 3 more days with an additional 37,580 passes. After 3 days of 18 kips load, a corner crack of 4 feet radius was observed at the south end of the slab, as shown in Figure 5-14-D.

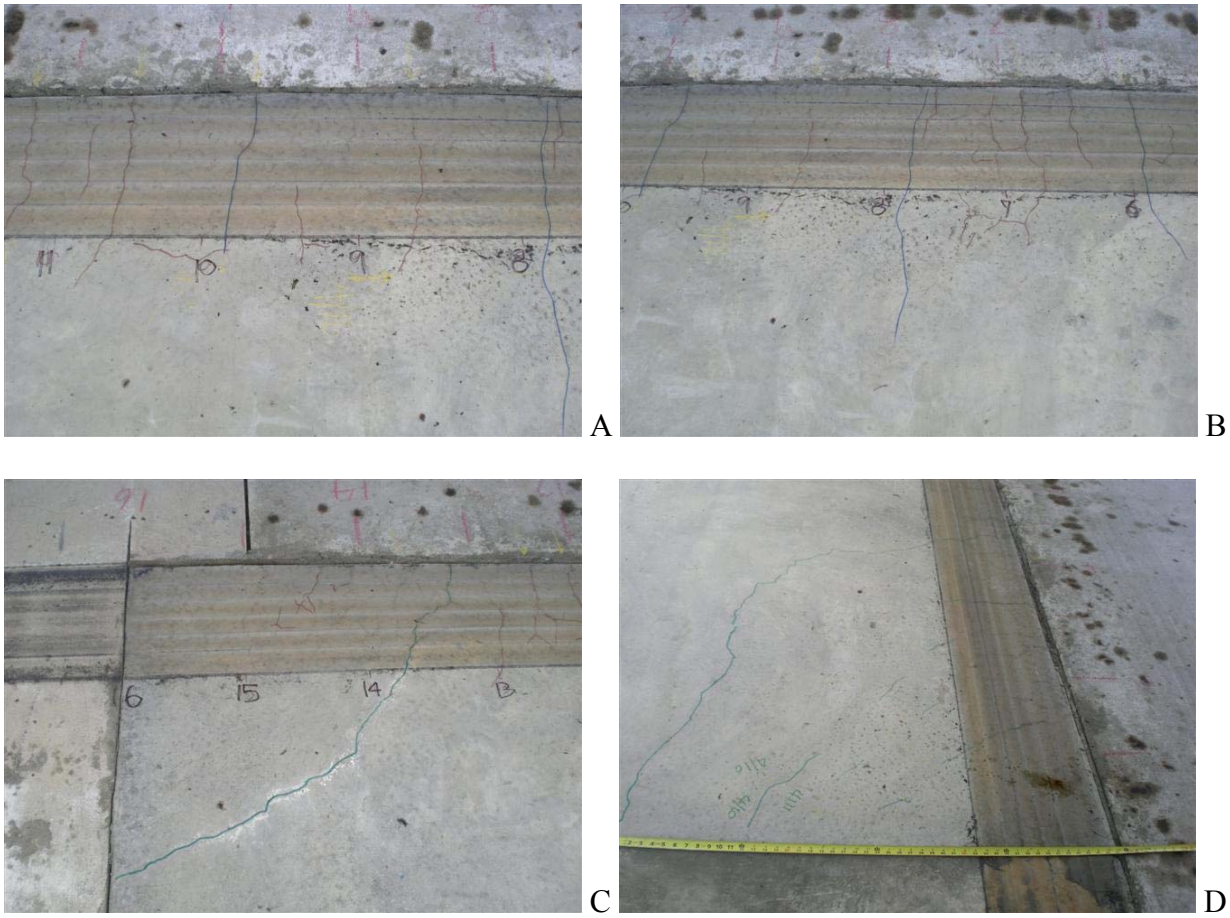

Figure 5-14. Cracks on Test Slab 3. A) First transverse crack 6 feet from the north end. B) Transverse cracks at mid edge. C) Corner crack at the north end. D) Corner crack at the south end.

Crack pattern and locations of the cracks after testing with 18-kip load are shown in Figure 5-15. Figure 5-15-B shows a drawing of the locations of the cracks on this test slab.

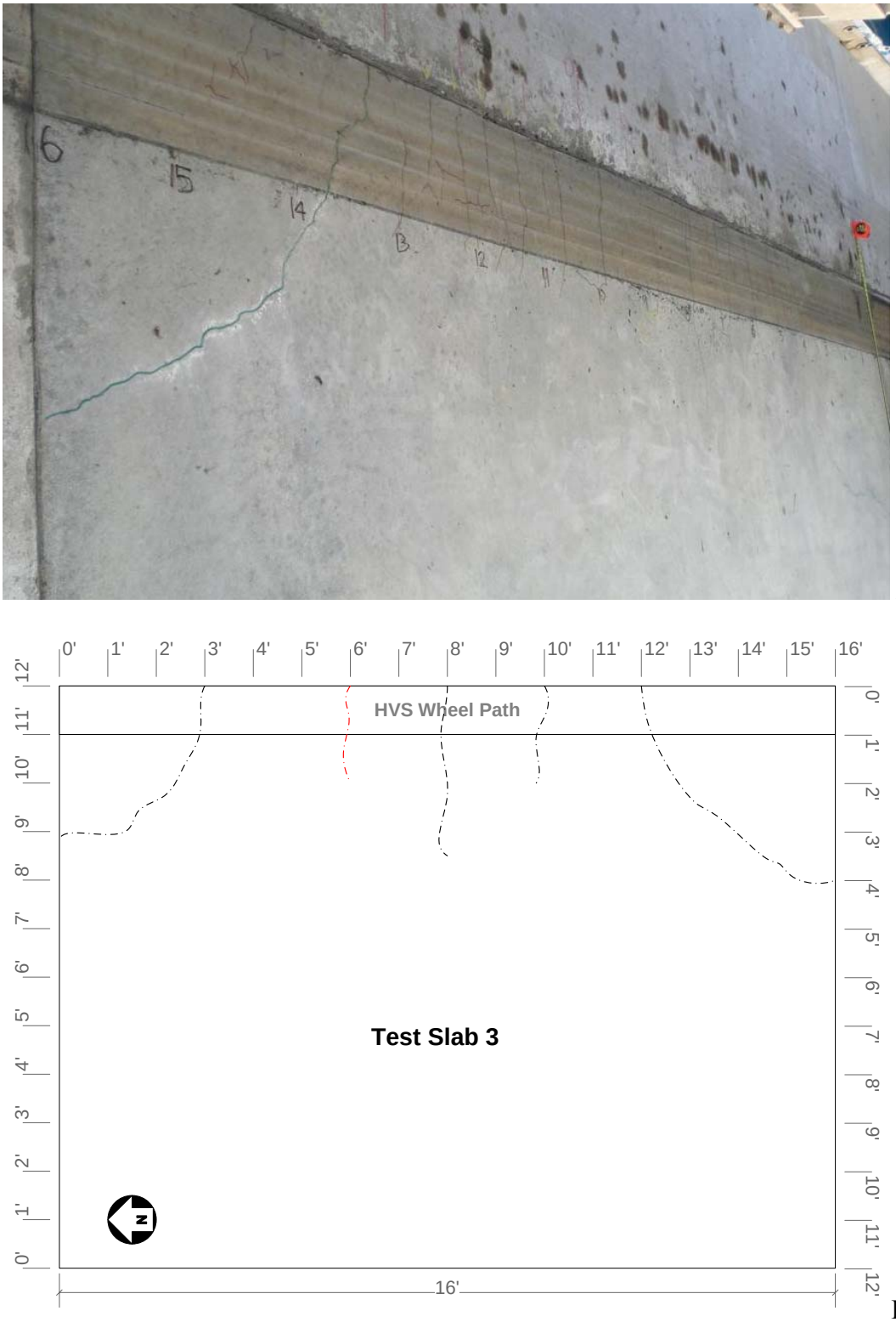

Figure 5-15. Cracks on Test Slab 3. A) Crack Pattern (a corner crack of about 3-feet radius after testing with 15-kip load). B) Locations of cracks.

5.5 Slab 4

5.5.1 Start of HVS Loading on Slab 4

Test Slab 4 used the same concrete mix as that used in Slab 3. HVS loading of Slab 4 was to start when the in-place concrete attained an estimated flexural strength of 300 psi. Therefore, the TTF of the in-place concrete was used to predict the flexural strength of the concrete using the maturity calibration of the concrete from Slab 3. Figure 5-16 shows the relationship between the flexural strength and the TTF of the concrete according to the maturity calibration of the concrete from Slab 3. To attain a flexural strength of 300 psi, the TTF had to be equal or greater than 370 C-hour. Figure 5-17 shows the plot of TTF versus time for the in-place concrete in Slab 4. It can be seen that TTF was equal to 400 C-hour at approximately 7 hours. This would give an estimated flexural strength of over 300 psi. Thus, HVS loading of Slab 4 was started at 7 hours after concrete placement.

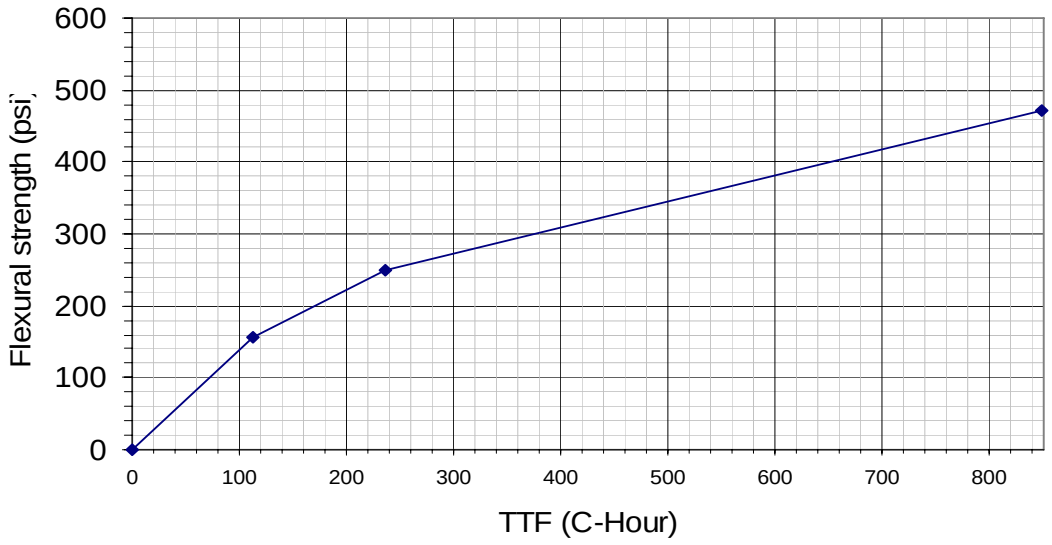

Figure 5-16. Flexural strength vs. TTF for concrete from Slab 3.

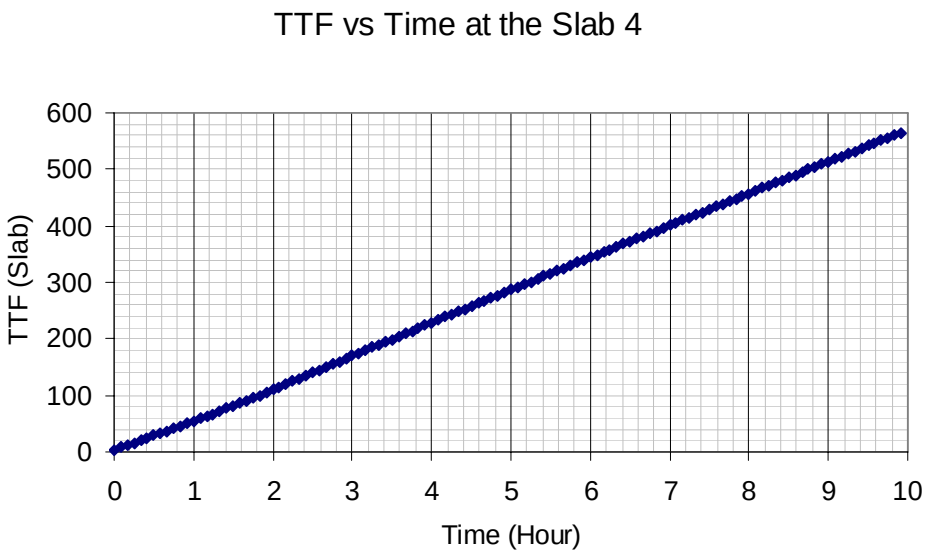

Figure 5-17. TTF vs. Time for In-Place Concrete in Slab 4.

5.5.2 Strength Determination using Maturity Calibration of Concrete Mix from Slab 4

Samples of the concrete mix used in Slab 4 were taken and used to perform the maturity calibration. The maturity calibration of the actual concrete used in Slab 4 was used to determine the strength of the in-place concrete at different times. Figure 5-18 shows the plots of compressive strength and flexural strength versus TTF for the concrete mix used in Slab 4.

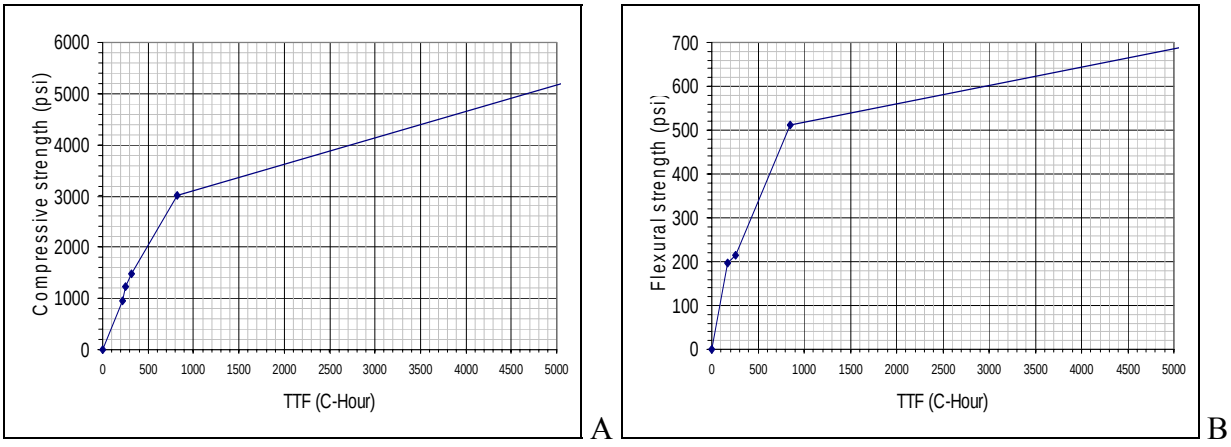

Figure 5-18. Strengths vs. TTF for the Concrete from Slab 4. A) Compressive Strength vs. TTF. B) Flexural Strength vs. TTF.

Table 5-4 shows the compressive strength, flexural strength and TTF of the laboratory cured samples of the concrete from Slab 4, which were used to determine maturity calibration of this mix. Figure 5-19 shows the temperature history of these specimens. Table 5-4 also shows the computed compressive strength and flexural strength of the in-place concrete in Slab 4 by using this maturity calibration.

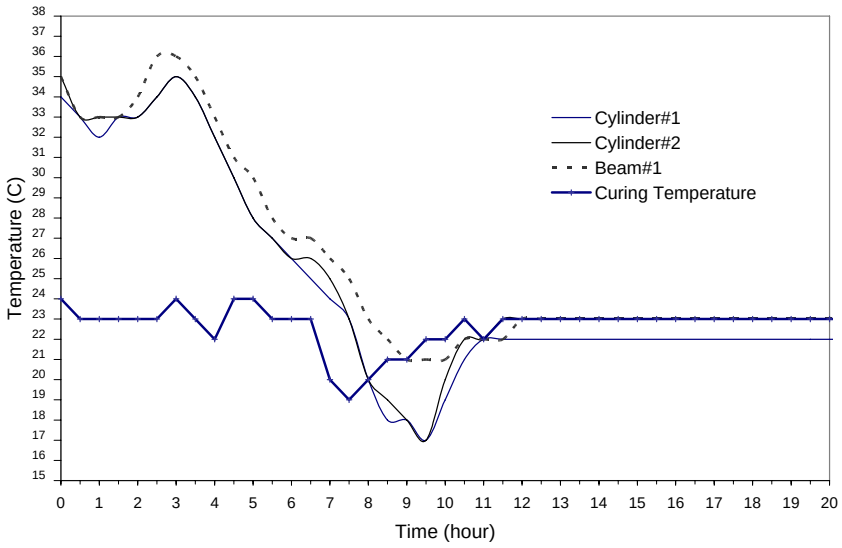

Figure 5-19. Temperature history of the specimens from Slab 4.

Table 5-4. Data for maturity calibration of concrete used in Slab 4.

Time	TTF (Beam)	TTF (Cylinder)	TTF (Slab)	R (Lab)	R (Slab)	f_c (Lab)	f_c (Slab)
4-hour	177.4	173.9	224.0	196	210	-	1,000
5-hour	218.8	214.0	282.2	-	230	952	1,400
6-hour	257.1	251.1	339.5	214.4	250	1218.9	1,500
7-hour	-	-	396.0	-	295 **(305*)**	-	1,700 **(2011*)**
8-hour	328.8	318.8	452.4	-	318	1485.7	1,900
24-hour	853.4	823.4	1,247.9	510.5	530	3023.2	3,190
41-Hour	-	-	2,033.0	-	560	-	3,650
168-hour	5,480.1	5,444.8	7,474.4	707.0	720.0	5388.1	5,500
672-hour	21,658.4	21,610.2	-	-	-	-	-

Note: * -Actual strength of samples placed by the test slab
TTF = time-temperature factor, hr-°C
R = Flexural strengths, psi
f_c = Compressive strengths, psi

Two beam specimens made with the actual concrete mix used in Slab 4 were placed next to the slab in order to have the same curing condition as the test slab. These specimens were tested for their flexural strength at the time of start of loading (7 hours). An average flexural strength of 305 psi was obtained from these samples at 7 hours. This measured flexural strength was very close to the predicted flexural strength value (295 psi) from the maturity calibration of the actual concrete from Slab 4.

5.5.3 Observed Performance of Slab 4

HVS loading of Test Slab 4 was started 7 hours after concrete placement. A 12-kip super single wheel with a tire contact pressure of 120 psi was applied repetitively along the free edge of the slab. On the second day, a corner crack of about 5 feet radius was formed at the south end, as shown in Figure 5-20. It was found out later from the strain data (as described in Chapter 8) that the first crack corner happened at about 41 hours after the placement or after 15,175 passes of 12-kip load. The slab was continuously loaded with the 12-kip load for 7 days with a total load repetition of 82,963 passes. Two 12-inch transverse cracks were observed at the mid-edge of the slab, as shown in Figure 5-21-A. Shrinkage cracks were also observed at about four feet away from the wheel path, as shown in Figure 5-21-B.

The wheel load was then increased to 15 kips, and the slab was loaded for an additional 3 days with an additional 53,420 passes of the 15-kip wheel load. The load was then increased to 18 kips, and the slab was loaded for 2 more days with an additional 18,243 passes. After 2 days of 18-kip loads, a corner crack of 4 feet radius at the north end of the slab and cracks at the mid edge was observed, as shown in Figure 5-22. It is to be noted that the new corner crack and the cracks at the mid edge were at the locations of maximum load-induced stresses according to the stress analyses.

A

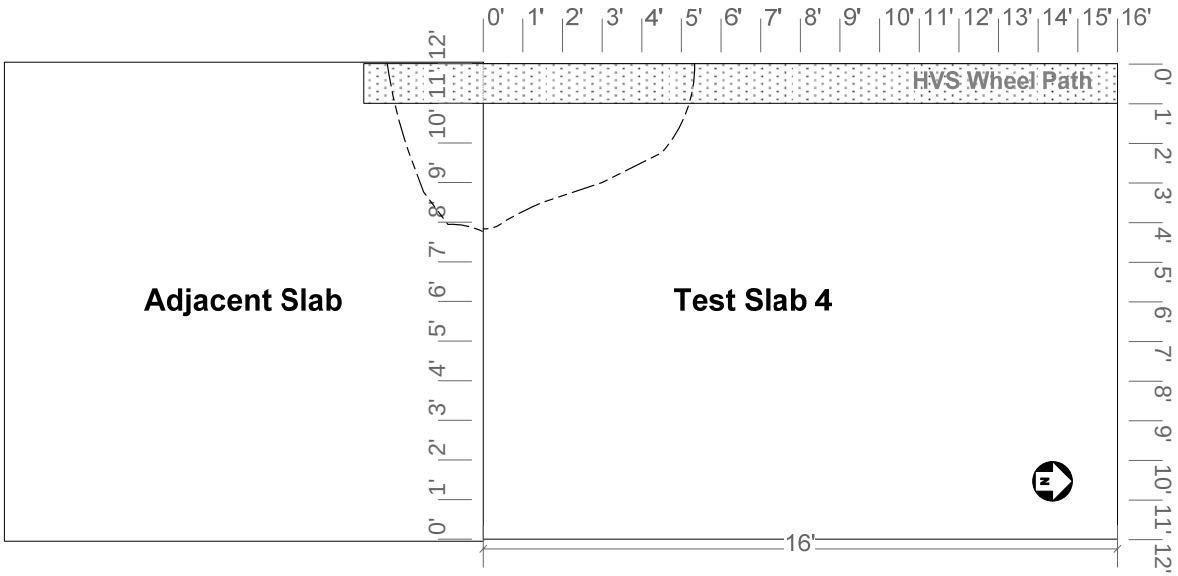

B

Figure 5-20. Cracks on the second day of loading on Test Slab 4. A) First corner crack at the south end. B) Corner cracks at the south end of Slab 4 and the adjacent slab.

A

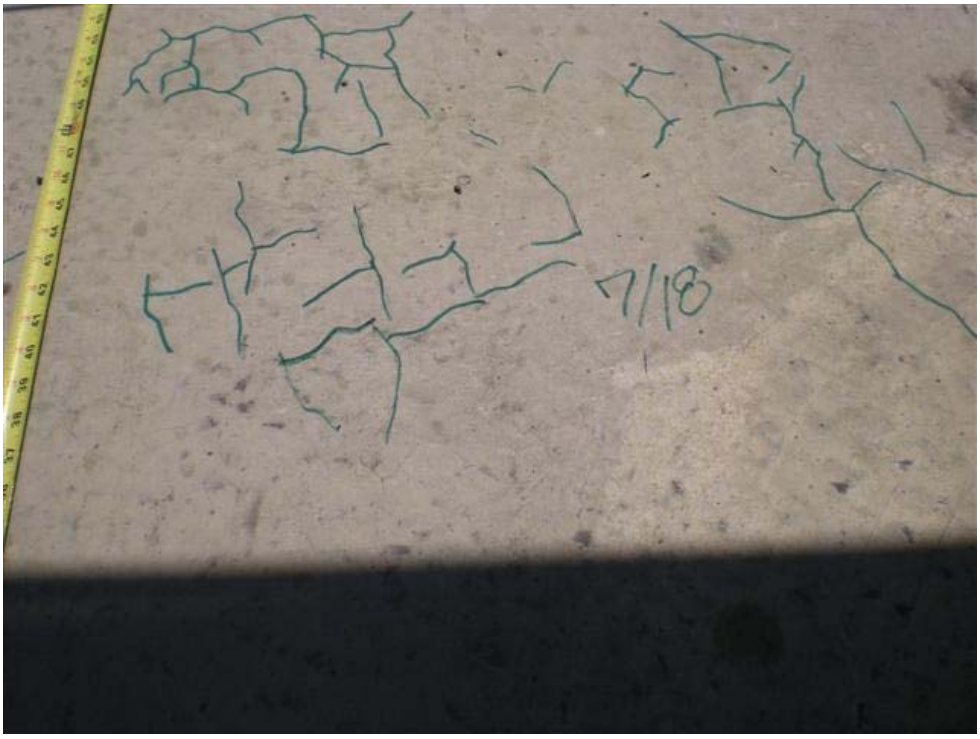

B

Figure 5-21. Cracks in Slab 4 on Day 7. A) Mid-edge cracks after the first corner crack. B) Drying shrinkage cracks at 3 to 4 Feet from the wheel path.

A

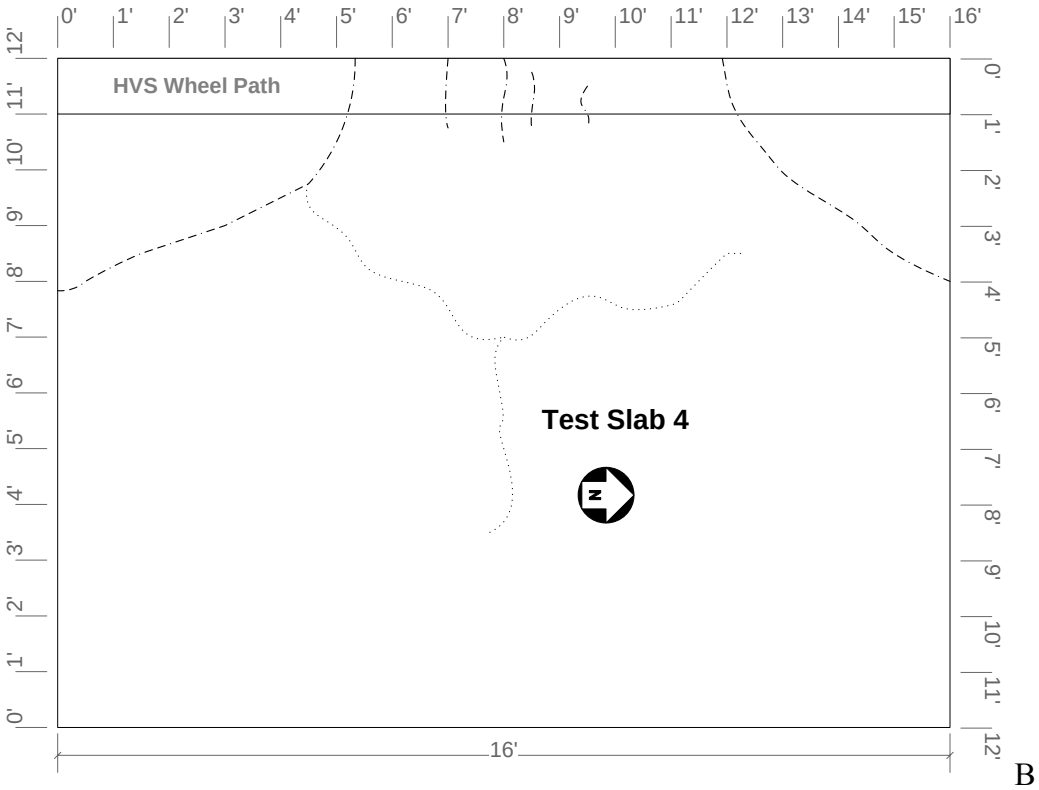

B

Figure 5-22. Cracks after loading with 18-kip wheel load on Test Slab 4. A) Crack pattern. B) Locations of corner and transverse cracks.

5.6 Slab 5

5.6.1 Start of HVS Loading on Slab 5

The concrete used for this Slab 5 had the same mix design as that used in Slabs 3 and 4. HVS loading of Slab 5 was to start when the in-place concrete attained an estimated flexural strength of 300 psi. Therefore, the TTF of the in-place concrete was used to predict the flexural strength of the concrete using the maturity calibration of the concrete from Slab 3 or Slab 4. To attain a flexural strength of 300 psi, the TTF had to be equal or greater than 370 C-hour. Figure 5-23 shows the plot of TTF versus time for the in-place concrete in Slab 5. It can be seen that TTF was equal to 380 C-hour at approximately 7 hours. This would give an estimated flexural strength of over 300 psi. Thus, HVS loading of Slab 5 was started at 7 hours after concrete placement.

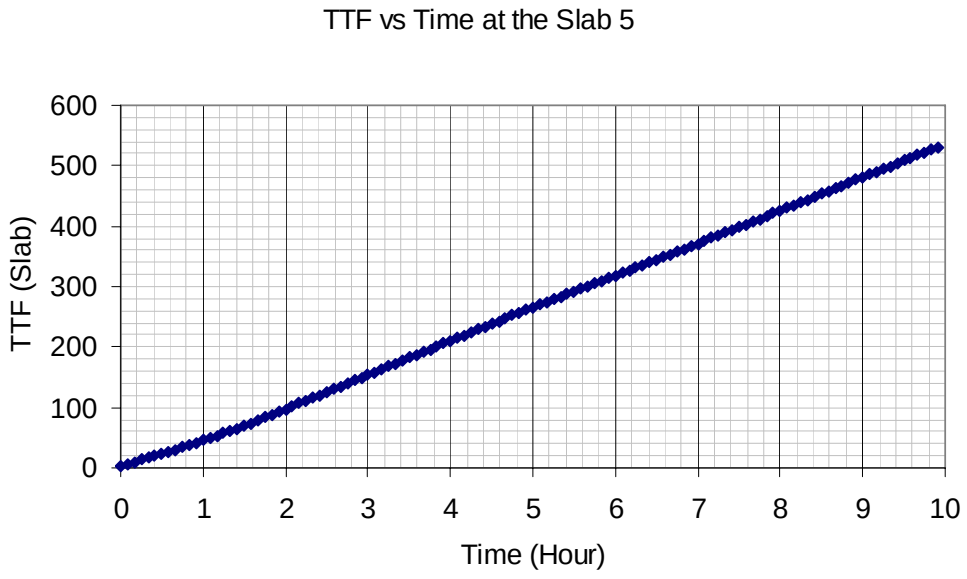

Figure 5-23. TTF vs. Time for In-Place Concrete in Slab 5.

5.6.2 Strength Determination using Maturity Calibration of Concrete Mix from Slab 5

Samples of the concrete mix used in Slab 5 were taken and used to perform the maturity calibration. The maturity calibration of the actual concrete used in Slab 5 was used to determine the strength of the in-place concrete at different times. Figure 5-24 show the plots of compressive strength and flexural strength versus TTF for the concrete mix used in Slab 5.

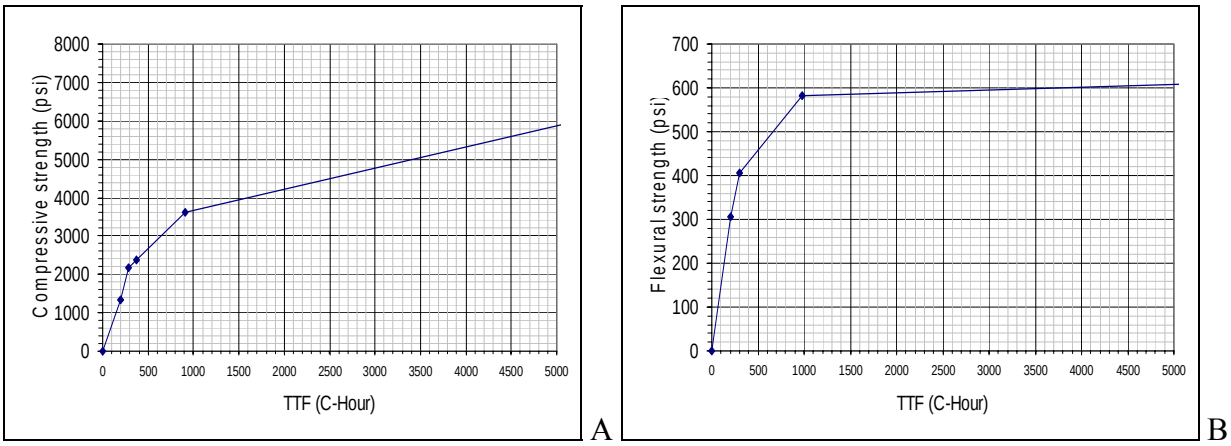

Figure 5-24. Strengths vs. TTF for the Concrete from Slab 5. A) Compressive Strength vs. TTF. B) Flexural Strength vs. TTF.

Table 5-5 shows the compressive strength, flexural strength and TTF of the laboratory cured samples of the concrete from Slab 5, which were used to determine maturity calibration of this mix. Figure 5-25 shows the temperature history of these specimens. Table 5-4 also shows the computed compressive strength and flexural strength of the in-place concrete in Slab 5 by using this maturity calibration.

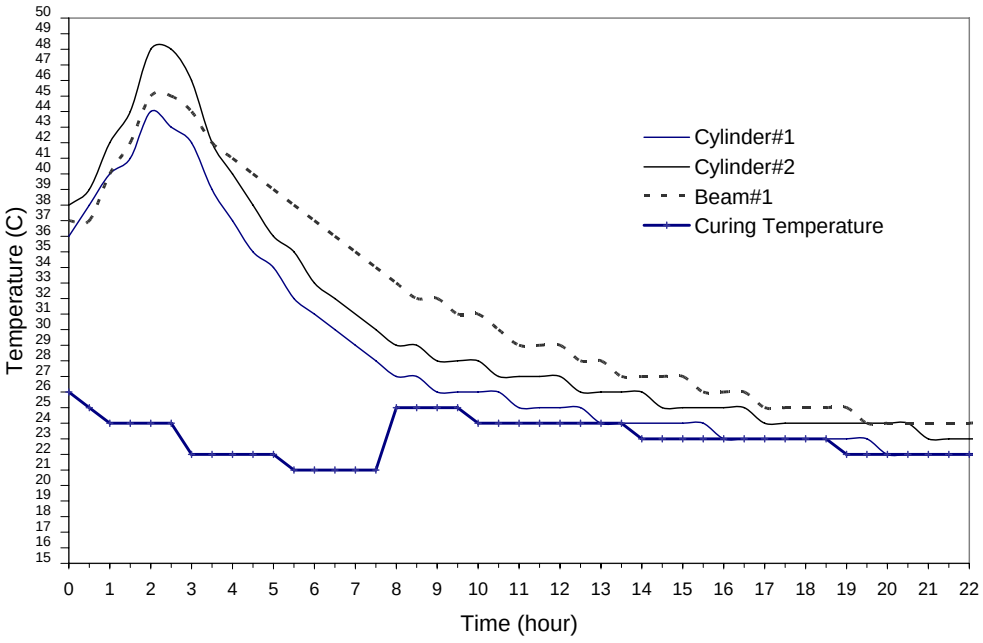

Figure 5-25. Temperature history of the specimens from Slab 5.

Table 5-5. Data for maturity calibration of concrete used in Slab 5.

Time	TTF (Beam)	TTF (Cylinder)	TTF (Slab)	R (Lab)	R (Slab)	f_c (Lab)	f_c (Slab)
4-hour	207.4	202.2	205.8	307.0	305	1,348.8	1350
6-hour	305.6	289.9	314.5	404.8	410	2,161.0	2,250
7-hour	351.7	330.0	366.9	-	420 **(371.1*)**	-	2400 **(2,828.4*)**
8-hour	395.8	368.1	421.2	-	430	2,371.7	2,500
24-hour	983.4	909.4	1192.2	581.9	585	3,623.6	3,800
168-hour	5,606.55	5,524.3	6546.5	612.1	620.0	6,155.9	6,300
672-hour	21,784.95	21,678.2	-	715.6	-	7,463.2	-

Note: * -Actual strength of samples placed by the test slab
TTF = time-temperature factor, hr-°C
R = Flexural strengths, psi
f_c = Compressive strengths, psi

Two beam specimens made with the actual concrete mix used in Slab 5 were placed next to the slab in order to have the same curing condition as the test slab. These specimens were tested for their flexural strength at the time of start of loading (7 hours). An average flexural strength of 371 psi was obtained from these samples at 7 hours. This measured flexural strength was higher than the value of 300 psi as predicted by the maturity calibration of concrete mix samples from Slab 3. However, the predicted flexural strength value (420 psi) at 7 hours matched well with the other predicted strength values from the maturity calibration of the actual concrete from Slab 5.

5.6.3 Observed Performance of Slab 5

HVS loading of Test Slab 5 was started 7 hours after concrete placement. A 12-kip super single wheel with a tire contact pressure of 120 psi was applied repetitively along the free edge of the slab. On the second day, a full-depth transverse crack of about 12 feet along the test slab was formed at the mid-slab, as shown in Figure 5-26. The slab was continuously loaded with the 12-kip load for 7 days with a total load repetition of 81,062 passes. Two longitudinal cracks that separated the test slab into 4 pieces were observed, as shown in Figure 5-27.

The wheel load was then increased to 15 kips, and the slab was loaded for an additional 3 days with an additional 49,748 passes of the 15-kip wheel load. The load was then increased to 18 kips, and the slab was loaded for 2 more days with an additional 22,551 passes. After 2 days of 18-kip loads, an additional 14-inch transverse crack was observed at the mid-edge on the wheel path, as shown in Figure 5-28.

A

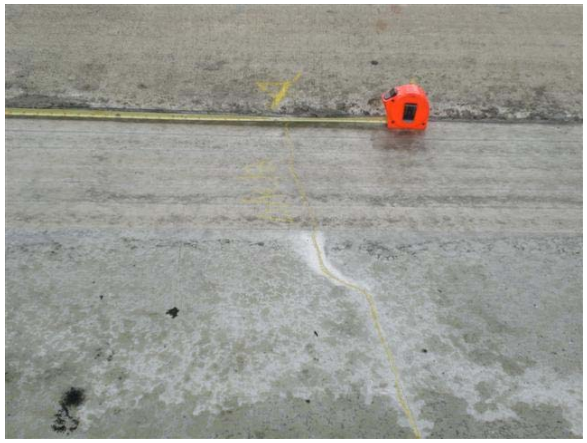

B

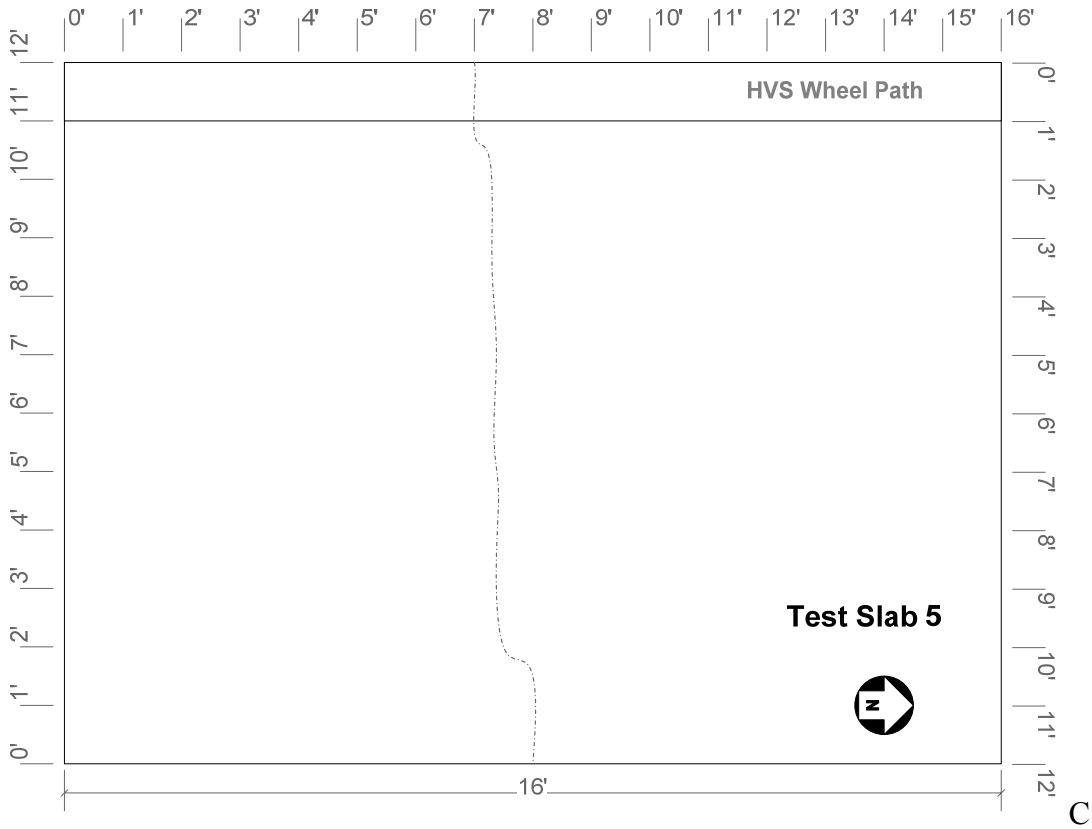

C

Figure 5-26. First crack on Slab 5 in Day 2 after HVS loading. A) First crack observed at the mid-slab. B) First crack on the wheel path at 7 feet from the South End. C) Location of the mid-slab crack.

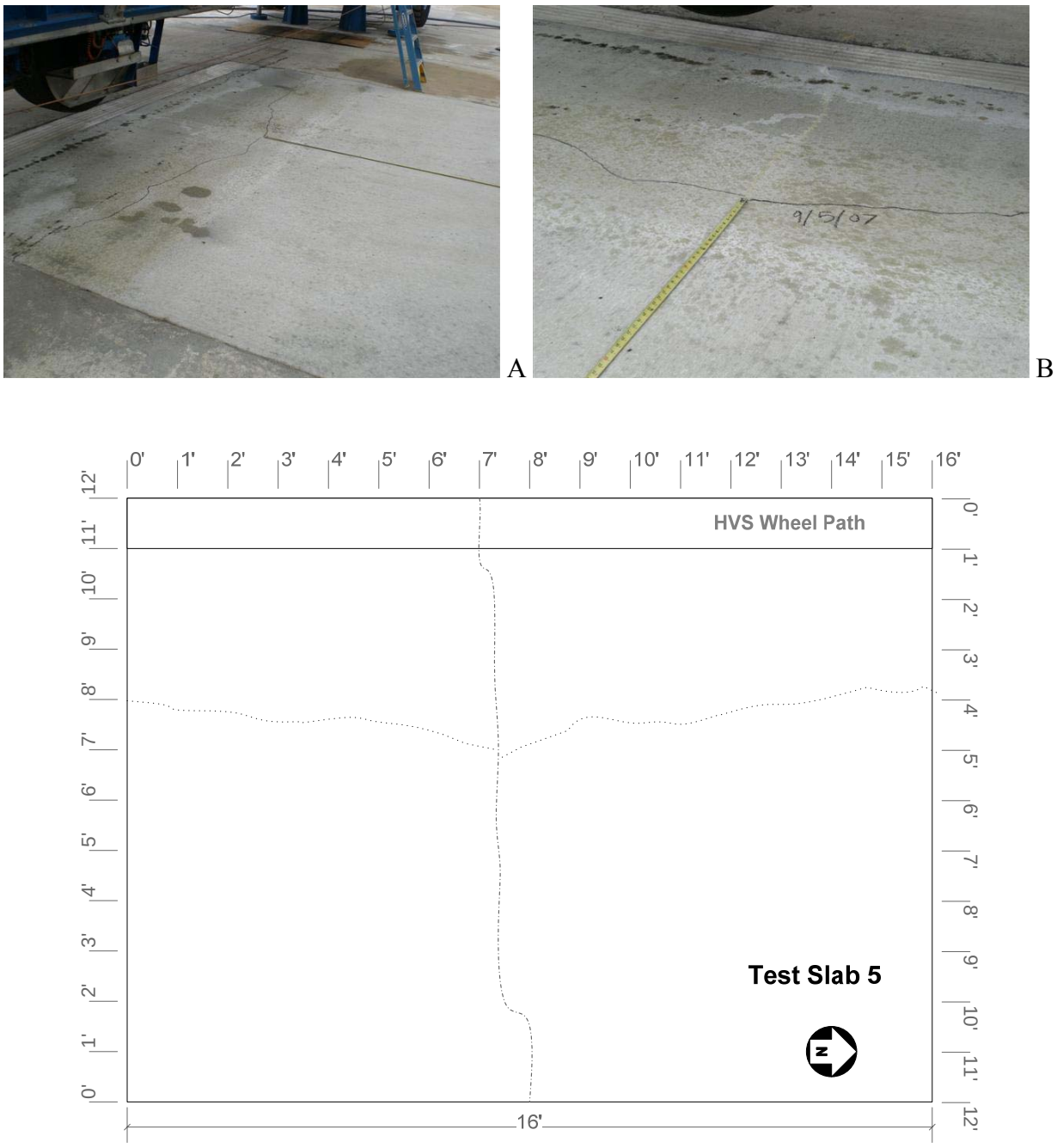

Figure 5-27. Cracks on Slab 5 in Day 7 after HVS loading. A) Cracks observed at the mid-slab. B) Cracks develop from the first crack to both side of the slab. C) Crack pattern.

A

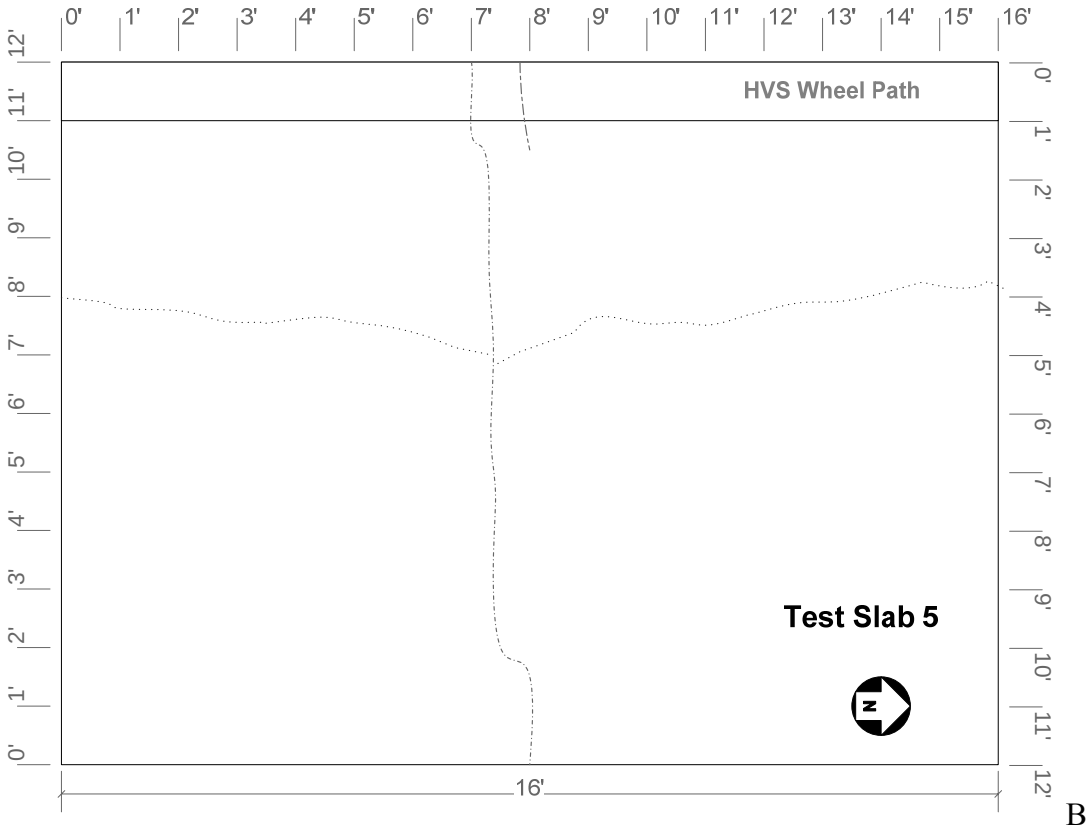

B

Figure 5-28. Cracks on Slab 5 at the finish of HVS testing. A) A 14-inch Transverse crack on the wheel path at the mid-edge. B) Crack pattern.

CHAPTER 6
CHARACTERIZATION OF CONCRETE MIXES AND TEST SLABS

6.1 Characterization of Concrete Mixes

6.1.1 Results of Tests on Concrete

The compressive strength, flexural strength, splitting tensile strength, modulus of elasticity, coefficient of thermal expansion and drying shrinkage of the concrete mixes used in this study are presented this section. The details of the mix designs and test methods are presented in Chapter 3 of this dissertation. The concrete mixes are divided into two groups. The first group of mixes that were to have a target cement content of 850 lb per cubic yard of concrete, they include Mix 1, Mix 3, Slab 1 and Slab 2. The second group includes Mix 2, Slab 3, Slab 4 and Slab 5 which have a target cement content of 725 lb per cubic yard of concrete.

Compressive Strength

The average compressive strengths from three specimens per condition are presented in Table 6-1.

Figure 6-1 shows the plots of average compressive strength at various curing times.

Table 6-1. Average compressive strength of the concrete mixes used.

Curing Time (hours)	Compressive Strength, *fc* (psi)							
	Mix 1	Mix 3	Slab 1	Slab 2	Mix 2	Slab 3	Slab 4	Slab 5
4	798	-	-	891	1,262	-	-	1,349
5	1,125	-	737	993	1,729	563	952	1,755
6	1,453	1,747	1,223	1,095	2,195	1,076	1,219	2,161
8	1,730	2,019	1,642	1,560	2,526	1,240	1,486	2,372
24	3,941	4,199	3,631	3,225	3,891	3,370	3,023	3,624
168	5,792	5,746	5,634	5,951	6,082	5,324	5,388	6,156
672	6,469	6,220	6,429	6,647	6,649	6,810	6,921	7,463

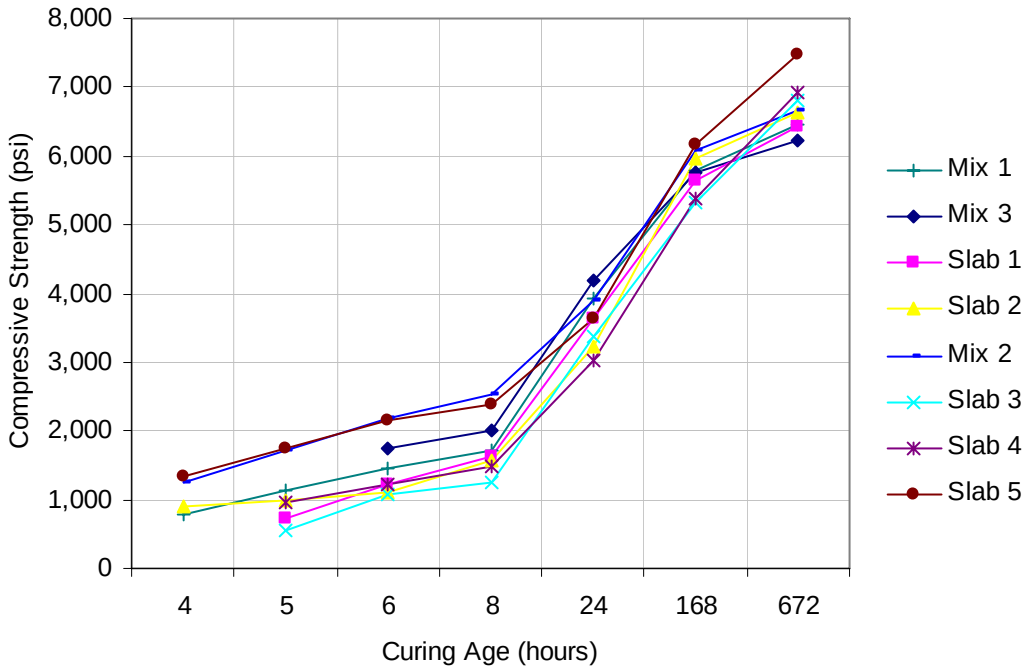

A

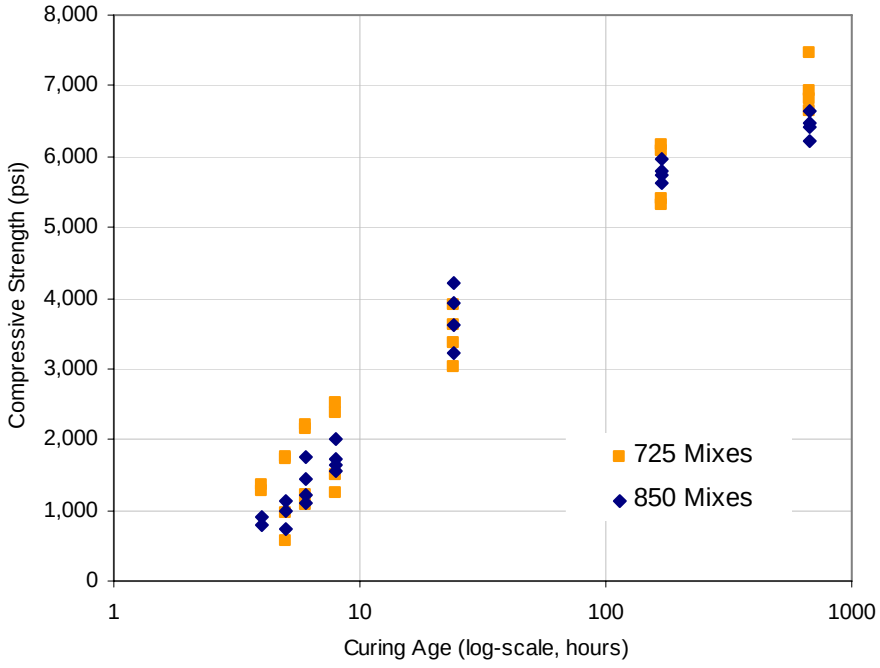

B

Figure 6-1. Compressive Strength at various times of all concrete mixes in this study. A) Average compressive strengths by each mix. B) Average compressive strengths grouped by cement content vs. curing age in log scale.

Flexural Strength

The average flexural strengths from two beams per curing time of two laboratory-prepared mixes, namely Mixes 1 and 2, and of five concrete mixes used in test slabs, namely Slabs 1, 2, 3, 4 and 5 are presented in Table 6-2. Figure 6-2 shows also the plots of average flexural strength of all these mixes at various curing times.

Table 6-2. Average flexural strength of the concrete mixes used.

Curing Time (hours)	Flexural Strength, f_R (psi)						
	Mix 1	Slab 1	Slab 2	Mix 2	Slab 3	Slab 4	Slab 5
4	250	-	-	266	187	196	307
5	319	-	-	358	219	205	356
6	388	292	390	450	250	214	405
24	607	592	576	686	472	511	582
168	740	762	724	831	556	707	612
672	770	801	775	887	805	819	716

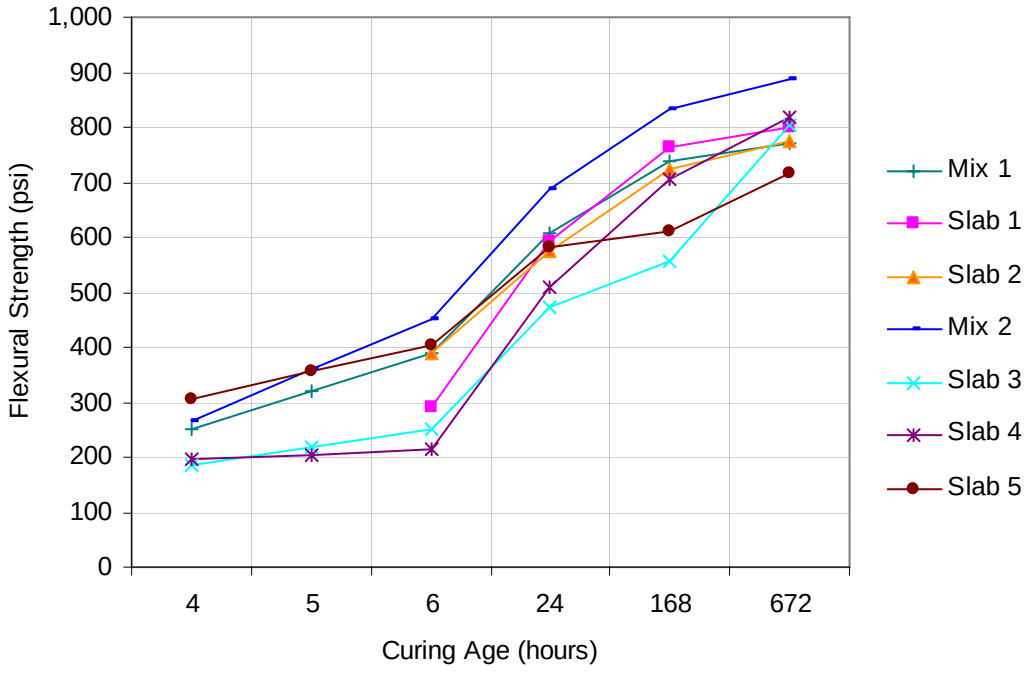

Figure 6-2. Average compressive strength of all mixes evaluated at various curing times.

Typical facture surfaces of a beam specimen are shown in Figure 6-3. It shows that at the early age (about 4 to 6 hours), at the breaking area, only some aggregate are fractured. At the later age, most aggregate are fractured at the breaking area.


A

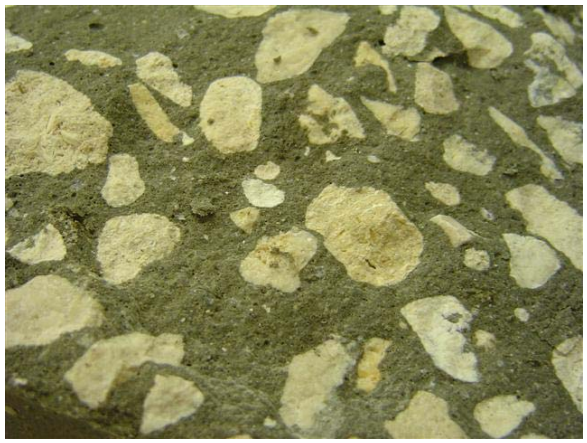
B

Figure 6-3. Typical facture of a beam. A) Beam facture at the early age (only some aggregate cut at the breaking area). B) Beam facture at the later age (most aggregate cut at the breaking area).

Splitting Tensile Strengths

The average splitting tensile strengths from three cylinders per curing time of five concrete mixes used in test slabs, namely Slabs 1, 2, 3, 4 and 5 are presented in Table 6-3. Figure 6-4 shows also the plots of average splitting tensile strength at various curing times.

Table 6-3. Average splitting tensile strength of the concrete mixes used.

Curing Time (hours)	Splitting Tensile Strength, f_{ST} (psi)				
	Slab 1	Slab 2	Slab 3	Slab 4	Slab 5
6	141	187	134	173	251
24	248	322	289	317	392
168	325	418	449	589	529
672	385	472	560	678	585

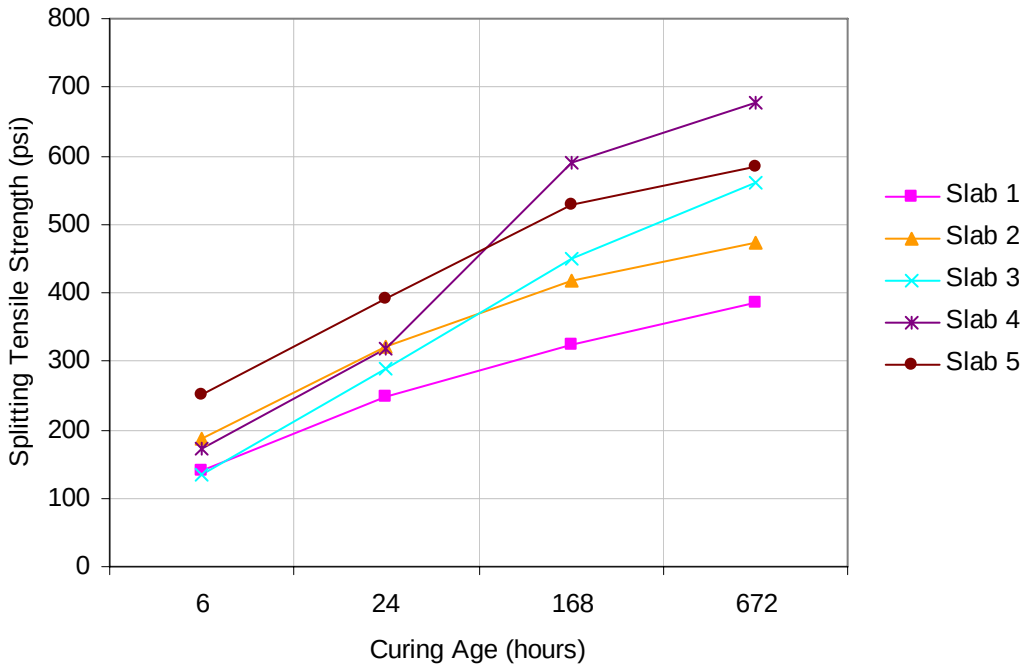

Figure 6-4. Average splitting tensile strength of all mixes evaluated at various curing times.

Modulus of Elasticity Test Results

The average elastic modulus from two cylinders (or four readings) per curing time of a laboratory-prepared Mix 1, and, of five concrete mixes used in test slabs, namely Slabs 1, 2, 3, 4 and 5 are presented in Table 6-4. Figure 6-5 shows the plots of average elastic modulus at various curing times.

Table 6-4. Average elastic modulus of the concrete mixes used.

Curing Time (hours)	Modulus of Elasticity, *E* (ksi)					
	Mix 3	Slab 1	Slab 2	Slab 3	Slab 4	Slab 5
4	-	-	1,047	-	-	1,900
5	-	739	1,129	1,288	1,600	2,238
6	1,800	1,434	1,211	1,563	1,763	2,575
8	1,961	1,559	1,700	1,813	1,925	2,875
24	3,250	2,662	1,913	2,813	3,150	3,563
168	3,800	3,481	3,470	3,250	3,488	3,863
672	4,413	3,752	3,825	3,650	3,875	4,288

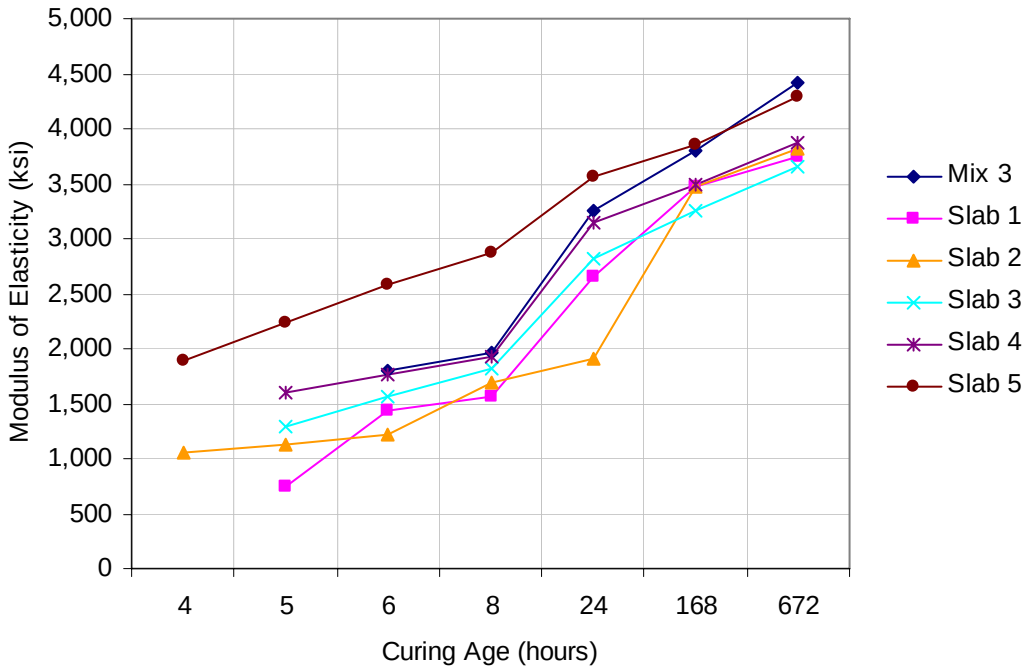

Figure 6-5. Elastic modulus at various curing times.

Drying Shrinkage Test Results

The average drying shrinkage strain from three square prisms per curing time of two laboratory-prepared Mixes 3 and 2, and of three concrete mixes used in test slabs, namely Slabs 3, 4 and 5 are presented in Table 6-5. Figure 6-6 shows the plots of average drying shrinkage strain at various curing times.

Table 6-5. Drying shrinkage strains of the concrete mixes used.

Curing Time (hours)	Drying Shrinkage Strain, ε_{sh} (in/in 10^{-6})				
	Mix 3	Mix 2	Slab 3	Slab 4	Slab 5
6	0.00	0.00	0.00	0.00	0.00
8	10.00	20.00	43.33	23.33	50.00
24	46.67	23.33	96.67	53.33	113.33
168	263.33	240.00	246.67	240.00	303.33
672	420.00	393.33	436.67	523.33	440.00

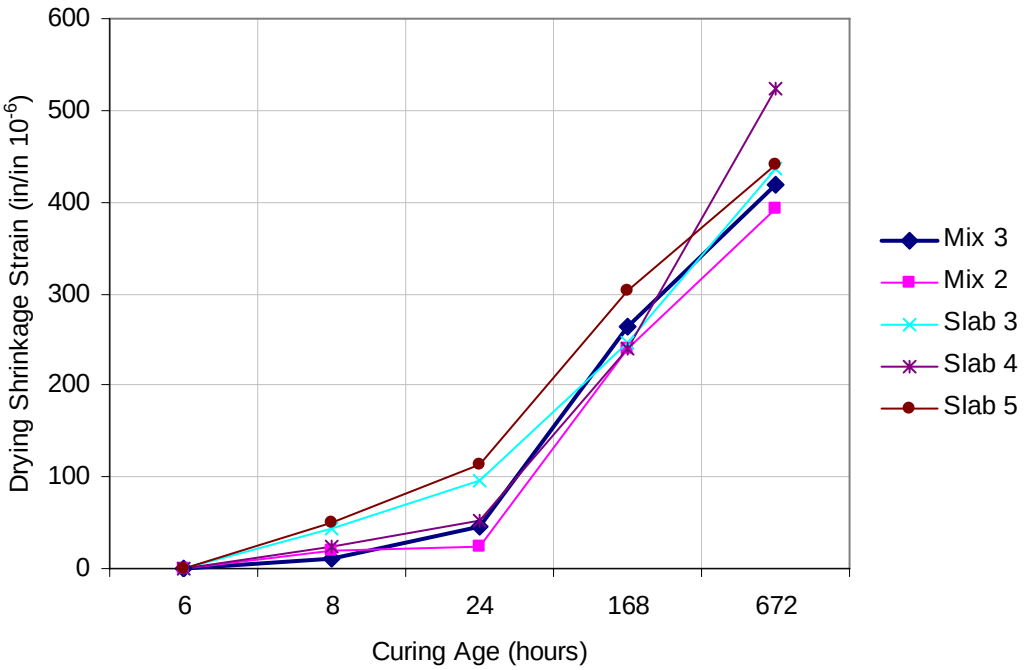

Figure 6-6. Drying shrinkage strains at various curing times.

Coefficient of Thermal Expansion

The average coefficient of thermal expansion from three cylinder specimen (or six readings) per curing time of two laboratory-prepared Mixes 3 and 2, and of five concrete mixes used in test slabs, namely Slabs 1, 2, 3, 4 and 5 are presented in Table 6-6. Figure 6-7 shows the plots of average coefficient of thermal expansion at various curing times.

Table 6-6. Coefficient of thermal expansion of the concrete mixes used.

Curing Time (hours)	Coefficient of Thermal Expansion, *CTE* (in/ºF 10^{-6})						
	Mix3	Slab 1	Slab 2	Mix 2	Slab 3	Slab 4	Slab 5
24	5.97	-	6.75	6.36	6.28	6.46	6.27
168	6.01	6.15	7.01	6.13	6.18	6.13	6.07
672	5.98	-	6.76	5.93	6.14	5.99	5.89

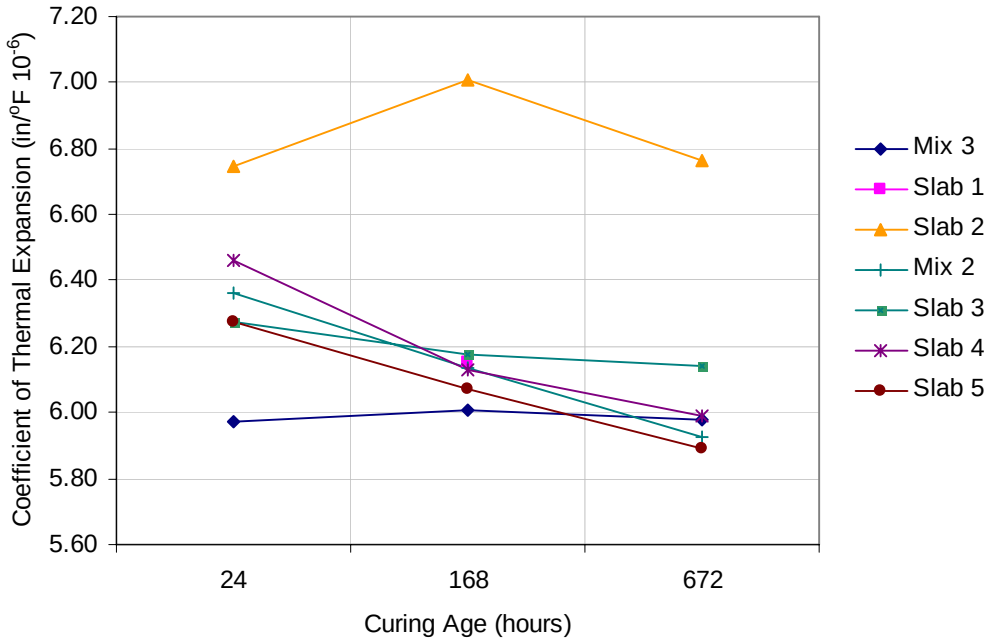

Figure 6-7. Coefficient of thermal expansion of the concrete mixes used.

6.1.2 Relationship among the Concrete Properties

Using the limited data from the mixes in this study, the relationships among the compressive strength, elastic modulus, flexural strength and splitting tensile strength of the concrete used were determined.

Since compressive strength of concrete is a common property to be obtained and considered in structural design, compressive strength is related to other concrete properties.

Relationship between Compressive Strength and Flexural Strength

The relationship between compressive strength and the flexural strength was developed, and plotted in Figure 6-8. Regression equation 6-1 was developed to present the best fit relationship between compressive strength and flexural strength. the ACI equation for this purpose is shown in equation 6-2.

Regression equation: $R = 5.3936 \times f_c^{0.5655}, R^2 = 0.9203$ (6-1)

ACI equation: $R = A \times f_c^B, A = 7.5, B = 0.5$ (6-2)

Or $R = 7.5 \times f_c^{0.5}$

Where: R = Flexural strength, in psi
f_c = Compressive strength, in psi
A, B = Coefficients

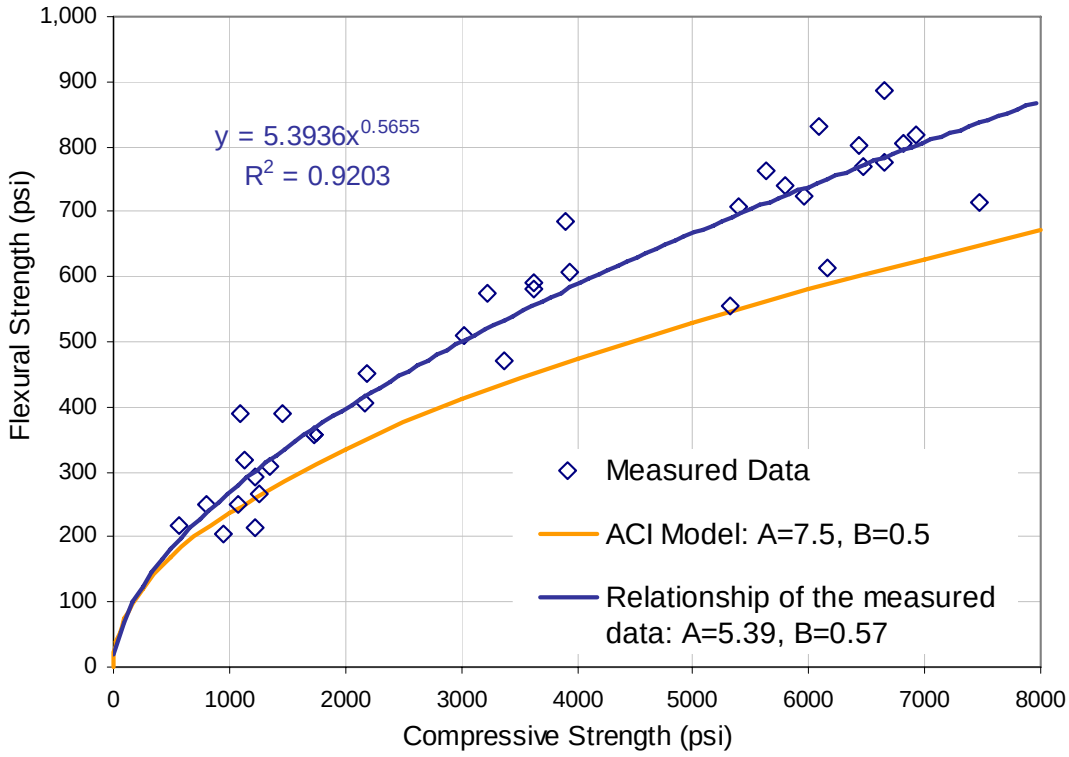

Figure 6-8. Relationship between compressive strength and flexural strength.

The power exponent (Coefficient B) of regression equation 6-1 is a little bit higher than the recommended coefficient B from equation 6-2, and coefficient A from equation 6-1 is also higher than that from equation 6-2. From the plots, it can be seen that using the recommended values A and B from the equation 6-3 may underestimate the flexural strength based on the experimental data in this study.

Relationship between Compressive Strength and Splitting Tensile Strength

The relationship between splitting tensile strength and compressive strength was plotted in Figure 6-9. Regression equation 6-3 was developed to present the best fit relationship between compressive strength and splitting tensile strength.

Regression equation: $f_{ct} = 1.3983 \times f_c^{0.6691}, R^2 = 0.8682$ (6-3)

Where: f_{ct} = Splitting tensile strength, in psi
f_c = Compressive strength, in psi

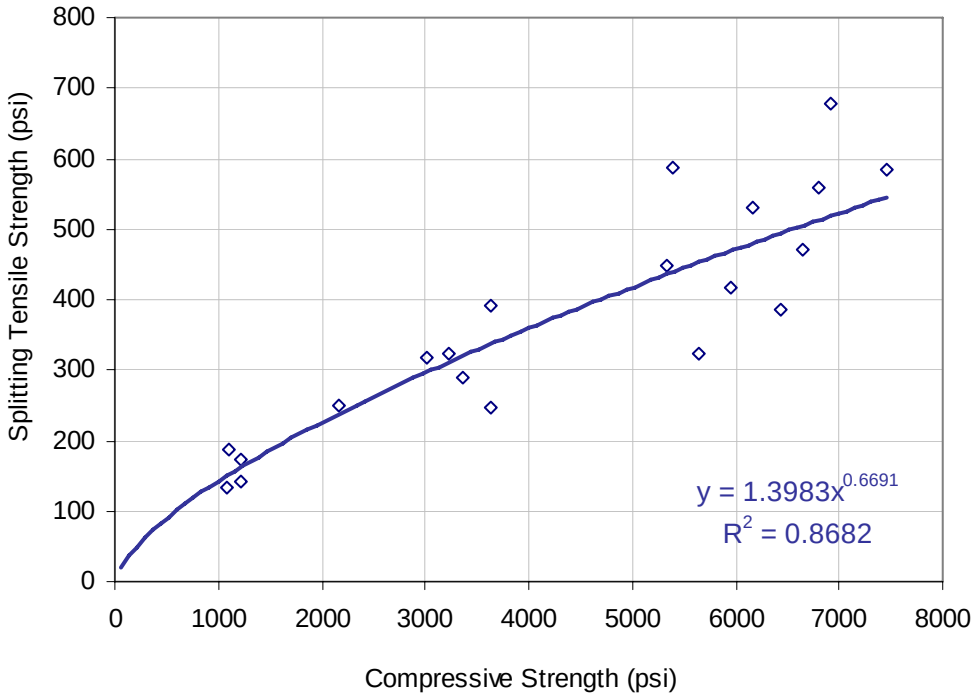

Figure 6-9. Relationship between compressive strength and splitting tensile strength.

Relationship between Splitting Tensile Strength and Flexural Strength

The relationship between flexural strength and splitting tensile strength was similarly plotted in Figure 6-10. Regression equation 6-4 was developed to present the best fit relationship between splitting tensile strength and flexural strength.

Regression equation: $R = 7.9828 \times f_{ct}^{0.7247}, R^2 = 0.7693$ (6-4)

Where: R = Flexural strength, in psi

f_{ct} = Splitting tensile strength, in psi

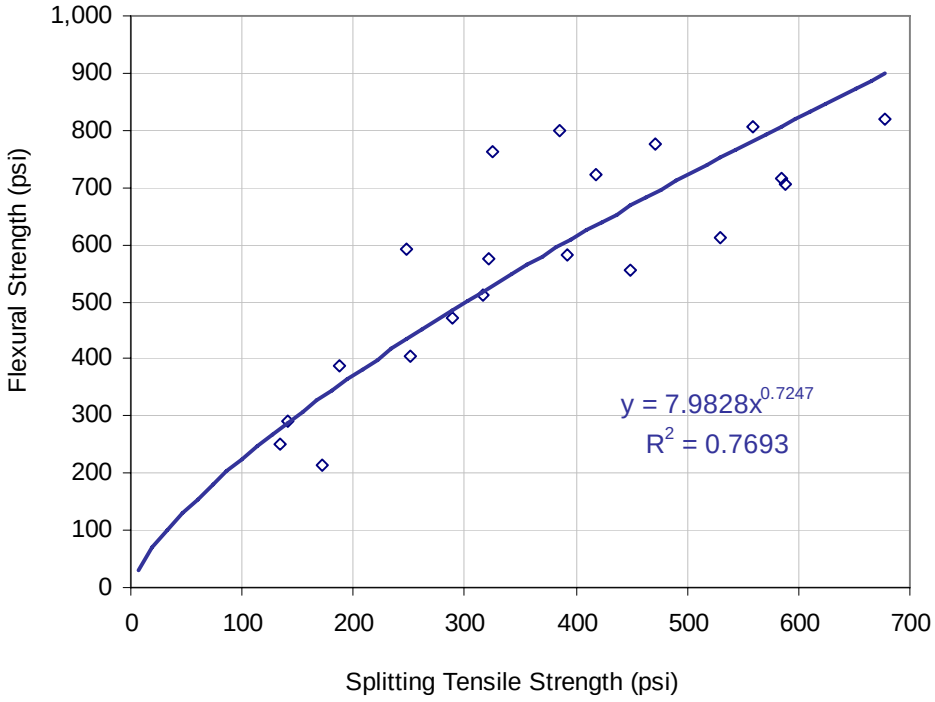

Figure 6-10. Relationship between splitting tensile strength and flexural strength.

Relationship between Compressive Strength and Modulus of Elasticity

The modulus of elasticity is an important material property that affects the stress/strain behavior of the concrete slab, and is a needed input to the FEACONS model. Having enough experimental data to develop the reliable relationship between compressive strength and modulus of elasticity for slab replacement concrete mixes is needed to analyze the stress/strain behavior of the concrete slabs.

The relationship between compressive strength and the modulus of elasticity was developed, and plotted in Figure 6-11. Regression equation 6-5 was developed to present the best fit relationship between compressive strength and modulus of elasticity. This is compared with the ACI equation (6-6 through 6-8) for this purpose.

Regression equation: $E = 28.802 \times f_c^{0.5606}, R^2 = 0.8801$ (6-5)

ACI equation: $E = \frac{A \times w^{1.5}}{1{,}000} \times f_c^{B}, A = 33, B = 0.5, w = 140$ (6-6)

$$E = \frac{33 \times (140)^{1.5}}{1{,}000} \times f_c^{0.5} \quad (6\text{-}7)$$

$$E = 54.665 \times f_c^{0.5} \quad (6\text{-}8)$$

Where: E = Elastic modulus, in ksi
f_c = Compressive strength, in psi
w = Unit weight, in pci
A, B = Coefficients

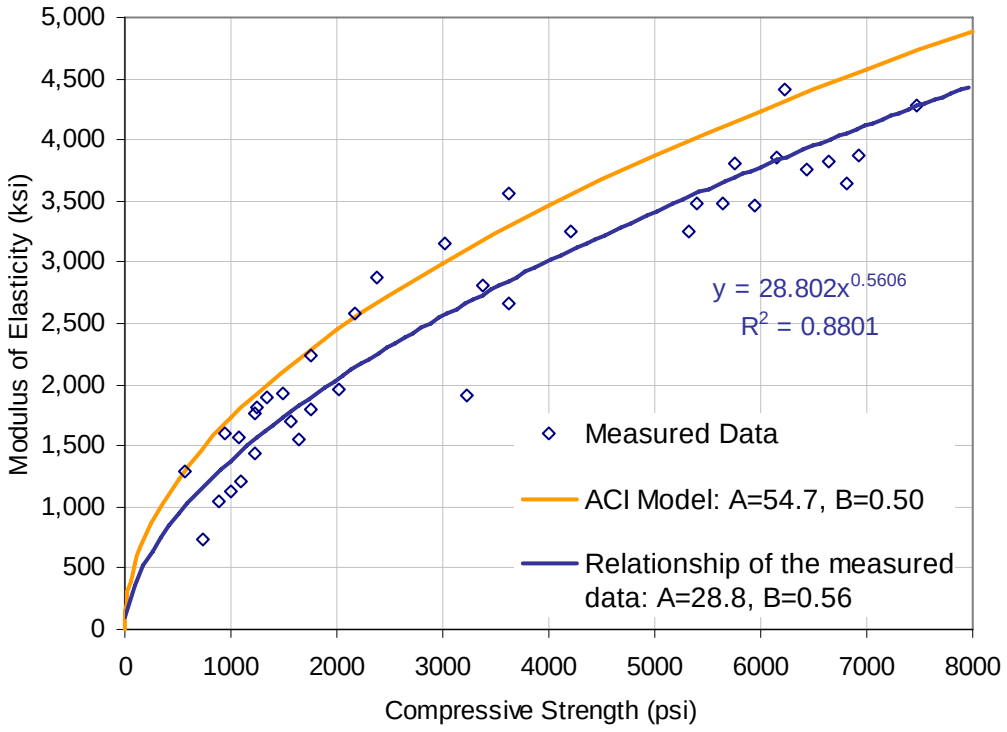

Figure 6-11. Relationship between compressive strength and elastic modulus.

The power exponent (Coefficient B) of regression equation 6-5 is a little higher than the recommended coefficient B from equation 6-8, and first constant from equation 6-5 is also higher than that from the equation 6-8. From these plots, it can be seen that using the recommended values A and B from equation 6-8 may overestimate the elastic modulus of the concrete based on the experimental data in this study.

Relationship between Compressive Strength and Drying Shrinkage Strain

A relationship between compressive strength and drying shrinkage strain was developed, and plotted in Figure 6-12. Regression equation 6-9 was developed to present the best fit relationship between compressive strength and drying shrinkage strain.

Regression equation: $\varepsilon_{sh} = 8.6286 \cdot e^{0.0006 \cdot f_c}, R^2 = 0.8193$ (6-9)

Where: ε_{sh} = Drying shrinkage strain, in in/in $x10^{-6}$
f_c = Compressive strength, in psi

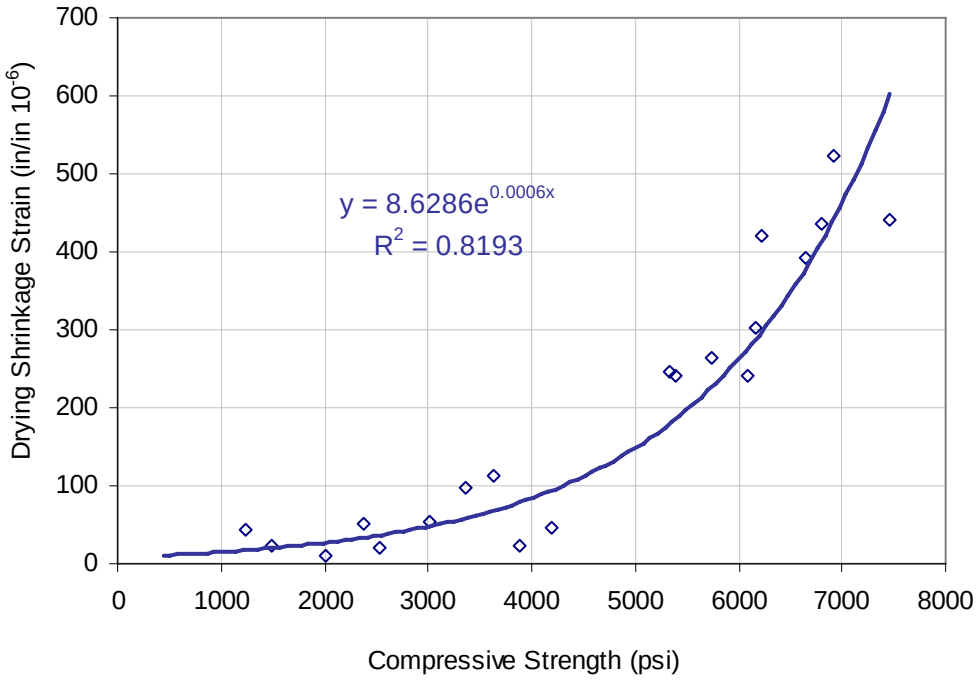

Figure 6-12. Relationship between compressive strength and drying shrinkage strain.

Relationship between Modulus of Elasticity and Drying Shrinkage Strain

The relationship between elastic modulus and drying shrinkage strain is shown in Figure 6-13. Regression equation 6-10 was developed to present the best fit relationship between modulus of elasticity and drying shrinkage strain.

Regression equation: $\varepsilon_{sh} = 1.6734 \cdot e^{0.0014 \cdot f_c}, R^2 = 0.8792$ (6-10)

Where: ε_{sh} = Drying shrinkage strain, in in/in $x10^{-6}$

f_c = Compressive strength, in psi

From the experimental data in this study, it shows that the relationship between elastic modulus and drying shrinkage strain gives a little bit better fit than the relationship between compressive strength and drying shrinkage strain.

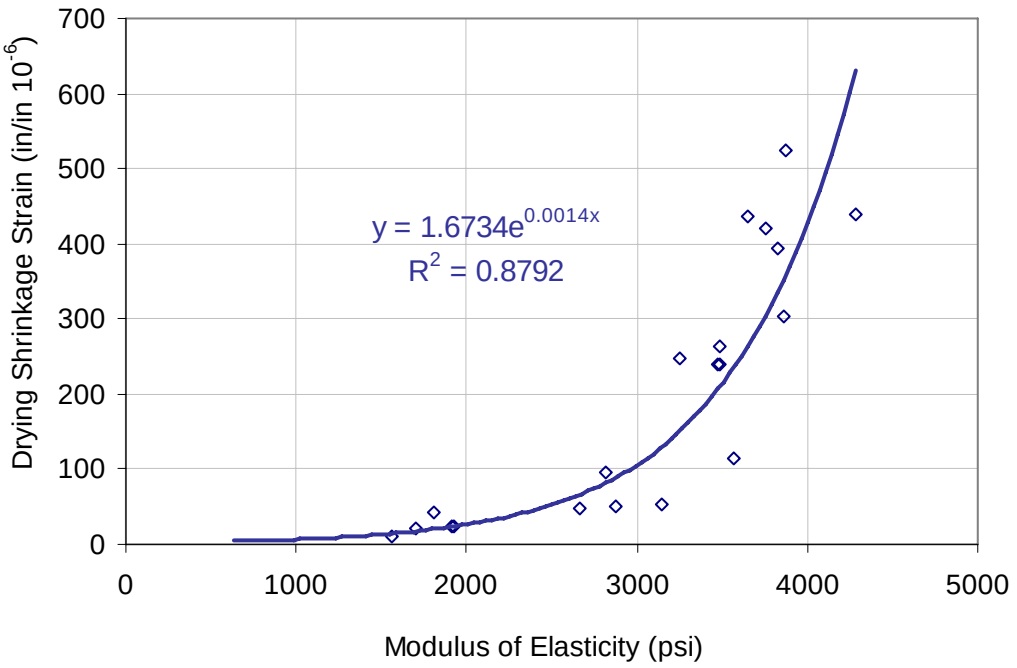

Figure 6-13. Relationship between modulus of elasticity and drying shrinkage strain.

6.2 Slab Characterization

Five test slabs were evaluated in this study. The characterization of the test slabs are presented in this section by means of temperature data, joint movement measurement, FWD testing and core testing. Figure 6-14 shows a plan view of typical location and configuration of a test slab confined with adjacent slabs.

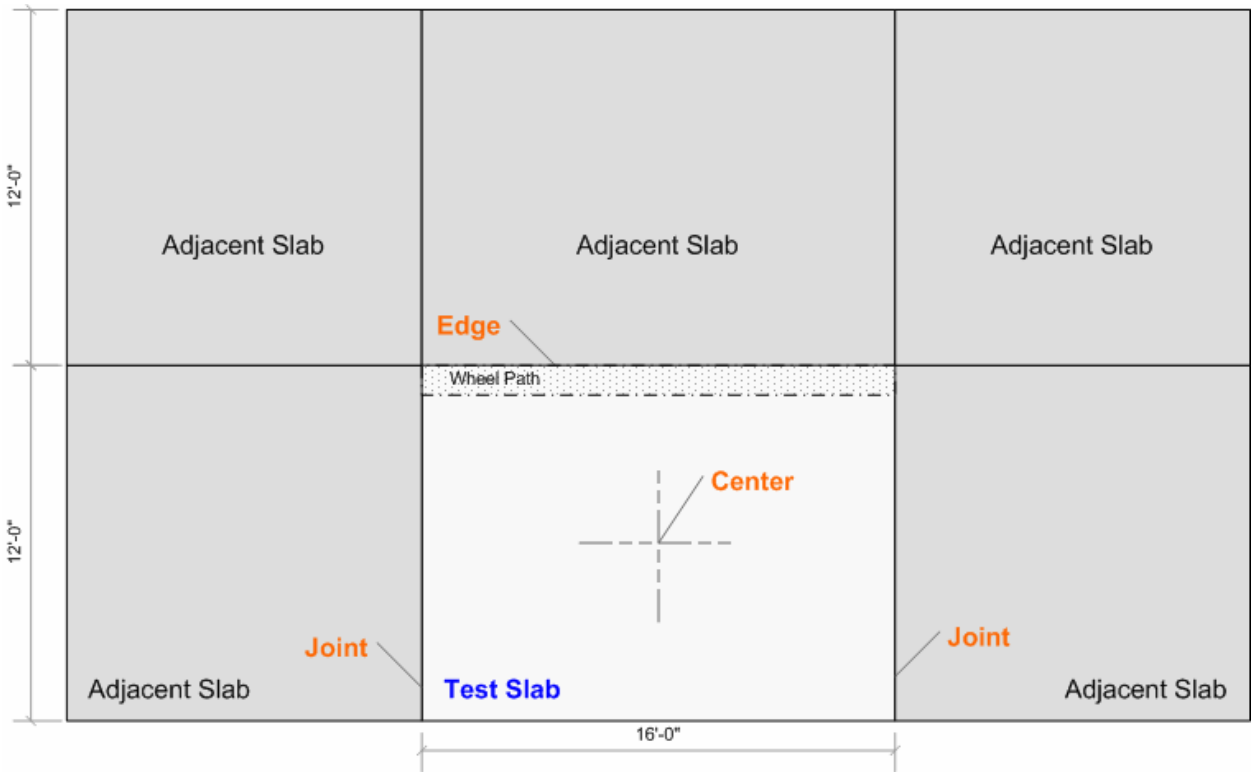

Figure 6-14. Plan view of the typical location and configuration of a test slab.

6.2.1 Analysis of Temperature Data

Thermocouples in the instrumentation plan (see detail in Chapter 4) were placed in three locations as shown in Figure 6-15, namely (1) the slab corner on the side of the slab not loaded by the HVS wheel, (2) the slab corner on the wheel path, and (3) the slab center. At each location, six thermocouples were placed at 0.5, 2.5, 4.5, 6.5, 8.5 inches from the concrete surface and at 1 inch below the surface of the asphalt base as shown in Figure 6-16.

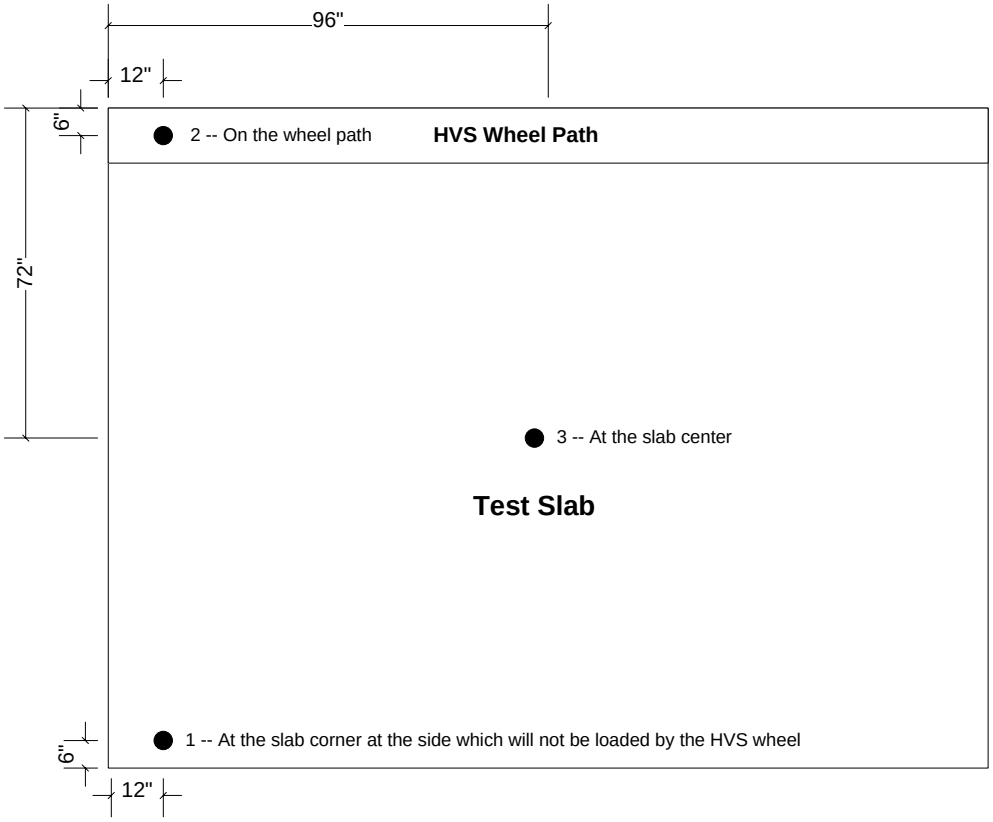

Figure 6-15. Plan view of locations of thermocouples.

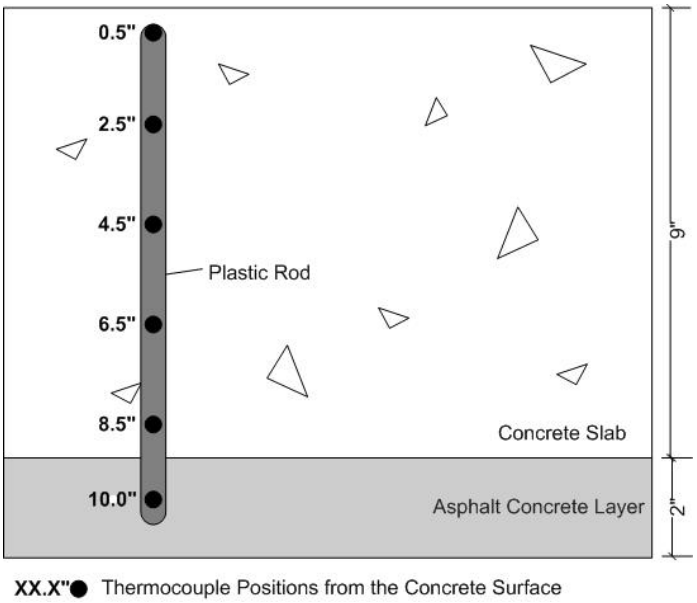

Figure 6-16. Vertical positions of thermocouples.

Temperature differentials in the concrete slab (as calculated from the temperature at 0.5" from the top of the slab the temperature at the base layer) slab are plotted against time for Slabs 1, 2, 3, 4 and 5 in Figures 6-17 to 6-21, respectively.

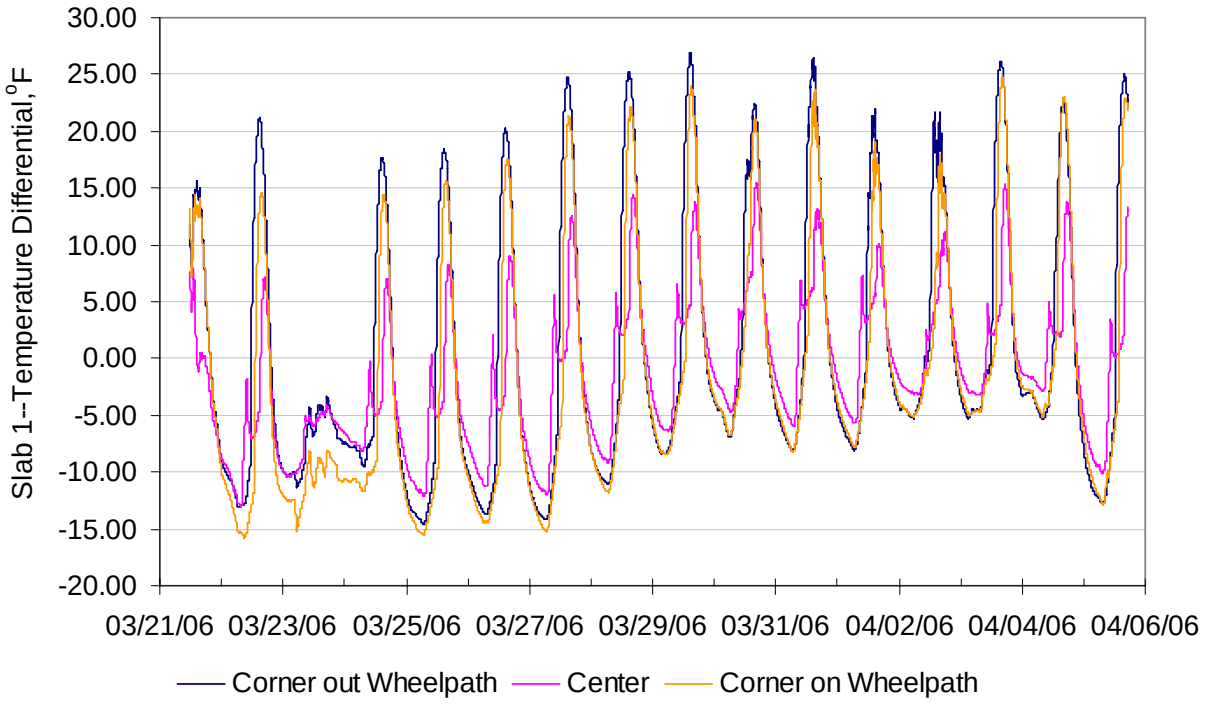

Figure 6-17. Temperature differential variation in Slab 1.

It can be seen that the temperature differentials fluctuated between positive values in the daytime to negative values at night. For Slabs 1 in March 2006, the maximum positive temperature differential was around +28 °F, while the maximum negative temperature differential was about -16 °F.

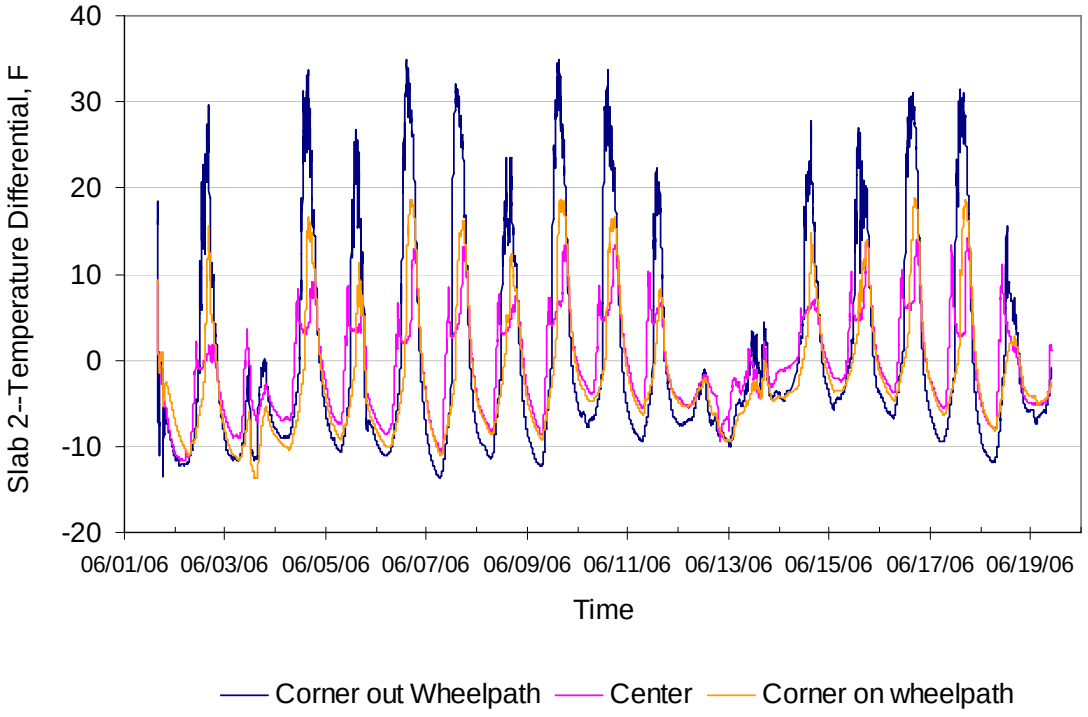

Figure 6-18. Temperature differential variation in Slab 2.

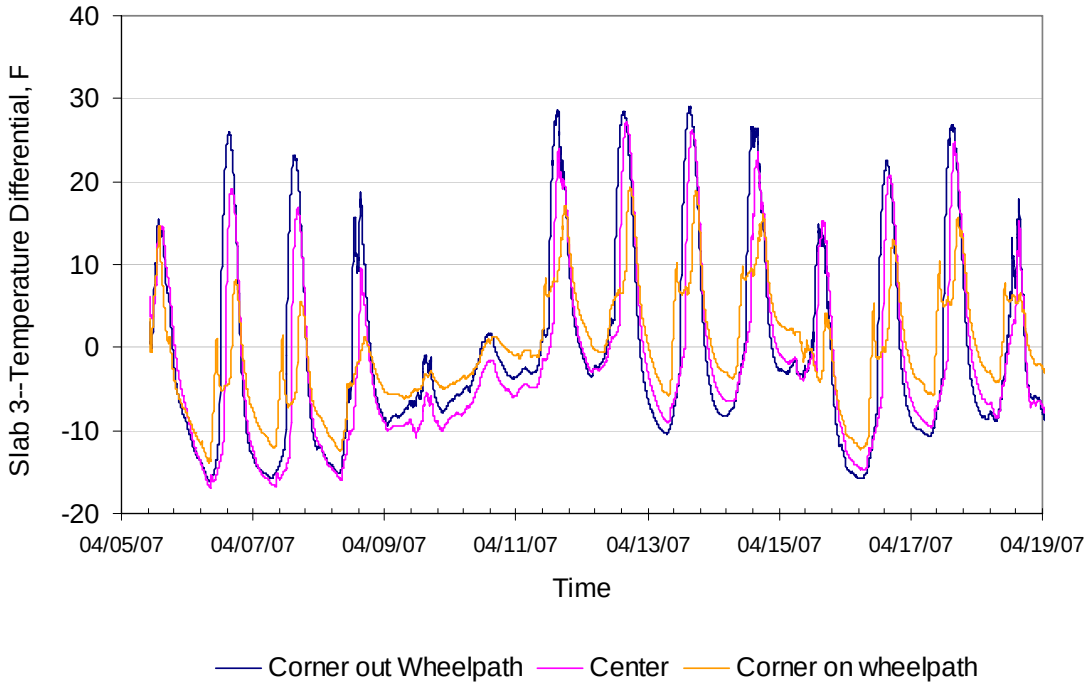

Figure 6-19. Temperature differential variation in Slab 3.

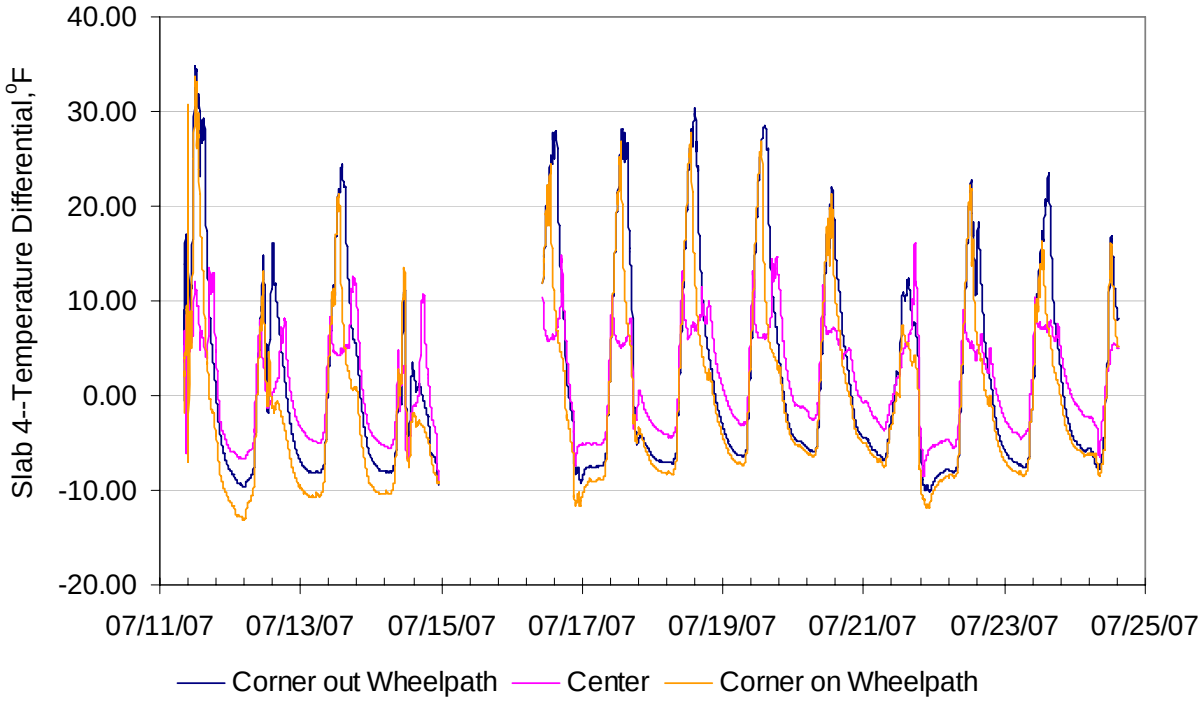

Figure 6-20. Temperature differential variation in Slab 4.

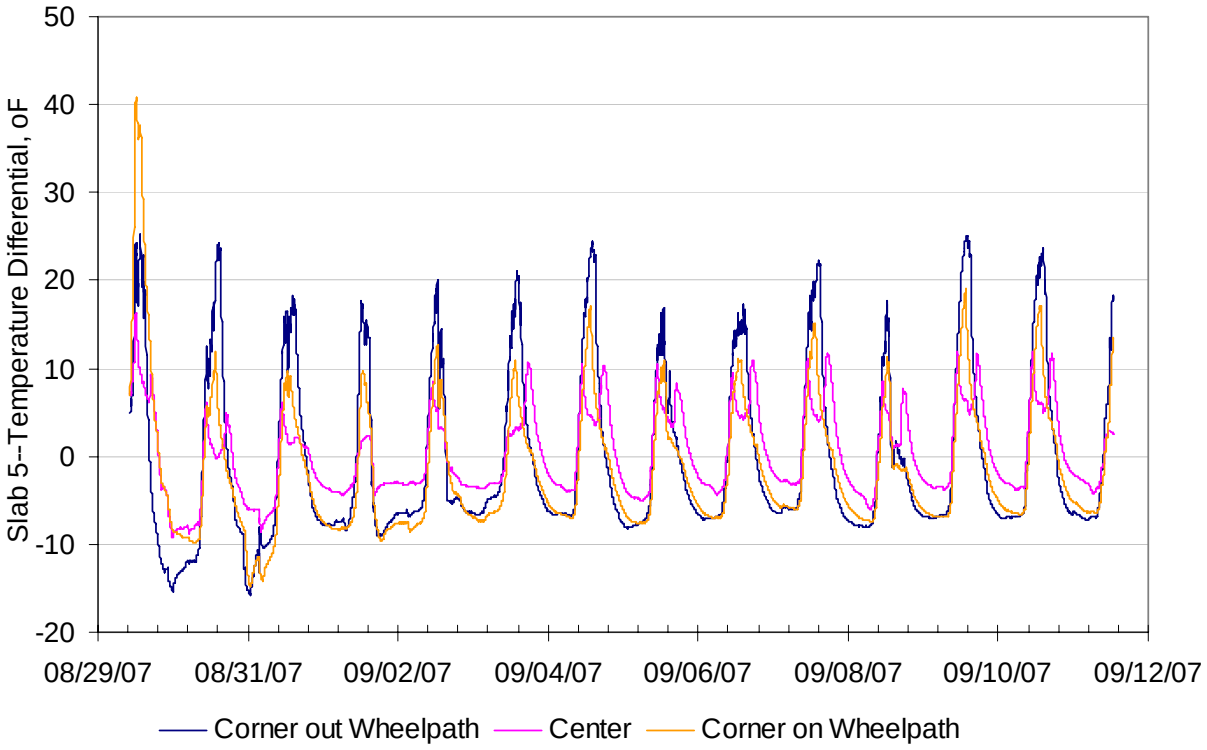

Figure 6-21. Temperature differential variation in Slab 5.

For Slab 2 in June 2006, the maximum positive temperature differential was around +35 °F, while the maximum negative temperature differential was around -14 °F. For Slab 3 in April 2007, the maximum positive temperature differential was around +29 °F, while the maximum negative temperature differential was around -17 °F. For Slab 4 in July 2007, the maximum positive temperature differential was around +35 °F, while the maximum negative temperature differential was around -13 °F. Finally for Slab 5 in September 2007, the maximum positive temperature differential was around +41 °F, while the maximum negative temperature differential was around -16 °F.

Table 6-7 presents the maximum positive and negative temperature differential data for the test slabs. From all test slabs observed at different times is this study, the maximum positive temperature differential was as high as high to about +41 °F, while the maximum negative temperature differential was about -17 °F. These maximum positive and negative temperatures are used to evaluate the maximum stresses due to temperature and load that might apply to replacement slabs in Florida conditions.

The base layer of test Slabs 1, 2, 3 and 4 was a 2-inch asphalt concrete (AC) layer, while it was a compacted limestone layer in Slab 5.

Figure 6-22 shows the temperature on the surface of the AC layer in Slab 1. This plot presents an example of the variation of the temperature in the AC layer which is an important parameter affecting the elastic modulus of the AC and the stress/strain behavior of the concrete test Slabs 1, 2, 3 and 4.

Table 6-7. Maximum temperature differential on the test slabs.

Slab 1, 3/21/06 - 4/6/06	Positive	Negative
Corner out the Wheel Path	26.94	-14.63
Corner on the Wheel Path	15.51	-13.01
Center	24.75	-15.78
Slab 2, 6/1/06 – 6/19/06	Positive	Negative
Corner out the Wheel Path	34.91	-13.78
Corner on the Wheel Path	14.07	-11.68
Center	18.77	-13.79
Slab 3, 4/5/07 – 4/19/07	Positive	Negative
Corner out the Wheel Path	29.02	-16.14
Corner on the Wheel Path	19.39	-13.83
Center	27.29	-16.92
Slab 4, 7/11/07 – 7/19/07	Positive	Negative
Corner out the Wheel Path	34.87	-10.16
Corner on the Wheel Path	33.80	-13.15
Center	24.07	-9.10
Slab 5, 8/29/07 – 9/11/07	Positive	Negative
Corner out the Wheel Path	25.20	-15.77
Corner on the Wheel Path	40.81	-14.84
Center	16.21	-9.21

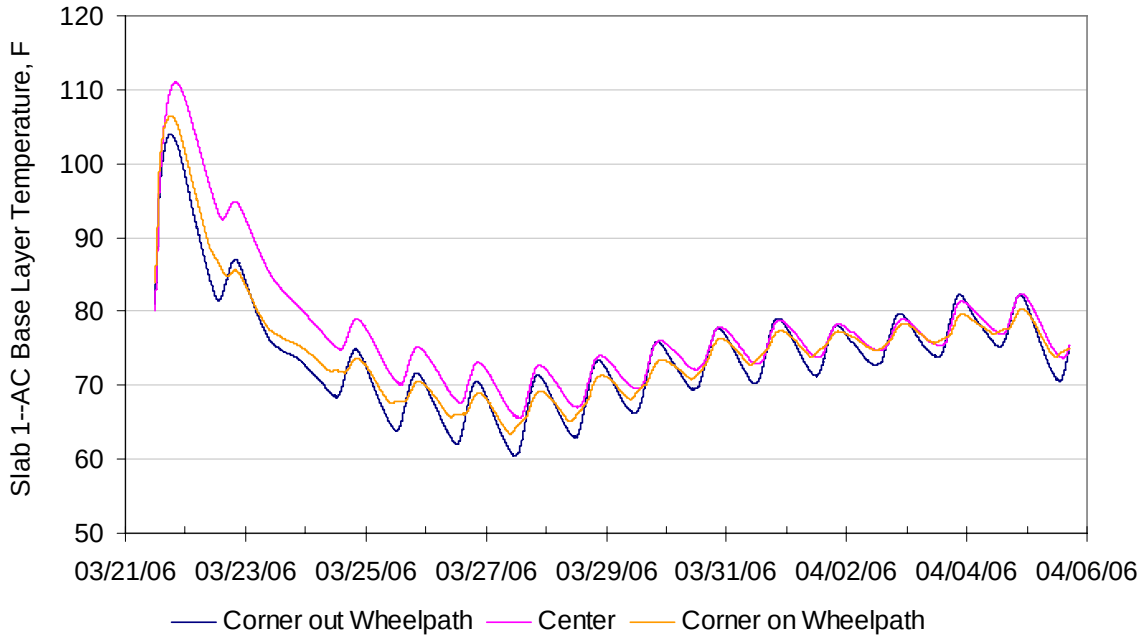

Figure 6-22. Temperature on the surface of the AC layer in the test Slab 1.

Figure 6-23 shows the variation of the temperature at the top (0.5" depth) and bottom (8.5" depth) of concrete slab as well as the temperature of the base layer (10.0" depth) at the corner of Test Slab 5. After placement of the test slab in day time, the temperature at the top of the concrete slab was higher than that at the bottom. At night, the temperature at the bottom of the slab appeared to be higher than that at the top. So the negative temperature differential was high. This high negative temperature differential might cause the concrete slab to curl up along the joints and edges for a few days after the placement. These negative temperature differentials at the first few days are to be considered in the evaluation of performance of the test slabs.

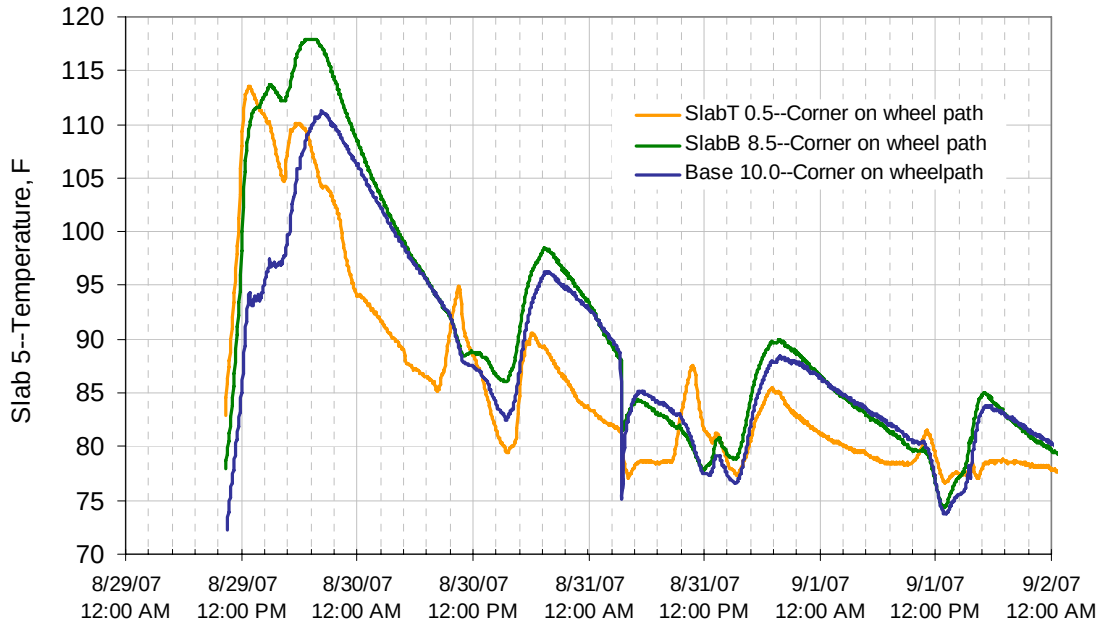

Figure 6-23. Variation of the temperature in the top (0.5") and bottom (8.5") of concrete slab and the temperature of the base layer (10.0") at the corner of Test Slab 5.

Figure 6-24 shows temperature distribution at the maximum positive and negative temperature in the concrete Slab 1. It can be seen that maximum positive temperature differential occurred in afternoon and maximum negative temperature differential occurred in early morning.

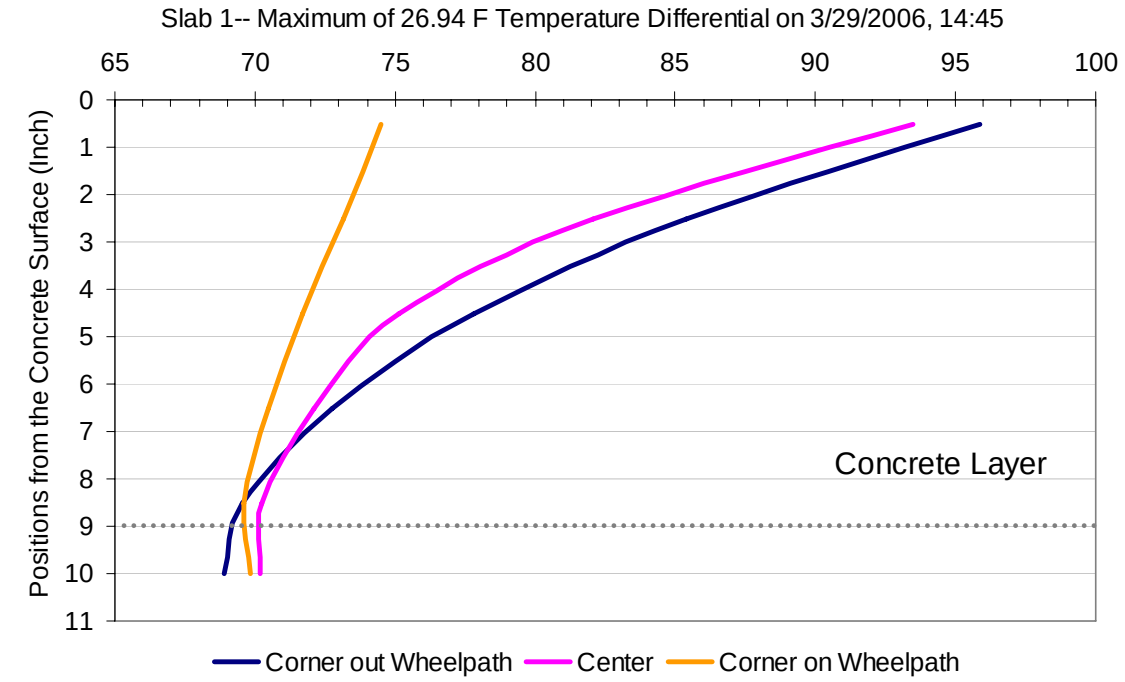

A

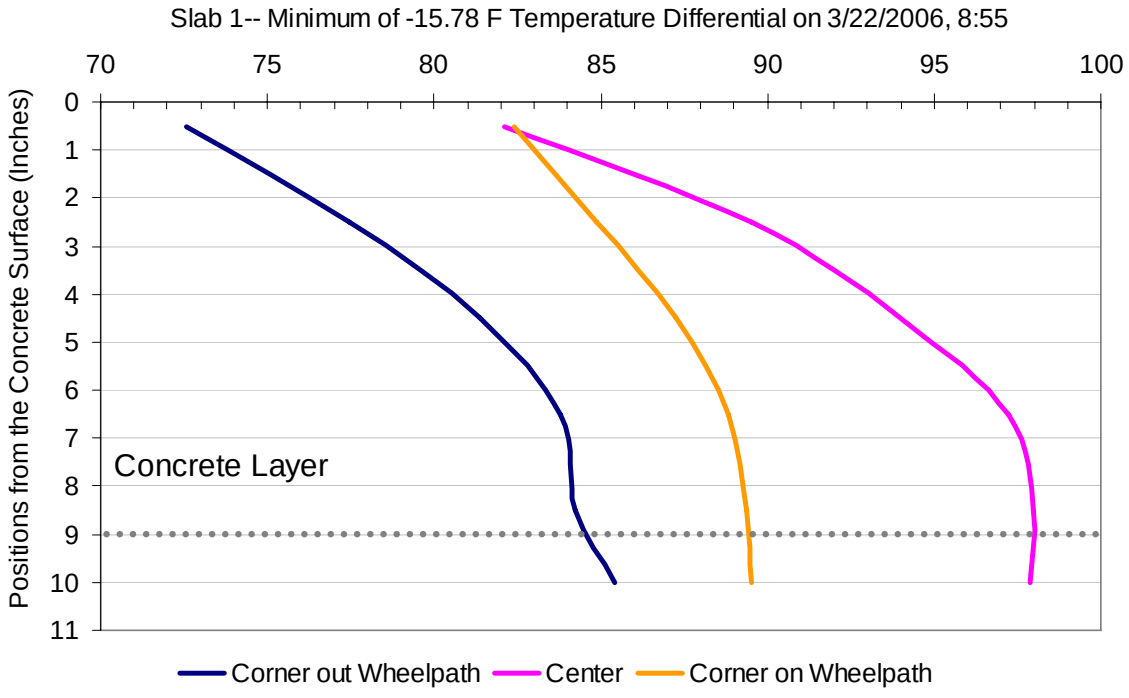

B

Figure 6-24. Temperature distribution at the maximum positive and negative temperature in Test Slab 1. A) Temperature distribution at the maximum positive temperature. B) Temperature distribution at the maximum negative temperature.

6.2.2 Joint Opening Measurement

Two pairs of Whittemore gauge inserts were placed at the joints of each test slab to measure joint movement. Each pair of Whittemore inserts were placed at two inches from the joint. The joint movement was measured by Whittemore gauge at different times of the day. These inserts were fixed to concrete before the fresh concrete stiffened during placement. Figure 6-25 shows the Whittemore inserts fixed at the joint and the standard Invar bar. The Invar bar is a reference bar which was used to calibrate the Whittemore gauge.

Table 6-8 shows the joint opening readings which were taken on Test Slabs 1 and 2. Figures 6-26 and 6-27 present the plots of joint movement versus time on Test Slabs 1 and 2 respectively. A negative value in the joint movement means that the joint was closing due to the expansion of the concrete slab, while a positive value means it was opening due to contraction. The maximum measured joint movement was about 0.04 in.


A


B

Figure 6-25. Joint opening measurements. A) Inserts on both sides of joint and calibration bar opening (Invar bar). B) Whittemore gauge for measuring joint.

Table 6-8. Joint Opening Readings.

Slab 1 Time	Calibration	Gauge Reading		Distance between inserts (inch)		Joint Movement (inch)	
		J1*	J2*	J1	J2	J1	J2
8:30 AM	0.073	0.0668	0.0143	4.0062	4.0587	-	-
10:00 AM	0.0725	0.0701	0.0156	4.0024	4.0569	-0.0038	-0.0018
11:00 AM	0.0727	0.0775	0.0201	3.9952	4.0526	-0.011	-0.0061
1:30 PM	0.073	0.091	0.023	3.982	4.05	-0.0242	-0.0087
2:30 PM	0.0725	0.099	0.0285	3.9735	4.044	-0.0327	-0.0147
3:30 PM	0.0726	0.103	0.0356	3.9696	4.037	-0.0366	-0.0217
4:30 PM	0.073	0.1035	0.0433	3.9695	4.0297	-0.0367	-0.029
5:30 PM	0.0729	0.0982	0.0395	3.9747	4.0334	-0.0315	-0.0253
Slab 2 Time	Calibration	Gauge Reading		Distance between inserts (inch)		Joint Movement (inch)	
		J1	J2	J1	J2	J1	J2
10:30 AM	0.0715	0.0585	0.152	4.013	3.9195	-	-
11:30 AM	0.072	0.0475	0.158	4.0245	3.914	0.0115	-0.0055
12:30 PM	0.0651	0.0535	0.1582	4.0116	3.9069	-0.0014	-0.0126

Note: J1 – Joint at the south corner of the test slab
J2 – Joint at the north corner of the test slab

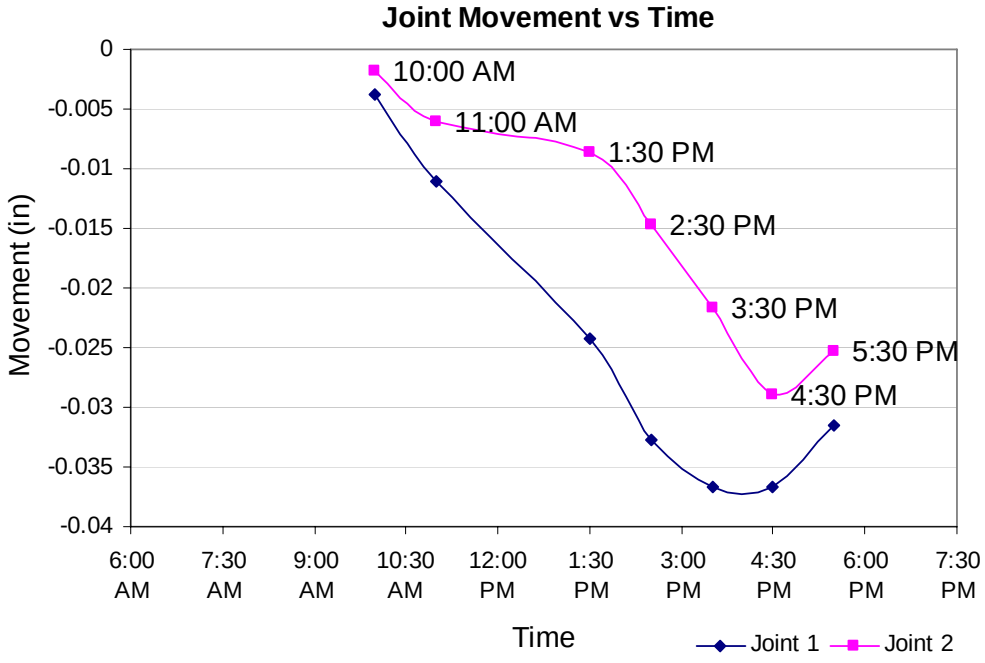

Figure 6-26. Joint movements on Slab 1.

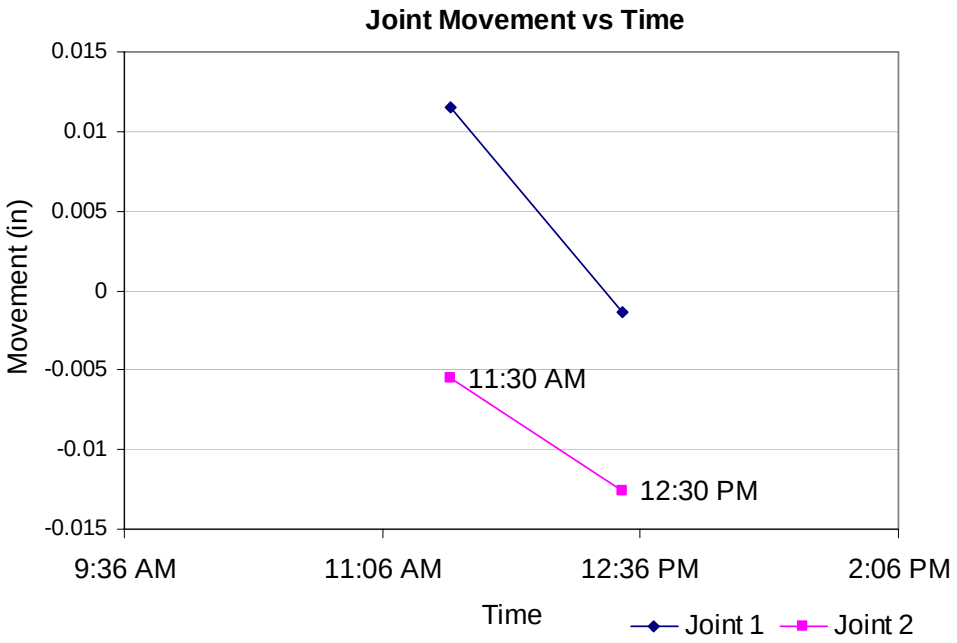

Figure 6-27. Joint movements on Slab 2.

6.2.3 Falling Weight Deflectometer Testing

Falling Weight Deflectometer (FWD) tests were performed on all test slabs. The measured FWD deflection basins were used to estimate the stiffness of the springs used to model the modulus of subgrade reaction and load transfer at the joints and edges through a back-calculation process. The back-calculation process also allowed for the verification of the elastic modulus of the concrete and the base layer, previously evaluated from laboratory testing. The details of calibration and verification of parameters used in a finite element model are presented in Chapter 7.

FWD tests were performed at early morning between 6 A.M. and 8 A.M. and at midday between 2 P.M. At early morning, the temperature differential tends to be negative and the slab tends to curl down at the center of the slab. This is an ideal time to run the FWD test at the center of the slab for evaluation of the condition of the concrete slab and the layer underneath.

At mid day, the temperature differential tends to be positive and slab tends to curl down at the edges and joints. This is the best time to run the FWD test for evaluation of joints because the slab is more likely to be in full contact with the layer underneath at both the edges and joints.

FWD tests were to run on the test slabs using different loads. A replicate test was run right after each test was completed to check for consistency.

Figure 6-28 shows the FWD load and sensor positions used for the FWD tests at the slab center. The FWD loading plate was place at the center of the test slab. Two sensor locations are along longitudinal and transversal directions. The same schemes were used for all the test slabs to be tested in the early morning to evaluate the elastic modulus of the layers.

Figure 6-29 and 6-30 show the FWD load and sensor positions used for the FWD tests at the slab edge and joint, respectively. For the edge loading, the FWD loading plate was place at the mid edge. One set of sensor locations are along the edge of the test slab and another set are along the adjacent slab. Similarly for the joint loading, the FWD loading plate was place at the middle of the test slab's joint. One set of sensor locations is along the joint on the test slab and another set are along the adjacent slab. The same schemes are used for all the test slabs to be test in the mid day to evaluate the load transfer condition.

The results of the FWD tests on five test slabs are presented in the Appendix A of this dissertation.

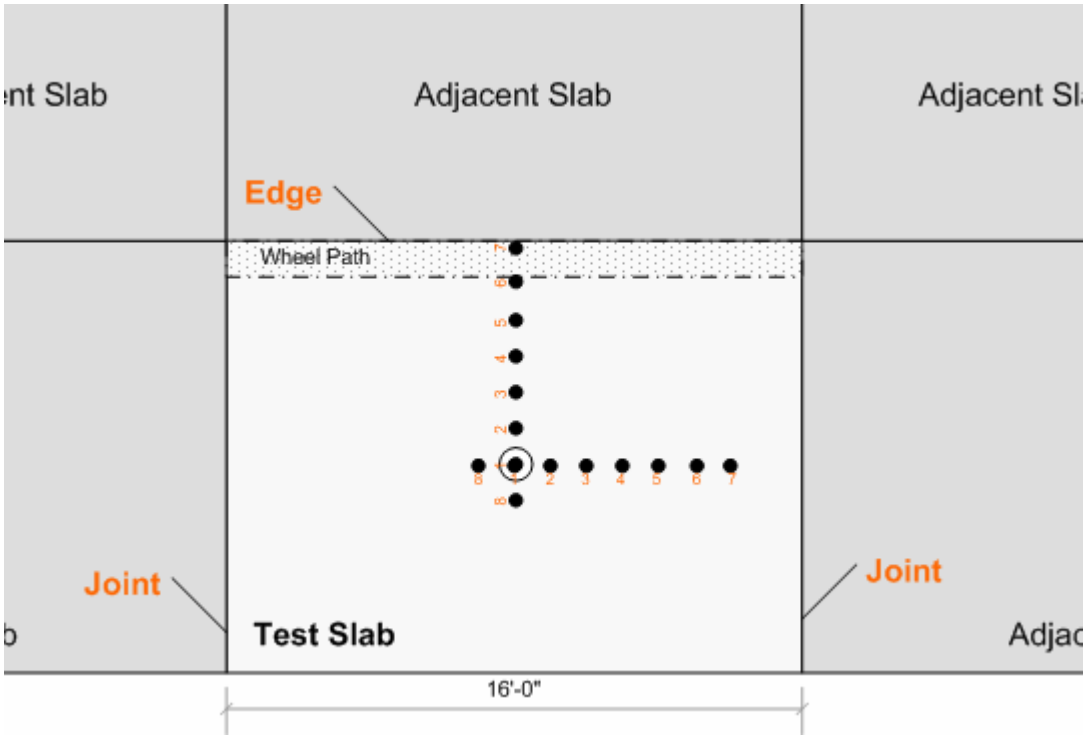

A

B

Figure 6-28. FWD tests at the slab center. A) FWD load and sensor locations at the slab center. B) FWD test at the slab center and measuring deflection on the longitudinal direction.

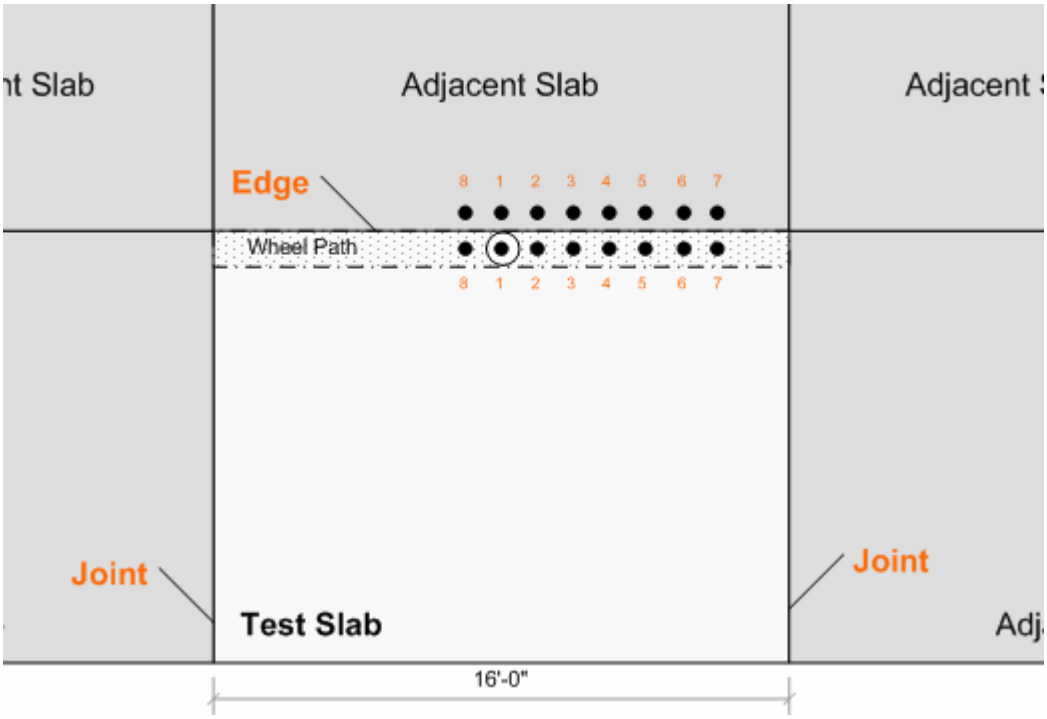

A

B

Figure 6-29. FWD tests at the slab edge. A) FWD load and sensor locations at the slab edge. B) FWD test at the slab edge and measuring deflection on the opposite slab.

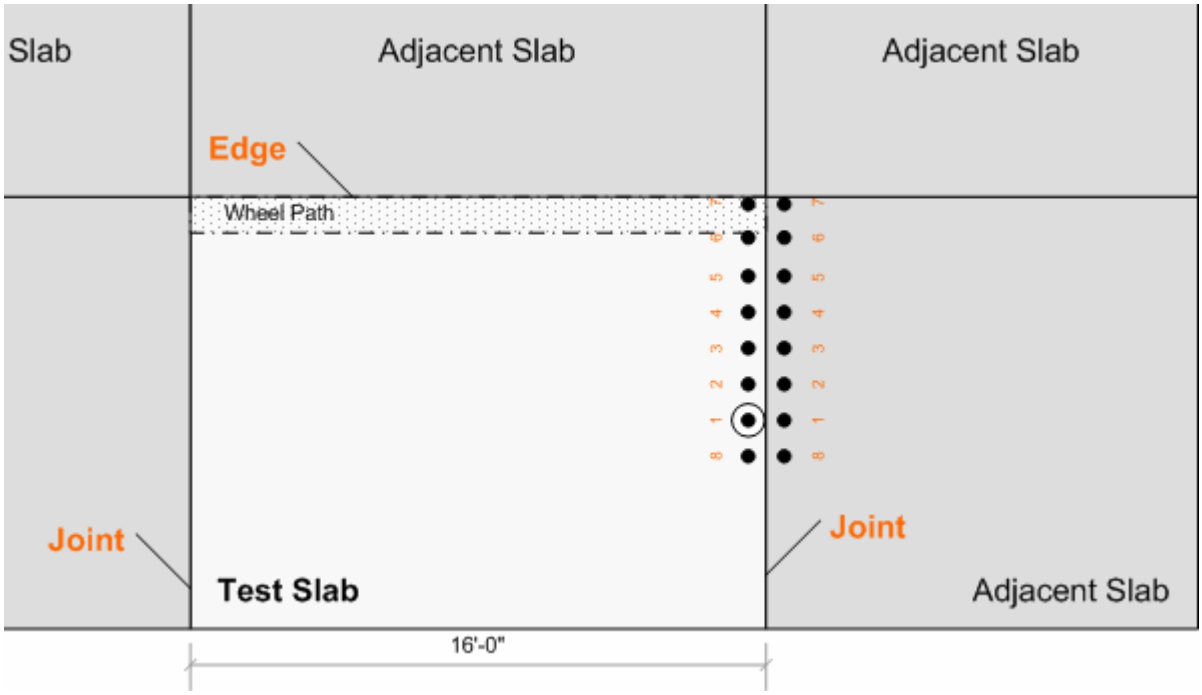

A

B

Figure 6-30. FWD tests at the slab joint. A) FWD load and sensor locations at the slab joint. B) FWD test at the slab joint and measuring deflection on the adjacent slab.

6.2.4 Measurement of the HVS Laser Profiles

A laser based profiling system was installed on the Florida Department of Transportation's Heavy Vehicle Simulator (HVS). This system enables a detailed analysis of the surface of the test pavement; primarily the system evaluates the vertical profile of the test section, which is scanned by the profiler. In this study, the laser profiling system was used to measure the curling of the concrete test slabs at and near the wheel path.

The HVS laser profile was run on the test section at early morning between 5 A.M. and 6 A.M. and at midday between 2 P.M. during the HVS loading of the test slabs.

Figure 6-31 shows the side-shifting pattern of the laser profiler as it scans over the test section. Figure 6-32 presents the test track matrix and the overlap area which is comprised of the 127 columns of data. Each laser produces 67 columns of data. There are a total of 134 columns of data with 7 overlapping columns. Each column contains 58 data points. Accordingly there are 58 rows of data. Each row of data represents the transverse profiles of the test track [FDOT, HVS laser profile data acquisition system].

The wheel path in this study is along the confined edge of the test slabs; therefore, one side of the laser obtains the surface data of the test slab, while another side obtains the opposite slab. From Figures 6-31 and 6-32, it can be seen that the surface data that were used in the analysis of the laser profile of the test slabs was to cover the area of the wheel path to about 38 inches from the edge of a test slab.

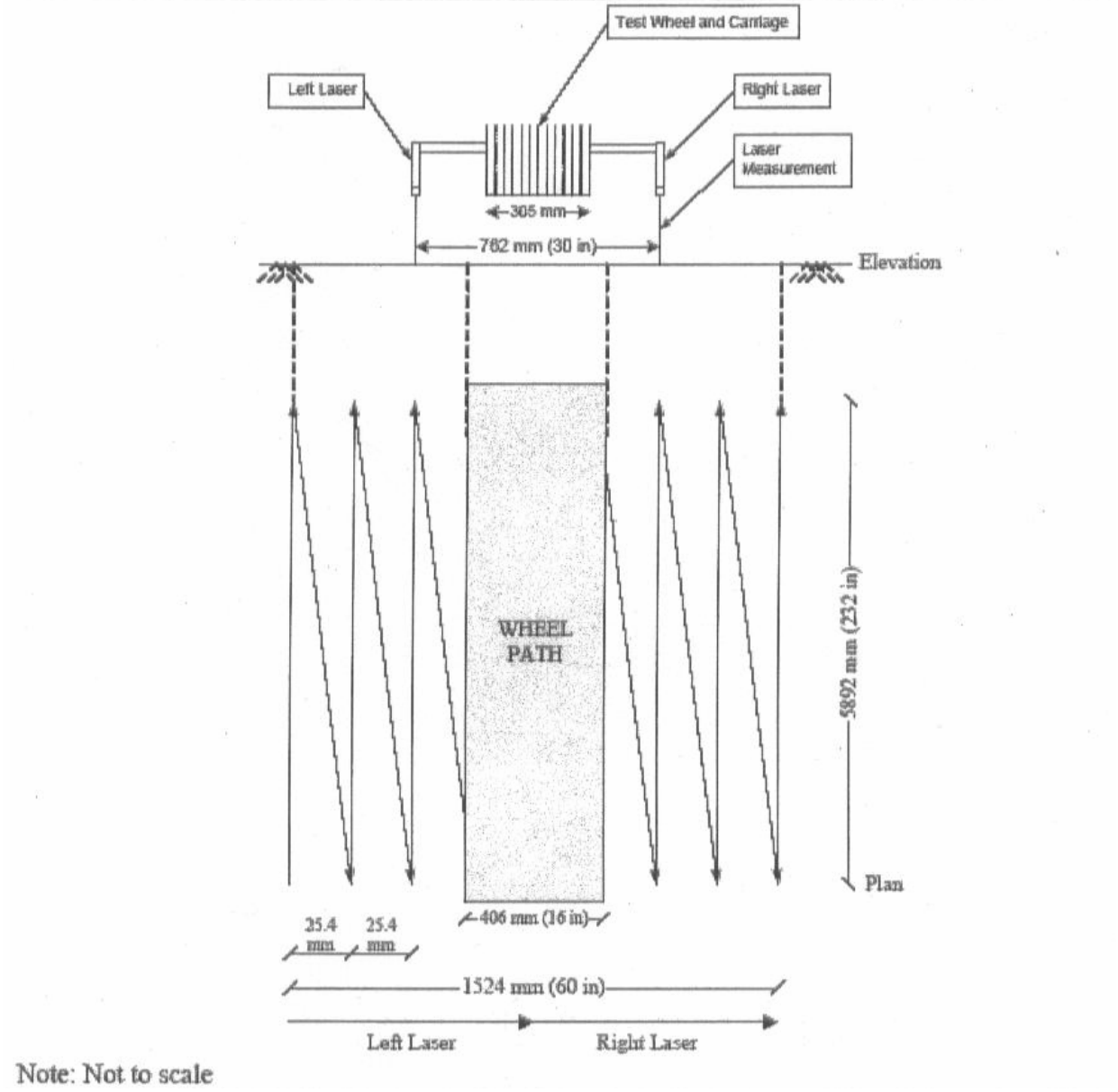

Figure 6-31. Side-shifting pattern of the laser profile. [Byron, Gokhale, Choubane, 2005]

The schedule for the laser profile measurement and list of analysis files of each test slab in this study are shown in Appendix B of this report.

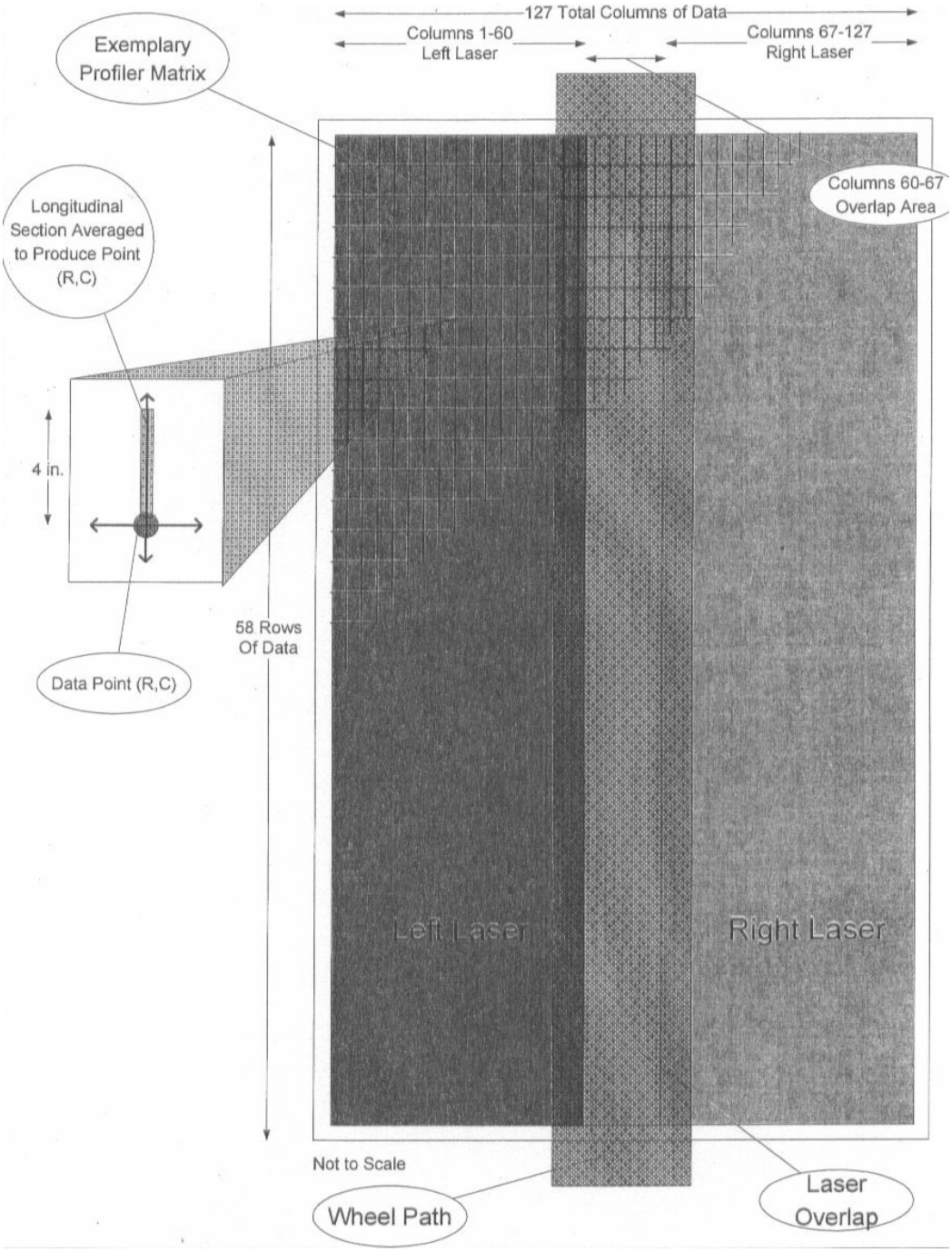

Figure 6-32. Approximate Profiler Matrix [FDOT, HVS laser profile data acquisition system].

Figure 6-33 depicts a typical laser profile data from Slab 2. The data was obtained after 82,815 passes of the HVS loading at 5 A.M. The figure shows the area on both the test slab and opposite slab, which were in the scan area of the HVS laser profiling system.

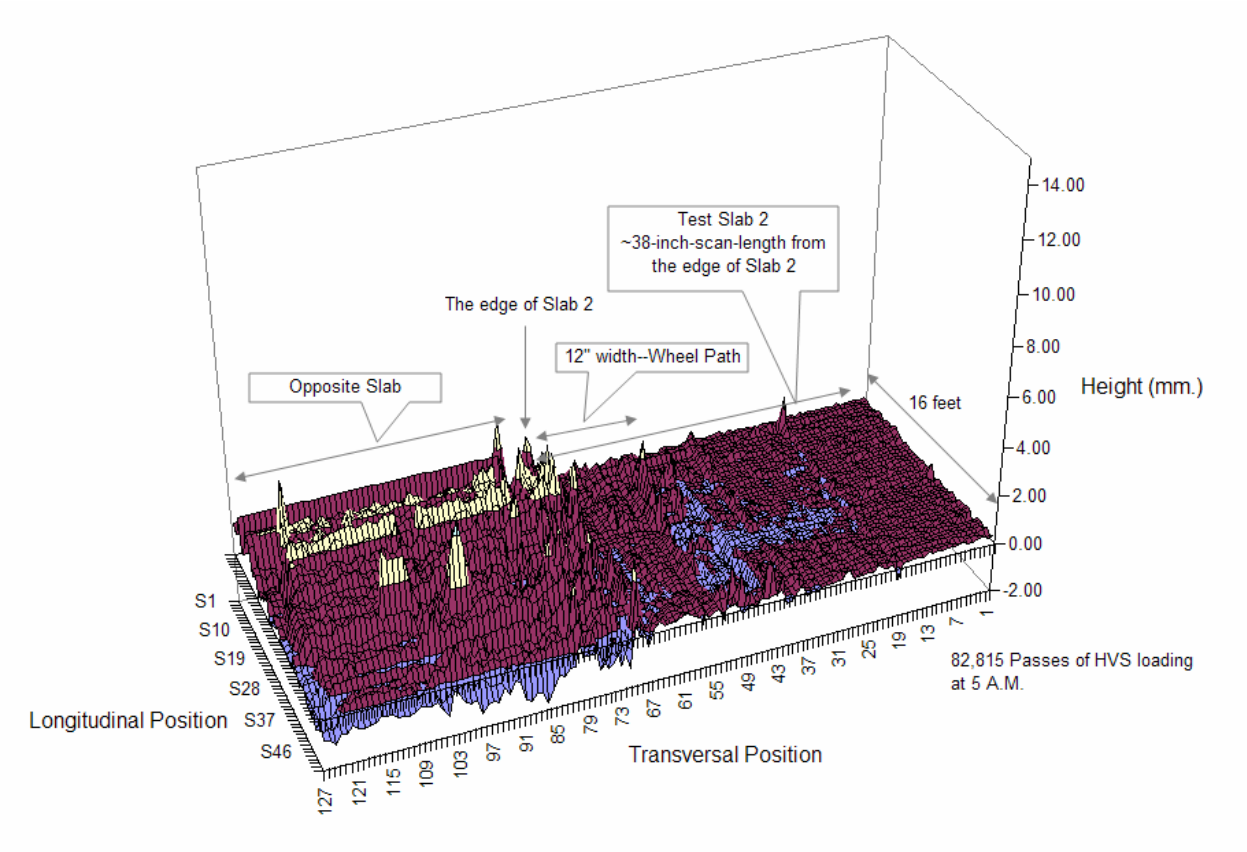

Figure 6-33. 3-D plot of a laser profile data from Slab 2.

The initial laser profile data were used as the reference, and were subtracted subsequent profile measurements to obtain the differential profile. The result is the difference in surface height from when the test was started to the time when the profiler was run.

Figure 6-34 presents the average differential profiles of Slab 5 at two different times. These two profiles were obtained at 5 A.M. and 2 P.M. in the same day. It can be seen that the shapes of the average transverse profiles are similar, but the slab at the 5 A.M. curled up from the edge of the test slab more than the slab at the 2 P.M. Figure 6-34 also shows that the average movement due to the curling effect at the testing period was about 0.62 mm.

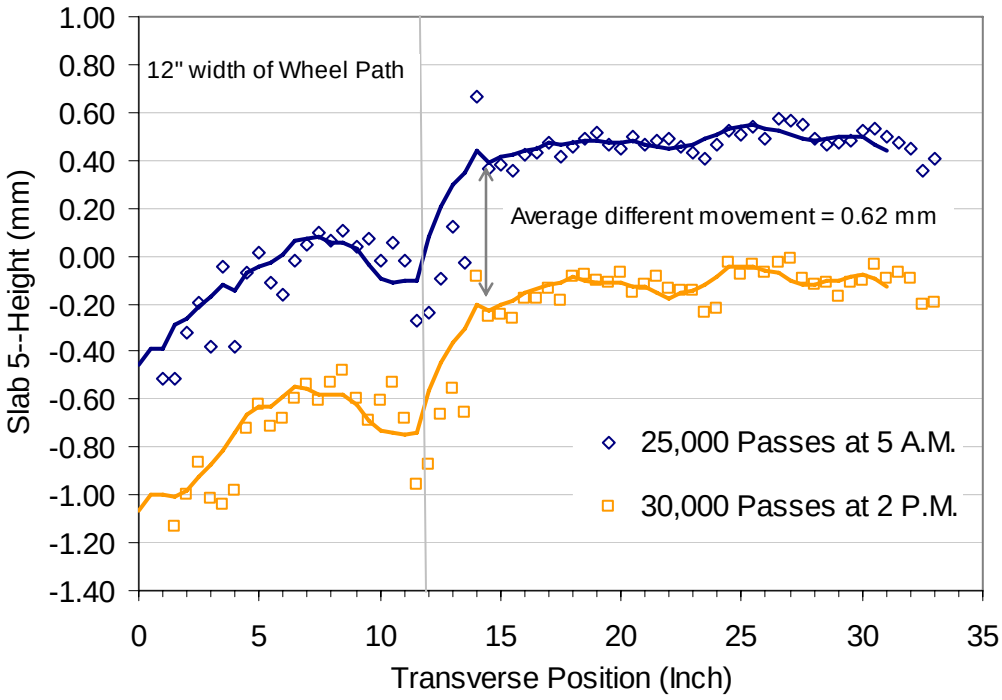

Figure 6-34. Average differential transverse profile of Slab 5 at two different times.

Figure 6-35 shows the differential transverse profile along the joint and center of Slab 1 at 5 A.M. testing. From the figure, it can be seen that the transverse profile along the joint of the test slab curls up more as compared with the profile along the center of the edge.

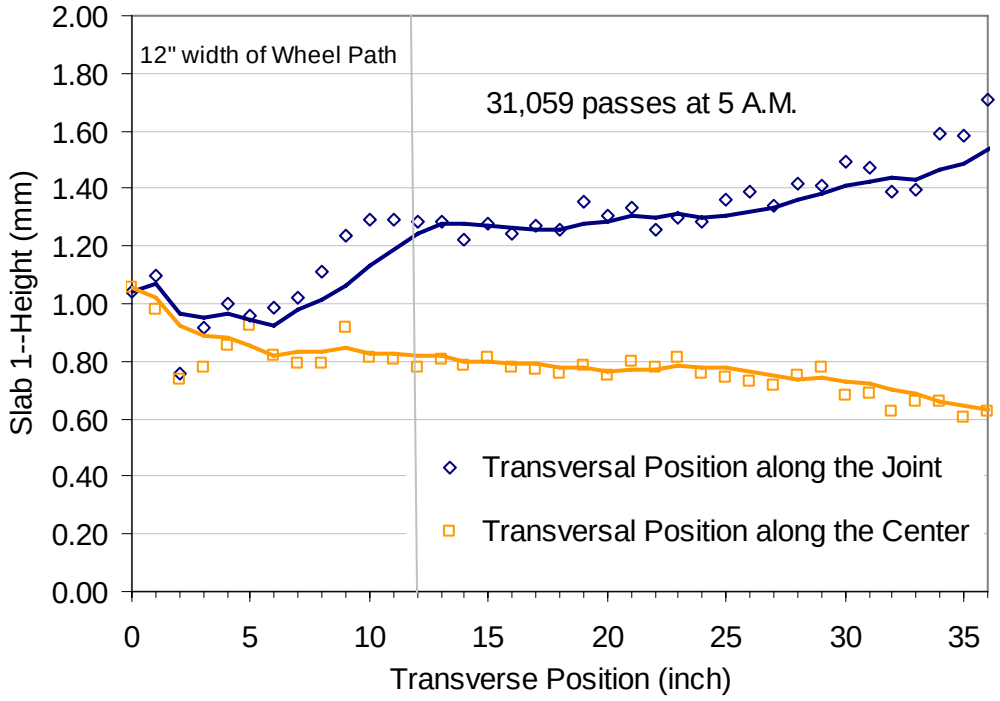

Figure 6-35. Curling effect along the joint and center in Slab 1.

6.2.5 Testing of Concrete Cores

Concrete cores from test slabs were taken after the HVS testing. Six cores from the wheel path were tested for their compressive strength (ASTM C39), elastic modulus (ASTM C469) and splitting tensile strength (ASTM C496). The other three cores from outside the wheel path were tested for their compressive strength.

Nine 4-inch diameter and 9-inch long concrete cores were taken from Slab 1 on October 11, 2006, about 7 months after the concrete placement, from Slab 2 on February 8, 2007, about 8 months after the concrete placement, from Slab 3 on June 22, 2007, about 2.5 months after concrete placement and from Slabs 4 and 5 on November 11, 2007, about 4 months and 2.5 months after the placement respectively.

In order to perform the tests mentioned above, the concrete cores were sawed to the length of 8 inches. Diameters and lengths of the concrete cores were measured to use in the calculation of the strengths and elastic modulus. Figure 6-36 shows concrete cores taken from a test slab.

A 
B

Figure 6-36. Concrete cores. A) Nine 4-inch diameter concrete cores. B) 9-inch length concrete cores.

Figure 6-37 shows the locations of the cores taken from Slabs 1, 2 and 3 respectively. Table 6-9 shows the average compressive strength, elastic modulus and splitting tensile strength of the cores taken from Slab 3, and those from the laboratory-cured concrete specimens.

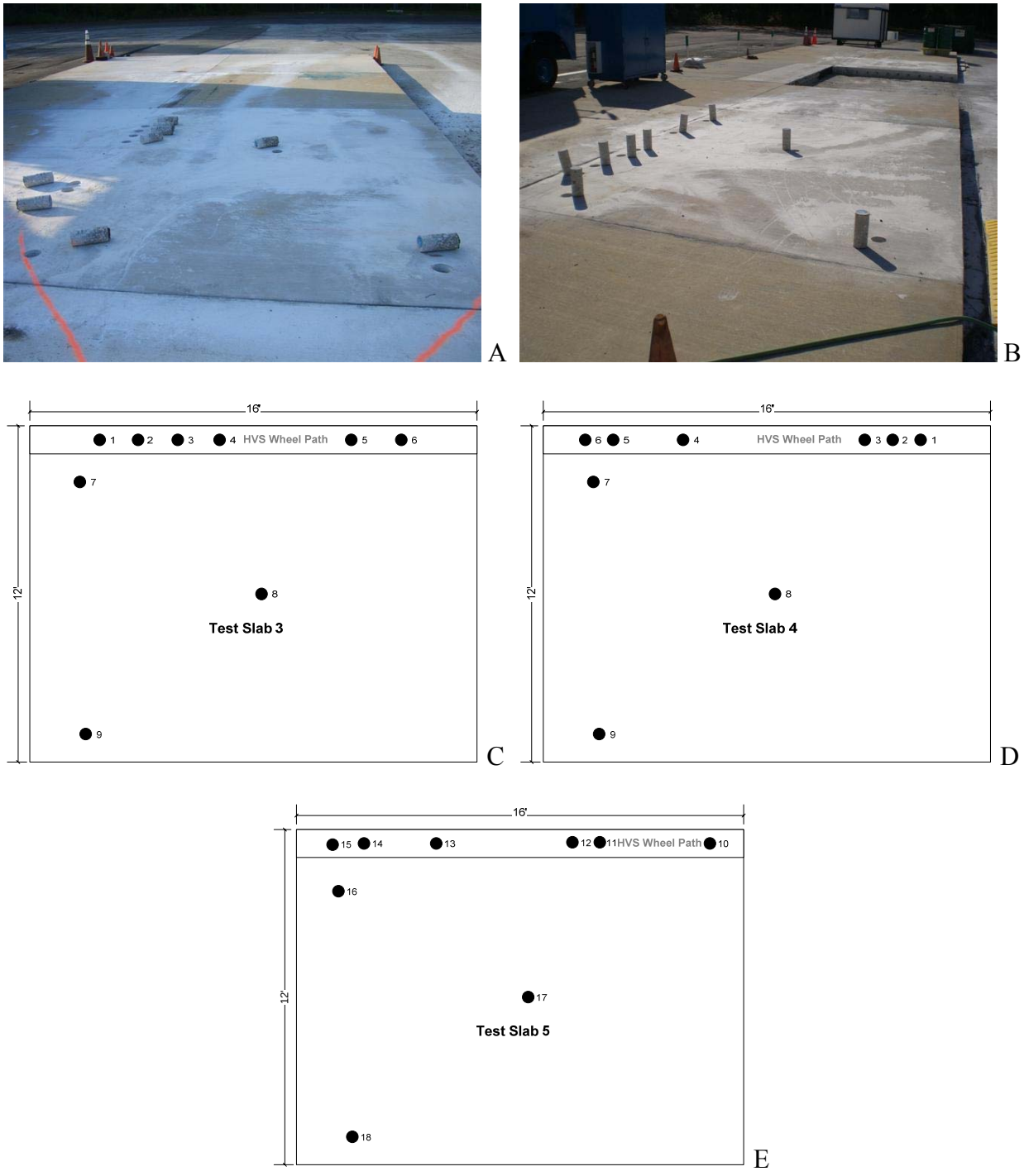

Figure 6-37. Locations of the cores taken. A) Locations of the cores taken from Slab 1. B) Locations of the cores taken from Slab 2. C) Locations of the cores taken from Slab 3. D) Locations of the cores taken from Slab 4. E) Locations of the cores taken from Slab 5.

Table 6-9. Properties of concrete cores from test slabs compared to laboratory-cured specimens from the test slabs concrete respectively.

Slab 1: Concrete Core Testing October 11, 2006 ~ 7 months	Compressive Strength (psi)	Elastic Modulus (ksi)	Splitting Tensile Strength (psi)
Cores on the wheel path	6,686.0	3,650	470.9
Cores outside the wheel path	7,561.8	3,725	-
28 days Laboratory cured	6,428.8	3,752	384.8
Slab 2: Concrete Core Testing February 8, 2007 ~ 8 months	Compressive Strength (psi)	Elastic Modulus (ksi)	Splitting Tensile Strength (psi)
Cores on the wheel path	6,439.1	3,725	527.6
Cores outside the wheel path	7,431.3	3,800	-
28 days Laboratory cured	6,646.8	3,825	471.6
Slab 3: Concrete Core Testing June 22, 2007 ~ 2.5 months	Compressive Strength (psi)	Elastic Modulus (ksi)	Splitting Tensile Strength (psi)
Cores on the wheel path	5,974.6	3,625	563.0
Cores outside the wheel path	6,497.4	3,925	-
Laboratory cured samples at same curing time as cores	6,813.1	3,950	574.1
Laboratory cured at 28 days	6,810.3	3,650	559.5
Slab 4: Concrete Core Testing November 11, 2007 ~ 4 months	Compressive Strength (psi)	Elastic Modulus (ksi)	Splitting Tensile Strength (psi)
Cores on the wheel path	7,234	4,197	611
Cores outside the wheel path	7,228	4,195	-
28 days Laboratory cured	6,921	3,875	678
Slab 5: Concrete Core Testing November 11, 2007 ~ 2.5 months	Compressive Strength (psi)	Elastic Modulus (ksi)	Splitting Tensile Strength (psi)
Cores on the wheel path	7,034	4,331	590
Cores outside the wheel path	6,749	4,237	-
28 days Laboratory cured	7,463	4,288	585

CHAPTER 7
MODEL CALIBRATION AND VERIFICATION

7.1 Overview of Model Calibration

The analytical model used in the FEACONS program as presented in Chapter 4 was used to perform stress analyses to determine the optimum locations for strain gauges. In those previous analyses, reasonable values for the various pavement parameters were used with the purpose of determining the locations of maximum stresses rather than determining correctly the magnitudes of the maximum stresses.

However, in analyzing the performance of the test slabs under the HVS loading, the temperature-load induced stresses on the test slabs needed to be determined accurately. In order for the analytical model to correctly analyze the behavior of the replacement slabs, it needs to have accurate properties of the test slab materials and the correct values of spring stiffness for modeling the behavior of joints and edges.

The elastic modulus of the concrete material was initially estimated from the results of laboratory tests on the concrete as described in Chapter 6. The modulus of subgrade reaction of the test slab was estimated by back-calculation of the FWD deflection basins using the FEACONS program. The deflection basins caused by FWD loads applied at the slab center was used in this case. The results of the FWD tests at the joints and edges were used to calibrate values of spring stiffness at the joints and edges of the test slabs. This process is called "calibration of model parameters" of the model in this study.

The estimation of the test slab parameters was further verified by matching the analytically computed strains with the measured strains in the test slabs caused by the HVS loading. This step is named as "verification of model parameters" in this study.

The loading area of the FWD is a 12-inch diameter circular plate. A twelve inch by twelve inch square loading area was used in the finite element mesh to model the loading plate. The other slab model parameters used in the FEACONS analyses are shown in the Table 7-1.

Table 7-1. Slab model parameters used in the FEACONS model calibrations.

Parameters in FEACONS	Values
Slab Size (ft. x ft.)	12 x 16
Number of Bonded Layers	2 Layers, 1 Layer
Thickness of Concrete Slab (inch)	9
Elastic Modulus of Concrete (ksi)	4,000 ksi
Density of Concrete (pcf)	140 pcf
Thickness of Asphalt Concrete (inch)	4 inches, N/A
Elastic Modulus of Asphalt Concrete (ksi)	1,400 ksi
Density of Asphalt Concrete (pcf)	100 pcf
Poison's ratio	0.2
Subgrade Condition	Linear
Modulus of Subgrade Reaction (kci)	from FWD results
Applied load (kip)	9 kips, 12 kips
Temperature Effect	No
Spring Coefficient for the Edge (ksi)	from FWD results
Linear Spring Coefficient for the Dowel Joint (ksi)	from FWD results
Torsional Spring Coefficient for the Dowel Joint (k-in/in)	from FWD results

7.2 Calibration of Model Parameters

7.2.1 Slab 1

Slab 1 was modeled as a 9-inch concrete slab bonded to a 4-inch asphalt over a Winkler foundation. The material properties used in this analysis are shown in the Table 7-1. A 9-kip FWD applied load was used in analysis.

Figure 7-1 shows the measured and computed deflections at the location of the geophones for Slab 1 caused by a 9-kip FWD load. The measured deflections in longitudinal direction were

noted to be similar to those in the transversal direction. The computed deflection basin was obtained by using a modulus of subgrade reaction of 0.80 kci.

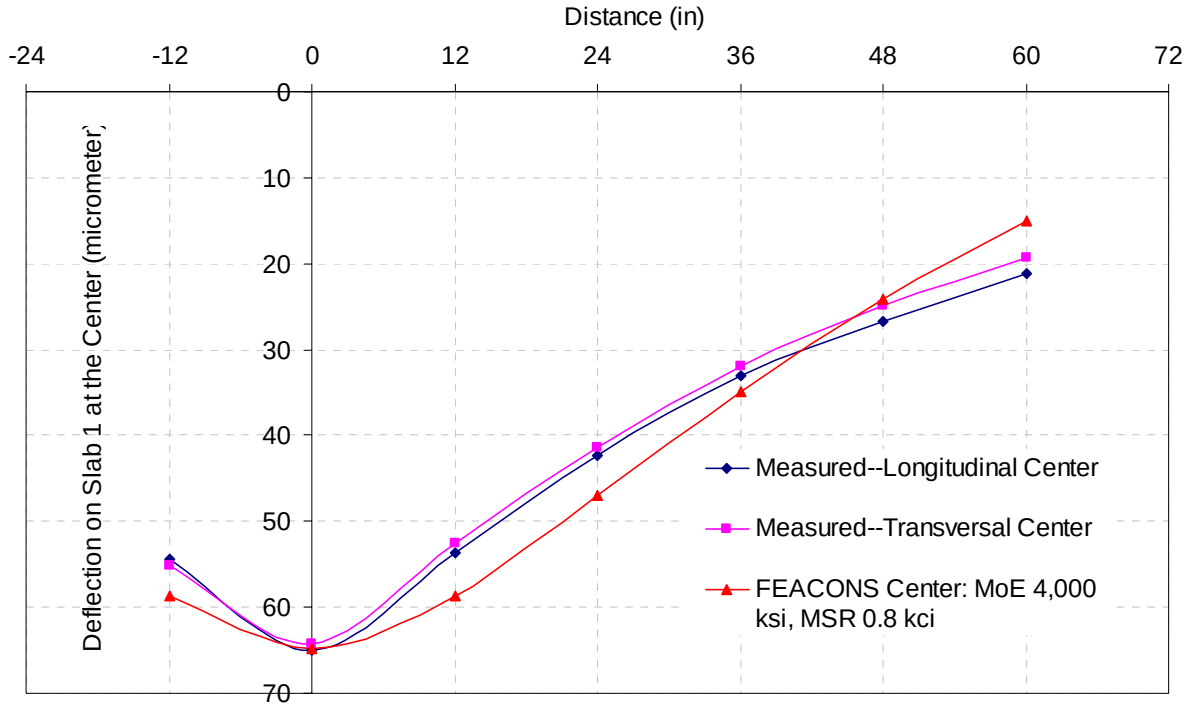

Figure 7-1. Measured and computed deflection basin caused by a 9-kip FWD load at slab center for Slab 1.

Slab deflections caused by FWD load applied at the confined edge of the test slab, the FWD test results were used to estimate the edge coefficient. The estimated subgrade modulus and the other known pavement parameters were used in the FEACONS program to compute the deflections caused by a 9-kip FWD load at the slab edge. An edge stiffness of 25 kci gave a fairly good match between the computed and measured deflection at the confined edge as shown in Figure 7-2.

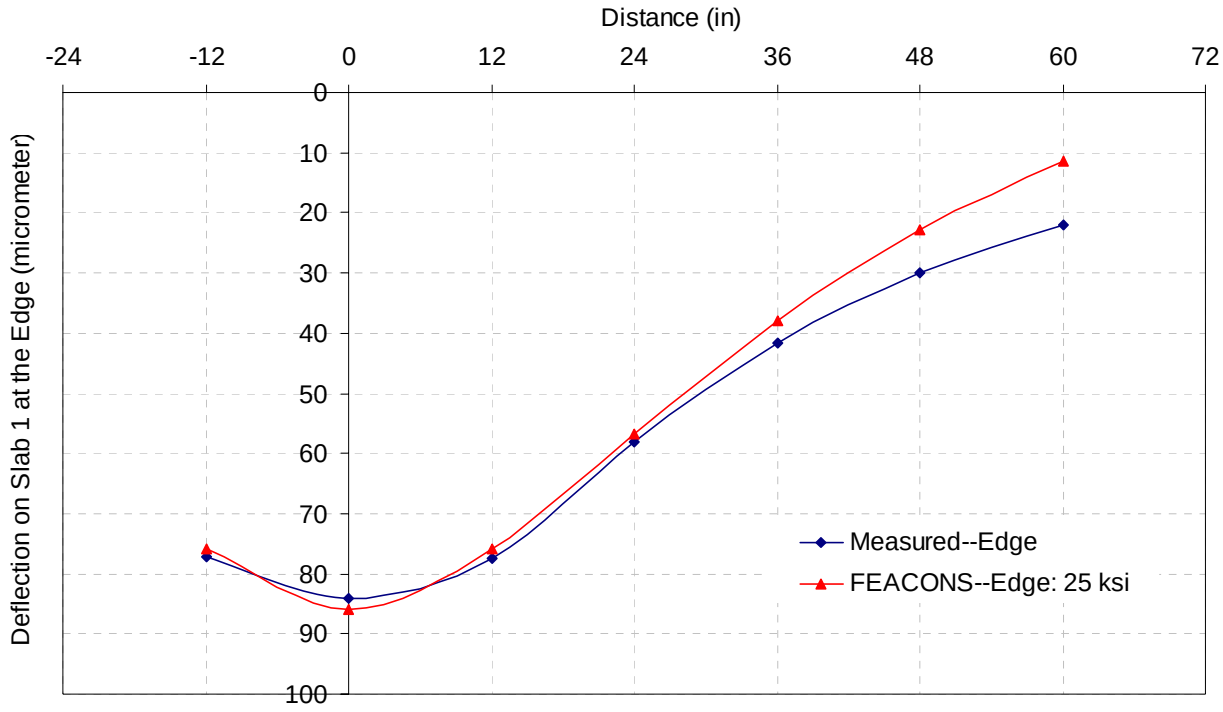

Figure 7-2. Measured and computed deflection basin caused by a 9-kip FWD load at slab edge for Slab 1.

Slab deflections caused by FWD load applied at the joint of the test slab, FWD tests results were also used to estimate the joint coefficients. With previous estimated parameters and values of the other known pavement parameters, the computed and measured deflections at the joint were matched fairly well by using a linear spring coefficient of 300 ksi and a torsional spring coefficients of 1,500 K-in/in at the joint as presented in Figure 7-3.

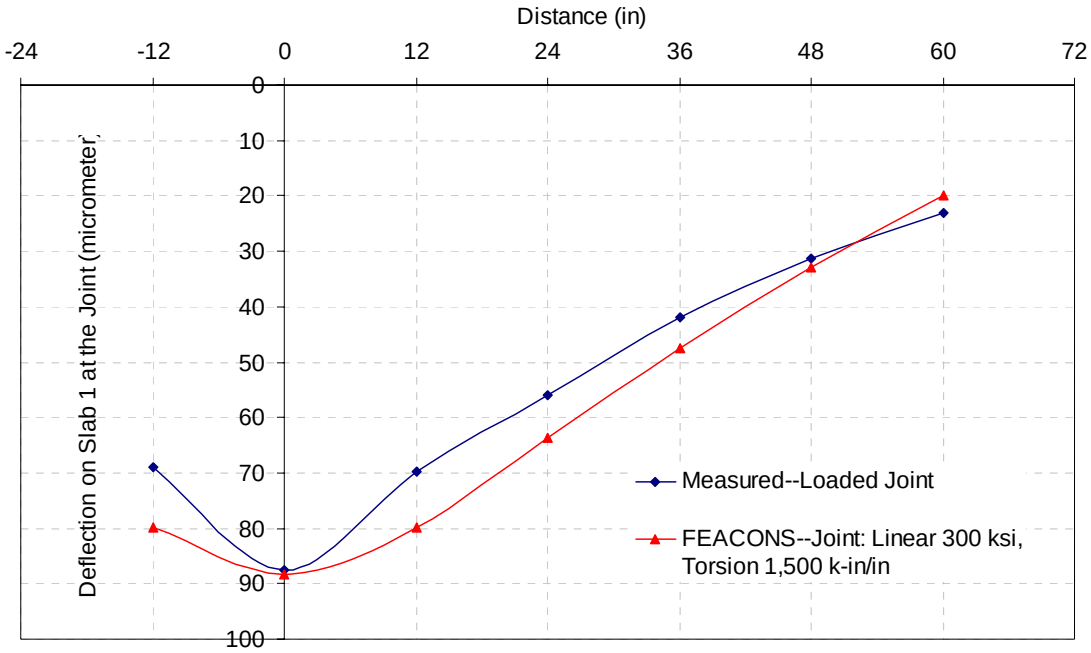

Figure 7-3. Measured and computed deflection basin caused by a 9-kip FWD load at slab joint for Slab 1.

7.2.2 Slab 2

A 9-kip FWD load is also used as the applied load in the model calibration for Slab 2. Similarly, the slab was modeled as a 9-inch concrete slab bonded to a 4-inch asphalt layer, placed over a Winkler foundation. Figure 7-4 shows the measured and computed FWD deflections at the location of the geophones for Slab 2. The measured deflections in the longitudinal direction were noted to be also similar to those in the transversal direction. The computed deflection basin matched to the measured one by using a higher modulus of subgrade reaction of 0.95 kci.

Slab deflections caused by FWD load applied at the confined edge of the test slab were used to estimate the edge coefficient. The estimated subgrade modulus and the other known pavement parameters were used in the FEACONS program to compute the deflections caused by a 9-kip FWD load at the slab edge. An edge stiffness of 8 kci gave a fairly good match between the computed and measured deflection at the confined edge as shown in Figure 7-5.

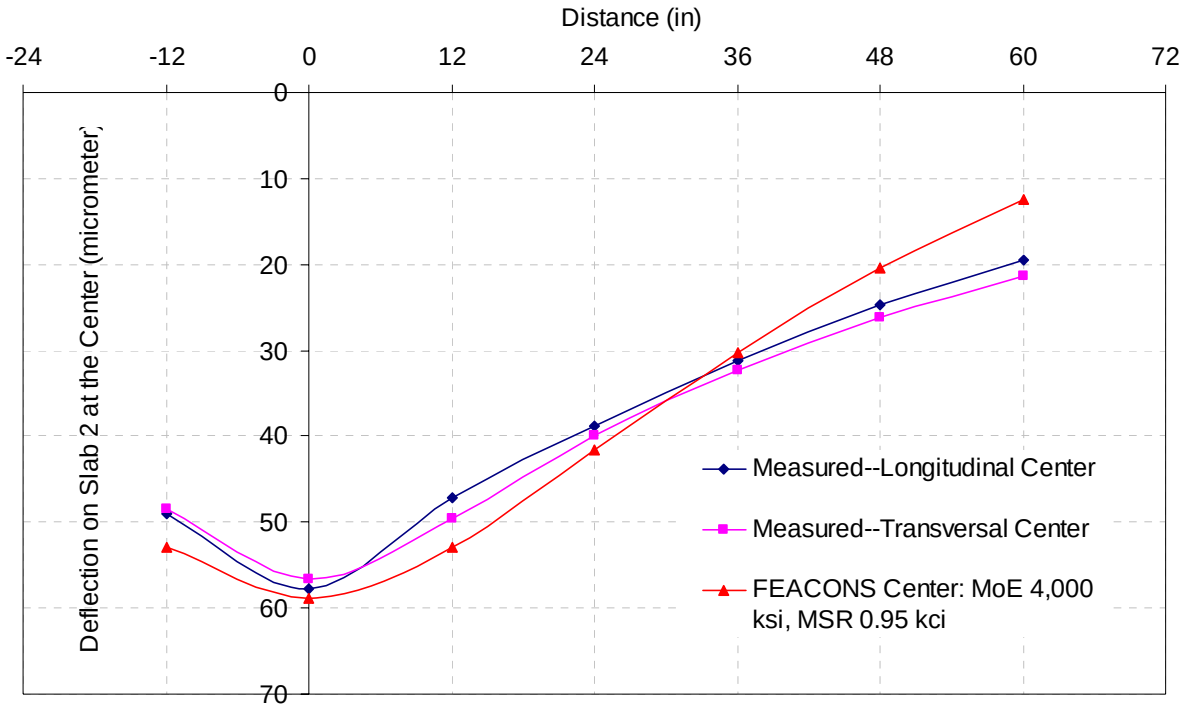

Figure 7-4. Measured and computed deflection basin caused by a 9-kip FWD load at slab center for Slab 2.

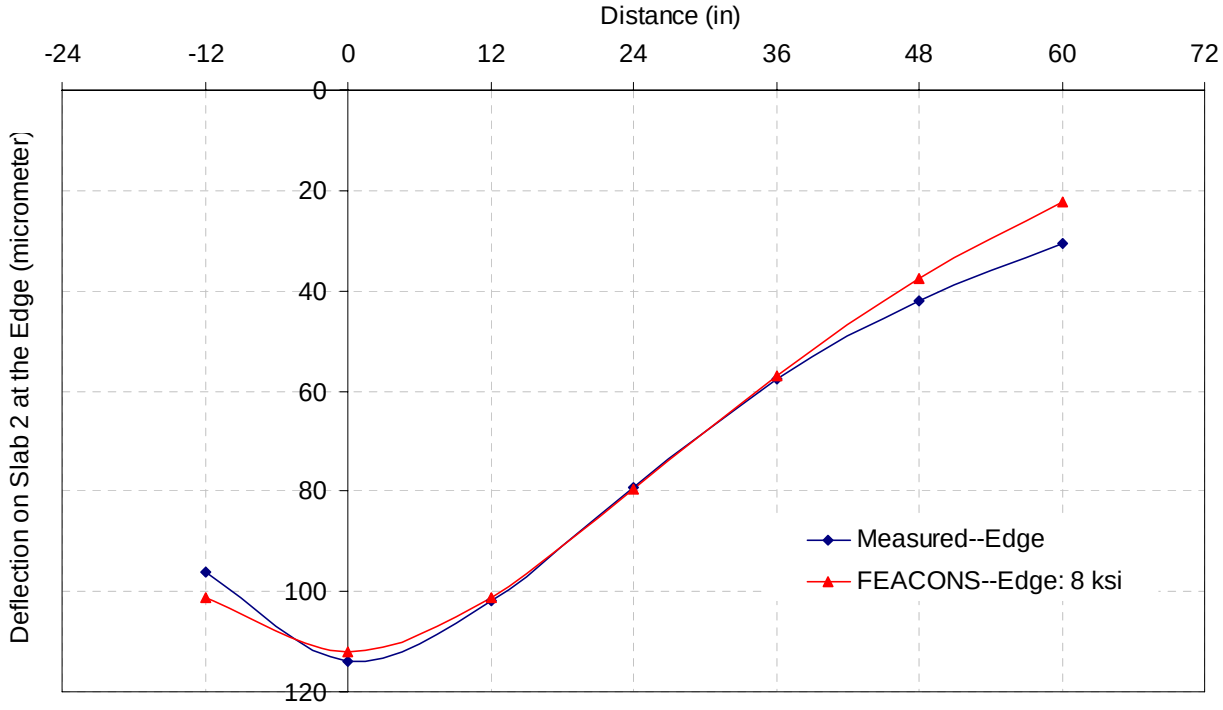

Figure 7-5. Measured and computed deflection basin caused by a 9-kip FWD load at slab edge for Slab 2.

FWD deflections at the joint of Slab 2 were also used to estimate the joint coefficients. With previous estimated parameters and values of the other known pavement parameters, the computed and measured deflection at the joint were matched fairly well by using a linear spring coefficient of 300 ksi and a torsional spring coefficient of 1,500 K-in/in at the joint as shown in Figure 7-6.

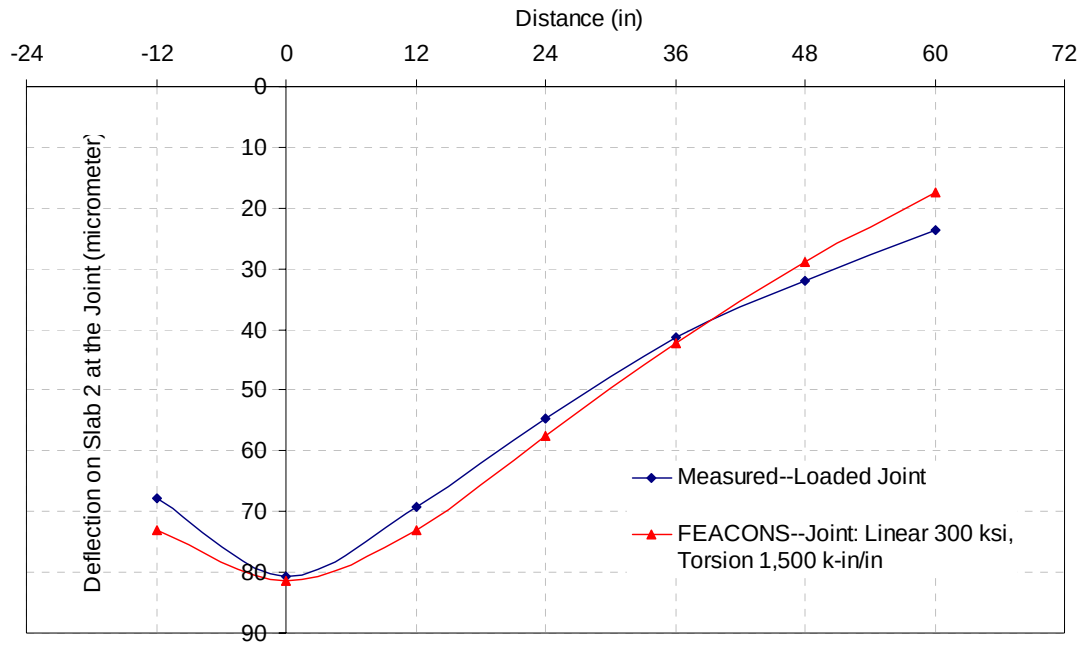

Figure 7-6. Measured and computed deflection basin caused by a 9-kip FWD load at slab joint for Slab 2.

7.2.3 Slab 3

For Slab 3, a 12-kip FWD load was used as the applied load for calibrating the analytical model. Using a similar process as in the previous two models, the matched computed deflection basin was obtained by using a modulus of subgrade reaction of 0.85 kci as shown in Figure 7-7. An edge stiffness of 5 kci gave a quite good match between the computed and measured deflection at the confined edge as shown in Figure 7-8. The computed and measured deflection at the joint were matched fairly well by using a linear spring coefficient of 300 ksi and a torsional spring coefficient of 1,500 K-in/in at the joint as shown in Figure 7-9.

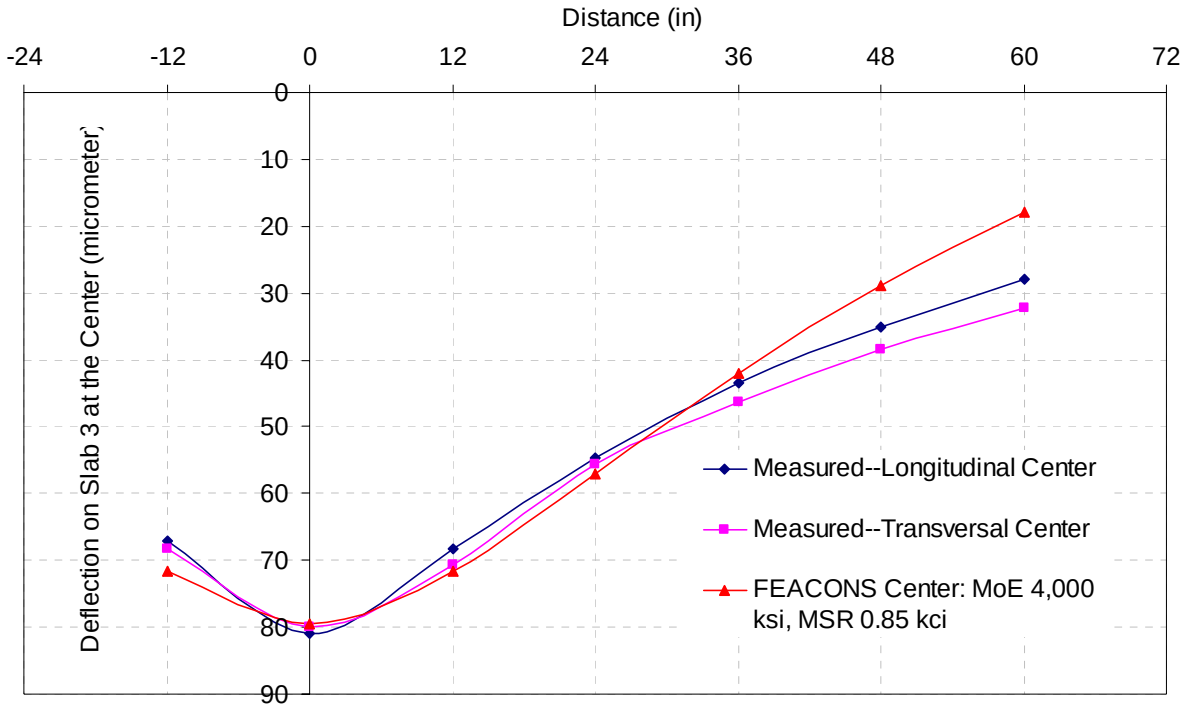

Figure 7-7. Measured and computed deflection basin caused by a 12-kip FWD load at slab center for Slab 3.

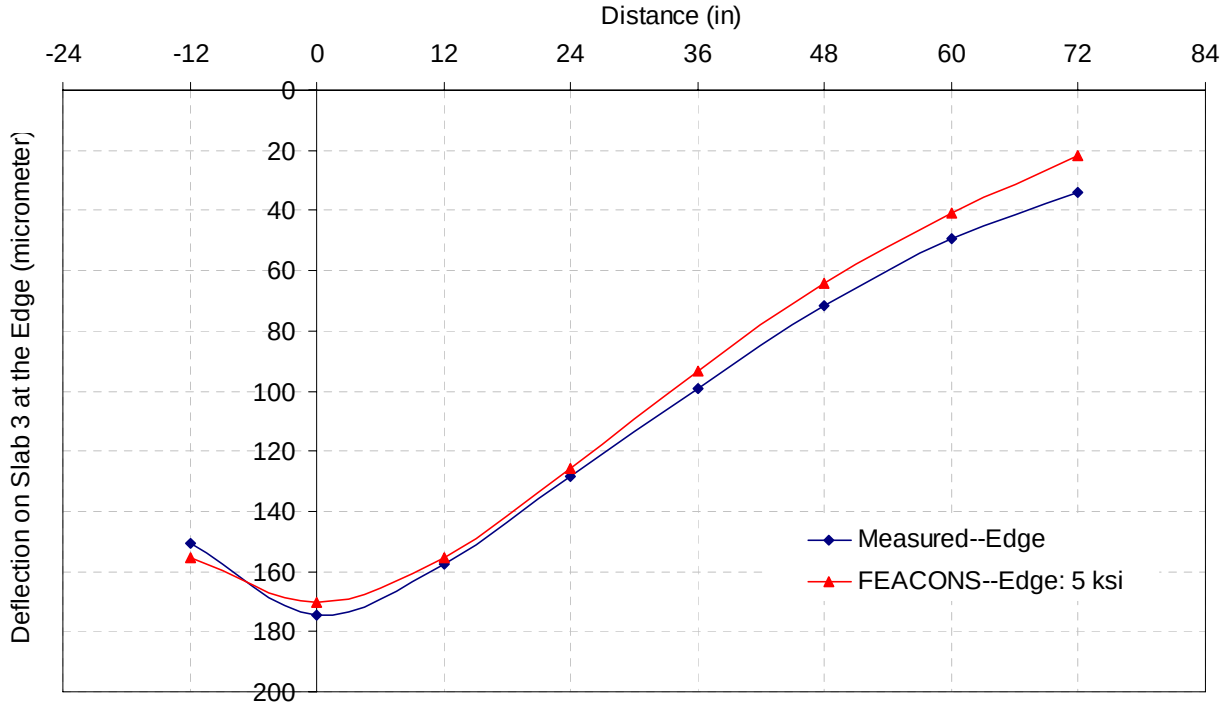

Figure 7-8. Measured and computed deflection basin caused by a 12-kip FWD load at slab edge for Slab 3.

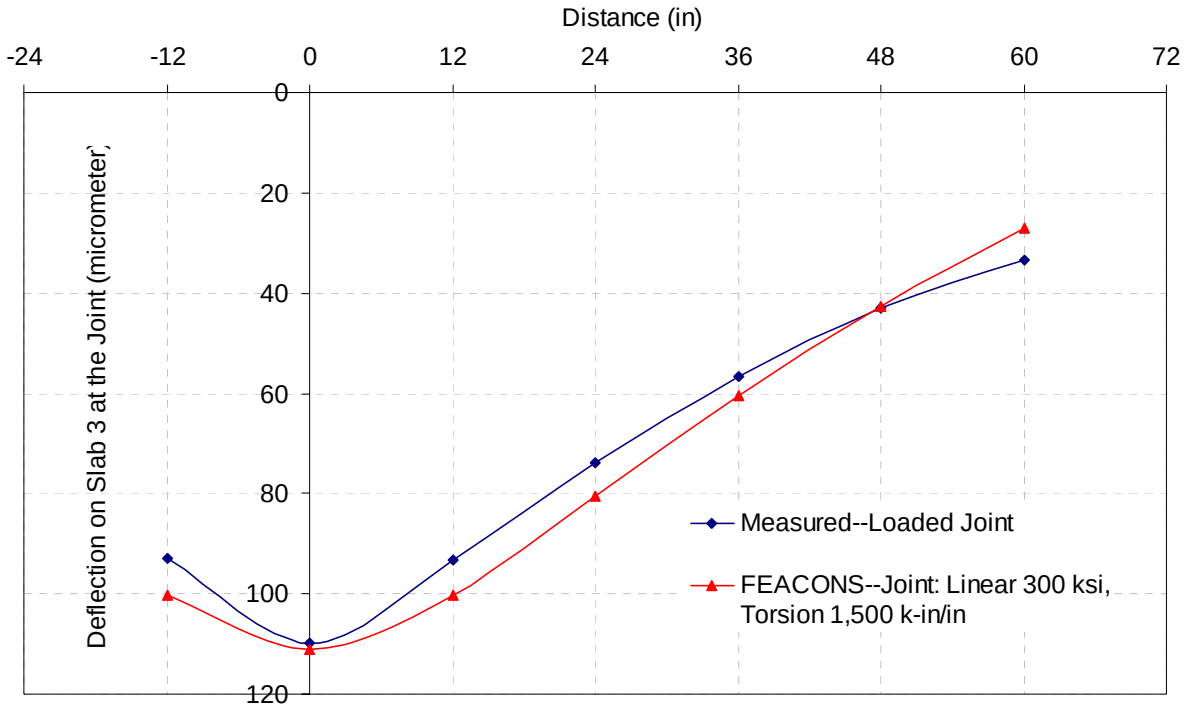

Figure 7-9. Measured and computed deflection basin caused by a 12-kip FWD load at slab joint for Slab 3.

7.2.4 Slab 4

For Slab 4, a 12-kip FWD load was again used as the applied load for calibrating the analytical model. Using a similar model and procedure, the computed deflection basin was matched to the measured one by using a modulus of subgrade reaction of 0.80 kci, as shown in Figure 7-10. An edge stiffness of 20 kci gave a fairly good match between the computed and measured deflection at the confined edge as shown in Figure 7-11. The computed and measured deflections at the joint were matched fairly well by using a higher linear spring coefficient of 1,000 ksi and a torsional spring coefficient of 2,000 K-in/in at the joint as shown in Figure 7-12.

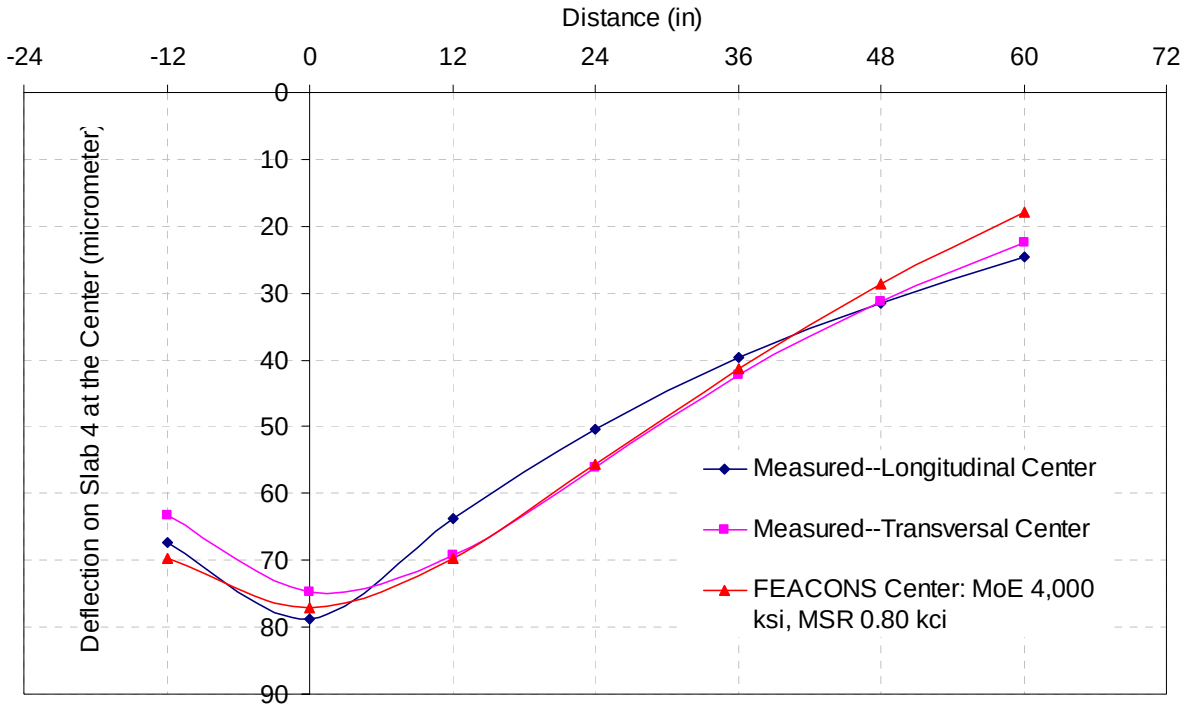

Figure 7-10. Measured and computed deflection basin caused by a 12-kip FWD load at slab center for Slab 4.

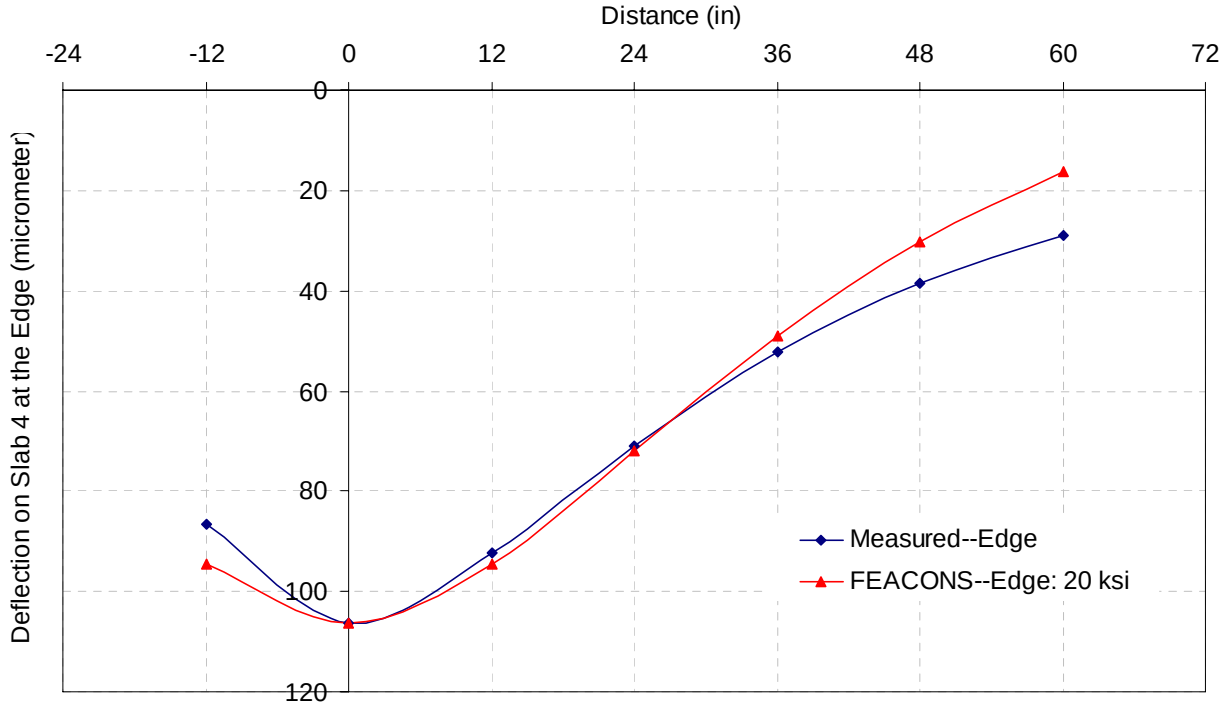

Figure 7-11. Measured and computed deflection basin caused by a 12-kip FWD load at slab edge for Slab 4.

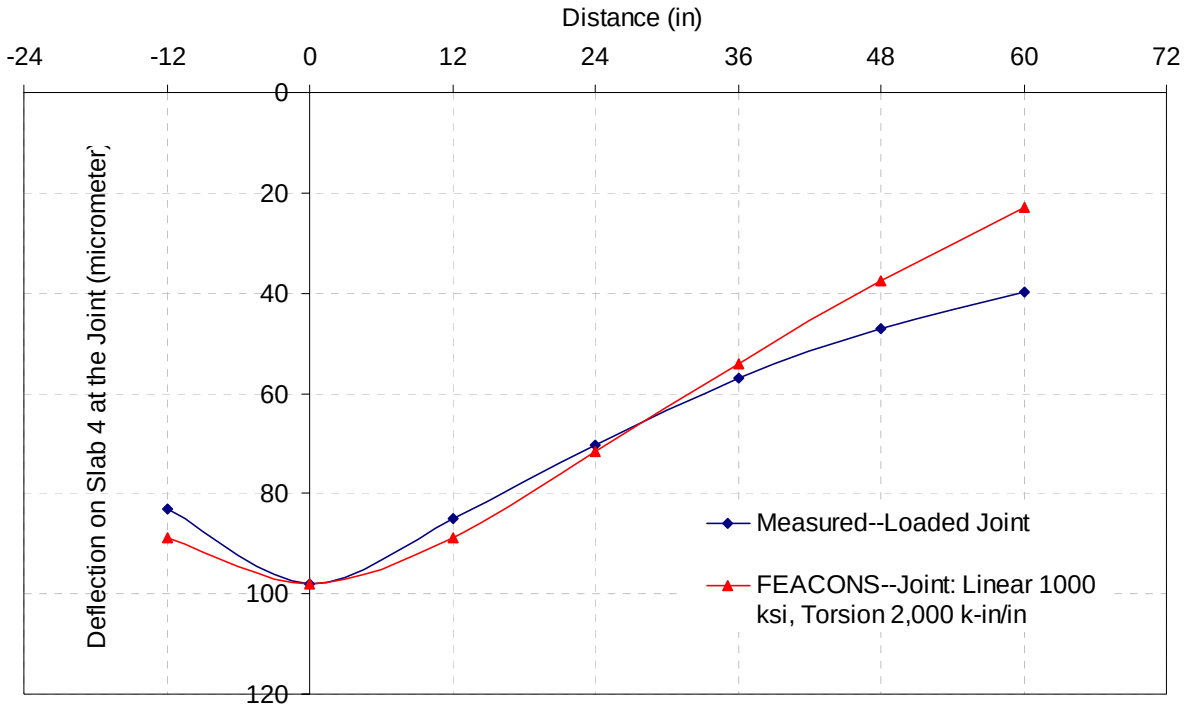

Figure 7-12. Measured and computed deflection basin caused by a 12-kip FWD load at slab joint for Slab 4.

7.2.5 Slab 5

Since Slab 5 was constructed over a compacted limerock base instead of an asphalt concrete base, The slab was modeled as a one layer of 9-inch concrete slab placed unbonded over a compacted limerock base (as a Winkler foundation). A 12-kip FWD load was used as the applied load for calibrating the FEACONS model. Material properties used in this calibration are also shown in the Table 7-1.

FWD testing was performed on the test slab after the HVS loading was finished. Cracks developed on Slab 5 such that the test slab was separated into four small slabs as shown in Figure 5-28. FWD loads were applied at locations away from the cracks to avoid the effect of the cracks as much as possible.

Figure 7-13 shows the measured and computed deflections at the location of the geophones for Slab 5. The measured deflections in the transversal direction were used to compare with the

computed deflection basin. A modulus of subgrade reaction of 0.40 kci gave a fair fit between the measured and the computed deflections.

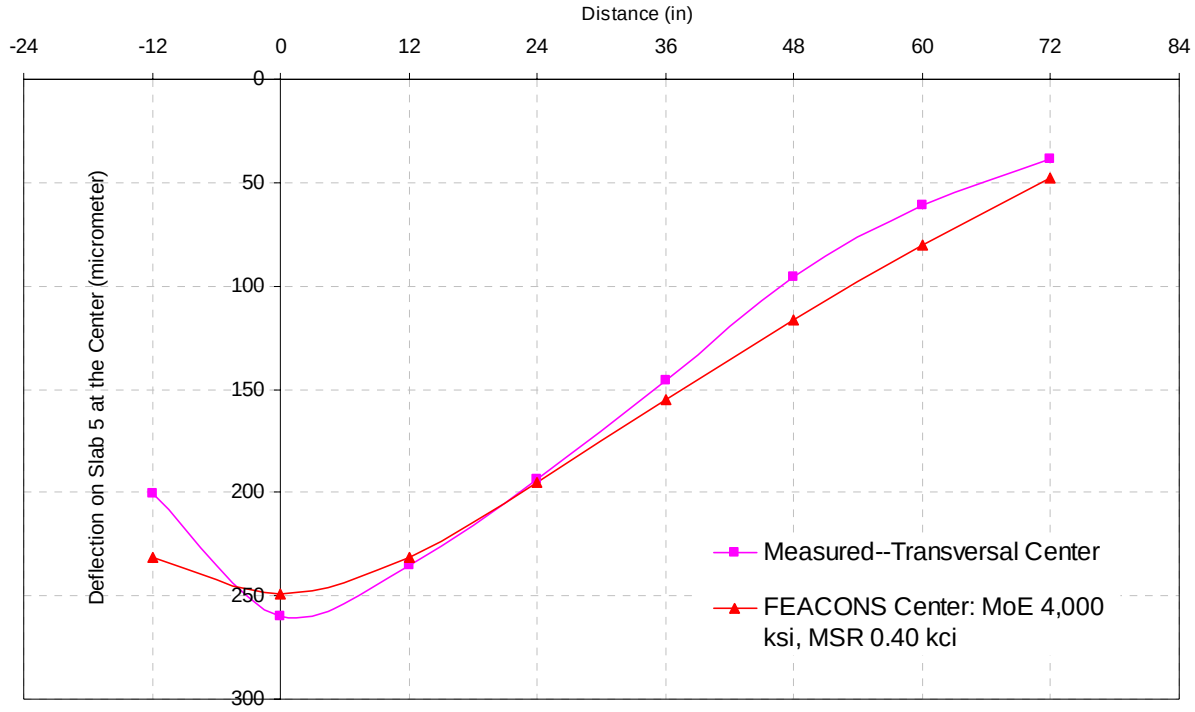

Figure 7-13. Measured and computed deflection basin caused by a 12-kip FWD load at slab center for Slab 5.

An edge stiffness of 5 kci gave a fair match between the computed and measured deflection at the confined edge as shown in Figure 7-14. It is to be noted that there was a crack at the location of loading plate.

The computed and measured deflection at the joint were matched at the joint of the test slab by using a linear spring coefficient of 1,000 ksi and a torsional spring coefficients of 2,000 K-in/in at the joint as shown in Figure 7-15.

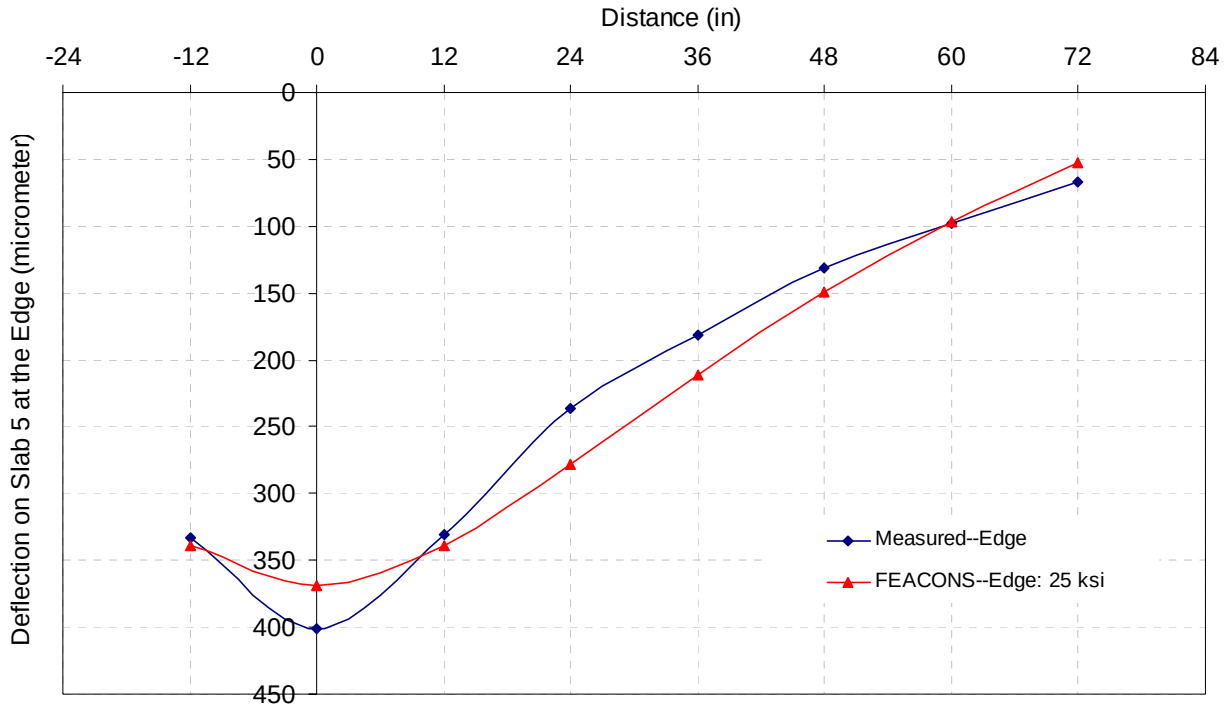

Figure 7-14. Measured and computed deflection basin caused by a 12-kip FWD load at slab edge for Slab 5.

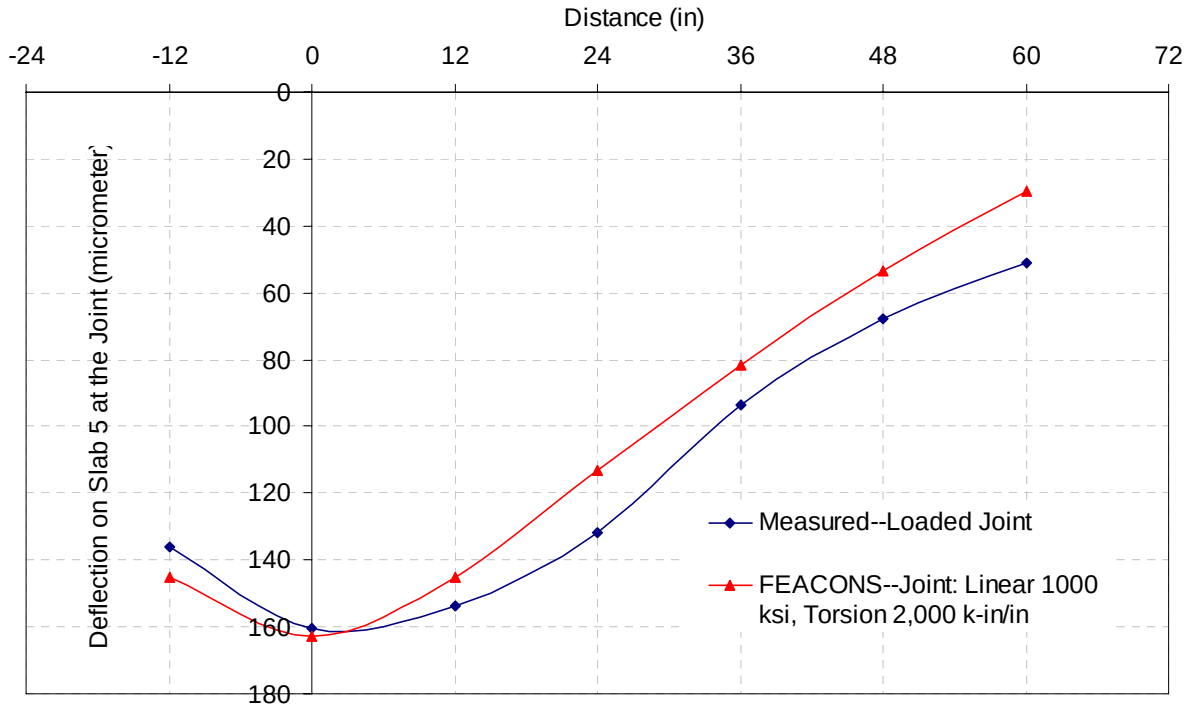

Figure 7-15. Measured and computed deflection basin caused by a 12-kip FWD load at slab joint for Slab 5.

7.3 Verification of Model Parameters

In order to verify the parameters for the FEACONS model, the computed strains at each gauge location are compared with the measured strains from strain gauges embedded in the test slab. The computed strains were computed from the computed stresses by using elastic modulus and Poisson's ratio of the concrete. The stress at each gauge location was computed by using the FEACONS model for the case of static load at several specified locations on the wheel path. The locations of the strain gauges in Slab 1 are shown in Figure 7-16. Figures 7-17 through 7-22 show the comparison of analytical strains using the FEACONS model and the measured dynamic strains at gauge location 1T, 2T, 3T, 4T, 6B and 7B on Slab 1 respectively.

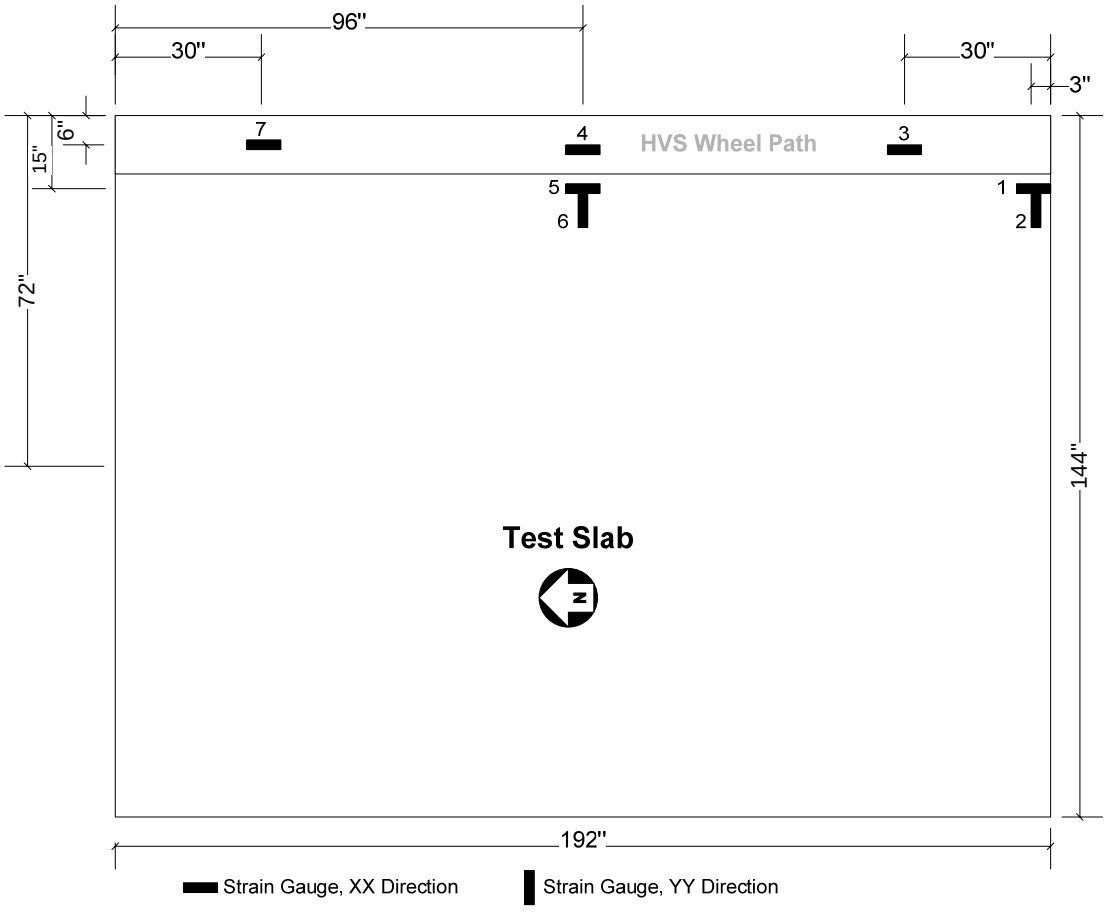

Figure 7-16. The locations of the strain gauges in Slab 1.

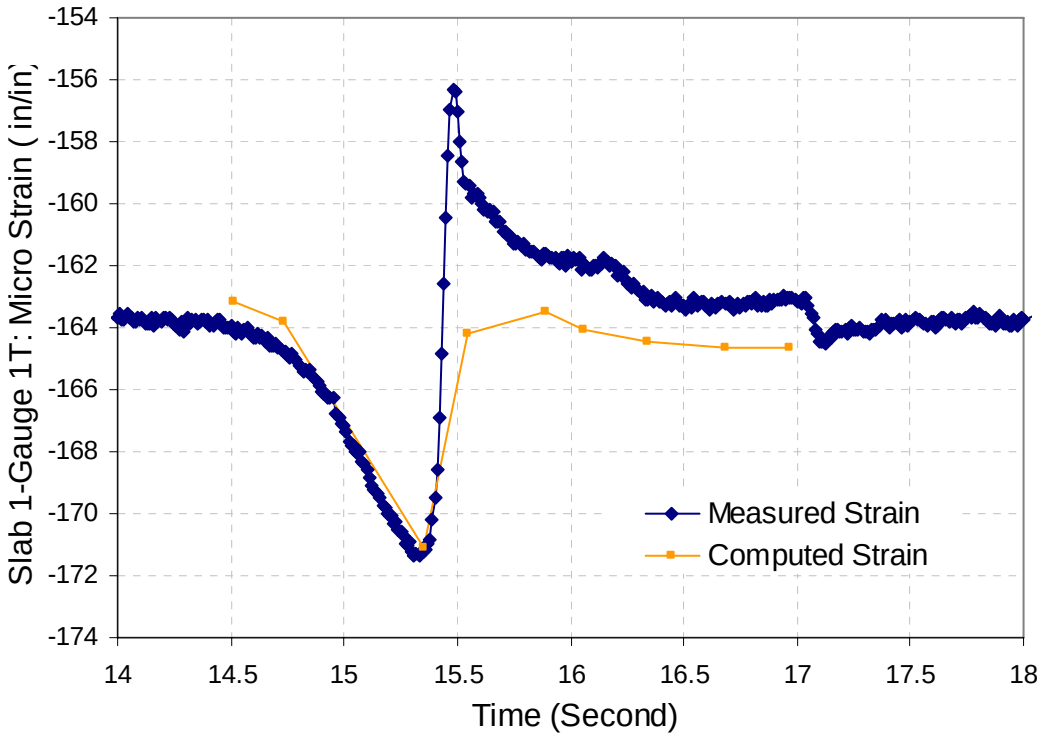

Figure 7-17. Measured and computed strains for Gauge 1T on Slab 1

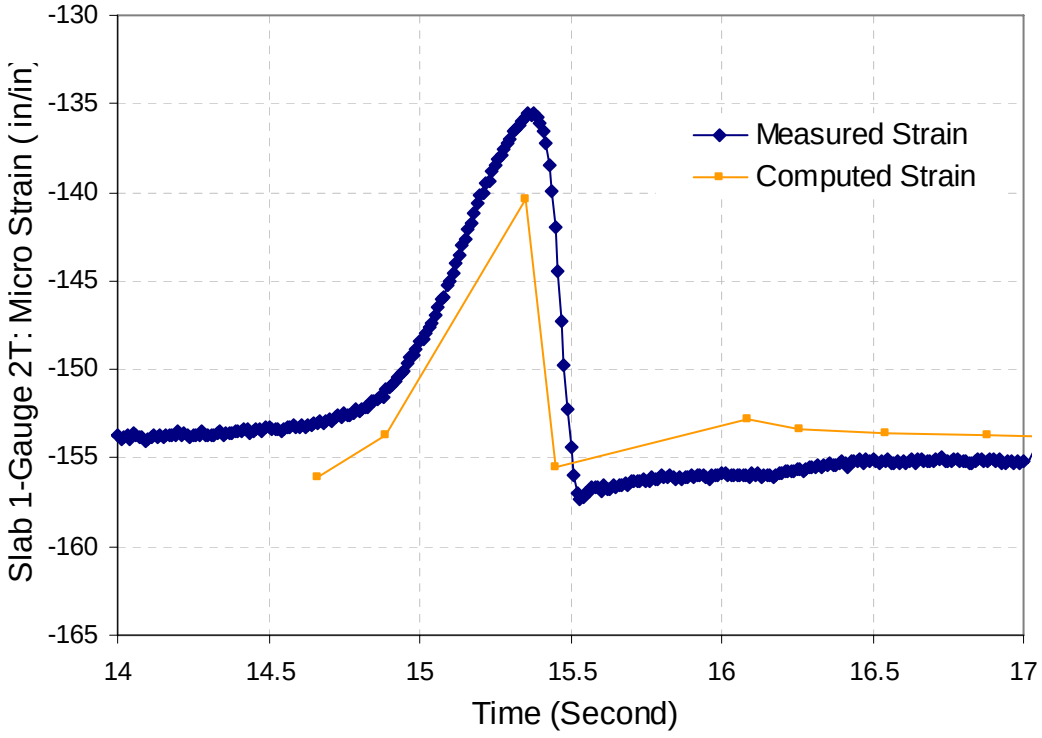

Figure 7-18. Measured and computed strains for Gauge 2T on Slab 1

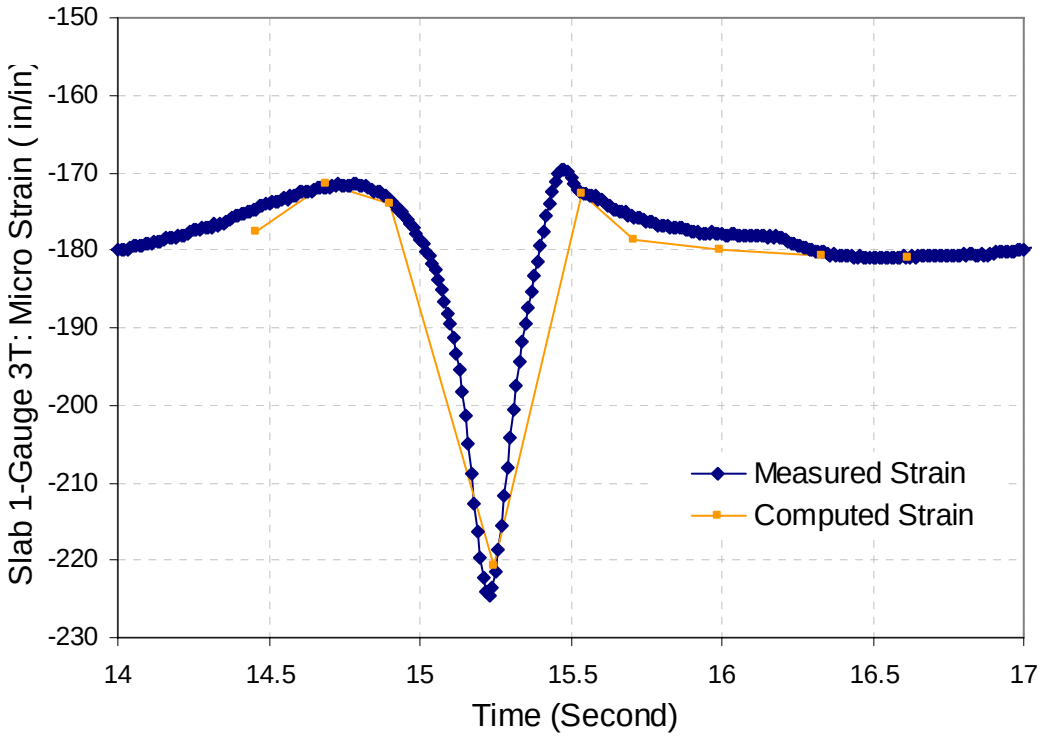

Figure 7-19. Measured and computed strains for Gauge 3T on Slab 1

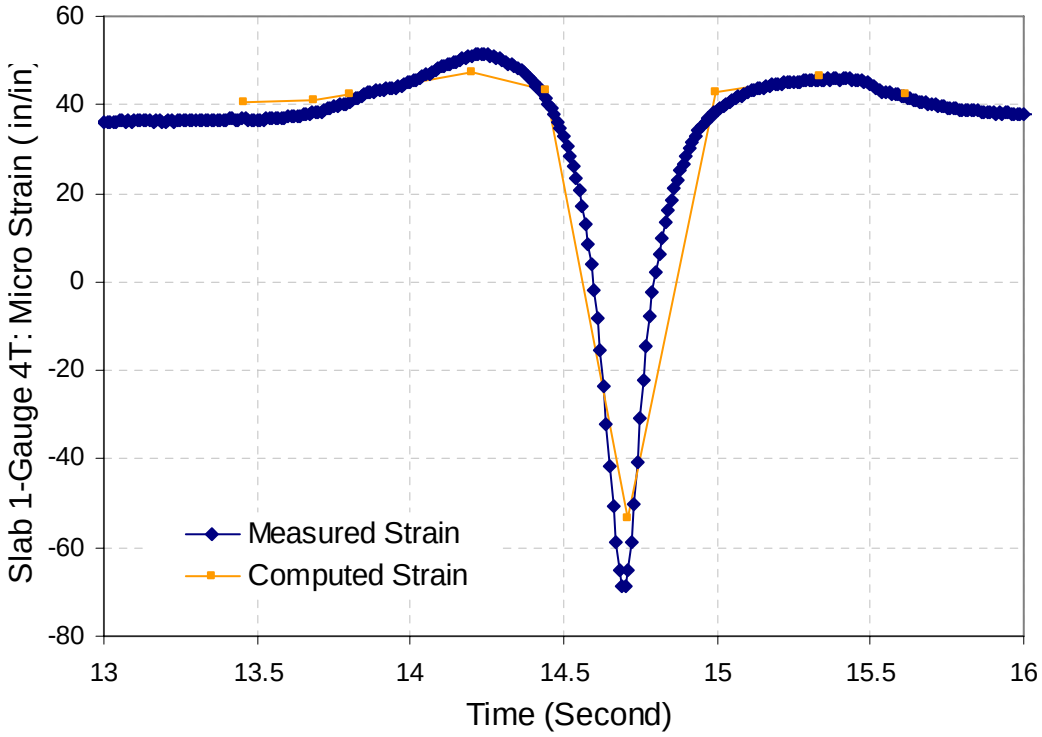

Figure 7-20. Measured and computed strains for Gauge 4T on Slab 1

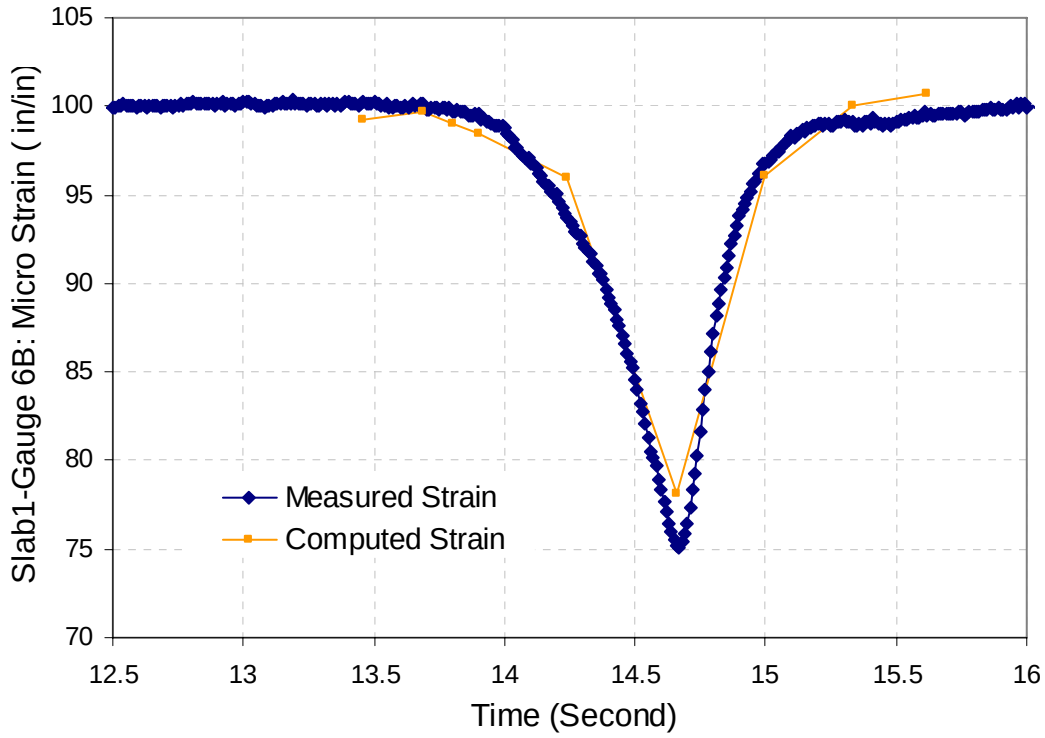

Figure 7-21. Measured and computed strains for Gauge 6B on Slab 1.

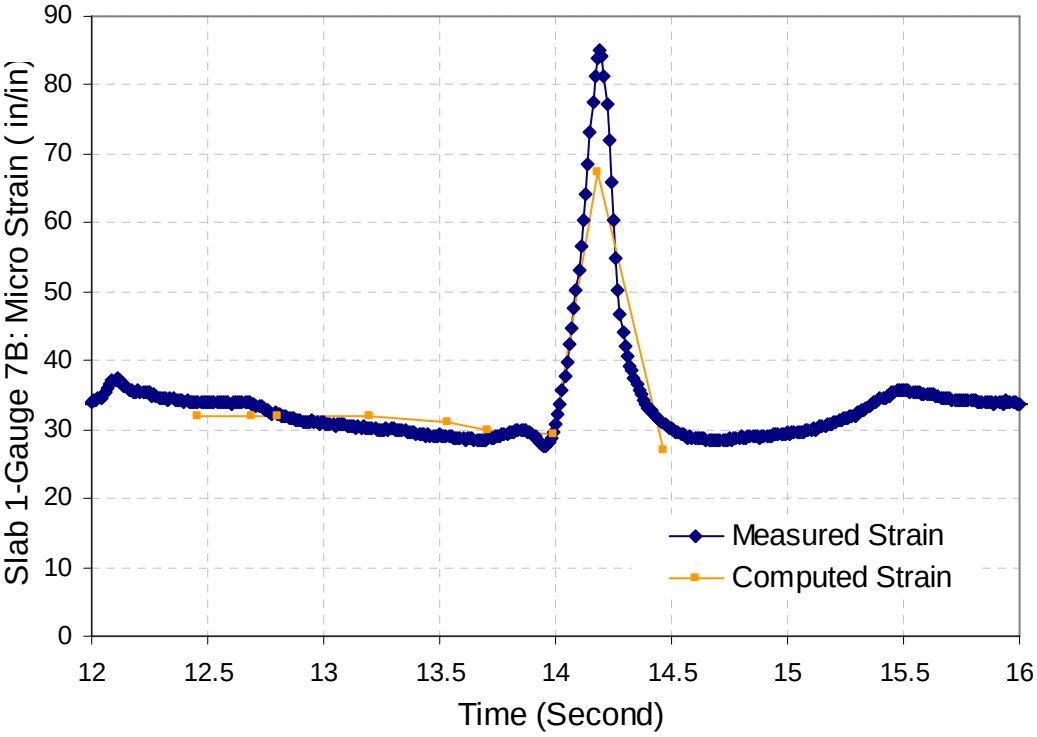

Figure 7-22. Measured and computed strains for Gauge 7B on Slab 1.

The locations of the strain gauges in Slab 5 are shown in Figure 7-23. Figures 7-24 through 7-31 show the comparison of analytical strains using the FEACONS model and the measured dynamic strains at gauge location 1B, 2B, 3B, 4B, 4T, 5T, 6T and 7T on Slab 5 respectively.

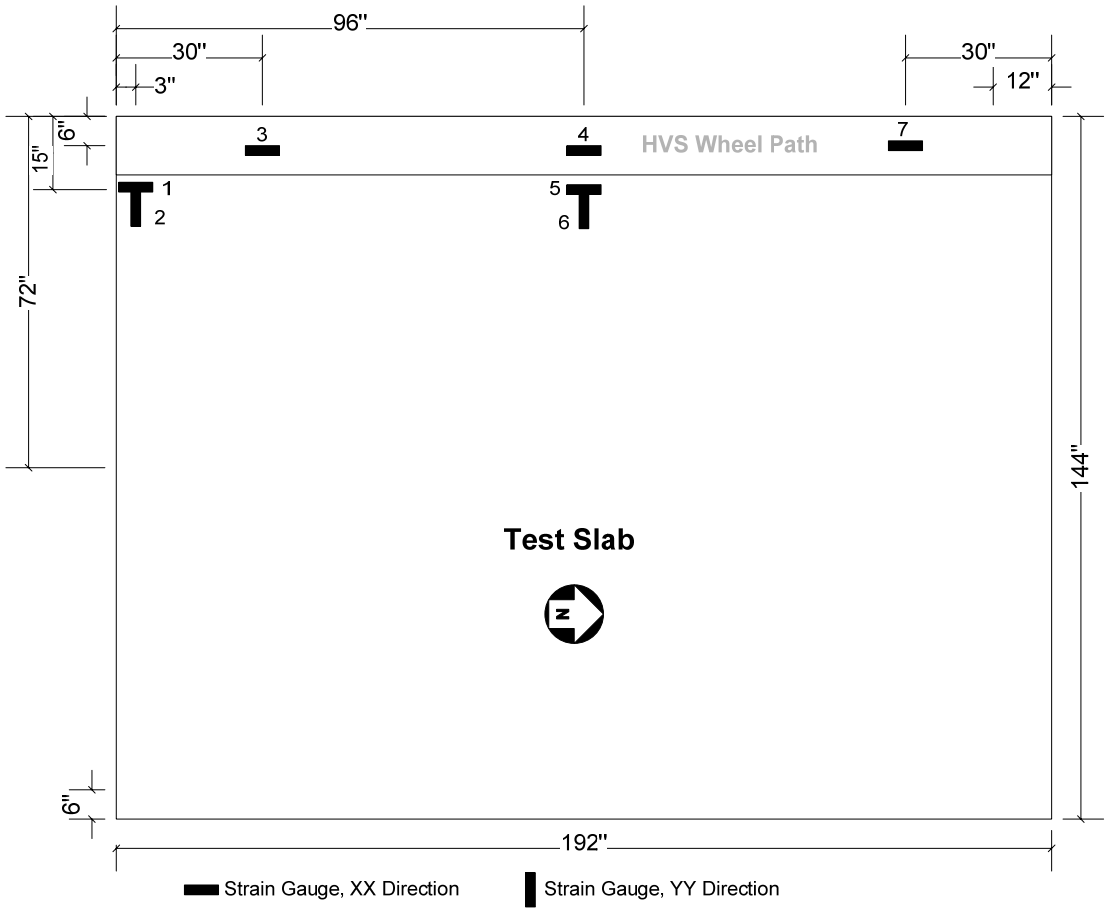

Figure 7-23. The locations of the strain gauges in Slab 5.

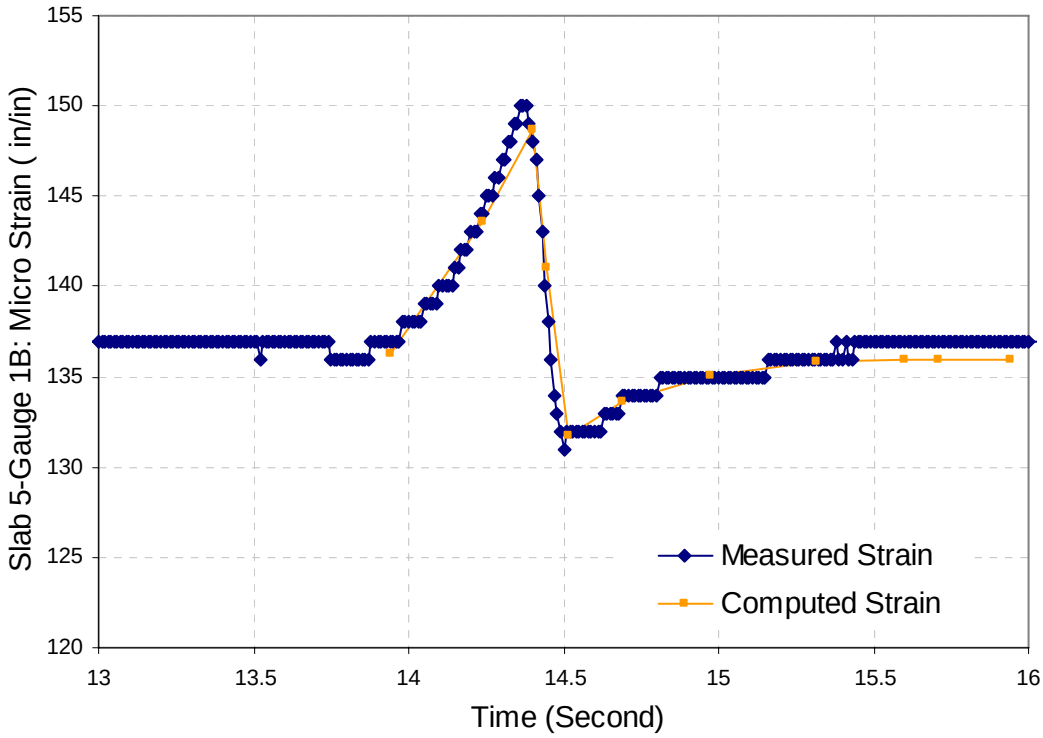

Figure 7-24. Measured and computed strains for Gauge 1B on Slab 5.

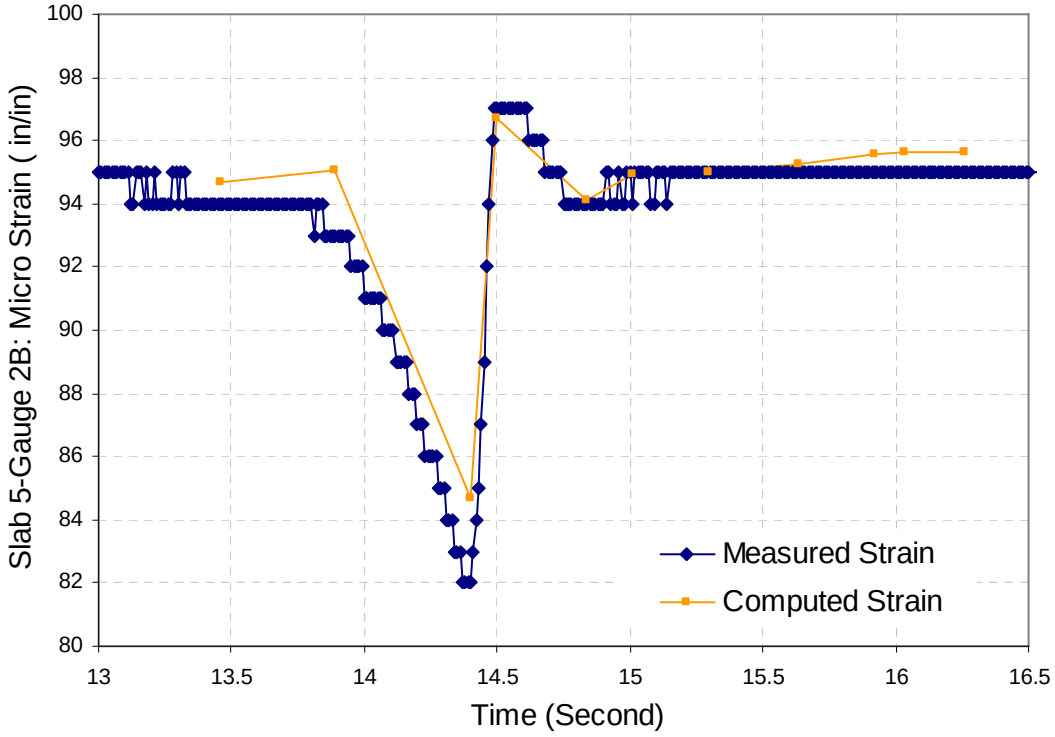

Figure 7-25. Measured and computed strains for Gauge 2B on Slab 5.

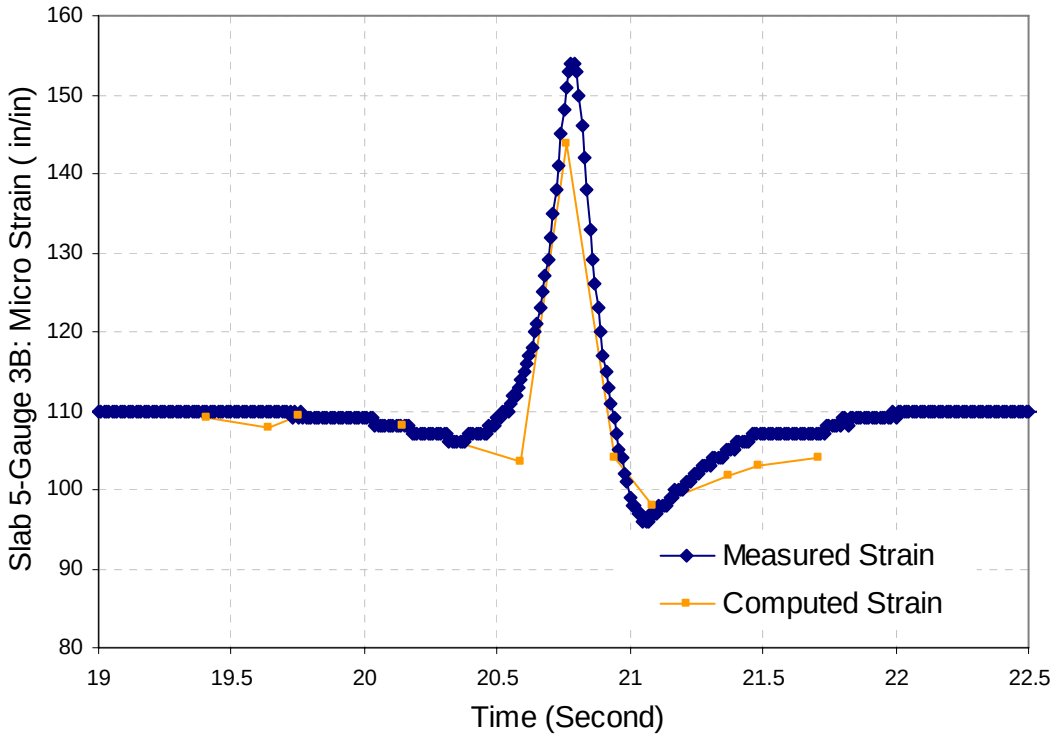

Figure 7-26. Measured and computed strains for Gauge 3B on Slab 5.

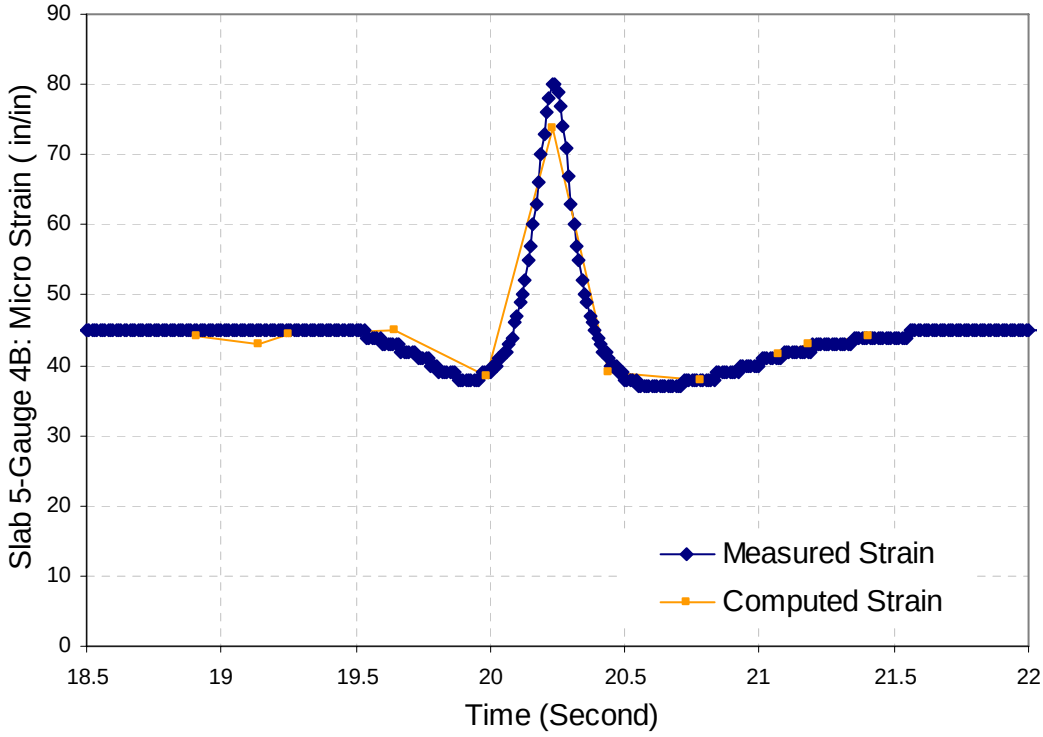

Figure 7-27. Measured and computed strains for Gauge 4B on Slab 5.

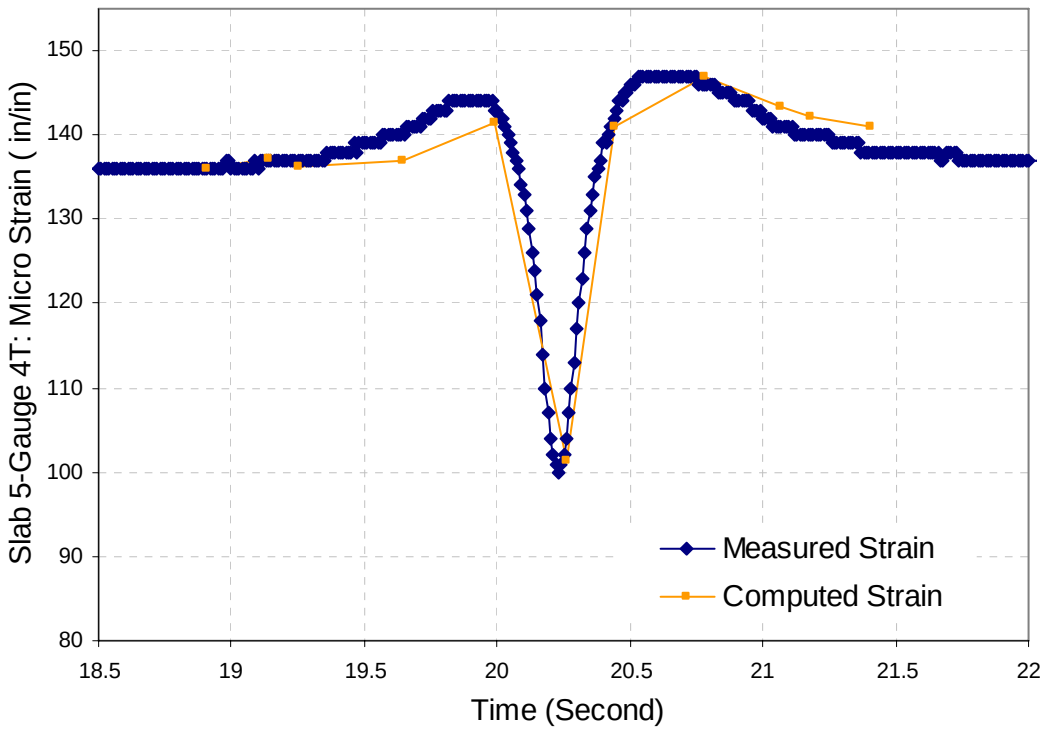

Figure 7-28. Measured and computed strains for Gauge 4T on Slab 5.

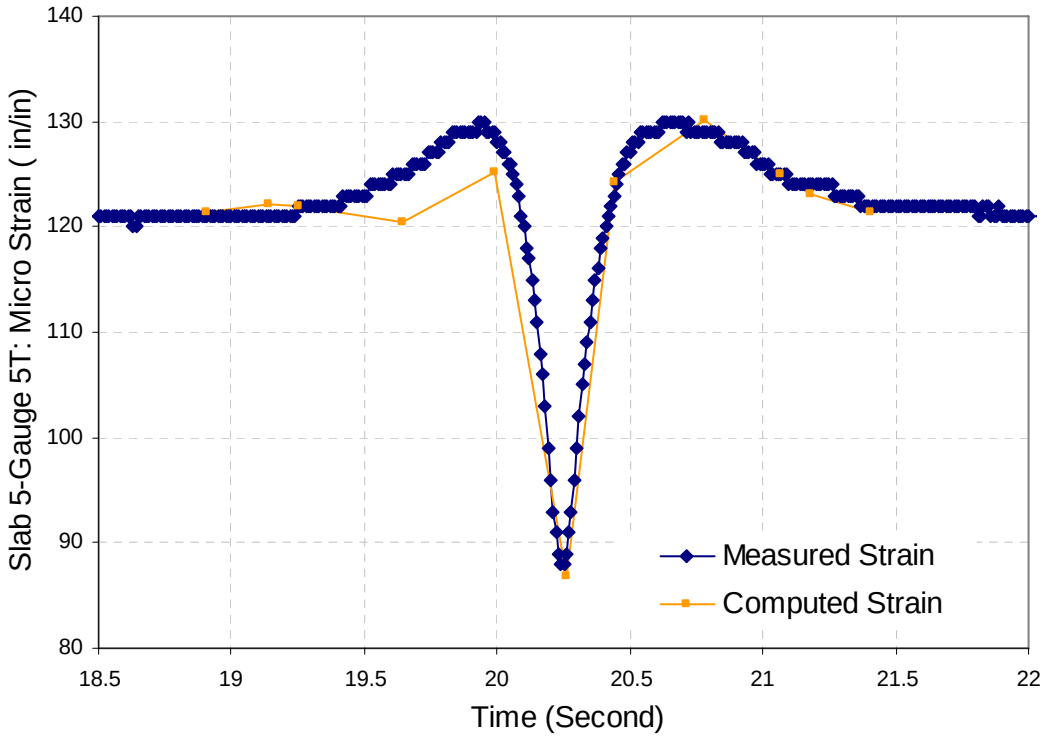

Figure 7-29. Measured and computed strains for Gauge 5T on Slab 5.

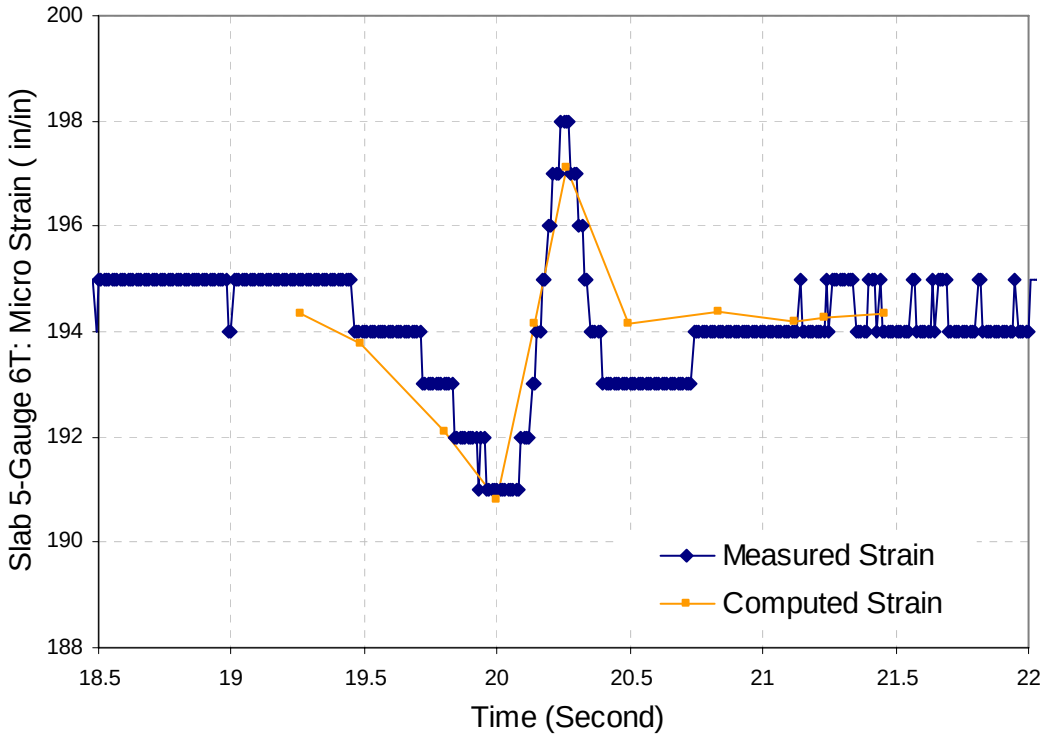

Figure 7-30. Measured and computed strains for Gauge 6T on Slab 5.

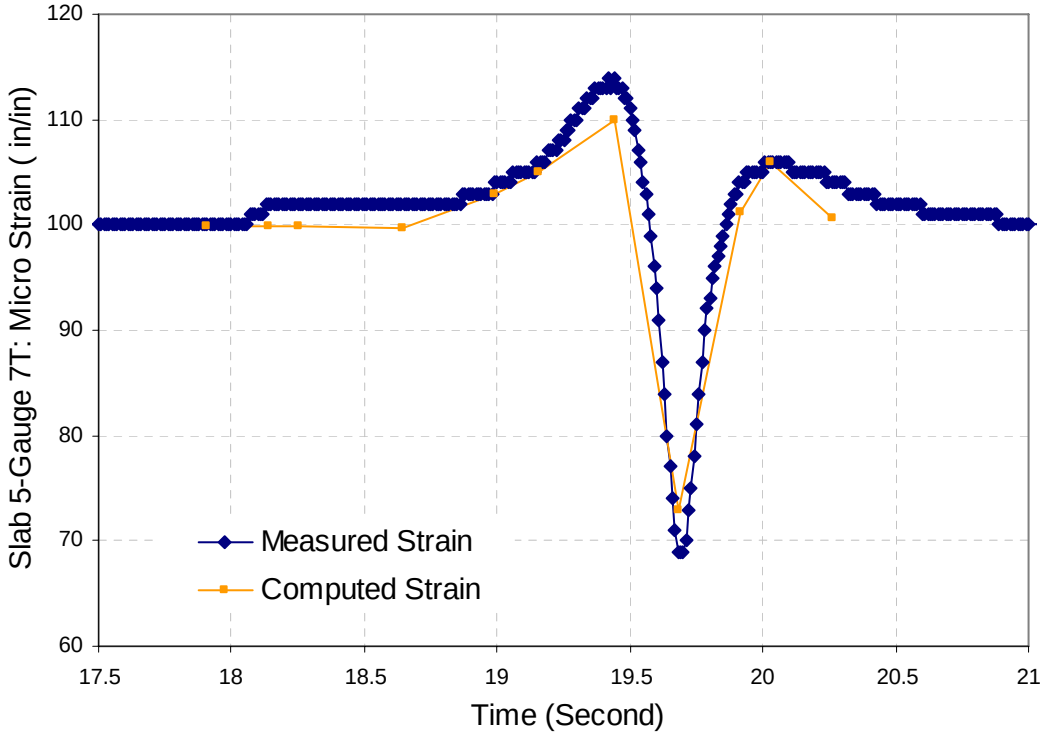

Figure 7-31. Measured and computed strains for Gauge 7T on Slab 5.

Table 7-2 presents a summary of model parameters calibrated for the test slabs in this study. The calibrated parameters and material test results were used to perform the analysis of stresses due to temperature and load in each test slab as presented in Chapter 8.

Table 7-2. Summary of model parameters calibrated for the test slabs.

Parameters Used in FEACONS Model	Slab 1	Slab 2	Slab 3	Slab 4	Slab 5
Slab Size (ft. x ft.)	12 x 16	12 x 16	12 x 16	12 x 16	12 x 16
Number of Bonded Layers	2	2	2	2	1
Thickness of Concrete Slab (inch)	9	9	9	9	9
Elastic Modulus of Concrete (ksi)	4,000	4,000	4,000	4,000	4,000
Density of Concrete (pcf)	140	140	140	140	140
Thickness of Asphalt Concrete (inch)	4	4	4	4	N/A
Elastic Modulus of Asphalt Concrete (ksi)	1,400	1,400	1,400	1,400	1,400
Density of Asphalt Concrete (pcf)	100	100	100	100	100
Poison's ratio	0.2	0.2	0.2	0.2	0.2
Subgrade Condition	Linear	Linear	Linear	Linear	Linear
Modulus of Subgrade Reaction (kci)	**0.80**	**0.95**	**0.85**	**0.80**	**0.40**
Applied load (kip)	9	9	12	12	12
Temperature Effect	No	No	No	No	No
Spring Coefficient for the Edge (ksi)	**25**	**8**	**5**	**20**	**5**
Linear Spring Coefficient for the Dowel Joint (ksi)	**300**	**300**	**300**	**1,000**	**1,000**
Torsional Spring Coefficient for the Dowel Joint (k-in/in)	**1,500**	**1,500**	**1,500**	**2,000**	**2,000**

CHAPTER 8
EVALUATION OF POTENTIAL PERFORMANCE

8.1 Introduction

This chapter presents the evaluation of the performance of replacement slabs by critical stress analysis. Stress analyses to determine the maximum stresses in each test slab under typical critical temperature-load condition were performed using the FEACONS model with the calibrated model parameters and the measured coefficient of thermal expansion of the each concrete used in each test slab in this study. The flexural strength of the concrete as determined by maturity method for each test slab was used to calculate the stress to strength ratio in each analysis. The observed performance of each test slab, as well as the characteristics of concrete mixes and test slabs were also used to evaluate the potential performance of the test slabs in this study.

8.2 Evaluation of Potential Performance of Test Slabs

A 12-kip single wheel load, which is slightly higher than the maximum legal single wheel load of 11 kips in Florida, was as a critical applied load in the analysis. In the analysis, the two critical loading positions used in the stress analysis were (1) the mid-edge and (2) the corner of the slab.

The potential performance of each test slab was evaluated based on the maximum stress to flexural strength ratio of the concrete at the early age. Other possible causes of cracking in a test slab were also evaluated. The fatigue curve recommended by the PCA, which relates the stress to strength ratios with the number of repetitions to produce fatigue failure in concrete, was used to estimate the number of load repetitions to failure.

8.2.1 Evaluation of Induced Stresses and Flexural Strength of Concrete in Slab 1

The HVS loading of Slab 1 was started at 7 hours after concrete placement. The test slab performed well without cracks under a 12-kip super single load, which was applied along its confined edge for 7 days with a total of 85, 254 passes, or an average of about 12,000 passes per day. Then the wheel load was increased to 15 kips and then to 18 kips as presented in Chapter 5.

The maximum induced stresses in Slab 1 due to the HVS load and the actual temperature differential in Slab 1 during the time of HVS loading were computed using the FEACONS program and compared with the strength of the concrete at the various times. The ratio between the maximum induced stress and the flexural strength at the various times were also computed. Table 8-1 presents the computed maximum induced stresses and the predicted flexural strengths of the in-place concrete in Slab 1 at the various times, and the computed stress to flexural strength ratios. It also lists the temperature differentials in the concrete slab and the elastic modulus at the various times, and the pavement parameters which were used in the FEACONS analysis.

Figure 8-1 shows the plot of the predicted flexural strength versus time of the in-place concrete, and the plot of the computed maximum stress due a 12-kip wheel load and the actual recorded temperature differential in the slab. Though the HVS load was not applied to Slab 1 until 7 hours after placement, the maximum stresses for the hypothetical case if the 12-kip load were applied at 5 hours and 6 hours were also computed and shown on the figure. It appears that if the HVS loading had started at 5 hours when the flexural strength was about 300 psi, the slab should still be strong enough to withstand the induced stresses. This hypothesis was tested in the testing of Slab 2.

Table 8-1. Predicted induced stresses and strength of concrete in Slab 1.

Time (hrs)	Temp. Diff. (^oF)	Applied Load, (kips)	Elastic Modulus (ksi)	Max. Computed Stress (psi)	Predicted Flexural Strength from Maturity (psi)	Predicted Stress/ Strength	No. of Repetition to Failure
5	0.41	12	739	191	320	0.60	35,055
6	0.19	12	1,434	232	360	0.64	9,067
7	-1.78	12	1,681	258	**397***	0.65	7,932
9	-4.91	12	1,622	287	480	0.60	34,032
24	-6.85	12	2,662	332	620	0.54	200,756
168	2.22	12	3,481	287	780	0.37	Unlimited

Note: * -actual strength of samples placed by the slab

Parameters used in the stress analysis:

The coefficient of thermal expansion: 6.15E-06 in/^oF
Concrete thickness: 9 inches
Asphalt Concrete Thickness: 4 inches
Poison's ratio: 0.2
Shear joint stiffness: 300 ksi
Torsional joint stiffness: 1,500 k-in/in
Confined edge stiffness: 25 ksi
Modulus of subgrade reaction: 0.80 kci

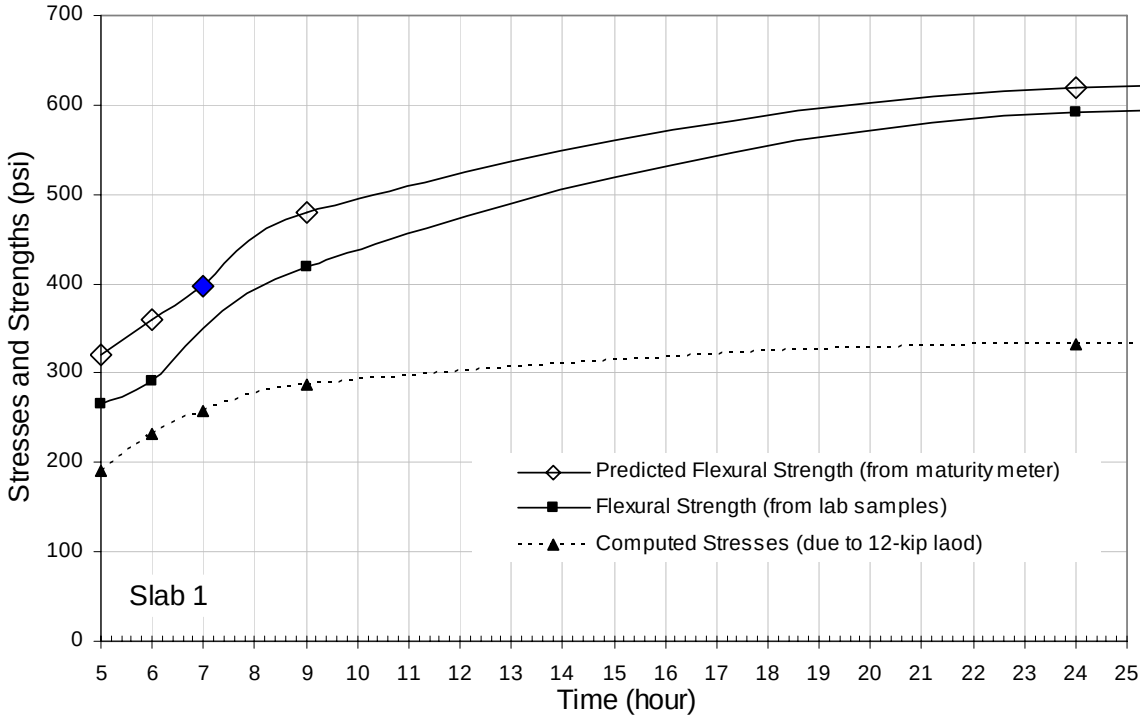

Figure 8-1. Computed stresses and flexural strengths for concrete in Slab 1.

Figure 8-1 also presents the flexural strength of the laboratory-cured samples of the same concrete mix. It can be seen that the laboratory-cured samples had a much lower strength than the strength of the in-place concrete as predicted from the maturity method, which was shown to match well with the strength of the specimens which were cured under the same condition as the test slab.

8.2.2 Evaluation of Induced Stresses and Flexural Strength of Concrete in Slab 2

The HVS loading of Slab 2 was started at 5 hours after concrete placement. The test slab performed well without cracks under a 12-kip super single load, which was applied along its confined edge for 7 days with a total of 87,785 passes, or an average of about 12,000 passes a day. Then the wheel load was increased to 15 kips and then to 18 kips as presented in Chapter 5.

The maximum induced stresses in Slab 2 due to the HVS load and the actual temperature differential in Slab 2 during the time of HVS loading were computed using the FEACONS program and compared with the strength of the concrete at the various times. The ratio between the maximum induced stress and the flexural strength at the various times were also computed. Table 8-2 presents the computed maximum induced stresses and the predicted flexural strengths of the in-place concrete in Slab 2 at the various times, and the computed stress to flexural strength ratios. It also lists the temperature differentials in the concrete slab and the elastic modulus at the various times, and the pavement parameters which were used in the FEACONS analysis.

Figure 8-2 shows the plot of the predicted flexural strength versus time of the in-place concrete, and the plot of the computed maximum stress due a 12-kip wheel load and the actual recorded temperature differential in the slab.

Table 8-2. Predicted induced stresses and strength of concrete in Slab 2.

Time (hrs)	Temp. Diff. (^oF)	Applied Load, (kips)	Elastic Modulus (ksi)	Max. Computed Stress (psi)	Predicted Flexural Strength from Maturity (psi)	Predicted Stress/ Strength	No. of Repetition to Failure
4	-3.57	12	1,047	223	360	0.62	18,455
5	-4.52	12	1,129	228	**402***	0.57	79,953
6	-6.48	12	1,211	230	450	0.51	401,390
8	-9.21	12	1,700	249	500	0.50	Unlimited
24	-0.23	12	1,913	215	590	0.36	Unlimited
168	3.48	12	3,470	229	730	0.31	Unlimited

Note: * -actual strength of samples placed by the slab

Parameters used in the stress analysis:

The coefficient of thermal expansion: 6.75E-06 in/^{o}F
Concrete thickness: 9 inches
Asphalt concrete Thickness: 4 inches
Poison's ratio: 0.2
Shear joint stiffness: 300 ksi
Torsional joint stiffness: 1,500 k-in/in
Confided edge stiffness: 8 ksi
Modulus of subgrade reaction: 0.95 kci

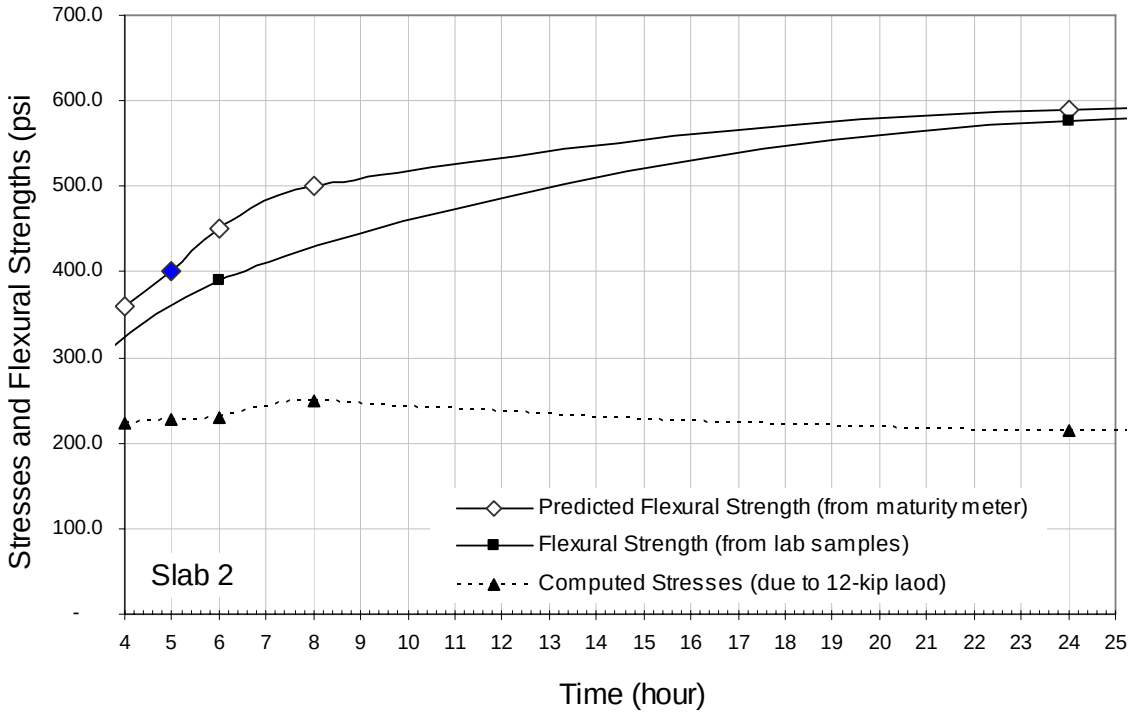

Figure 8-2. Computed stresses and flexural strengths for concrete in Slab 2.

Figure 8-2 also presents the flexural strength of the laboratory-cured samples of the same concrete mix. It can be seen that the laboratory-cured samples had a substantially lower strength than the strength of the in-place concrete as predicted from the maturity method, which was shown to match well with the strength of the specimens which were cured under the same condition as the test slab.

It can be seen from Figure 8-2 that the induced stresses in Slab 2 after the start of HVS load were lower than the flexural strength of the in-place concrete. This explains why Slab 2 held up very well under the HVS loading.

Figure 8-3 shows the comparison of compressive strengths from laboratory samples with predicted compressive strength from maturity meter for the concrete in Slab 2. Similarly, the in-place concrete can be seen to have higher strength than the laboratory-cured concrete.

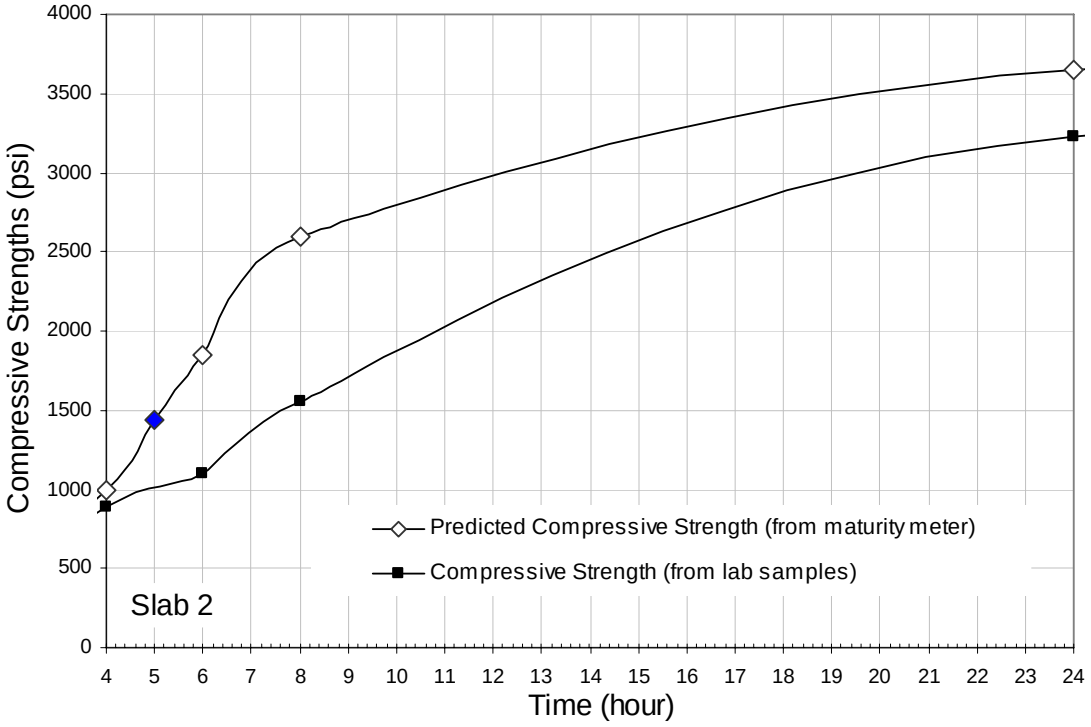

Figure 8-3. Comparison of compressive strengths for concrete in Slab 2.

8.2.3 Evaluation of Induced Stresses and Flexural Strength of Concrete in Slab 3

The HVS loading of Slab 3 was started at 4 hours after concrete placement. On the second days, a 12-inch transverse crack was first observed at the mid-edge of the slab. After repetitions of 47,170 passes of the 12-kip load, a few transverse cracks have also occurred at the mid-edge of the slab. The slab was loaded with the 12 kip-load for 7 days with a total load repetition of 95,042 passes, or an average of about 13,000 passes a day. Then the wheel load was increased to 15 kips and then to 18 kips presented in Chapter 5.

The maximum induced stresses in Slab 3 due to the HVS load and the actual temperature differential in Slab 3 during the time of HVS loading were computed using the FEACONS program and compared with the strength of the concrete at the various times. The ratio between the maximum induced stress and the flexural strength at the various times were also computed.

Table 8-3 presents the computed maximum induced stresses and the predicted flexural strengths of the in-place concrete in Slab 3 at the various times, and the computed stress to flexural strength ratios. It also lists the temperature differentials in the concrete slab and the elastic modulus at the various times, and the pavement parameters which were used in the FEACONS analysis.

Figure 8-4 shows the plot of the predicted flexural strength versus time of the in-place concrete, and the plot of the computed maximum stress due a 12-kip wheel load and the actual recorded temperature differential in the slab. Since the HVS load was applied to Slab 3 at 4 hour after placement, the computed maximum stresses due to the 12-kip load were higher than predicted flexural strength at the time. Table 8-3 also presents the low number of repetition to failure. As predicted by the high stress/strength ratio, transverse cracks were observed at mid edge of the slab after 1 day of the HVS loading.

Table 8-3. Predicted Induced Stresses and Flexural Strength of Concrete in Slab 3.

Time (hrs)	Temp. Diff. (^oF)	Applied Load, (kips)	Elastic Modulus (ksi)	Max. Computed Stress (psi)	Predicted Flexural Strength from Maturity (psi)	Predicted Stress/ Strength	No. of Repetition to Failure
4	6.85	12	825.0	215	**184.0 ***	1.17	0
5	1.07	12	1,287.5	232	235.0	0.99	1
6	-2.61	12	1,562.5	239	255.0	0.94	2
8	-4.64	12	1,812.5	213	285.0	0.75	486
24	-3.43	12	2,812.5	230	475.0	0.48	Unlimited
168	2.28	15	3,250.0	215	560.0	0.38	Unlimited

Note: * -actual strength of samples placed by the slab

Parameters used in the stress analysis:

The coefficient of thermal expansion: 6.28E-06 in/^{o}F
Concrete thickness: 9 inches
Asphalt concrete thickness: 4 inches
Poison's ratio: 0.2
Shear joint stiffness: 300 ksi
Torsional joint stiffness: 1,500 k-in/in
Free edge stiffness: 5 ksi
Modulus of subgrade reaction: 0.85 kci

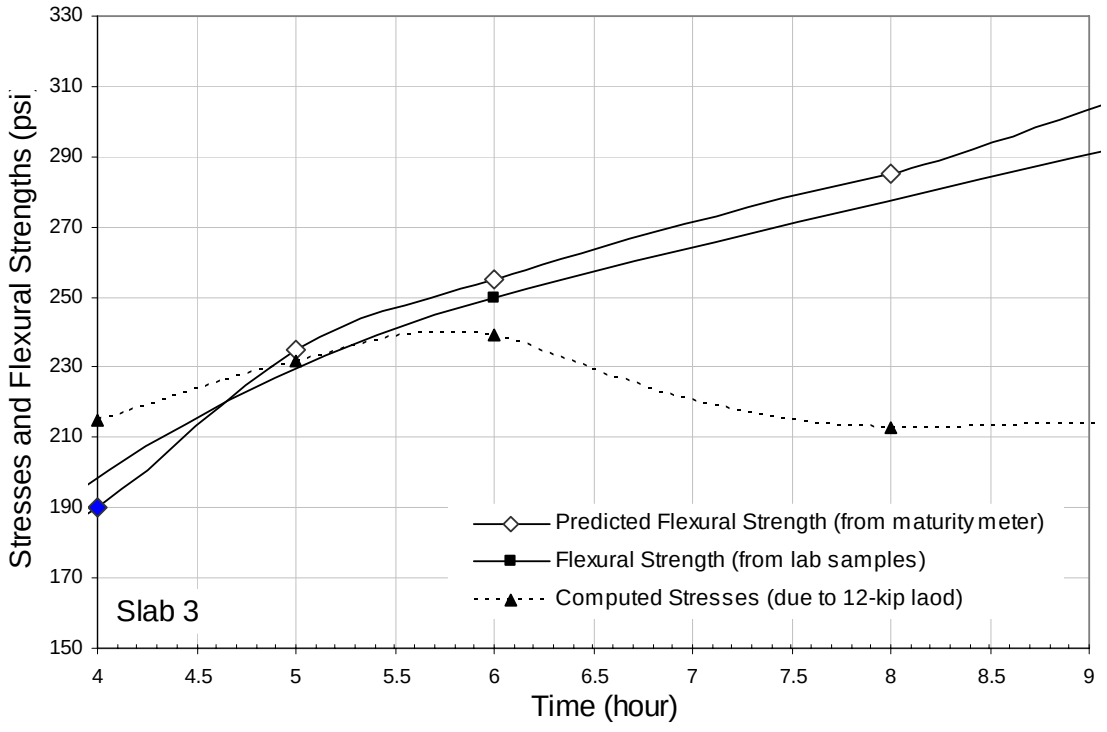

Figure 8-4. Computed stresses and flexural strengths for the concrete in Slab 3.

Figure 8-4 also presents the flexural strength of the laboratory-cured samples of the same concrete mix. It can be seen that the laboratory-cured samples had a much lower strength than the strength of the in-place concrete as predicted from the maturity method, which was shown to match well with the strength of the specimens which were cured under the same condition as the test slab.

8.2.4 Evaluation of Induced Stresses and Flexural Strength of Concrete in Slab 4

The HVS loading of Slab 4 was started at 7 hours after concrete placement. On the second days, a corner crack of about 5 feet radius was first formed at the south end of the slab. It was found out later from the strain data that the first crack corner happened at about the 41 hours after the placement of about 15,175 passes of the 12-kip load.

The time at which there was a change in the measured dynamics strains marked the time when the cracks were formed in Slab 4. Figure 8-5 shows the plots of dynamic strains as measured by Gauge 3T as a HVS wheel passed over it, before and after a crack developed on Slab 4. A change in the plots can be observed at 41 hours after concrete placement, when the first corner crack was determined to have formed.

The slab was continuously loaded with the 12 kip-load for 7 days with a total of 82,963 passes, or an average of about 12,000 passes a day. Then the wheel load was increased to 15 kips and then to 18 kips as presented in Chapter 5.

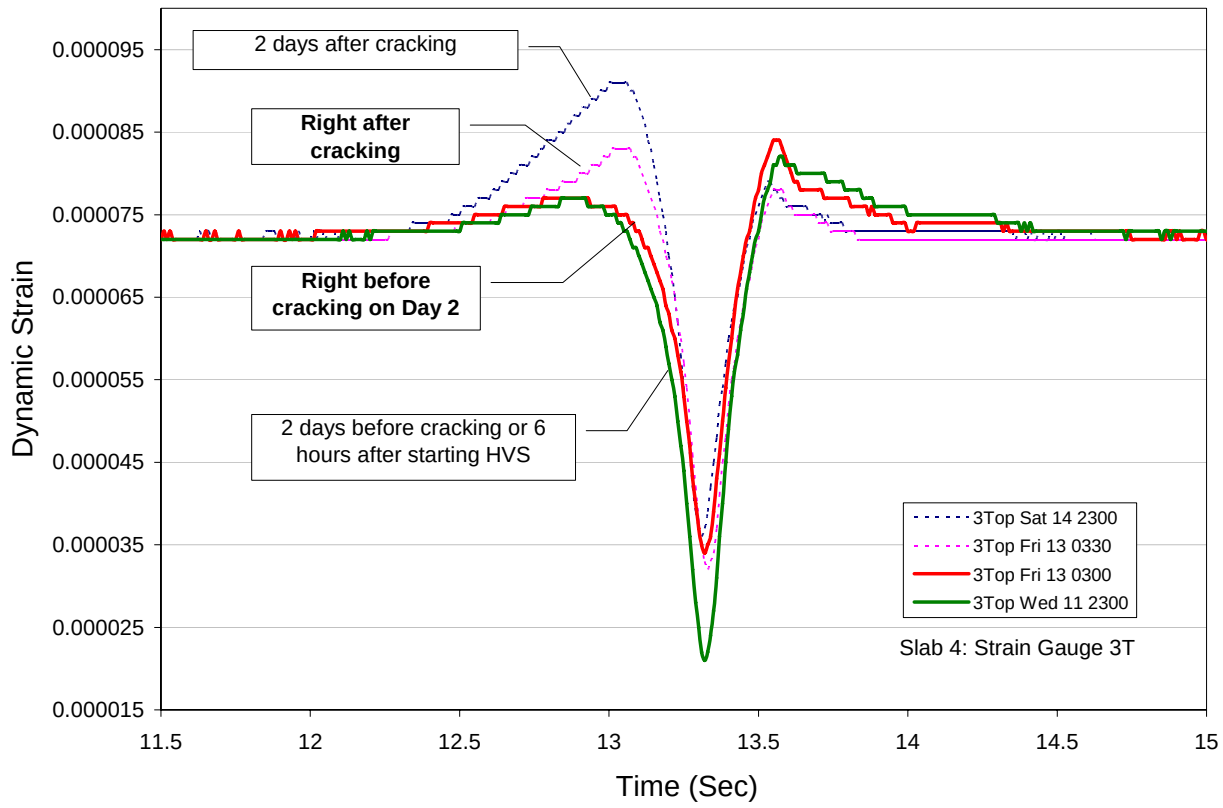

Figure 8-5. Measured dynamic strains from Gauge 3T on Slab 4.

Possible Causes of Cracking in Slab 4

The maximum induced stresses in Slab 4 due to the HVS load and the actual temperature differential in Slab 4 during the time of HVS loading were computed using the FEACONS program and compared with the strength of the concrete at the various times. The ratio between the maximum induced stress and the flexural strength at the various times were also computed. Table 8-4 presents the computed maximum induced stresses and the predicted flexural strengths of the in-place concrete in Slab 4 at the various times, and the computed stress to flexural strength ratios. It also lists the temperature differentials in the concrete slab and the elastic modulus at the various times, and the pavement parameters which were used in the FEACONS analysis.

Table 8-4. Computed load-induced stresses and predicted flexural strength of concrete in Slab 4.

Time (hrs)	Temp. Diff. (^oF)	Applied Load, (kips)	Elastic Modulus (ksi)	Max. Computed Stress (psi)	Predicted Flexural Strength from Maturity (psi)	Predicted Stress/ Strength	No. of Repetition to Failure
5	9.84	12	1,600.0	167	230	0.73	890
6	3.96	12	1,762.5	199	250	0.80	122
7	1.25	12	1,825.0	213	**305***	0.70	1,958
8	-1.66	12	1,925.0	241	330	0.73	790
24	4.57	12	3,150.0	225	530	0.42	Unlimited
168	8.91	12	3,487.5	244	720	0.29	Unlimited

Note: * -actual strength of samples placed by the slab

Parameters used in the stress analysis:

The coefficient of thermal expansion: 6.46E-06 in/^oF
Concrete thickness: 9 inches
Asphalt concrete thickness: 4 inches
Poison's ratio: 0.2
Shear joint stiffness: 1,000 ksi
Torsional joint stiffness: 2,000 k-in/in
Confined edge stiffness: 5 ksi
Modulus of subgrade reaction: 0.80 kci

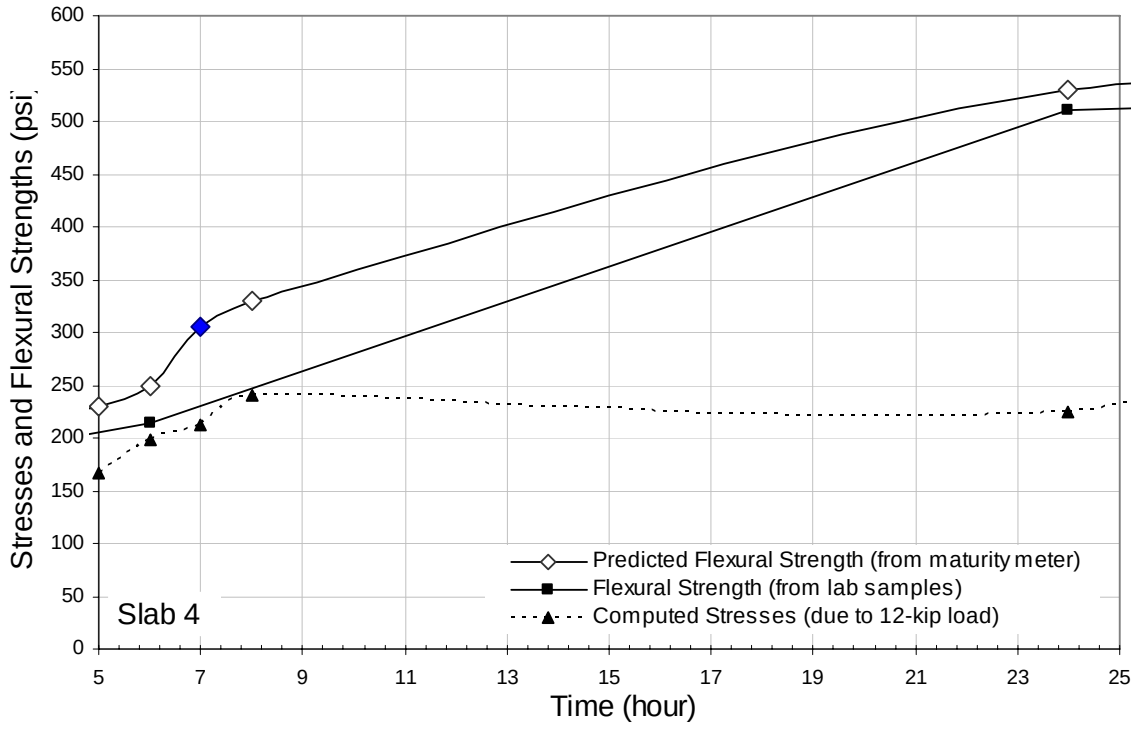

Figure 8-6. Computed stresses and flexural strengths for the concrete in Slab 4.

Figure 8-6 shows the plot of the predicted flexural strength versus time of the in-place concrete, and the plot of the computed maximum stress due a 12-kip wheel load and the actual recorded temperature differential in the slab.

Since the HVS load was applied to Slab 4 at 7 hours after concrete placement, the computed maximum stresses due to the 12-kip loads were lower than the predicted flexural strength at the time of start of loading and throughout the entire period of 12-kip loads. The corner crack which occurred on day 2 could not be explained by the load-induced stresses alone. The first corner crack is shown in Figures 8-7 and 8-8.

It is postulated that the corner crack in the adjacent slab was formed first and then propagated to the test slab. It happened that the holes for the dowel bars were drilled at the wrong positions initially. Figure 8-9 shows a picture of the improperly drilled holes. The vertical lines on the vertical face of the joint show where the correct locations of the holes should be. Note in the picture that there was a crack extending from a drilled hole at about 4 feet away from the edge. The location of this crack matched with the location where the corner crack extended from the joint.

The improperly drilled holes were later patched with an epoxy, and new holes were drilled at the right locations. Figure 8-10 shows the joint after the holes were patched. It happened to rain at that time, and accumulation of water was formed at the base, as can be observed from this picture. This might have weakened the base and further helped the formation of the corner crack in the adjacent slab.

Figure 8-7. First Corner Crack at the South End of Slab 4.

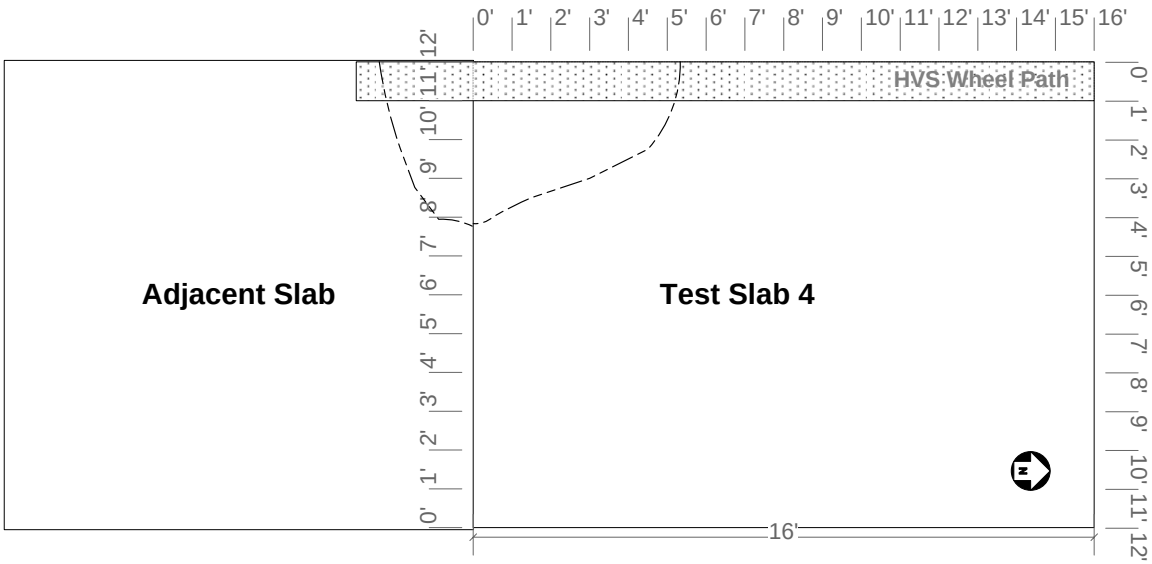

Figure 8-8. Corner cracks at the south end of Slab 4 and the adjacent slab.

Figure 8-9. Holes for dowel bars in wrong positions at the south end joint.

Figure 8-10. Holes patched at the south end joint. (Note that base was flooded with water.)

8.2.5 Evaluation of Induced Stresses and Flexural Strength of Concrete in Slab 5

The HVS loading of Slab 5 was started at 7 hours after concrete placement. On the second day, a full-depth transverse crack of about 12 feet along the test slab was first observed at the mid slab. After repetitions of 47,170 passes of the 12-kip load, a few transverse cracks have also occurred at the mid-edge of the slab. The slab was loaded with the 12 kip-load for 7 days with a total of 81,062 passes. Then the wheel load was increased to 15 kips and then to 18 kips as presented in Chapter 5.

The maximum induced stresses in Slab 5 due to the HVS load and the actual temperature differential in Slab 5 during the time of HVS loading were computed using the FEACONS program and compared with the strength of the concrete at the various times. The ratio between the maximum induced stress and the flexural strength and the number of repetitions to failure at the various times were also computed.

Table 8-5 presents the computed maximum induced stresses and the predicted flexural strengths of the in-place concrete in Slab 5 at the various times, and the computed stress to flexural strength ratios. It also lists the temperature differentials in the concrete slab and the elastic modulus at the various times, and the pavement parameters which were used in the FEACONS analysis.

Figure 8-11 shows the plot of the predicted flexural strength versus time of the in-place concrete, and the plot of the computed maximum stress due a 12-kip wheel load and the actual recorded temperature differential in the slab.

Table 8-5. Computed load-induced stresses and predicted flexural strength of concrete in Slab 5.

Time (hrs)	Temp. Diff. (^{o}F)	Applied Load, (kips)	Elastic Modulus (ksi)	Max. Computed Stress (psi)	Predicted Flexural Strength from Maturity (psi)	Predicted Stress/ Strength	No. of Repetition to Failure
4	22.97	12	1,900.0	373	305	1.22	0
6	14.47	12	2,575.0	361	410	0.88	11
7	8.41	12	2,725.0	347	420 (**371***)	0.83 (**0.94**)	52
8	-7.86	12	2,875.0	330	430	0.77	275
24	2.22	12	3,563.0	340	585	0.58	54,741
168	3.10	12	3,863.0	331	620	0.53	210,175

Note: * -actual strength of samples placed by the slab

Parameters used in the stress analysis:

The coefficient of thermal expansion: 6.27E-06 /^{o}F
Concrete Thickness: 9 inches
Poison's ratio: 0.2
Shear joint stiffness: 1,000 ksi
Torsional joint stiffness: 2,000 k-in/in
Confined edge stiffness: 5 ksi
Modulus of subgrade reaction: 0.40 kci

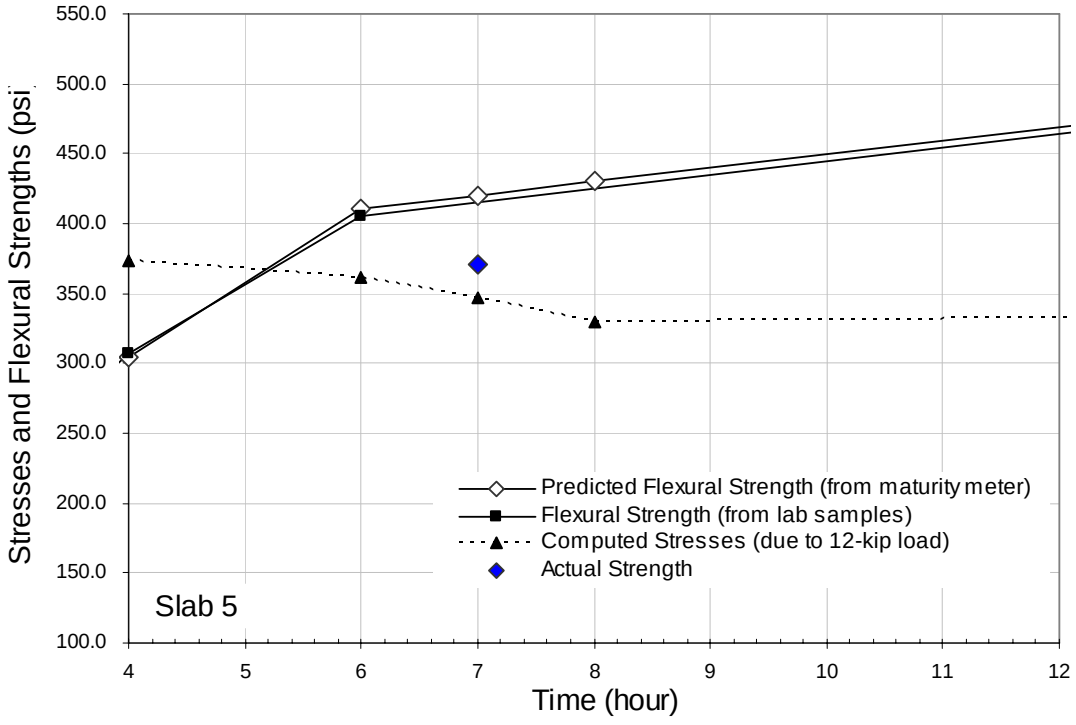

Figure 8-11. Computed Stresses and Flexural Strengths for the Concrete in Slab 5.

It can be seen from the Figure 8-11 that the computed maximum stresses due to the 12-kip load at 7 hour after placement of the HVS loading on Slab 5 were a little lower than predicted flexural strength at the time. Table 8-5 shows the low number of repetition to failure at the time of loading. As predicted by the high stress to strength ratio or low number of repetitions to failure at the time of loading, the full-depth transverse crack was observed at mid slab of the slab after 1 day of the HVS loading.

8.3 Required Concrete Properties for Adequate Performance

Analysis was performed to determine the required properties of concrete for adequate performance in a typical 9-inch replacement slab in Florida.

The FEACONS program was used to calculate the maximum stresses in a 9-inch slab (with similar condition as the test slabs in this study) under various critical loading conditions. A slab width of 12 feet, a joint spacing of 16 feet, a modulus of subgrade reaction of 0.4 kci, an edge stiffness of 5 ksi, a shear joint stiffness of 300 ksi, and a torsional joint stiffness of 1,500 k-in/in were used to model the slab in the analysis. The applied load in the analysis was a 12-kip wheel load placed at the corner and mid-edge of the slab under different temperature differentials in the slab. Temperature differentials of -20^{o}F, -10 ^{o}F, 0^{o}F, +10 ^{o}F, +20 ^{o}F and +30^{o}F were considered in this analysis with the average coefficient of thermal expansion of 6.28 x 10^{-6} / ^{o}F obtained from this study.

Since the load-induced stresses in the slab are affected by the elastic modulus of the concrete, analysis was performed for concrete of different elastic moduli. The ratios of the maximum stress to flexural strength were also computed for the various conditions analyzed.

The following regression equations (from Chapter 6) relating flexural strength to compressive strength, and elastic modulus to compressive strength were used in this analysis:

Regression equation 6-1: $R = 5.3936 \times f_c^{0.5655}, R^2 = 0.9203$

Regression equation 6-5: $E = 28.802 \times f_c^{0.5606}, R^2 = 0.8801$

Table 8-6 presents the maximum computed stresses caused by a 12-kip load at various conditions of temperature differentials in the slab for concrete of various flexural strengths (and their corresponding compressive strength and elastic modulus. Table 8-7 presents the computed stress to flexural strength ratios for the various conditions. Figure 8-12 shows the plot of computed stress to strength ratio versus flexural strength.

Table 8-6. Maximum computed stress due to 12-kip load at various temperature differentials

Flexural Strength (psi)	Computed Compressive Strength (psi)	Computed Elastic Modulus (ksi)	Maximum Computed Stress due to 12-kip load (psi) at Different Temperature Differentials					
			-20 °F	-10 °F	0 °F	+10 °F	+20 °F	+30 °F
150	358	778	149	170	186	211	236	264
250	883	1,291	135	171	207	249	291	338
300	1,220	1,547	130	175	214	265	317	372
400	2,028	2,058	119	168	225	294	369	437
500	3,010	2,567	105	159	234	322	413	499
600	4,155	3,076	92	149	242	347	455	558

Table 8-7. Stress to strength ratio at various temperature differentials

Flexural Strength (psi)	Stress (due to12-kip load) / Flexural Strength Ratio at Different Temperature Differentials					
	-20 °F	-10 °F	0 °F	+10 °F	+20 °F	+30 °F
150	0.99	1.13	1.24	1.41	1.57	1.76
250	0.54	0.68	0.83	1.00	1.16	1.35
300	0.43	0.58	0.71	0.88	1.06	1.24
400	0.30	0.42	0.56	0.74	0.92	1.09
500	0.21	0.32	0.47	0.64	0.83	1.00
600	0.15	0.25	0.40	0.58	0.76	0.93

From Table 8-7, it can be seen that when the temperature differential is +10 °F, a slab with a concrete flexural strength of 300 psi will have a stress strength ratio of less than 1. When

the temperature differential is +20 °F, a slab with a concrete flexural strength of 400 psi will have a stress ratio of less than 1.0. This means that when the expected temperature differential in the slab is +10 and +20 °F, specifying a minimum flexural strength of 300 and 400 psi, respectively, before opening to traffic, will ensure adequate performance of the replacement slab at early age.

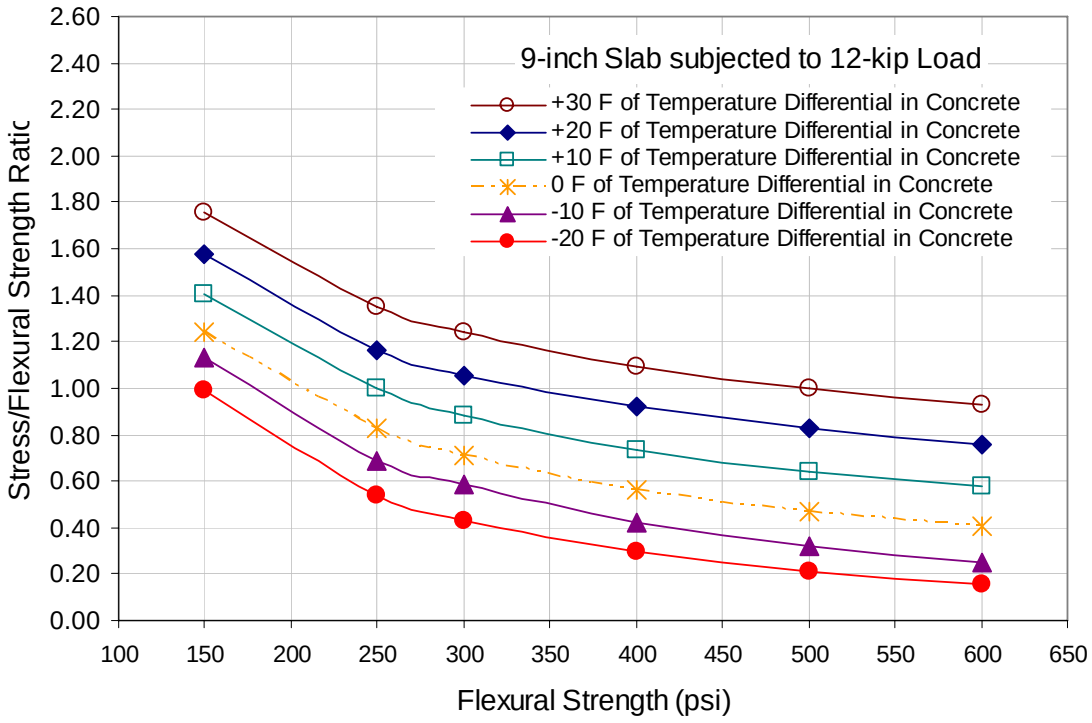

Figure 8-12. Computed stress to strength ratio at different temperature differentials as a function of flexural strength using the developed relationship between flexural strength compressive strength, and elastic modulus.

CHAPTER 9
CONCLUSIONS AND RECOMMENDATIONS

9.1 Summary of Findings

Five instrumented 9-inch thick concrete slabs were constructed and tested under accelerated pavement testing by means of a Heavy Vehicle Simulator (HVS) to study the behavior of concrete replacement slabs at early age and the effects of concrete properties on the performance of the replacement slabs.

Two test slabs (Slabs 1 and 2) used a concrete mix with a cement content of 850 lbs per cubic yard of concrete, while the other three test slabs (Slabs 3, 4 and 5) used a concrete mix with a cement content of 725 lbs per cubic yard of concrete. All the concrete mixes used in the test slabs maintained the same water-cement ratio of 0.36.

Determination of the flexural strength of the in-place concrete at early age was evaluated by the maturity method in this study. The HVS loading was planned to start when the strengths of the test slabs reached a certain strength. The HVS loading of Slab 1 was to start when the in-place concrete attained an estimated compressive strength of 2,200 psi, which is the current FDOT specification for a replacement slab at 7 hours after the placement. The required flexural strength of 300 psi or higher was used as an indicator to start the HVS loading in Slabs 2, 3, 4 and 5, where the required strength of the in-place concrete was reached at 5, 4, 7 and 7 hours after the placement, respectively.

The concrete mixes used in this study were evaluated in the laboratory for their compressive strength, flexural strength, splitting tensile strength, modulus of elasticity, drying shrinkage and coefficient of thermal expansion. The relationships among these concrete properties were developed and used to evaluate the performance of concrete mixes and the concrete test slabs.

The maximum stresses in the concrete slabs due to the applied loads and the temperature differentials in the slabs were calculated using the FEACONS (Finite Element Analysis of CONcrete Slabs) program. The model parameters were estimated by performing back-calculations from FWD data, and verified by comparing computed strains with measured strains from embedded strain gauges in the test slabs, which were loaded by the HVS.

Test Slabs 1, 2, 3 and 4, which had an asphalt base, were modeled as a 9-inch concrete layer bonded to a 4-inch asphalt concrete layer over a Winkler foundation using the FEACONS program. Test Slab 5, which had a limerock base, was modeled as a 9-inch concrete slab over a Winkler foundation.

The results of the experiments indicated that Slabs 1 and 2 performed well under the 12-kip load and the temperature conditions, while Slabs 3, 4 and 5 cracked at early age. The maturity method was found to be reliable to predict the flexural strength of the in-place concrete. Slabs 3 and 5 cracked at early age due to high temperature-load induced stresses in the test slabs that had either exceeded or were very close to the in-place flexural strength of the concrete at early age. Slab 4 cracked prematurely due to propagation of cracks from an adjacent slab.

Investigation was also made to evaluate the use of the maximum stress to flexural strength ratio of the concrete at the early age as an indicator of potential performance of a concrete replacement slab. This was done by comparing the stress to strength ratio with the observed performance of test slabs in this study. This method was found to be effective in predicting the potential performance of the replacement slabs.

Based on the test results from this study, relationships among flexural strength, compressive strength, splitting tensile strength, elastic modulus and drying shrinkage strain were developed for concrete used in replacement slabs.

Analysis of temperature data of the 9-inch concrete slabs at various times of year shows that a positive temperature differential was found to be as high as +30^{o}F and a negative temperature differential as low as -20^{o}F. These temperature differential ranges were used to evaluate stresses due to temperature conditions in Florida.

9.2 Conclusions

The use of the maturity method to determine the flexural strength of the in-place concrete at early age was found to be convenient to use and to have produced reliable determination of the flexural strength of the in-place concrete. This method can be used as a tool to predict the flexural strength of the in-place concrete for slab replacement at the time to open to the traffic. Higher cement content concrete tends to gain the in-place flexural strength faster. The strength development of a concrete slab depends not only on the mix design but also the condition under which the concrete is cured.

The anticipated stresses in the concrete slab can be calculated from the FEACONS (Finite Element Analysis of CONcrete Slabs) program or a similar finite element model which considers the effects of the applied load, temperature differential in the slab, elastic modulus and coefficient of thermal expansion of concrete, slab thickness, joint characteristics and effective subgrade stiffness. The anticipated stress needs to be lower than the anticipated flexural strength of the concrete at all times to ensure good performance.

The maximum stress to flexural strength ratio of the concrete at the early age can be used as an indicator of potential performance of a concrete replacement slab.

Based on the test results from this study, for a 9-inch slab placed on a fair foundation (minimum modulus of subgrade reaction of 0.4 kci) with the temperature differential of +10 $^{\circ}$F, a minimum required flexural strength of 300 psi at the time to open to the traffic would be needed

for adequate performance. When the temperature differential is +20 °F, a minimum required flexural strength of 400 psi would be needed.

9.3 Recommendations

The following recommendations are made with respect to specifications for concrete used in slab replacement:

- The use of the maturity method testing as specified in ASTM C 1074 is recommended for use in determination of concrete strength at the time of opening a replacement slab to traffic.

- The use of a minimum required flexural strength of concrete at the time of opening to traffic, instead of a minimum compressive strength, is recommended. If compressive strength is to be used, a relationship between the flexural strength and compressive strength for the specific concrete must be established so that the flexural strength can be more accurately determined from its compressive strength.

It is also recommended that further testing and research in this subject area be conducted, with particular focus on the following areas:

- Determination of the relationships between compressive strength, flexural strength and elastic modulus and drying shrinkage strain of typical concretes used in replacement slabs in Florida. Accurate determination of these relationships is needed in order to determine the required strength of the concrete before a concrete slab can be opened to traffic.

- Determination of temperature distributions in typical concrete pavement slabs in Florida. This information is needed in order to accurately determine the maximum temperature-load induced stresses in the concrete slabs. The strength of the concrete needs to be higher than this maximum induced stress to avoid cracking.

9.4 Contributions of the Research

The main contributions from this research are as follows:

- The development of a reliable model for analysis of concrete pavements where the analytical results were successfully verified by experimental results.

- The successive use of a systematic method to evaluate the required properties of concrete for slab replacement with consideration of additional factors such as anticipated temperature distribution in the slab and coefficient of thermal expansion of the concrete.

- The verification of the reliability of the maturity method based on flexural strength as the primary predicted property.

- The development of a relationship between compressive strength and flexural strength of concrete for use in slab replacement in Florida.

APPENDIX A
FWD TEST DATA

Table A-1. FWD test data from Slab 1.

Slab1 - Center Longitudinal		Deflections at Each Sensor Positions (mils)							
Load (kips)	Pressure (psi)	1	2	3	4	5	6	7	8
6.73	59.50	1.66	1.4	1.14	0.89	0.7	0.54	0.41	1.45
9.72	85.90	2.56	2.11	1.67	1.3	1.05	0.83	0.65	2.14
12.28	108.60	3.27	2.71	2.16	1.69	1.35	1.08	0.84	2.74
15.62	138.10	4.24	3.55	2.85	2.23	1.78	1.41	1.11	3.61
Slab1 - Center Transversal 01		Deflections at Each Sensor Positions (mils)							
Load (kips)	Pressure (psi)	1	2	3	4	5	6	7	8
6.67	59.00	1.63	1.36	1.06	0.81	0.65	0.5	0.39	1.45
9.67	85.50	2.49	2.06	1.61	1.24	0.96	0.75	0.59	2.15
12.19	107.80	3.21	2.65	2.08	1.62	1.25	0.98	0.78	2.77
15.69	138.70	4.2	3.5	2.79	2.17	1.67	1.3	1.05	3.67
Slab1 - Center Transversal 02		Deflections at Each Sensor Positions (mils)							
Load (kips)	Pressure (psi)	1	2	3	4	5	6	7	8
6.73	59.50	1.65	1.38	1.07	0.83	0.65	0.5	0.4	1.46
9.70	85.80	2.53	2.07	1.63	1.26	0.98	0.76	0.6	2.17
12.18	107.70	3.2	2.66	2.09	1.63	1.26	0.98	0.78	2.79
15.73	139.10	4.22	3.52	2.8	2.18	1.69	1.3	1.04	3.69
Slab 1 - Edge loaded		Deflections at Each Sensor Positions (mils)							
Load (kips)	Pressure (psi)	1	2	3	4	5	6	7	8
6.62	58.5	3.26	2.11	1.59	1.15	0.85	0.64	0.47	2.08
9.72	85.9	3.39	3.17	2.4	1.76	1.3	0.99	0.75	3.12
12.33	109	4.63	4.07	3.1	2.29	1.72	1.31	0.98	4.02
15.71	138.9	6.24	5.28	4.09	3.04	2.29	1.74	1.32	5.16
Slab 1 - Edge unloaded		Deflections at Each Sensor Positions (mils)							
Load (kips)	Pressure (psi)	1	2	3	4	5	6	7	8
6.85	60.6	1.24	1.2	1.06	0.91	0.77	0.64	0.47	1.12
9.88	87.4	1.88	1.82	1.59	1.39	1.15	0.95	0.72	1.69
12.00	106.1	2.33	2.3	1.98	1.76	1.45	1.19	0.91	2.12
15.74	139.2	3.19	3.15	2.74	2.45	2.03	1.66	1.26	2.92
Slab 1--Joint loaded		Deflections at Each Sensor Positions (mils)							
Load (kips)	Pressure (psi)	1	2	3	4	5	6	7	8
7.77	68.7	2.35	2.13	1.69	1.27	0.93	0.69	0.5	2.09
9.92	87.7	3.45	2.75	2.2	1.65	1.23	0.91	0.67	2.71
12.06	106.6	4.28	3.4	2.71	2.05	1.52	1.13	0.85	3.33
15.83	140	5.45	4.68	3.75	2.85	2.14	1.59	1.21	4.56
Slab 1--Joint unloaded		Deflections at Each Sensor Positions (mils)							
Load (kips)	Pressure (psi)	1	2	3	4	5	6	7	8
7.53	66.6	2.04	1.91	1.55	1.18	0.89	0.67	0.49	1.87
9.98	88.2	2.74	2.56	2.09	1.59	1.21	0.91	0.69	2.52
11.98	105.9	3.34	3.12	2.56	1.95	1.48	1.12	0.85	3.07
15.79	139.6	4.67	4.28	3.54	2.71	2.07	1.56	1.2	4.21

Table A-2. FWD test data from Slab 2.

Slab 2 - Center Longitudinal		Deflections at Each Sensor Positions (mils)							
Load (kips)	Pressure (psi)	1	2	3	4	5	6	7	8
6.81	60.20	1.53	1.29	1.05	0.83	0.66	0.57	0.44	1.31
9.74	86.10	2.27	1.86	1.53	1.23	0.97	0.77	0.61	1.93
12.38	109.50	2.93	2.47	2.02	1.61	1.31	1.04	0.83	2.52
15.72	139.00	3.87	3.31	2.68	2.13	1.73	1.36	1.09	3.35
Slab 2 - Center Transversal		Deflections at Each Sensor Positions (mils)							
Load (kips)	Pressure (psi)	1	2	3	4	5	6	7	8
6.85	60.60	1.51	1.33	1.07	0.85	0.69	0.56	0.46	1.3
9.69	85.70	2.23	1.95	1.57	1.27	1.03	0.84	0.7	1.91
12.30	108.80	2.89	2.57	2.1	1.7	1.37	1.13	0.93	2.5
15.71	138.90	3.84	3.39	2.78	2.25	1.83	1.5	1.26	3.3
Slab 2 - Edge loaded		Deflections at Each Sensor Positions (mils)							
Load (kips)	Pressure (psi)	1	2	3	4	5	6	7	8
6.60	58.4	3.17	2.7	2.08	1.5	1.11	0.79	0.55	2.56
9.57	84.6	4.49	4.01	3.12	2.27	1.66	1.2	0.86	3.79
12.09	106.9	6.01	5.21	4.07	2.98	2.15	1.57	1.15	4.93
15.68	138.6	8.02	6.95	5.48	4.03	2.94	2.13	1.56	6.64
Slab 2 - Edge unloaded		Deflections at Each Sensor Positions (mils)							
Load (kips)	Pressure (psi)	1	2	3	4	5	6	7	8
7.17	63.4	1.17	1.15	1.05	0.93	0.81	0.7	0.56	1.15
9.67	85.5	1.63	1.61	1.46	1.31	1.14	0.98	0.78	1.59
12.35	109.2	2.11	2.08	1.9	1.72	1.5	1.3	1.05	2.06
15.94	140.9	2.72	2.67	2.45	2.22	1.95	1.71	1.39	2.65
Slab 2 - Joint loaded		Deflections at Each Sensor Positions (mils)							
Load (kips)	Pressure (psi)	1	2	3	4	5	6	7	8
7.89	69.8	2.6	2.21	1.73	1.31	1	0.73	0.55	2.16
9.96	88.1	3.18	2.73	2.15	1.63	1.26	0.93	0.73	2.67
12.00	106.1	3.91	3.34	2.64	2.02	1.56	1.16	0.89	3.28
15.97	141.2	5.61	4.76	3.77	2.87	2.22	1.65	1.29	4.67
Slab 2 - Joint unloaded		Deflections at Each Sensor Positions (mils)							
Load (kips)	Pressure (psi)	1	2	3	4	5	6	7	8
7.03	62.2	1.61	1.53	1.33	1.03	0.81	0.63	0.48	1.57
9.82	86.8	2.3	2.2	1.91	1.48	1.18	0.91	0.71	2.24
12.01	106.2	2.83	2.72	2.38	1.86	1.49	1.14	0.9	2.79
15.81	139.8	3.94	3.81	3.33	2.59	2.09	1.59	1.27	3.86

Table A-3. FWD test data from Slab 3.

Slab 3 - Center Longitudinal 01		Deflections at Each Sensor Positions (mils)							
Load (kips)	Pressure (psi)	1	2	3	4	5	6	7	8
7.89	69.74	1.93	1.6	1.29	1.02	0.84	0.69	0.52	1.59
9.34	82.62	2.33	1.98	1.59	1.25	1	0.8	0.61	1.94
12.52	110.71	3.3	2.79	2.26	1.8	1.44	1.14	0.89	2.77
15.56	137.54	4.22	3.56	2.88	2.29	1.83	1.44	1.12	3.53
Slab 3 - Center Longitudinal 02		Deflections at Each Sensor Positions (mils)							
Load (kips)	Pressure (psi)	1	2	3	4	5	6	7	8
7.87	69.54	1.94	1.63	1.29	1.01	0.83	0.65	0.52	1.6
9.18	81.17	2.28	1.92	1.56	1.21	0.98	0.8	0.6	1.9
12.36	109.26	3.19	2.69	2.15	1.71	1.38	1.1	0.86	2.64
15.54	137.44	4.14	3.46	2.8	2.22	1.79	1.41	1.11	3.44
Slab 3 - Center Transversal 01		Deflections at Each Sensor Positions (mils)							
Load (kips)	Pressure (psi)	1	2	3	4	5	6	7	8
7.46	65.96	1.84	1.59	1.23	1.03	0.86	0.71	0.59	1.55
9.38	82.91	2.32	2.06	1.62	1.34	1.12	0.93	0.77	1.99
12.27	108.48	3.15	2.78	2.19	1.82	1.51	1.27	1.07	2.69
15.57	137.63	4.12	3.64	2.86	2.39	1.98	1.67	1.43	3.53
Slab 3 - Center Transversal 02		Deflections at Each Sensor Positions (mils)							
Load (kips)	Pressure (psi)	1	2	3	4	5	6	7	8
7.613	67.31	1.89	1.67	1.3	1.07	0.89	0.74	0.61	1.61
9.256	81.84	2.33	2.07	1.62	1.36	1.12	0.93	0.78	2
12.159	107.51	3.18	2.79	2.21	1.84	1.52	1.28	1.07	2.71
15.314	135.41	4.12	3.61	2.85	2.38	1.97	1.66	1.42	3.5
Slab 3 - Edge loaded 01		Deflections at Each Sensor Positions (mils)							
Load (kips)	Pressure (psi)	1	2	3	4	5	6	7	8
7.41	65.47	4.08	3.89	3.11	2.37	1.70	1.17	0.81	3.27
9.19	81.27	5.20	4.52	3.61	2.76	2.00	1.37	1.00	3.78
11.98	105.96	6.56	5.96	4.87	3.73	2.71	1.89	1.38	5.11
15.15	133.96	8.69	7.69	6.31	4.91	3.58	2.52	1.83	6.59
Slab 3 - Edge loaded 02		Deflections at Each Sensor Positions (mils)							
Load (kips)	Pressure (psi)	1	2	3	4	5	6	7	8
7.24	64.02	4.31	4.03	3.23	2.48	1.76	1.19	0.79	3.76
9.18	81.17	5.68	4.94	3.98	3.07	2.20	1.50	1.02	4.67
11.92	105.38	6.87	6.21	5.06	3.91	2.82	1.94	1.33	5.94
15.07	133.27	8.74	7.86	6.32	4.88	3.57	2.48	1.71	7.43
Slab 3 - Edge unloaded 01		Deflections at Each Sensor Positions (mils)							
Load (kips)	Pressure (psi)	1	2	3	4	5	6	7	8
7.13	63.05	1.33	1.27	1.19	1.05	0.90	0.76	0.61	1.33
9.11	80.59	1.77	1.71	1.60	1.41	1.21	1.02	0.83	1.70
11.84	104.71	2.37	2.28	2.14	1.88	1.60	1.36	1.09	2.20
15.05	133.08	3.10	3.00	2.81	2.48	2.12	1.78	1.44	3.09

Table A-3. Continued.

Slab 3 - Edge unloaded 02		Deflections at Each Sensor Positions (mils)							
Load (kips)	Pressure (psi)	1	2	3	4	5	6	7	8
7.19	63.54	1.33	1.30	1.18	1.06	0.92	0.76	0.62	1.30
9.14	80.78	1.77	1.73	1.54	1.41	1.21	1.02	0.82	1.76
11.78	104.12	2.35	2.30	2.03	1.88	1.61	1.35	1.08	2.30
15.15	133.96	3.13	3.06	2.78	2.50	2.13	1.80	1.45	3.02
Slab 3 - Joint loaded 01		Deflections at Each Sensor Positions (mils)							
Load (kips)	Pressure (psi)	1	2	3	4	5	6	7	8
7.92	70.03	2.86	2.42	1.91	1.45	1.09	0.83	0.66	2.42
9.31	82.33	3.18	2.68	2.10	1.59	1.20	0.92	0.72	2.70
12.35	109.16	4.32	3.67	2.91	2.23	1.69	1.31	1.05	3.66
15.63	138.22	5.59	4.72	3.77	2.90	2.21	1.71	1.37	4.74
Slab 3 - Joint loaded 02		Deflections at Each Sensor Positions (mils)							
Load (kips)	Pressure (psi)	1	2	3	4	5	6	7	8
7.635	67.51	2.64	2.22	1.71	1.3	0.97	0.74	0.58	2.2
9.191	81.27	3.19	2.68	2.11	1.59	1.2	0.92	0.72	2.68
12.148	107.41	4.28	3.62	2.86	2.18	1.64	1.26	1.01	3.66
15.522	137.24	5.54	4.68	3.73	2.86	2.17	1.67	1.34	4.74
Slab 3 - Joint unloaded 01		Deflections at Each Sensor Positions (mils)							
Load (kips)	Pressure (psi)	1	2	3	4	5	6	7	8
7.42	65.57	1.87	1.74	1.48	1.17	0.92	0.69	0.54	1.82
9.16	80.97	2.35	2.18	1.87	1.49	1.17	0.89	0.69	2.27
12.04	106.45	3.18	2.95	2.55	2.05	1.60	1.23	0.97	3.06
15.44	136.48	4.15	3.85	3.35	2.69	2.11	1.62	1.29	3.97
Slab 3 - Joint unloaded 02		Deflections at Each Sensor Positions (mils)							
Load (kips)	Pressure (psi)	1	2	3	4	5	6	7	8
7.58	67.02	1.96	1.81	1.56	1.24	0.96	0.74	0.57	1.90
8.93	78.94	2.30	2.14	1.83	1.47	1.15	0.88	0.69	2.24
11.94	105.57	3.15	2.93	2.54	2.04	1.59	1.23	0.96	3.04
15.36	135.79	4.13	3.84	3.34	2.69	2.11	1.63	1.29	3.97

Table A-4. FWD test data from Slab 4.

Slab 4 - Center Longitudinal 01		Deflections at Each Sensor Positions (mils)							
Load (kips)	Pressure (psi)	1	2	3	4	5	6	7	8
9.15	80.9	2.35	1.93	1.5	1.18	0.93	0.75	0.57	2.04
11.58	102.4	3.1	2.51	1.98	1.56	1.24	0.97	0.78	2.65
15.43	136.4	4.27	3.47	2.76	2.17	1.71	1.36	1.07	3.67
17.85	157.8	4.91	4.07	3.23	2.54	2.02	1.6	1.25	4.3
Slab 4 - Center Longitudinal 02		Deflections at Each Sensor Positions (mils)							
Load (kips)	Pressure (psi)	1	2	3	4	5	6	7	8
9.03	79.8	2.35	1.93	1.51	1.18	0.93	0.73	0.57	2.04
11.45	101.2	3.13	2.51	1.98	1.56	1.23	0.98	0.77	2.66
15.28	135.1	4.28	3.46	2.74	2.17	1.69	1.35	1.06	3.66
17.77	157.1	4.96	4.09	3.25	2.56	2.02	1.61	1.26	4.31
Slab 4 - Center Transversal 01		Deflections at Each Sensor Positions (mils)							
Load (kips)	Pressure (psi)	1	2	3	4	5	6	7	8
9.14	80.8	2.26	2.09	1.69	1.28	0.93	0.67	0.49	1.92
11.50	101.7	2.94	2.73	2.21	1.66	1.23	0.88	0.65	2.49
15.35	135.7	4.09	3.78	3.09	2.3	1.72	1.25	0.94	3.46
17.88	158.1	4.8	4.46	3.64	2.67	2.02	1.48	1.13	4.07
Slab 4 - Center Transversal 02		Deflections at Each Sensor Positions (mils)							
Load (kips)	Pressure (psi)	1	2	3	4	5	6	7	8
8.93	79	2.24	2.08	1.68	1.26	0.93	0.66	0.49	1.9
11.41	100.9	2.96	2.74	2.24	1.68	1.24	0.89	0.64	2.51
15.30	135.3	4.12	3.8	3.09	2.3	1.72	1.26	0.96	3.47
17.81	157.5	4.81	4.48	3.65	2.72	2.04	1.49	1.17	4.09
Slab 4 - Edge loaded 01		Deflections at Each Sensor Positions (mils)							
Load (kips)	Pressure (psi)	1	2	3	4	5	6	7	8
8.63	76.3	3.38	2.94	2.24	1.65	1.2	0.88	0.67	2.67
11.14	98.5	4.21	3.65	2.83	2.07	1.54	1.15	0.9	3.39
15.19	134.3	5.98	5.24	4.05	2.97	2.21	1.66	1.28	4.8
17.62	155.8	6.86	6.25	4.74	3.49	2.59	1.94	1.5	5.74
Slab 4 - Edge loaded 02		Deflections at Each Sensor Positions (mils)							
Load (kips)	Pressure (psi)	1	2	3	4	5	6	7	8
8.67	76.7	3.24	2.81	2.15	1.57	1.17	0.88	0.68	2.62
11.02	97.4	4.18	3.63	2.8	2.05	1.52	1.14	0.88	3.41
15.05	133.1	5.9	5.13	4.01	2.94	2.19	1.64	1.27	5.31
17.50	154.7	6.94	6.13	4.7	3.46	2.57	1.93	1.49	6.07
Slab 4 - Edge unloaded 01		Deflections at Each Sensor Positions (mils)							
Load (kips)	Pressure (psi)	1	2	3	4	5	6	7	8
8.62	76.2	2.09	1.92	1.64	1.38	1.1	0.86	0.66	1.96
11.04	97.6	2.75	2.51	2.17	1.82	1.45	1.13	0.88	2.57
15.16	134	3.85	3.54	3.09	2.6	2.04	1.61	1.26	3.62
17.60	155.6	4.56	4.15	3.63	3.05	2.39	1.89	1.47	4.25

Table A-4. Continued.

Slab 4 - Edge unloaded 02		Deflections at Each Sensor Positions (mils)							
Load (kips)	Pressure (psi)	1	2	3	4	5	6	7	8
8.61	76.1	2.11	1.95	1.67	1.41	1.12	0.88	0.68	1.99
10.97	97	2.77	2.5	2.15	1.8	1.41	1.1	0.83	2.57
15.06	133.2	3.83	3.56	3.09	2.61	2.05	1.61	1.26	3.65
17.47	154.5	4.47	4.16	3.64	3.06	2.4	1.89	1.48	4.26
Slab 4 - Joint loaded 01		Deflections at Each Sensor Positions (mils)							
Load (kips)	Pressure (psi)	1	2	3	4	5	6	7	8
9.15	80.9	2.64	2.19	1.71	1.3	1	0.74	0.57	2.13
11.54	102	3.29	2.77	2.2	1.67	1.29	0.99	0.77	2.7
15.43	136.4	4.55	3.96	3.14	2.4	1.85	1.42	1.13	3.82
17.61	155.7	5.3	4.58	3.66	2.81	2.17	1.67	1.33	4.46
Slab 4 - Joint loaded 02		Deflections at Each Sensor Positions (mils)							
Load (kips)	Pressure (psi)	1	2	3	4	5	6	7	8
9.06	80.1	2.54	2.19	1.7	1.29	1	0.75	0.59	2.12
11.35	100.4	3.3	2.8	2.2	1.67	1.29	0.98	0.77	2.71
15.17	134.1	4.41	3.89	3.11	2.37	1.83	1.41	1.12	3.78
17.52	154.9	5.26	4.54	3.63	2.79	2.14	1.64	1.32	4.44
Slab 4 - Joint unloaded 01		Deflections at Each Sensor Positions (mils)							
Load (kips)	Pressure (psi)	1	2	3	4	5	6	7	8
8.99	79.5	1.97	1.83	1.54	1.2	0.95	0.74	0.59	1.86
11.38	100.6	2.52	2.35	1.99	1.57	1.23	0.96	0.75	2.4
15.36	135.8	3.55	3.33	2.82	2.23	1.75	1.37	1.09	3.38
17.61	155.7	4.13	3.88	3.3	2.62	2.05	1.6	1.29	3.94
Slab 4 - Joint unloaded 02		Deflections at Each Sensor Positions (mils)							
Load (kips)	Pressure (psi)	1	2	3	4	5	6	7	8
8.96	79.2	1.94	1.8	1.51	1.18	0.92	0.72	0.56	1.84
11.34	100.3	2.52	2.34	1.98	1.57	1.23	0.96	0.76	2.4
15.23	134.7	3.53	3.31	2.81	2.22	1.73	1.37	1.08	3.36
17.52	154.9	4.13	3.88	3.3	2.61	2.04	1.62	1.29	3.94

Table A-5. FWD test data from Slab 5.

Slab 5 - Center Longitudinal 01		Deflections at Each Sensor Positions (mils)							
Load (kips)	Pressure (psi)	1	2	3	4	5	6	7	8
9.35	82.70	9.36	6.64	4.70	3.20	2.22	1.48	0.93	4.13
12.76	112.80	11.28	7.90	5.50	3.74	2.61	1.79	1.17	5.39
15.88	140.40	13.94	9.84	6.86	4.67	3.26	2.20	1.45	6.82
18.63	164.70	16.12	11.42	7.98	5.44	3.80	2.58	1.69	7.89
Slab 5 - Center Longitudinal 02		Deflections at Each Sensor Positions (mils)							
Load (kips)	Pressure (psi)	1	2	3	4	5	6	7	8
9.51	84.10	10.09	7.13	4.87	3.29	2.13	1.38	0.93	4.14
12.54	110.90	12.38	8.76	6.01	4.03	2.70	1.80	1.21	5.43
15.55	137.50	14.72	10.45	7.20	4.91	3.26	2.13	1.44	6.80
18.45	163.10	16.83	12.02	8.30	5.64	3.81	2.50	1.69	8.00

Table A-5. Continued.

Slab 5 - Center Transversal 01		Deflections at Each Sensor Positions (mils)							
Load (kips)	Pressure (psi)	1	2	3	4	5	6	7	8
9.55	84.40	10.44	8.34	6.39	3.82	1.69	1.06	0.44	7.35
12.64	111.80	12.68	11.43	7.63	4.72	2.15	1.44	0.74	9.67
15.66	138.50	14.95	13.43	9.04	5.57	2.74	1.80	1.00	11.70
18.50	163.60	16.85	14.81	10.30	6.28	3.36	2.21	1.39	13.47
Slab 5 - Center Transversal 02		Deflections at Each Sensor Positions (mils)							
Load (kips)	Pressure (psi)	1	2	3	4	5	6	7	8
9.43	83.40	10.72	8.62	6.35	3.96	1.83	1.05	0.53	7.52
12.52	110.70	13.07	11.33	7.69	4.93	2.27	1.42	0.69	10.14
15.47	136.80	15.28	13.39	9.08	5.72	2.81	1.87	1.12	11.96
18.45	163.10	17.21	14.83	10.39	6.41	3.40	2.28	1.28	13.69
Slab 5 - Center Small Long 01		Deflections at Each Sensor Positions (mils)							
Load (kips)	Pressure (psi)	1	2	3	4	5	6	7	8
9.75	86.20	3.76	3.54	3.16	2.82	2.60	1.82	2.36	2.90
12.68	112.10	4.82	4.38	4.05	3.58	3.25	2.42	3.09	3.79
15.56	137.60	6.01	5.45	5.01	4.40	3.96	3.06	3.88	4.74
18.45	163.10	7.06	6.42	5.84	5.11	4.57	3.62	4.58	5.63
Slab 5 - Center Small Long 02		Deflections at Each Sensor Positions (mils)							
Load (kips)	Pressure (psi)	1	2	3	4	5	6	7	8
9.73	86.00	3.81	3.48	3.26	2.90	2.68	1.87	2.40	2.97
12.57	111.10	4.91	4.44	4.12	3.65	3.33	2.45	3.13	3.84
15.43	136.40	6.02	5.49	5.06	4.45	4.01	3.07	3.90	4.78
18.23	161.20	7.13	6.53	5.88	5.15	4.62	3.64	4.60	5.63
Slab 5 - Center Small Trans 01		Deflections at Each Sensor Positions (mils)							
Load (kips)	Pressure (psi)	1	2	3	4	5	6	7	8
9.79	86.60	3.73	2.96	2.31	1.74	1.28	3.97	3.85	3.72
12.67	112.00	4.71	3.74	2.98	2.28	1.71	4.84	4.76	4.62
15.51	137.10	5.97	4.68	3.70	2.84	2.11	6.14	6.06	5.92
18.42	162.90	7.06	5.54	4.34	3.33	2.46	7.36	7.24	7.10
Slab 5 - Center Small Trans 02		Deflections at Each Sensor Positions (mils)							
Load (kips)	Pressure (psi)	1	2	3	4	5	6	7	8
9.95	88.00	3.76	2.94	2.30	1.75	1.32	4.02	3.89	3.45
12.42	109.80	4.75	3.66	2.91	2.22	1.67	4.97	4.85	4.24
15.57	137.70	6.00	4.65	3.67	2.82	2.11	6.29	6.18	5.52
18.54	163.90	7.15	5.52	4.34	3.33	2.46	7.39	7.36	6.70
Slab 5 - Edge loaded 01		Deflections at Each Sensor Positions (mils)							
Load (kips)	Pressure (psi)	1	2	3	4	5	6	7	8
9.23	81.60	13.81	11.41	8.37	6.35	4.72	3.56	2.49	3.09
12.20	107.90	15.03	12.22	8.84	6.67	4.91	3.56	2.46	3.70
15.18	134.20	17.54	14.38	10.23	7.84	5.76	4.31	2.98	4.76
18.27	161.50	19.87	16.35	11.48	8.31	6.49	4.93	3.43	5.93
Slab 5 - Edge loaded 02		Deflections at Each Sensor Positions (mils)							
Load (kips)	Pressure (psi)	1	2	3	4	5	6	7	8
9.01	79.70	13.50	11.58	7.80	6.23	4.43	3.44	2.34	5.38
12.02	106.30	15.77	13.02	9.29	7.14	5.15	3.86	2.65	3.92
15.01	132.70	17.97	14.97	10.64	8.22	5.90	4.44	3.08	5.11
18.17	160.70	20.09	16.75	11.85	9.26	6.61	5.05	3.51	6.13

Table A-5. Continued.

Slab 5 - Edge loaded 03		Deflections at Each Sensor Positions (mils)							
Load (kips)	Pressure (psi)	1	2	3	4	5	6	7	8
8.98	79.40	13.58	11.67	7.96	6.27	4.48	3.53	2.43	2.06
12.04	106.50	16.05	13.29	9.39	7.26	5.23	3.95	2.72	2.77
15.01	132.70	18.18	15.14	10.74	8.30	5.98	4.48	3.15	3.63
18.19	160.80	20.02	16.67	11.87	9.22	6.63	5.01	3.54	4.59
Slab 5 - Joint loaded 01		Deflections at Each Sensor Positions (mils)							
Load (kips)	Pressure (psi)	1	2	3	4	5	6	7	8
9.62	85.10	5.04	4.87	4.18	2.93	2.10	1.58	1.17	4.31
12.71	112.40	6.32	6.06	5.18	3.69	2.67	2.02	1.53	5.35
15.64	138.30	7.89	7.54	6.46	4.66	3.38	2.59	1.98	6.58
18.55	164.00	9.33	9.03	7.64	5.51	4.02	3.12	2.39	7.95
Slab 5 - Joint loaded 02		Deflections at Each Sensor Positions (mils)							
Load (kips)	Pressure (psi)	1	2	3	4	5	6	7	8
9.59	84.80	5.19	4.98	4.39	3.03	2.16	1.56	1.15	4.41
12.60	111.40	6.62	6.37	5.56	3.87	2.78	2.08	1.56	5.50
15.51	137.10	8.11	7.83	6.71	4.78	3.47	2.62	2.00	6.59
18.38	162.50	9.48	9.18	7.81	5.58	4.08	3.13	2.39	7.87

APPENDIX B
HVS LASER PROFILE DATA COLLECTION SCHEDULE

Table B-1. Data collection schedule of the HVS laser profile for Slab 1.

Profile Number	Passes	Date	Time
1	0	03/21/06	15:52
2	5869	03/22/06	5:01
3	5869	03/22/06	5:14
4	10418	03/22/06	14:01
5	10418	03/22/06	14:13
6	18343	03/23/06	5:00
7	18343	03/23/06	5:13
8	22840	03/23/06	14:00
9	22840	03/23/06	14:12
10	31059	03/24/06	5:05
11	31059	03/24/06	5:19
12	35555	03/24/06	14:00
13	43946	03/25/06	5:07
14	43946	03/25/06	5:21
15	48460	03/25/06	14:01
16	48460	03/25/06	14:14
17	56800	03/26/06	5:01
18	56800	03/26/06	5:13
19	61217	03/26/06	14:03
20	61217	03/26/06	14:16
21	69408	03/27/06	5:00
22	69408	03/27/06	5:08
23	69408	03/27/06	5:21
24	72901	03/27/06	14:00
25	72901	03/27/06	14:14
26	80721	03/28/06	5:00
27	80721	03/28/06	5:13
28	80721	03/28/06	5:24
29	85254	03/28/06	14:00
30	85254	03/28/06	14:13
31	85254	03/28/06	14:25
32	93140	03/29/06	5:00
33	93140	03/29/06	5:12
34	97709	03/29/06	14:00
35	97709	03/29/06	14:13
36	105877	03/30/06	5:00
37	105877	03/30/06	5:15

Table B-1. Continued.

Profile Number	Passes	Date	Time
38	10630	03/30/06	14:15
39	10630	03/30/06	14:26
40	10630	03/30/06	14:37
41	118735	03/31/06	5:00
42	118735	03/31/06	5:15
43	123134	03/31/06	14:03
44	123134	03/31/06	14:14
45	131121	04/01/06	5:03
46	131121	04/01/06	5:16
47	135282	04/01/06	14:00
48	135282	04/01/06	14:13
49	135282	04/01/06	14:28
50	142764	04/02/06	5:12
51	142764	04/02/06	5:24
53	146509	04/02/06	14:00
54	146509	04/02/06	14:16
55	154836	04/03/06	5:00
56	154836	04/03/06	5:15
57	158810	04/03/06	14:00
58	158810	04/03/06	14:14
59	167031	04/04/06	5:00
60	167031	04/04/06	5:15
61	167031	04/04/06	5:20
62	171051	04/04/06	14:00
63	171051	04/04/06	14:12
64	179316	04/05/06	5:00
65	179316	04/05/06	5:15
66	179316	04/06/06	5:25
67	179316	04/06/06	5:40

Table B-2. Analysis files of the HVS laser profile for Slab 1.

Passes	File Name	File Date	Time
0	06_03_1H.p0	21/03/2006	15:32:35
5869	06_03_1H.p2	22/03/2006	5:01:29
10418	06_03_1H.p4	22/03/2006	14:01:14
18343	06_03_1H.p6	23/03/2006	5:00:59
22840	06_03_1H.p8	23/03/2006	14:00:58
31059	06_03_1H.p10	24/03/2006	5:05:49
35555	06_03_1H.p12	24/03/2006	14:00:54
43946	06_03_1H.p13	25/03/2006	5:07:06
48460	06_03_1H.p15	25/03/2006	14:01:19
56800	06_03_1H.p17	26/03/2006	5:01:43
61217	06_03_1H.p19	26/03/2006	14:03:21
69408	06_03_1H.p23	27/03/2006	5:21:21
72901	06_03_1H.p24	27/04/2006	14:01:09
80721	06_03_1H.p26	28/04/2006	5:00:50
85254	06_03_1H.p29	28/04/2006	14:00:52
93140	06_03_1H.p32	29/04/2006	5:00:34
97709	06_03_1H.p34	29/04/2006	14:00:49
105877	06_03_1H.p36	30/04/2006	5:00:56
110630	06_03_1H.p38	30/03/2006	14:15:03
118735	06_03_1H.p41	31/03/2006	5:00:32
123134	06_03_1H.p43	31/03/2006	14:03:08
131121	06_03_1H.p45	1/4/2006	5:02:50
135282	06_03_1H.p47	1/4/2006	14:00:38
142764	06_03_1H.p50	2/4/2006	4:01:12
143323	06_03_1H.p52	2/4/2006	6:24:01
146509	06_03_1H.p53	2/4/2006	14:00:34
154836	06_03_1H.p55	3/4/2006	5:00:51
158810	06_03_1H.p57	3/4/2006	14:00:51
167031	06_03_1H.p59	4/4/2006	5:00:55
171051	06_03_1H.p62	4/4/2006	14:00:41

Table B-3. Data collection schedule of the HVS laser profile for Slab 2.

Profile Number	Passes	Date	Time
0	0	6/1/2006	14:05
1	0	6/1/2006	14:20
2	7780	6/2/2006	5:00
3	7780	6/2/2006	5:00
4	12490	6/2/2006	14:10
5	12490	6/2/2006	14:30
6	20718	6/3/2006	5:00
7	20718	6/3/2006	5:24
8	25405	6/3/2006	14:00
9	25405	6/3/2006	14:15
10	34230	6/4/2006	5:05
11	34230	6/4/2006	5:34
12	38166	6/4/2006	14:00
13	38166	6/4/2006	14:09
14	46588	6/5/2006	5:00
15	46588	6/5/2006	5:00
16	51165	6/5/2006	14:00
17	51165	6/5/2006	14:15
18	59478	6/6/2006	5:00
19	59478	6/6/2006	5:15
20	62645	6/6/2006	14:00
21	62645	6/6/2006	14:15
22	70769	6/7/2006	5:00
23	70769	6/7/2006	5:13
24	74800	6/7/2006	14:15
25	74800	6/7/2006	14:30
26	82816	6/8/2006	5:00
27	82816	6/8/2006	5:15
28	82816	6/8/2006	5:30
29	86967	6/8/2006	14:10
30	86967	6/8/2006	14:10
31	86967	6/8/2006	15:30
Changed load from 12 kips to 15 kips			
32	94911	6/9/2006	5:00
33	94911	6/9/2006	5:15
34	99814	6/9/2006	15:15
35	99814	6/10/2006	15:30
36	99814	6/11/2006	15:45
37	106840	6/10/2006	5:05

Table B-3. Continued.

Profile Number	Passes	Date	Time
38	106840	6/10/2006	5:23
39	111385	6/10/2006	14:00
40	111385	6/10/2006	14:10
HVS down from 00:30 to 10:30 6/10/06 for Maintenance trouble.			
41	119279	6/11/2006	14:00
42	119279	6/11/2006	14:10
43	119279	6/11/2006	14:23
HVS down from 1:00am to 4:30am 12/11 from personel issue			
44	125367	6/12/2006	5:00
45	125367	6/12/2006	5:13
46	130024	6/12/2006	14:30
47	130024	6/12/2006	14:45
HVS down from 8:30am to 8:30pm on 6/13 do to FDOT Closing from storm			
Changed load from 15 kips to 18 kips at 08:30 pm on 6/13/06.			
48	137946	6/14/2006	5:00
49	137946	6/15/2006	5:13
50	147617	6/16/2006	14:30
51	147617	6/17/2006	14:45
53	157017	6/15/2006	5:00
54	157017	6/15/2006	5:00
55	160361	6/16/2006	14:20
56	160361	6/17/2006	14:30
57	168585	6/16/2006	5:00
58	168585	6/16/2006	5:10
59	173204	6/16/2006	14:00
60	173204	6/16/2006	14:20
61	173204	6/16/2006	14:30
62	175415	6/17/2006	5:12
63	175415	6/17/2006	5:22

Table B-4. Analysis files of the HVS laser profile for Slab 2.

Passes	File Name	File Date	Time
0	06jun_1e.p2	2/6/2006	4:59:00
7779	06jun_1e.p3	2/6/2006	5:12:39
12490	06jun_1e.p4	2/6/2006	14:07:50
25405	06jun_1e.p8	3/6/2006	13:59:07
34230	06jun_1e.p10	4/6/2006	5:43:43
38166	06jun_1e.p12	4/6/2006	13:58:54
46587	06jun_1e.p14	5/6/2006	4:58:53
51165	06jun_1e.p16	5/6/2006	13:59:29
59402	06jun_1e.p18	6/6/2006	5:00:49
62645	06jun_1e.p20	6/6/2006	13:59:13
70768	06jun_1e.p22	7/6/2006	4:58:40
75235	06jun_1e.p24	7/6/2006	14:14:17
82815	06jun_1e.p26	8/6/2006	5:00:10
86937	06jun_1e.p30	8/6/2006	14:03:09
94911	06jun_1e.p32	9/6/2006	4:58:42
99813	06jun_1e.p34	9/6/2006	14:57:10
106840	06jun_1e.p37	10/6/2006	4:59:40
111384	06jun_1e.p39	10/6/2006	13:58:50
119279	06jun_1e.p41	11/6/2006	13:58:43
125366	06jun_1e.p44	12/6/2006	4:58:38
130023	06jun_1e.p46	12/6/2006	14:28:39
137946	06JUN_1E.p48	13/06/2006	5:02:18
148756	06JUN_1E.p51	14/06/2006	14:00:14

Table B-5. Data collection schedule of the HVS laser profile for Slab 3.

Profile Number	Passes	Date	Time
0	0	04/04/07	13:35
1	0	03/21/07	13:50
2	1730	04/05/07	17:09
3	1730	04/05/07	17:28
4	8266	04/06/07	5:00
5	8266	04/06/07	5:15
6	12925	04/06/07	14:10
7	12925	04/06/07	14:25
8	20690	04/07/07	5:27
9	20690	04/07/07	5:28
10	25300	04/07/07	14:00
11	25300	04/07/07	14:15
12	33156	04/08/07	5:00
13	33156	04/08/07	5:13
14	37758	04/08/07	14:00
15	37758	04/08/07	14:15
15	46783	04/09/07	6:30

Table B-5. Continued.

Profile Number	Passes	Date	Time
16	46783	04/09/07	6:45
17	50849	04/09/07	14:30
18	50849	04/09/07	14:45
19	53574	04/10/07	5:00
20	53574	04/10/07	5:15
21	62852	04/10/07	14:10
22	62852	04/10/07	14:25
23	70910	04/11/07	5:00
24	70910	04/11/07	5:15
25	75482	04/11/07	14:30
26	75482	04/11/07	14:45
27	82534	04/12/07	5:00
28	82534	04/12/07	5:15
29	86546	04/12/07	14:30
30	94051	04/13/07	5:00
31	94051	04/13/07	5:11
Changed from 12kips to 15kips 4/13/07 @ 8:00am and 95042 passes			
32	95042	04/12/07	14:30
33	95042	04/12/07	14:45
34	105067	04/14/07	5:05
35	105067	04/14/07	5:45
35	108582	04/14/07	14:00
36	108583	04/14/07	14:12
37	116918	04/15/07	3:27
38	116918	04/15/07	3:39
39	121545	04/15/07	14:00
40	121545	04/15/07	14:15
41	129639	04/16/07	5:00
42	129639	04/16/07	5:15
Changed from 15kips to 18kips 4/16/07 @ 8:00am and 130957 passes			
43	132946	04/16/07	14:00
44	132946	04/12/07	14:20
45	141131	04/17/07	5:00
46	141131	04/17/07	5:15
47	144484	04/17/07	14:05
48	144484	04/17/07	14:25
49	152799	04/18/07	5:00
50	152799	04/18/07	5:15
51	157337	04/17/07	14:05

Table B-5. Continued.

Profile Number	Passes	Date	Time
52	157337	04/17/07	14:25
53	164545	04/19/07	5:00
54	164545	04/19/07	5:15
55	168537	04/19/07	14:05
56	168537	04/19/07	14:25

Table B-6. Analysis files of the HVS laser profile for Slab 3.

Passes	File Name	File Date	Time
0	07APR1H.p0	5/4/2007	14:26:13
1730	07APR1H.p2	5/4/2007	18:05:09
24924	07APR1H.p10	7/4/2007	13:58:57
37757	07APR1H.p13	8/4/2007	13:58:45
46764	07APR1H.p15	9/4/2007	6:33:55
58573	07APR1H.p19	10/4/2007	4:59:24
62851	07APR1H.p21	10/4/2007	14:00:21
70910	07APR1H.p23	11/4/2007	5:01:56
75482	07APR1H.p25	11/4/2007	13:58:50
85868	07APR1H.p29	12/4/2007	13:59:32
97971	07APR1H.p32	13/04/2007	14:03:50
105066	07APR1H.p34	14/04/2007	5:07:18
108583	07APR1H.p35	14/04/2007	12:27:12
116918	07APR1H.p37	15/04/2007	3:27:50
121545	07APR1H.p39	15/04/2007	13:59:47
129640	07APR1H.p41	16/04/2007	5:00:28
132946	07APR1H.p43	16/04/2007	14:00:55
141130	07APR1H.p45	17/04/2007	5:00:10
145347	07APR1H.p47	17/04/2007	14:03:02
152799	07APR1H.p49	18/04/2007	5:03:31
157337	07APR1H.p51	18/04/2007	14:06:16
164544	07APR1H.p53	19/04/2007	5:01:16
168537	07APR1H.P55	19/04/2007	14:01:39

Table B-7. Data collection schedule of the HVS laser profile for Slab 4.

Profile Number	Passes	Date	Time
0	0	07/11/07	17:00
1	6262	07/12/07	8:00
2	8934	07/12/07	14:30
3	8934	07/12/07	15:00
4	16031	07/13/07	5:04
5	16031	07/13/07	5:21
9	19923	07/13/07	14:00
10	19923	07/13/07	14:15
11	28479	07/14/07	5:12
12	28479	07/14/07	5:23
13	32865	07/14/07	14:05
14	32865	07/14/07	14:20
15	41030	07/15/07	5:05
16	41030	07/15/07	5:16
17	45823	07/15/07	14:05
18	45823	07/15/07	14:20
19	54281	07/16/07	5:15
20	54281	07/16/07	5:25
21	58400	07/16/07	14:25
22	58400	07/16/07	14:35
23	64686	07/17/07	2:00
24	64686	07/17/07	2:15
25	66029	07/17/07	5:09
26	66029	07/17/07	5:25
29	78118	07/18/07	5:11
30	78118	07/18/07	5:21
31	82471	07/18/07	
32	82471	07/18/07	
Changed from 12kip to 15kip at 7/18 3:34pm @ 82963 passes			
33	90998	07/19/07	5:20
34	90998	07/19/07	5:35
35	93923	07/19/07	14:05
36	93923	07/19/07	14:20
37	103430	07/20/07	5:20
38	103430	07/20/07	5:31
39		07/20/07	14:05
40		07/20/07	14:20
41	115291	07/21/07	5:22
42	115291	07/21/07	5:43

Table B-7. Continued.

Profile Number	Passes	Date	Time
45	120080	07/21/07	14:19
46	120080	07/21/07	14:30
47	125813	07/22/07	5:05
48	125813	07/22/07	5:30
49	132244	07/22/07	14:00
50	132244	07/22/07	14:12
Changed from 15kip to 18 kip: 7/22 10:11pm @ 136,365 passes			
51	140705	07/23/07	5:11
52	140705	07/23/07	5:22
55	154608	07/24/07	5:02
56	154608	07/24/07	5:10
57	154608	07/24/07	5:25
58	154608	07/24/07	5:35

Table B-8. Analysis files of the HVS laser profile for Slab 4.

Pass #	File Name	File Date	File Time
0	07JUL2G.p0	11/7/2007	16:59:53
17457	07JUL2G.p6	13/07/2007	9:19:54
69920	07JUL2G.p27	17/07/2007	14:07:02
82471	07JUL2G.p31	18/07/2007	14:00:26

Table B-9. Data collection schedule of the HVS laser profile for Slab 5.

Profile Number	Passes	Date	Time
0	0	08/29/07	13:30
1	0	08/29/07	13:45
2	4861	08/30/07	14:15
3	4861	08/30/07	14:30
4	11618	08/31/07	5:11
5	11618	08/31/07	5:22
6	16800	08/31/07	14:15
7	16800	08/31/07	14:30
8	25345	09/01/07	5:45
9	25345	09/01/07	5:55
10	30001	09/01/07	14:00
11	30001	09/01/07	14:03
12	30001	09/01/07	14:13
13	38283	0/02/07	5:13
14	38283	09/02/07	5:20
15	43176	09/02/07	14:00

Table B-9. Continued.

Profile Number	Passes	Date	Time
16	43176	09/02/07	14:10
18	53553	09/03/07	14:10
20	63780	09/04/07	5:00
21	63780	09/04/07	5:15
23	68264	09/04/07	14:30
24	68264	09/04/07	14:45
25	74763	09/05/07	5:10
26	74763	09/05/07	5:20
27	81062	09/05/07	14:00
28	81062	09/05/07	14:10
Changed from 12kip to 15kip 9/5/07 2:30pm @ 81062 passes			
29	88360	09/06/07	5:00
30	88360	09/06/07	5:30
31	91868	09/06/07	14:00
32	91868	09/06/07	14:10
33	100296	09/07/07	5:10
34	100296	09/07/07	5:20
35	104491	09/07/07	14:00
36	104491	09/07/07	14:10
37	113046	09/08/07	5:19
38	113046	09/08/07	5:29
39	117392	09/08/07	14:00
40	117392	09/08/07	14:09
41	130810	09/09/07	14:00
42	130810	09/09/07	14:20
Changed from 15kip to 18kip 9/9/07 2:30pm @ 130810 passes			
43	139009	09/10/07	5:10
44	139009	09/10/07	5:21
45	143750	09/10/07	14:00
46	143750	09/10/07	14:10
47	152239	09/11/07	5:00
48	152239	09/11/07	5:15
153361 Total Passes			

Table B-10. Analysis files of the HVS laser profile for Slab 5.

Passes	File Name	File Date	Time
0	07AUGCON.p0	29/08/2007	11:54:45
4860	07AUGCON.p2	30/08/2007	14:16:53
13213	07AUGCON.p4	31/08/2007	4:59:55
16809	07AUGCON.p6	31/08/2007	13:48:04
25345	07AUGCON.p8	1/9/2007	5:33:07
30002	07AUGCON.p11	1/9/2007	14:02:16
38283	07AUGCON.p13	2/9/2007	4:59:23
43176	07AUGCON.p15	2/9/2007	14:00:14
55586	07AUGCON.p17	3/9/2007	13:59:11
63780	07AUGCON.p20	4/9/2007	5:00:15
68259	07AUGCON.p23	4/9/2007	15:00:02
76187	07AUGCON.p25	5/9/2007	4:59:27
81062	07AUGCON.p27	5/9/2007	14:03:54
88360	07AUGCON.p29	6/9/2007	5:01:14
91868	07AUGCON.p31	6/9/2007	13:59:29
100296	07AUGCON.p33	7/9/2007	4:59:12
104491	07AUGCON.p35	7/9/2007	14:03:52

LIST OF REFERENCES

ACI 318-02: Building Code Requirements for Structural Concrete and Commentary. American Concrete Institute, Detroit, Mich., 2002.

Armaghani, J. M, Comprehensive Analysis of Concrete Pavement Response to Temperature and Load Effects. Ph.D. Dissertation, University of Florida, Gainesville, Florida, 1987.

Armaghani, J. M., Factors Affecting Performance of Concrete Pavements.Proc., 5th International Conference on Copncrete Pavement Design and Rehabilitation, Purdue University, West Lafayette, Indiana, April 1993.

Armaghani, J. M.,T. J. Larsen, and L. L. Smith. Design-Related Distress in Concrete Pavements, Florida's Interstate 75. Concrete International, Design and Construction, ACI, Vol.10, No 8, Aug. 1988, pp 43-49.

Blab, R., L. G. Wiman, and J. Litzka. Heavy Vehicle Simulator Experiment on A Semi-Rigid Pavement Structure Of A Motorway. Proc., 2nd International Conference on Accelerated Pavement Testing, Minneapolis, Minnesota , September, 2004.

Byron, T., Gokhale, S. and Choubane, B. Laser Based Technology for Automated Rut Measurement in Accelerated Pavement Testing. Presented at the 84th Annual Meeting of the Transportation Research Board, Washington D.C., January 2005

California Department of Transportation, Slab replacement guidelines, January 2004.

Chou, Y. T., Structural Analysis Computer Programs for Rapid Multicomponent Pavement Structures with Discontinuities-WESLIQUID and WESLAYER. Technical Report 1, 2, and 3, US Army Engineering Waterways Experiment Station, Vicksburg, MI, May 1981.

Coetzee, N. F., W. Nokes, C. Monismith, J. Metcalf, and J. Mahoney. Full-Scale/Accelerated Pavement Testing: Current Status and Future Directions. Presented at the Transportation Research Board 82nd Annual Meeting, Washington D.C., 2003.

Davids, W.G., Z. M. Wang, G. Turkiyyah, J. Mahoney, and D. Bush.3D Finite Element Analysis of Jointed Plain Concrete Pavement with EverFE2.2. Transportation Research Record, No 1853, National Research Council, Washington D.C., 2003, pp92-99.

Florida Department of Transportation, HVS Laser Profile Data Acquisition System, State Materials Research Park, Gainesville, FL.

Florida Department of Transportation, Standard specification for Road and bridges., Tallahassee, FL, 2004.

Foppl, A. and B. B. Teubner. Vorlesungen uber Technische Mechanik, Vol. 3, 4th ed., Leipzig, Germany ,1909.

Fwa, T. F., X. P. Shi, and S. A. Tan. Analysis of Concrete Pavements by Rectangular Thick – Plate Model. Journal of Transportation Engineering, ASCE, Vol. 122, No. 2, 1996, pp 146-154.

Harvey, J., L.D. Plessis, and J. Roesler. Accelerated Pavement Testing on Concrete Pavements: A Review of Some Lessons Learned. Proc., 2nd International Conference on Accelerated Pavement Testing, Minneapolis, Minnesota , September 2004.

Hetenyi, M. A General Solution for the Bending Beams on an Elastic Foundation of Arbitrary Continuity. Journal of Applied Physics, Vol. 21, 1950, pp 55-58.

Hetenyi, M. Beams of Elastic Foundations, The University of Michigan Press, Ann Arbor, Michigan, 1946.

Hogg, A., and A. Hall. Equilibrium of a Thin Plate Symmetrically Loaded, Resting on an Elastic Subgrade of Infinite Depth. Philosophical Mag., Series 7, 1938.

Horvath, J. S. Beam-Column-Analogy Model for Soil-Structure Interaction Analysis. Journal of Geotechnical Engineering, Vol. 119, No. 2, 1992, pp 358-364.

Horvath, J. S. New Subgrade Model Applied to Mat Foundations. Journal of Geotechnical Engineering, Vol. 109, No 12, 1983, pp 1567-1587.

Horvath, J. S. Subgrade Models for Soil-Structure Interaction Analysis Proc., Foundation Engineering: Current Principles and Practice, Evanston, Illinois, June 1989.

Hu, H. C. Variational Principal and Its Application in Elastics. Science Press, China, 1981, pp 465-477.

Huang, Y. H. Pavement Analysis and Design, 1st ed., Prentice Hall, Upper Saddle River, NJ, 1993.

Hudson, W. R., and H. Matlock. Analysis of Discontinuous Orthotropic Pavement Slabs Subjected to Combined Loads. Highway Research Record, Vol. 131, 1966, pp 1-48.

Ioannides, A. M., M. R. Thompson, and E. J. Barenberg. Westergaard Solutions Reconsidered. Transportation Research Record, No. 1043, National Research Council, Washington D.C., 1985, pp 13-23.

Kumara, W., Analysis and Verification of Stresses and Strains and Their Relationship to Failure in Concrete Pavements under Heavy Vehicle Simulator Loading, Ph.D. dissertation, University of Florida, Gainesville, FL, 2005

Kumara, W., M. Tia, C.-L. Wu, B. Choubane. Evaluation of Applicability of Ultrathin Whitetopping in Florida. Transportation Research Record, No 1823, National Research Council, Washington D.C.,2002, pp39-46.

Luke, A. et al., Implementation of Concrete Maturity Meters, New Jersey Institute of Technology, Report# FHWA-NJ-2002-003, 2002.

Mancio, M et al., Evaluation of the Maturity Method for Flexural Strength Estimation in Concrete Pavement, Draft report prepared for the California Department of Transportation (Caltrans). Pavement Research Center, Institute of Transportation Studies, 2004.

Melhem et al., Accelerated Testing for Studying Pavement Design and Performance (FY 2000), Final report of Kansas Department of Transportation, Kansas, 2003.

Metcalf, J. B, Application of Full-Scale Accelerated Pavement Testing. Transportation Research Record, NCHRP Synthesis of Highway Practice 235, National Research Council, Washington D.C.,1996.

Mindlin, R. D. Influence of Rotatory Inertia and Shear on Flexural Motion of Isotropic Plates. Journal of Applied Mechanics, Vol. 23, 1951, pp 31-38.

Okamoto, P. A., C. L. Wu, S. M. Tarr, and L. W. Cole. Early Opening of PCC Pavements to Traffic",Proc., 5th International Conference on Copncrete Pavement Design and Rehabilitation, Purdue University, West Lafayette, Indiana, April 1993.

Okamoto, P.A., P. J. Nussbaum, K. D. Smith, T. P.Darter, T. P. Wilson, C. L. Wu, and S. D. Tayabji. Guidelines for Timing Contraction Joint Sawing and Earlist Loading for Concrete Pavements. FHWA-RD-91-079,080, Federal Highway Administration Washington DC, 1991.

Pasternak, P. L. On a New Method of Analysis of an Elastic Foundation by Means of Two Foundation Constants. Moscow: Gps. Izd. Lit.po. Strait I Arkh, 1954.

Pickett, G., and G. K. Ray. Influence Charts for Concrete Pavements, Transactions, ASCE, Vol. 116, 1951.

Plessis, L. D., D. Bush, F. Jooste, D. Hung, C. Scheffy, J. Roesler, L. Popescu, and J. Harvey. HVS Test Results on Fast-Setting Hydraulic Cement Concrete Palmadale, California Test Sections, South Tangent, Draft Report, California Department of Transportation, July 2003.

Rao, S., and J. Roesler. Cumulative Fatigue Damage Analysis of Concrete Pavement Using Accelerated Pavement Testing Results. Proc., 2nd International Conference on Accelerated Pavement Testing, Minneapolis, Minnesota , September 2004.

Rasmussen R. O. et al., Strength Measurements Using Maturity for Portland Cement Concrete Pavement Construction at Airfields, Innovative Pavement Research Foundation, Report DOT/FAA-01-G-002-4, 2003

Reissner, E. A Note on Deflections of Plates on a Viscoelastic Foundation. Journal of Applied Mechanics, Trans., ASME, Vol. 80, 1958, pp 144-145.

Reissner, E. Effect of Transverse Shear Deformation on Elastic Plates. Journal of Applied Mechanics, Vol. 12, 1945, pp 69-77.

Reissner, E. On a Variational Theorem in Elasticity. Journal of Mechanics amd Physics, July 1950, pp 90-95.

Sansalone, M.J. and W. B. Streett. Impact Echo, Nondestructive Evaluation of Concrete and Masonry, Bullbrier Press, Ithaca, N.Y. 1997.

Shi, X. P., S. A. Tan, and T. F. Fwa. Rectangular Thick Plate With Free Edges on Pasternak Foundation. Journal of Engineering Mechanics, Vol. 120, No. 5, 1994, pp 971-988.

Suh, C., The Effect of Early Opening to Traffic on Fatigue Life of Concrete Pavement, Dissertation, University of Texas at Austin, 2005.

System 6000- Model 6100 Scanner, Instruction Manual," Vishay Micro- Measurements, Raleigh, North Carolina, 2002.

Tabatabaie, A. M. and E. J. Barenberg. Finite Element Analysis of Jointed of Cracked Concrete Pavements. Transportation Research Record, No. 671, TRB, National Research Council, Washington D.C. 1978, pp. 11-17.

Tayabji, S. P., and B. E. Colley. Analysis of Jointed Concrete Pavements. Federal Highway Administration, National Technical Information Service, 1981.

Tia, M. and Kumara W., Evaluation of Early Strength Requirement of Concrete for Slab Replacement Using APT, Final Report for Florida Department of Transportation, Gainesville, FL, March 2005.

Tia, M., C. L. Wu, B. E. Ruth, D. Bloomquist, and B. Choubane. Field Evaluation of Rigid Pavements for the Development of A Rigid Pavement Design System- PhaseIV. Final Report, State Project# 99700-7359-010, Florida Department of Transportation, August 1989.

Tia, M., M. Armaghani, C.-L. Wu, S. Lei, and K. L. Toye. FEACONS III Computer program for an Analysis of Jointed Concrete Pavements. Transportation Research Record, No 1136, National Research Council, Washington D.C., 1987, pp12-22.

Tia, M., Wu, C. L., Ruth, B. E., Bloomquist, D., and Choubane, B., 1989. "Field Evaluation of Rigid Pavement Design System--Phase IV," Final Report, Project 4910450424912, Department of Civil Engineering, University of Florida.

Tikalsky, P. J., B. E. Scheeze, and D. G. Tepke. Using the Concrete Maturity Meter for QA/QC. Report for the Pennsylvania DOT, January 2001.

Transportation Research Board, Guidelines for Early-Opening-to-Traffic Portland Cement Concrete for Pavement Rehabilitation, NCHRP report 540, 2005

Trost, S. et al., Using Maturity Testing for Airfield Concrete Pavement Construction and Repair, Research Report on Innovation Pavement Research Foundation, 2006.

Turan O. T. et al., Early-Age Behavior of Jointed Plain Concrete Pavement System, the 2005 Mid-Continent Transportation Research Symposium, Iowa, 2005.

Venckovskii, B. K. Bending of Annular and Circular Plates on a Generalized Foundation under the Combined Action of Lateral and Radial Forces. Raschety na Prochnost, Collection of Papers, Vol. 3, Mashgiz, Moscow, USSR, 1958.

Vora, M. R., and H. A. Matlock. A Discrete-Element Analysis for Anisotropic Skew Plates and Grids Research Report No. S6-18, Center for Highway research, University of Texas, Austin, 1970.

Westergaard, H. M. Stresses Concentration in Plates Loaded Over Small Area. Transactions, ASCE, Vol. 108, 1943, pp 831-856.

Westergaard, H. M. Stresses in Concrete Runways of Airports. Proceedings of Highway Research Board, Vol. 19, 1939, pp 197-202.

Westergaard, H. M. Theory of Concrete Pavement Design. Proceedings of Highway Research Board, Vol. 7, Part 1, 1927, pp 175-181

Westergaard, H. M., Analysis of Stresses in Concrete Roads. Proceedings of Highway Research Board, Vol. 5, 1926, pp 90-112.

Westergaard, H. M., Analytical tools for Judging Results of Structural Tests of Concrete Pavements. Public Roads, Vol. 14, No. 10, 1933, pp 185-188.

Westergaard, H. M., New Formula for Stresses in Concrete Pavement of Airfields. American Society of Civil Engineers, ASCE, Vol. 113, 1947, pp 425-444.

William, G.W. and S. N. Shoukry, 3D Finite Element Analysis of Temperature-InducedStresses in Dowel Jointed Concrete Pavements. International Journal of Geomechanics, 1(3), 2001, pp291-308.

Yui, H.T., J. Mallela, and M. I. Darter. Long-Term Performance of Fast-Track Full-Depth Repairs. Presented at the Transportation Research Board 81st Annual Meeting, Washington D.C., 2002.

Zhang, J., J. T. Harvey, A. Ali, and J. Roesler. Goal 4 Long Life Pavement Rehabilitation Strategies—Rigid: Laboratory Strength, Shrinkage, and Thermal Expansion of Hydraulic Cement Concrete Mixes. Draft report prepared for the California Department of Transportation (Caltrans). Pavement Research Center, Institute of Transportation Studies, 2004.

BIOGRAPHICAL SKETCH

Kitti Manokhoon, the son of Mr.Chaisit and Mrs.Arunee Manokhoon, was born in 1977, Thailand. He graduated with the Bachelor of Engineering from the Department of Civil Engineering at the Khon-Kaen University (KKU), Thailand in April 1998. After the graduation, he was awarded a scholarship to continue his study at the Asian Institute of Technology (AIT), Thailand. He earned the Master of Engineering in Transportation Engineering from the School of Civil Engineering at AIT in April 2000. He was then appointed as a lecturer in the Department of Civil Engineering at the Mahanakorn University of Technology (MUT), Thailand until August 2002.

In 2002, he was awarded the Royal Thai Government scholarship to start his Ph.D. program in civil engineering at the University of Florida (UF), USA in Fall 2002. At UF, he also earned a graduate research assistantship to work on research projects as well as to complete his Ph.D. During the time of his Ph.D. plan, in August 2004, he was awarded the Master of Engineering from the Department of Civil and Coastal Engineering at UF. In April, 2005 he was granted the Outstanding International Student Academic Award from the College of Engineering at UF. Throughout his studies at UF, he has achieved the highest grade point average attainable of 4.0/4.0.